Impact of Dissolved Organic Matter Photodegradation on Carbon and Nitrogen Cycling in Freshwaters

by

Jennifer Carolyn Bowen

A dissertation submitted in partial fulfillment
of the requirements for the degree of
Doctor of Philosophy
(Earth and Environmental Sciences)
in the University of Michigan
2021

Doctoral Committee:

Associate Professor Rose M. Cory, Chair
Professor Gregory J. Dick
Research Scientist Emeritus Louis A. Kaplan, Stroud Water Research Center
Professor George W. Kling
Associate Professor Kerri A. Pratt

Jennifer Bowen

bowenjc@umich.edu

ORCID iD: 0000-0002-3085-3229

Dedication

To Grandma Jean and Grandpa Jim

Acknowledgements

First, I would like to thank my advisor Rose Cory for all of her guidance, support, and patience over the years. I appreciate how you would always make the time to provide feedback for your students and encourage us to help and support one another. You have provided me with valuable insight on becoming a better scientist and collaborator. Thank you to Lou Kaplan and George Kling for your feedback, advice, and time while working together on research projects and as members on my dissertation committee. I admire how much you both truly care about effective science communication and appreciate you putting in the time to push me as a writer and communicator. Thanks to both of you and the rest of my committee, Greg Dick and Kerri Pratt, for constantly challenging me to think about my results in new ways, asking big-picture questions on the implications of my findings, and providing advice for my future career.

Thank you to all the current and former Cory Lab members for passing on knowledge and being a source of support and encouragement for me over the years, especially Adrianna Trusiak who has been around throughout my time in the lab and has always been there to talk or provide critical feedback on my work. Thank you to Collin Ward for patiently teaching me about photochemistry and mass spectrometry in my first year, and then later welcoming me into your research group. I appreciate all the valuable insight you have provided on experimental design, building a research group, and developing a research career. Thank you to Lija and Katie for thinking deeply about science with me, helping with experiments, and making the challenges and hiccups of research fun.

Thank you to all of the scientists and staff at Michigan, Stroud, Toolik, EMSL, and WHOI who have made the research in this dissertation possible. Specifically, thank you to Li Xu and Josh Burton for teaching me how to use the extraction lines at NOSAMS and patiently answering my questions, and Rosey Chu for teaching me all you know about FTICR-MS. Thank you to the logistical support at Stroud and Toolik who helped make five field campaigns run smoothly. Thank you to Nancy and Anne at the University of Michigan for putting through last-minute orders or shipments and being an incredible resource for students.

Lastly, I would like to thank all of the friends that I have made while at Michigan, who have talked science with me over beers and celebrated the little milestones over the years. Thank you to my family for supporting me through the highs and lows, providing a different perspective on life, and reminding me to slow down when I needed it, especially Harold and Ira for always believing in me.

Table of Contents

List of Figures

List of Tables

Abstract

Freshwaters emit comparable amounts of carbon dioxide (CO_2) to the atmosphere as the net amount taken up by all land on Earth. The degradation of dissolved organic matter (DOM) to CO_2 impacts these emissions from freshwaters, making the fate of DOM a critical component of the global carbon (C) cycle. Yet, controls on DOM degradation remain too poorly understood to quantify how much CO_2 will be emitted from freshwaters as our planet warms. The sunlight-driven or photochemical degradation of DOM can impact freshwater CO_2 emissions by producing CO_2 or altering DOM to forms that are more or less labile to bacterial respiration to CO_2. Photodegradation of DOM can also produce ammonium (NH_4^+), providing a source of nitrogen (N) to the primary producers carrying out photosynthetic uptake of CO_2 in freshwaters. Here, chemical controls on these three photodegradation pathways were investigated and their impacts on C and N cycles were assessed in arctic and temperate freshwaters.

First, the photochemical production of NH_4^+ from DOM was investigated as a source of inorganic N to oligotrophic, arctic lakes. NH_4^+ was produced during the photodegradation of protein-like compounds within DOM, but rates of NH_4^+ photo-production were limited by the availability of protein-like compounds because they were also degraded by bacteria in the water column. The NH_4^+ photo-produced could account for ~5% of the N taken up by primary producers in arctic lakes, suppling N at rates comparable to the export of inorganic N from land to streams and streams to lakes. These findings demonstrate how the photodegradation of DOM creates a strong linkage between land and freshwater N cycling.

Second, the impact of thawing permafrost soils on freshwater CO_2 emissions was determined by showing that millennia-aged DOM from arctic permafrost is rapidly photodegraded to CO_2. Dissolved iron was identified as a major control on this photo-production of CO_2 from permafrost DOM because it catalyzed the photo-decarboxylation of terrestrially-derived compounds to CO_2. Rates of CO_2 photo-production from permafrost DOM were two-fold higher than rates from DOM currently draining from thawed surface soils to arctic freshwaters. These findings demonstrate that more DOM will be photodegraded to CO_2 as deeper permafrost soils thaw and deliver DOM to freshwaters in proportion to the amount of dissolved iron present.

Lastly, the effect of photodegradation on the amount of DOM respired by bacteria in the streambed to CO_2 was studied in a temperate stream. This effect of sunlight exposure depended strongly on the photodegradation rate and which compounds were photo-produced. For instance, photodegradation rates were fast enough to impact the respiration of terrestrially-derived compounds that take longer for bacteria to respire in the streambed. Photodegradation increased the respiration of terrestrially-derived compounds by breaking down higher molecular weight aromatic compounds and decreased their respiration by altering them to less labile forms. The balance of these DOM compounds photo-produced resulted in positive effects of sunlight on respiration after short exposures and negative effects after longer exposures. Given that only minutes to hours of sunlight exposure in the stream were needed to change bacterial respiration by ~50%, these findings indicate that photodegradation greatly impacts the amount of DOM respired to CO_2 even in periodically-shaded streams. Together, this dissertation demonstrates that DOM photodegradation substantially impacts freshwater CO_2 emissions now and will impact them in the future, improving our predicting understanding of this process.

Chapter 1

Introduction

1.1 The role of DOM photodegradation in the freshwater carbon and nitrogen cycles

Freshwaters emit comparable amounts of carbon dioxide (CO_2) to the atmosphere as the net amount taken up by all land on Earth (~1.2 Pg C per year), making freshwater CO_2 emissions a critical component of the global carbon (C) cycle.[1-3] The amount of CO_2 emitted from freshwaters depends largely on the degradation of dissolved organic matter (DOM) derived from decaying plant biomass to CO_2,[4-6] although uptake of CO_2 from the atmosphere during photosynthesis can offset this production. It is estimated that only half of the DOM in freshwaters globally is degraded to CO_2 before it reaches the ocean,[6] but this amount should change as more DOM drains from soils to freshwaters with land use and climate change.[7-10] Thus, changes to the fate of freshwater DOM (CO_2 released to the atmosphere versus DOM entering the ocean) due to land use and climate change are poised to impact the global C cycle in the future. Yet, controls on DOM degradation remain too poorly understood to estimate how much CO_2 will be released to the atmosphere from freshwaters in part because the sunlight-driven or photochemical pathways are not well constrained.

In sunlit freshwaters, the aromatic, chromophoric fraction of DOM (CDOM) absorbs sunlight, initiating photochemical reactions that can degrade DOM directly to CO_2 (photomineralization)[11-12] or alter the chemical composition of DOM by producing different DOM compounds (photo-alteration).[13-16] The photo-altered products formed during sunlight exposure can be more susceptible or less susceptible to bacterial respiration (i.e., more versus

less labile),[13,17-19] impacting the amount of DOM that is respired by heterotrophic bacteria to CO_2 in freshwaters.[17,20-22] Only recently was it reported that these pathways for photochemical degradation (photodegradation) of DOM can account for up to 30% of the CO_2 produced in freshwaters,[23-25] contradicting the long-held understanding that nearly all DOM degradation to CO_2 in freshwaters is attributed to bacterial respiration alone.[11,26-28] These findings demonstrate that the photodegradation of DOM may contribute a considerable portion of the CO_2 produced in freshwaters.

Photodegradation of DOM can also impact nitrogen (N) cycling in freshwaters by producing ammonium (NH_4^+).[29-32] In freshwaters, the amount of CO_2 taken up during photosynthesis can be limited by N when the availability of dissolved inorganic N (DIN; e.g., NH_4^+, NO_3^-, NO_2^-) is low[33-36] because primary producers use this form of N to carry out photosynthesis.[37] Previous work has estimated that NH_4^+ produced during the photodegradation of DOM can account for ~5% of the N taken up by primary producers in freshwaters.[38-39] Thus, the photochemical production of NH_4^+ from DOM in freshwaters may provide a source of DIN to primary producers that carry out photosynthesis in freshwaters.

Together, these previous findings demonstrate that DOM photodegradation can impact C and N cycling in freshwaters as well as the CO_2 emitted from freshwaters. However, there are two major limitations in the field of freshwater photochemistry that currently inhibit our ability to quantify the impacts of DOM photodegradation on C and N cycling in freshwaters: knowledge of mechanistic controls on these photodegradation pathways and the approaches used to estimate the importance of DOM photodegradation in sunlit freshwaters.

1.2 Identifying mechanistic controls on DOM photodegradation

Identifying mechanistic controls on DOM photodegradation pathways that produce NH_4^+, CO_2, or photo-altered DOM compounds requires knowledge of the compositions and structures of DOM compounds that undergo photodegradation. Yet, identifying the composition and structures of individual DOM compounds has been a challenge because DOM is a mixture of thousands of organic compounds varying in their size, composition, and structure. The compounds comprising the DOM pool are derived from biomolecules that make up dead plant and microbial biomass, including lignin, tannins, proteins, lipids, and carbohydrates.[40] The degradation of dead biomass to form DOM results in changes to the size and chemical properties of organic compounds, making them indistinguishable from intact biomolecules. As a result of this chemical alteration, current approaches to analyze the size, composition, and structure of DOM compounds are limited to average or bulk measures of the entire DOM pool instead of individual compounds.[41] For example, ultra-high resolution mass spectrometry can be used to determine the elemental composition of DOM compounds,[42-44] nuclear magnetic resonance can be used to characterize the distribution of functional groups on DOM compounds,[45-47] and measures of absorbance and fluorescence spectroscopy can be used to interpret the chemical properties of aromatic compounds within DOM.[15,48-50] In addition, there are currently no analytical approaches that concurrently measure the composition and assign structure to compounds comprising the DOM pool, both which are needed to test mechanisms of photodegradation. Thus, these bulk measures of DOM chemistry that cannot assign structure to specific DOM compositions limit our ability to trace the DOM compounds that undergo photodegradation to form NH_4^+, CO_2, or photo-altered products.

To overcome this limitation, previous studies have tested whether the production of NH_4^+, CO_2, or photo-altered products increases with certain chemical properties or compositions within DOM to infer mechanisms of photodegradation. For example, it has been reported that NH_4^+ photo-production increases with concentrations of dissolved organic N (DON),[31] CO_2 production from DOM photomineralization increases with the aromatic content of DOM[51] or loss of aromatic compounds,[12,52-54] and the photo-production of low molecular weight acids increases with the aromatic content of DOM.[55-56] However, this approach to testing mechanistic controls on photodegradation does not account for differences in the amount of aromatic compounds present, which strongly impact the extent of photodegradation because they are needed to initiate photochemical reactions. As such, higher amounts of NH_4^+, CO_2, or lower molecular weight acids photo-produced could be due to more aromatic compounds available to absorb sunlight, not a greater susceptibility of DOM to photodegradation.

The estimation of apparent quantum yields for photochemical reactions allows for direct comparisons of DOM photodegradation between freshwaters varying in aromatic DOM content. This is because the apparent quantum yield quantifies the susceptibility of DOM to a photochemical reaction as the moles of product formed per mole of photons absorbed by the aromatic compounds within DOM.[57-60] However, when differences in the aromatic content between freshwater DOM samples have been accounted for by quantifying apparent quantum yields, there are no observed relationships between the chemical properties of DOM and yields for NH_4^+ production,[61] CO_2 production,[23,62] or the formation of photo-altered DOM compounds.[63-64]

It is likely that no single chemical property of DOM determines its susceptibility to photodegradation because there are multiple mechanistic controls on the production of NH_4^+, CO_2, or photo-altered compounds. For example, DOM photomineralization is thought to occur through the photochemical loss of aromatic compounds,[51,53] the indirect oxidation of DOM compounds by hydroxyl radical (a reactive oxygen species),[58,65-66] and the oxidation of carboxyl groups within DOM by dissolved iron during a ligand-metal-charge-transfer reaction (photo-decarboxylation).[58,68-70] Thus, photomineralization could depend on the presence of aromatic compounds as well as the number of carboxylic groups, concentrations of dissolved iron, and the efficiency that DOM produces hydroxyl radical.[67,71] The photo-production of NH_4^+ from DOM is thought to occur through one mechanism involving the photochemical loss of primary amine groups, which are located on the ends of amino acids, peptides, and proteins (i.e., N-terminus).[72] Peptides and proteins also undergo peptide bond cleavage during sunlight exposure, which increases the number of primary amines available to undergo photodegradation to yield NH_4^+.[14,73] As such, the susceptibility of DOM to NH_4^+ photo-production could depend on the abundance of amino acids, peptides, and proteins within DOM (collectively known as protein-like DOM) as well as their susceptibility to peptide bond cleavage during DOM photodegradation.

In contrast to these inorganic products of DOM photodegradation (NH_4^+ and CO_2), far less is known about mechanistic controls on the formation of photo-altered DOM compounds that impact bacterial respiration of DOM. For instance, previous studies have shown that low molecular weight carboxylic acids and amino acids are produced during the photochemical oxidation of DOM by hydroxyl radical.[65,73] However, these low molecular weight compounds account for a small portion of the DOM respired by bacteria on a mass basis.[13,74-75] On the other

hand, the higher molecular weight compounds expected to have a larger impact on bacterial respiration on a mass basis[76] have been shown to undergo photodegradation in the presence of reactive oxygen species,[18,77-79] but the structures and compositions of photo-altered products are too poorly understood to infer mechanisms of their formation.[77-78]

Instead, mechanistic controls on the formation of photo-altered DOM compounds that are more versus less oxidized may be tested because these photo-products are thought to come from mechanisms of partial photo-oxidation and photo-decarboxylation, respectively.[70,78-79] For example, more oxidized compounds should be produced during the partial photo-oxidation of DOM by reactive oxygen species because this mechanism incorporates oxygen into DOM compounds.[18,60,79] Less oxidized compounds should be produced during the photo-decarboxylation of DOM because the conversion of a carboxyl group within DOM to CO_2 decrease the oxidation state of the compound remaining.[70] Previous findings suggest that the formation of more oxidized DOM compounds could depend the chemical properties of aromatic compounds present within the DOM pool because they control rates of reactive oxygen species production.[67,80-81] In addition, the formation of less oxidized compounds could depend on the number of carboxyl groups within DOM and concentrations of dissolved iron present to catalyze the photo-decarboxylation of DOM.[68-69]

However, estimating the impacts of DOM photodegradation on bacterial respiration of DOM to CO_2 is also confounded by the fact that the photo-altered products formed can be more versus less labile to freshwater bacteria. For instance, the formation of partially oxidized photo-products by reactive oxygen species may increase or decrease the lability of DOM to bacteria.[18-19] In addition, the breakdown of high molecular weight compounds to produce lower molecular weight acids or aldehydes can increase the lability of DOM to bacteria,[13,74] whereas some

aromatic and aliphatic photo-products are less labile than the initial DOM (i.e., relatively more recalcitrant to bacterial respiration).[18-19] The extent that each of these photo-altered products (labile vs. recalcitrant) are formed should determine whether sunlight has a positive or negative effect on bacterial respiration of DOM.[82-83] Thus, knowledge of mechanistic controls on the formation of labile vs. recalcitrant photo-products is needed to quantify the magnitude and direction of sunlight-altered bacterial respiration in freshwaters. Given that the impact of photo-altered products on respiration also depends strongly on which bacterial species are present[84-85] and their metabolic capacity,[19,85] it is essential that labile and recalcitrant photo-products are defined based on measurements of bacterial responses to these compounds using native bacterial communities from the freshwater ecosystem being studied, not based on the structures and oxidation states of photo-altered products alone.

In summary, we have yet to identify mechanistic controls on the DOM photodegradation pathways that produce NH_4^+, CO_2, or photo-altered products because previous approaches have not quantified apparent quantum yields of their formation or accounted for more than one control on their formation. Because there is more than one mechanism that can produce CO_2 photochemically[58,65,68] or form photo-altered products[18,65,73,78] testing controls in freshwaters and at wavelengths where one mechanism is expected to dominate should provide insight to the chemical properties controlling their production. Likewise, quantifying bacterial responses to the photodegradation of specific classes of compounds within DOM (e.g., lignin, tannins, proteins) should provide more insight to the chemical properties controlling the formation of labile and recalcitrant photo-products than measures of bulk changes in bacterial respiration of DOM. While knowledge of these mechanistic controls is needed to quantify water column rates

of DOM photodegradation in freshwaters, there are other limitations to estimating the importance of these DOM photodegradation pathways in freshwaters.

1.3 Estimating the importance of DOM photodegradation in freshwaters

Current estimates of the importance of DOM photodegradation in freshwaters are limited in part by our knowledge of the capacity for sunlight to outcompete bacteria for the degradation of DOM. It is well known that there is overlap between the DOM compounds degraded by sunlight and bacteria.[17-19,86] For example, bacteria degrade high molecular weight, aromatic compounds in freshwaters where these compounds are abundant within the DOM pool[19,76,87-88] and proteins in freshwaters where concentrations of small N-containing compounds are low.[89-91] Sunlight is expected to degrade these same DOM compounds to form NH_4^+, CO_2, or photo-altered products.[60,73,78] Thus, the photodegradation of DOM compounds to form NH_4^+, CO_2, or photo-altered products in freshwaters may be limited if rates of photodegradation are much slower than rates of bacterial degradation of these same compounds.

It is more likely that rates of photodegradation are fast enough to compete with bacterial degradation of high molecular weight, aromatic compounds than N-containing compounds like proteins because high molecular weight, aromatic compounds are degraded by bacteria at a slower rate than N-containing compounds.[92-94] Slower rates of bacterial degradation indicate that there could be more time for sunlight to degrade DOM compounds and alter their chemical properties before bacteria degrade them. In contrast, higher rates of bacterial degradation of N-containing compounds could mean that there is not enough time for sunlight to degrade protein-like compounds within DOM and thus, for any amino acids or NH_4^+ to be produced in freshwaters. Thus, direct comparisons of photodegradation rates to bacterial degradation for

specific compound classes are needed to evaluate the importance of DOM photodegradation pathways that produce NH_4^+, CO_2, or photo-altered compounds in freshwaters.

Accurate assessment of whether sunlight outcompetes bacteria for DOM compounds requires comparing photodegradation rates in the water column to rates of bacterial degradation in the water column and benthic zone. The few studies that have directly compared rates of DOM photodegradation to bacterial degradation showed that photodegradation can be faster than or equal to bacterial degradation in the water column.[23,95] Yet, benthic respiration can exceed water column rates of bacterial respiration by two orders of magnitude in streams.[96] Thus, comparisons of photodegradation to bacterial degradation in the water column could overestimate the importance of DOM photodegradation in freshwaters where rates of bacterial degradation in the benthic zone exceed those in the water column.

In addition, accurate assessment of the rate at which sunlight degrades DOM compounds relative to bacteria requires certainty in the wavelength dependence of the photochemical reaction. For instance, water column rates of DOM photodegradation pathways depend on three variables that vary as a function of sunlight wavelength: the amount of sunlight reaching freshwaters, the amount of DOM available to absorb that light in the water column, and the apparent quantum yield of products formed.[60,97] Of the three, the greatest uncertainty lies with the shape and magnitude of the apparent quantum yield spectrum,[60,95] which is challenging to measure.[98] Previous studies have reported apparent quantum yield spectra that decrease exponentially with increasing wavelength for NH_4^+ production[99] and CO_2 production.[97,100-102] Given that there is a ~10-fold greater flux of visible light reaching freshwaters than ultraviolet (UV),[23,57,97] DOM photodegradation rates are disproportionately impacted by the yield of products formed at visible wavelengths of light. It follows that estimated DOM

photodegradation rates are most sensitive to small changes in the apparent quantum yield at visible wavelengths of sunlight due to a shift in the slope or magnitude of the yield spectrum. Thus, direct measurements of apparent quantum yield spectra for DOM photodegradation pathways in freshwaters are needed to constrain estimates of DOM photodegradation rates in freshwaters and thus, accurately assess whether sunlight outcompetes bacteria for the degradation of DOM.

In summary, understanding of the importance of DOM photodegradation pathways in freshwaters is limited by our knowledge of how rates of photodegradation of DOM compounds compare to bacterial degradation of these same compounds as well as the measurements used to quantify these rates. Given that it is less likely for photodegradation rates to be fast enough to compete with bacterial degradation of N-containing DOM compounds, comparing photodegradation rates to rates of bacterial degradation of protein-like compounds should provide insight on the extent that sunlight produces NH_4^+ in freshwaters. Likewise, estimating the importance of DOM photodegradation pathways in freshwaters with high rates of bacterial degradation in the benthic zone, such as streams, requires comparing water column rates of photodegradation to rates of bacterial degradation in the benthic zone of the streambed.

1.4 Approach to test controls and the importance of DOM photodegradation in freshwaters

Thus, the goals of this dissertation were to (i) identify controls on the three DOM photodegradation pathways that impact freshwater CO_2 emissions and (ii) better constrain the importance of these DOM photodegradation pathways in freshwaters by comparing photodegradation rates to bacterial degradation of specific DOM compound classes and comparing them to bacterial degradation in the benthic zone when applicable. My approach to

test mechanistic controls on the photo-production of NH_4^+ and CO_2 involved quantifying apparent quantum yields of their production and combining analytical approaches to measure changes in DOM chemical properties during sunlight exposure for waters ranging in DOM chemical composition and water chemistry. I tested controls on the photo-production of more oxidized and less oxidized compounds by quantifying changes to the oxidation state and chemical properties of DOM at UV and visible wavelengths of sunlight. Lastly, my approach to test controls on the photo-production of labile and recalcitrant DOM compounds was to measure changes in bacterial degradation of specific classes of compounds within DOM following sunlight exposure. Together, I used these approaches to test the following hypotheses on NH_4^+, CO_2, and photo-altered compound production:

1. Photo-produced NH_4^+ comes from the degradation of protein-like compounds within DOM.

2. Dissolved iron is a major control on the photomineralization of DOM because iron catalyzes the photo-decarboxylation of carboxyl groups to CO_2.

3. The photo-production of less oxidized DOM compounds depends on the extent of iron-catalyzed photo-decarboxylation of DOM, whereas the photo-production of more oxidized compounds is controlled by the aromatic content of DOM.

4. Contrasting effects of sunlight on bacterial respiration of DOM to CO_2 can be explained by the balance of labile and recalcitrant DOM compounds photo-produced.

I tested the first hypothesis in **Chapter 2** using DOM from arctic streams, rivers, and lakes, which provided a natural gradient in the content and composition of N-containing compounds that could undergo photodegradation.[103-104] This work was carried out in the Alaskan Arctic because the majority of dissolved nitrogen draining from arctic soils to

freshwaters is in the organic form,[103,105] the lakes in this region are limited by available DIN,[34,106-107] and the photodegradation of DON to NH_4^+ could provide a major portion of the DIN fueling primary production arctic lakes.[108] Thus, I identified how much and when photo-produced NH_4^+ could contribute to DIN uptake by primary producers during the ice-free summer season in an arctic lake.

Findings from this work demonstrated that photo-produced NH_4^+ came from the degradation of protein-like compounds within DOM. Similar percentages of DON photodegraded to produce NH_4^+ across the arctic freshwaters indicated that NH_4^+ photo-production depended more on the amount of protein-like compounds present than the chemical properties of these compounds. I directly measured apparent quantum yield spectra for NH_4^+ photo-production to estimate rates of its production in arctic freshwaters. I found that photodegradation rates were 16% of rates that bacteria incorporated N into their biomass in an arctic lake. Given that the bacteria in these lakes primarily obtain N from protein-like compounds, these findings suggest that NH_4^+ photo-production rates are likely limited by available protein-like N to undergo photodegradation due to the competition between sunlight and bacteria for these same compounds. When NH_4^+ was photo-produced, it could supply an average of 5% of the N taken up by primary producers in an arctic lake, which was similar to that previously estimated in other freshwaters.[38-39] However, NH_4^+ photo-production rates were comparable to rates of DIN export from soils to streams[105] and inlet streams to lakes in the Arctic.[108] Thus, my findings indicate that the photodegradation of DON draining from soils to sunlit arctic lakes can supply DIN to primary producers at rates comparable to other fluxes of DIN, creating a strong linkage between soil and freshwater ecosystems.

In **Chapter 3**, I tested the second hypothesis using DOM draining from arctic permafrost soils, which contains a low abundance of aromatic compounds compared to DOM currently draining from the active soil layer.[109-110] A low aromatic content of DOM is expected to reduce the amount of CO_2 produced from direct and indirect mechanisms involving these light-absorbing compounds,[51,58,67] but not affect the extent that dissolved iron catalyzes the photo-decarboxylation of carboxyl groups to CO_2.[68] Consistent with this expectation, previous work estimated that 90% of the CO_2 produced during photodegradation of permafrost DOM came from the loss of carboxyl C.[70] Thus, I used permafrost DOM to test chemical controls on its photodegradation to CO_2 and provide experimental evidence for the iron-catalyzed mechanism of photo-decarboxylation.

My findings showed that the photo-production of CO_2 from permafrost DOM depended on the concentration of dissolved iron present because iron catalyzes the photo-decarboxylation of carboxyl groups within DOM. I used measures of the stable and radiocarbon isotopic composition of CO_2 produced from DOM photodegradation to demonstrate that the carboxyl groups were associated with lignin- and tannin-like compounds within DOM and that these compounds were >4,000 years old. By directly measuring apparent quantum yield spectra, I found that rates of CO_2 produced during the photodegradation of permafrost DOM are 2-fold higher than those for the modern DOM currently draining soils to freshwaters. These findings indicate that DOM photodegradation will account for more of the CO_2 produced from arctic freshwaters in the future as permafrost soils thaw. Including the CO_2 photo-produced from permafrost DOM in future predictions of net ecosystem C loss from thawing permafrost show that current estimates of amplified global warming may be underestimated by ~14%.

In **Chapter 4**, I tested the third hypothesis by quantifying photochemical changes to the oxidation state of DOM leached from the same permafrost soils used in **Chapter 3**. The iron-catalyzed removal of carboxyl groups during photo-decarboxylation is expected to increase with the wavelengths of light because the complexation of dissolved iron with DOM compounds (e.g., carboxylic acids)[111] increases its capacity to absorb light at longer wavelengths compared to shorter wavelengths.[58,112] In contrast, the incorporation of oxygen into DOM compounds during the partial photo-oxidation by reactive oxygen species may be higher at UV wavelengths because apparent quantum yields of reactive oxygen species production decrease with the wavelength of light.[59,113] Thus, I exposed the permafrost DOM to UV versus visible wavelengths of light to test chemical controls on the extent that permafrost DOM became more oxidized with partial photo-oxidation and less oxidized with photo-decarboxylation.

Findings from this work showed that less oxidized DOM compounds were photo-produced from permafrost DOM at visible wavelengths than UV wavelengths due to a greater extent of iron-catalyzed photo-decarboxylation taking place at longer wavelengths of light. The extent that more oxidized DOM compounds were photo-produced from partial photo-oxidation at either waveband was limited by the abundance of aromatic compounds likely because they were needed initiate the partial photo-oxidation of permafrost DOM. These results demonstrate that sunlight exposure of permafrost DOM can increase or decrease its oxidation state depending on the aromatic content of DOM draining from thawing permafrost soils and the amount of dissolved iron present in neighboring freshwaters. Given that the oxidation state of DOM can impact its susceptibility to bacterial respiration to CO_2,[19,114] my findings improve our knowledge of controls on the formation of photo-altered DOM compounds that may impact bacterial respiration of DOM in freshwaters.

In **Chapter 5**, I tested the fourth hypothesis using DOM from a temperate headwater stream and plug-flow biofilm reactors (bioreactors) that measure bacterial degradation of DOM in the benthic zone of the streambed.[115] Prior work scaled bacterial degradation of DOM in the bioreactors to the stream, where degradation occurring in the bioreactors over minutes and centimeters occurred in the stream over hours to days and hundreds of meters to kilometers.[116] In addition, it has been shown that protein-like compounds are degraded quickly by bacteria in the stream, whereas high molecular weight, aromatic compounds are degraded more slowly.[94,117] Thus, I used the bioreactors to identify which classes of DOM compounds became more versus less labile to bacteria following sunlight exposure and determine whether DOM photodegradation rates in the stream were fast enough to impact their degradation by bacteria in the streambed.

My findings showed that DOM photodegradation increased the lability of aromatic and N-containing compounds to bacteria by breaking down higher molecular weight aromatics into lower molecular weight aromatic compounds and by liberating amino acids from protein residues, respectively. DOM photodegradation also decreased the lability of these compounds by altering them to less labile forms and by mineralizing them to CO_2. I found that sunlight had a net positive effect on bacterial respiration of the bulk DOM pool until longer exposure times when the greatest extent of decreased lability for DOM compounds was observed. These results indicate that the balance of labile and recalcitrant DOM compounds photo-produced can explain contrasting effects of sunlight on bacterial respiration of DOM to CO_2. By quantifying the rates at which that sunlight alters bacterial degradation of DOM compounds quickly versus more slowly in the stream, I found that photodegradation rates were fast enough to impact bacterial degradation of compounds degraded more slowly, like high molecular weight aromatics.[117] In

contrast, DOM photodegradation rates in the stream were too slow to impact bacterial degradation of the most labile compounds, such as N-containing compounds.[94] These findings indicate that sunlight impacts bacterial degradation of DOM compounds that make up a large portion of the DOM respired on a mass basis.[76] Given that only minutes to hours of sunlight exposure in the stream were needed to increase or decrease the respiration of these compounds by ~50%, findings from this work suggest that DOM photodegradation can substantially impact the amount of CO_2 produced from DOM, even in periodically shaded freshwaters.

1.5 References

1. Cole, J. J., Y. T. Prairie, N. F. Caraco, W. H. McDowell, L. J. Tranvik, R. G. Striegl, et al. (2007). Plumbing the global carbon cycle: Integrating inland waters into the terrestrial carbon budget. *Ecosystems* 10(1): 171-184.

2. Battin, T. J., L. A. Kaplan, S. Findlay, C. S. Hopkinson, E. Marti, A. I. Packman, et al. (2008). Biophysical controls on organic carbon fluxes in fluvial networks. *Nat. Geosci.* 1: 95-100.

3. Aufdenkampe, K., E. Mayorga, P. A. Raymond, J. M. Melack, S. C. Doney, S. R. Alin, et al. (2011). Riverine coupling of biogeochemical cycles between land, oceans, and atmosphere. *Front. Ecol. Environ.* 9(1): 53-60.

4. Kling, G. W., G. W. Kipphut, and M. C. Miller (1991). Arctic lakes and streams as gas conduits to the atmosphere: Implications for tundra carbon budgets. *Science* 251: 298-301.

5. Tranvik, L. J., J. A. Downing, J. B. Cotner, S. A. Loiselle, R. G. Striegl, T. J. Ballatore, et al. (2009). Lakes and reservoirs as regulators of carbon cycling and climate. *Limnol. Oceanogr.* 54: 2298-2314.

6. Raymond, P. A, J. Hartmann, R. Lauerwald, S. Sobek, C. McDonald, M. Hoover, et al. (2013). Global carbon dioxide emissions from inland waters. *Nature* 503: 355-359.

7. Laudon, H., J. Hedtjärn, J. Schelker, K. Bishop, R. Sørensen, and A. Ågren (2009). Responses of dissolved organic carbon following forest harvesting in a boreal forest. *Ambio* 38: 381-386.

8. Singh, N. K., W. M. Reyes, E. S. Bernhardt, R. Bhattacharya, J. L. Meyer, J. D. Knoepp, and R. E. Emanuel (2016). Hydro-climatological influences on long-term dissolved organic carbon in a mountain stream of the southeastern United States. *J. Environ. Qual*. 45: 1286-1295.

9. Corman, J. R., B. L. Bertolet, N. J. Casson, D. Sebestyen, R. K. Kolka, and E. H. Stanley (2018). Nitrogen and phosphorous loads to temperate seepage lakes associated with allochthonous dissolved organic loads. *Geophys. Res. Lett.* 45: 5481-5491.

10. Plaza, C., E. Pegoraro, R. Bracho, G. Celis, K. G. Crummer, J. A. Hutchings, et al. (2019). Direct observation of permafrost degradation and rapid soil carbon loss in tundra. *Nat. Geosci.* 12: 627-631.

11. Granéli, W., M. Lindell, and L. Tranvik (1996). Photo-oxidative production of dissolved inorganic carbon in lakes of different humic content. *Limnol. Oceanogr.* 41: 698-706.

12. Lindell, M. J., H. W. Granéli, and S. Bertilsson (2000). Seasonal photoreactivity of dissolved organic matter from lakes with contrasting humic content. *Can. J. Fish. Aquat. Sci.* 57: 875-885.

13. Wetzel, R. G., P. G. Hatcher, and T. S. Bianchi (1995). Natural photolysis by ultraviolet irradiance of recalcitrant dissolved organic matter to simple substrates for rapid bacterial metabolism. *Limnol. Oceanogr*. 40: 1369-1380.

14. Jørgensen, N. O. G., L. Tranvik, H. Edling, W. Granéli, and M. Lindell (1998). Effects of sunlight on occurrence and bacterial turnover of specific carbon and nitrogen compounds in lake waters. *FEMS Microbol. Ecol*. 25: 217-227.

15. Helms, J. R., A. Stubbins, J. D. Ritchie, E. C. Minor, D. J. Kieber, and K. Mopper (2008). Absorption spectral slopes and slope ratios as indicators of molecular weight, source, and photobleaching of chromophoric dissolved organic matter. *Limnol. Oceanogr.* 53: 955-969.

16. Gonsoir, M., B. M. Peake, W. T. Cooper, D. Podgorski, J. D'Andrilli, and W. J. Cooper (2009). Photochemically induced changes in dissolved organic matter identified by ultrahigh resolution Fourier transform ion cyclotron resonance mass spectrometry. *Environ. Sci. Technol.* 43: 698-703.

17. Moran, M. A., W. M. Sheldon, and R. G. Zepp (2000). Carbon loss and optical property changes during long-term photochemical and biological degradation of estuarine dissolved organic matter. *Limnol. Oceanogr.* 45: 1254-1264.

18. Cory, R. M., K. McNeill, J. P. Cotner, A. Amado, J. M. Purcell, and A. G. Marshall (2010). Singlet oxygen in the coupled photochemical and biochemical oxidation of dissolved organic matter. *Environ. Sci. Technol*. 44: 3683-3689.

19. Ward, C. P., S. G. Nalven, B. C. Crump, G. W. Kling, and R. M. Cory (2017). Photochemical alteration of organic carbon draining permafrost soils shifts microbial metabolic pathways and stimulates respiration. *Nat. Commun*. 8, 772.

20. Amon, R. M. W., and R. Benner (1996). Photochemical and microbial consumption of dissolved organic carbon and dissolved oxygen in the Amazon River. *Geochim. Cosmochim. Acta* 60(10): 1783-1792.

21. Fasching, C., and T. J. Battin (2012). Exposure of dissolved organic matter to UV-radiation increases bacterial growth efficiency in a clear-water Alpine stream and its adjacent groundwater. *Aquat. Sci.* 74: 143-153.

22. Cory, R. M., B. C. Crump, J. A. Dobkowski, and G. W. Kling (2013). Surface exposure to sunlight stimulates CO_2 release from permafrost soil carbon in the Arctic. *Proc. Natl. Acad. Sci. USA* 110: 3429-3434.

23. Cory, R. M., C. P. Ward, B. C. Crump, and G. W. Kling (2014). Sunlight controls water column processing of carbon in arctic freshwaters. *Science* 345: 925-928.

24. Koehler, B., T. Landelius, G. A. Weyhenmeyer, N. Machida, and L. J. Tranvik (2014). Sunlight-induced carbon dioxide emissions from inland waters. *Global Biogeochem. Cycles* 28: 696-711.

25. Vachon, D., J.-F. Lapierre, and P. A. del Giorgio (2016). Seasonality of photochemical dissolved organic carbon mineralization and its relative contribution to pelagic CO_2 production in northern lakes. *J. Geophys. Res. Biogeosci*. 121: 864-878.

26. Ziegler, S., and R. Benner (2000). Effects of solar radiation on dissolved organic matter cycling in a subtropical seagrass meadow. *Limnol. Oceanogr*. 45(2): 257-266.

27. Jonsson, A., M. Meili, A.-K. Bergström, and M. Jansson (2001). Whole-lake mineralization of allochthonous and autochthonous organic carbon in a large humic lake (örträsket, N. Sweden). *Limnol. Oceanogr*. 46(7): 1691-1700.

28. Remington, S., A. Krusche, and J. Richey (2011). Effects of DOM photochemistry on bacterial metabolism and CO_2 evasion during falling water in a humic and a whitewater river in the Brazilian Amazon. *Biogeochem.* 105: 185-200.

29. Bushaw, K. L., R. G. Zepp, M. A. Tarr, D. Schulz-Jander, R. A. Bourbonniere, R. E. Hodson, et al. (1996). Photochemical release of biologically available nitrogen from aquatic dissolved organic matter. *Nature* 381: 404-407.

30. Smith, E. M., and R. Benner (2005). Photochemical transformation of riverine dissolved organic matter: effects on estuarine bacterial metabolism and nutrient demand. *Aquat. Microb. Ecol.* 40: 37-50.

31. Jeff, S., K. Hunter, D. Vandergucht, and J. Hudson (2012). Photochemical mineralization of dissolved organic nitrogen to ammonia in prairie lakes. *Hydrobiol.* 693: 71-80.

32. Porcal, P., J. Kopáček, and I. Tomkova (2014). Seasonal photochemical transformations of nitrogen species in a forest stream and lake. *PLoS ONE* 9(12), e116364.

33. Vincent, W. F., W. Wurtsbaugh, C. L. Vincent, and P. J. Richerson (1984). Seasonal dynamics of nutrient limitation in a tropical high-altitude lake (Lake Titicaca, Peru-Bolivia): Application of physiological bioassays. *Limnol. Oceanogr*. 29(3): 540-552.

34. Miller, M. C., G. R. Hater, P. Spatt, P. Westlake, and P. Yeakel (1986). Primary production and its controls in Toolik Lake, Alaska. *Arch. Hydrobiol*. 74: 97-134.

35. Elser, J. J., E. R. Marzolf, and C. R. Goldman (1990). Phosphorous and nitrogen limitation of phytoplankton growth in the freshwaters of North America: a review and critique of experimental enrichments. *Can. J. Fish. Aquat. Sci.* 47: 1468-1477.

36. Dodds, W. K., and V. H. Smith (2016). Nitrogen, phosphorous, and eutrophication in streams. *Inland Waters* 6: 155-164.

37. Anita, N. J., P. J. Harrison, and L. Oliveira (1991). The role of dissolved organic nitrogen in phytoplankton nutrition, cell biology and ecology. *Phycologia* 30(1): 1-89.

38. Buffam, I., and K. J. McGlathery (2003). Effect of ultraviolet light on dissolved nitrogen transformations in coastal lagoon water. *Limnol. Oceanogr*. 48(2): 723-734.

39. Vähätalo, A. V., K. Salonen, U. Münster, M. Järvinen, and R. G. Wetzel (2003). Photochemical transformation of allochthonous organic matter provides bioavailable nutrients in a humic lake. *Arch. Hydrobiol*. 156(3): 287-314.

40. Thurman, E. M. (Ed.) (1985). *Organic Geochemistry of Natural Waters*. Dordrecht, The Netherlands: Marinus Nijhoff/Dr W. Junk Publishers.

41. Kaplan, L. A., and R. M. Cory (2016). Dissolved organic matter in stream ecosystems: Forms, functions, and fluxes of watershed tea. In J. B. Jones and E. H. Stanley (Eds.), *Stream Ecosystems in a Changing Environment* (pg. 241-320). Oxford, UK: Elsevier.

42. Kim, S., R. W. Kramer, and P. G. Hatcher (2003). Graphical method for analysis of ultrahigh-resolution broadband mass spectra of natural organic matter, the van Krevelen diagram. *Anal. Chem*. 75: 5336-5344.

43. Koch, B. P., M. Witt, R. Engbrodt, T. Dittmar, and G. Kattner (2005). Molecular formulae of marine and terrigenous dissolved organic matter detected by electrospray ionization Fourier transform ion cyclotron resonance mass spectrometry. *Geochem. Cosmochim. Acta* 69(13): 3299-3308.

44. Minor, E. C., C. J. Steinbring, K. Longnecker, and E. B. Kujawinski (2012). Characterization of dissolved organic matter in Lake Superior and its watershed using ultrahigh resolution mass spectrometry. *Org. Geochem*. 43: 1-11.

45. Kaiser, E., A. J. Simpson, K. J. Dria, B. Sulzberger, and P. G. Hatcher (2003). Solid-state and multidimensional solution-state NMR of solid phase extracted and ultrafiltered riverine dissolved organic matter. *Environ. Sci. Technol.* 37: 2929-2935.

46. Lam, B., A. Baer, M. Alaee, B. Lefebvre, A. Moser, A. Williams, and A. J. Simpson (2007). Major structural components in freshwater dissolved organic matter. *Environ. Sci. Technol*. 41: 8240-8247.

47. Mao, J.-D., L. Tremblay, J.-P. Gagné, S. Kohl, and K. Schmidt-Rohr (2007). Humic acids from particulate organic matter in the Saguenay Fjord and the St. Lawrence Estuary investigated by advanced solid-state NMR. *Geochim. Cosmochim. Acta* 71(22): 5483-5499.

48. McKnight, D. M., E. W. Boyer, P. K. Westerhoff, P. T. Doran, T. Kulbe, and D. T. Andersen (2001). Spectrofluorometric characterization of dissolved organic matter for indication of precursor organic material and aromaticity. *Limnol. Oceanogr.* 46(1): 38-48.

49. Weishaar, J. L., G. R. Aiken, B. A. Bergamaschi, M. S. Fram, R. Fujii, and K. Mopper (2003). Evaluation of specific ultraviolet absorbance as an indicator of the chemical composition and reactivity of dissolved organic carbon. *Environ. Sci. Technol*. 37: 4702-4708.

50. Cory, R. M., and D. M. McKnight (2005). Fluorescence spectroscopy reveals ubiquitous presence of oxidized and reduced quinones in dissolved organic matter. *Environ. Sci. Technol.* 39: 8142-8149.

51. Mann, P. J., A. Davydova, N. Zimov, R. G. M. Spencer, S. Davydov, E. Bulygina, et al. (2012). Controls on the composition and lability of dissolved organic matter in Siberia's Kolyma River basin. *J. Geophys. Res.* 117, G01028.

52. Miller, W. L., and R. G. Zepp (1995). Photochemical production of dissolved inorganic carbon from terrestrial organic matter: Significance to the oceanic organic carbon cycle. *Geophys. Res. Lett.* 22: 417-420.

53. Granèli, W., M. Lindell, B. M. de Faria, and F. de Assis Esteves (1998). Photoproduction of dissolved organic carbon in temperate and tropical lakes – Dependence on wavelength band and dissolved organic carbon concentration. *Biogeochem.* 43: 175-195.

54. Osburn, C. L., L. Retamal, and W. F. Vincent (2009). Photoreactivity of chromophoric dissolved organic matter transported by the Mackenzie River to the Beaufort Sea. *Mar. Chem.* 115: 10-20.

55. Kieber, R. J., X. Zhou, and K. Mopper (1990). Formation of carbonyl compounds from UV-induced photodegradation of humic substances in natural waters: Fate of riverine carbon in the sea. *Limnol. Oceanogr*. 35(7): 1503-1515.

56. Bertilsson, S., and L. J. Tranvik (2000). Photochemical transformation of dissolved organic matter in lakes. *Limnol. Oceanogr*. 45(4): 753-762.

57. Leifer, A. (Ed.). (1988). *The Kinetics of Environmental Aquatic Photochemistry.* Salem, MA: American Chemical Society.

58. Gao, H., and R. G. Zepp (1998). Factors influencing photoreactions of dissolved organic matter in a coastal river of the southeastern United States. *Environ. Sci. Technol.* 32: 2940-2946.

59. Andrews, S. S., S. Caron, and O. C. Zafiriou (2000). Photochemical oxygen consumption in marine waters: A major sink for colored dissolved organic matter? *Limnol. Oceanogr*. 45: 267-277.

60. Cory, R. M., and G. W. Kling (2018). Interactions between sunlight and microorganisms influence dissolved organic matter degradation along the aquatic continuum. *Limnol. Oceanogr.: Lett.* 3: 102-116.

61. Stedmon, C. A., S. Markager, L. Tranvik, L. Kronberg, T. Slätis, and W. Martinsen (2007). Photochemical production of ammonium and transformation of dissolved organic matter in the Baltic Sea. *Mar. Chem*. 104: 227-240.

62. Powers, L. C., and W. L. Miller (2015). Photochemical production of CO and CO_2 in the Northern Gulf of Mexico: Estimates and challenges for quantifying the impact of photochemistry on carbon cycles. *Mar. Chem*. 171: 21-35.

63. de Bruyn, W. J., C. D. Clark, L. Pagel, and C. Takehara (2011). Photochemical production of formaldehyde, acetaldehyde, and acetone from chromophoric dissolved organic matter in coastal waters. *J. Photochem. Photobiol*. 226: 16-22.

64. Reader, H. E., and W. L. Miller (2014). The efficiency and spectral photon dose dependence of photochemically induced changes to the bioavailability of dissolved organic carbon. *Limnol. Oceanogr*. 59: 182-194.

65. Goldstone, J. V., M. J. Pullin, S. Bertilsson, and B. M. Voelker (2002). Reactions of hydroxyl radical with humic substances: Bleaching, mineralization, and production of bioavailable carbon substrates. *Environ. Sci. Technol*. 36: 364-372.

66. White, E. M., P. P. Vaughan, and R. G. Zepp (2003). Role of the photo-Fenton reaction in the production of hydroxyl radicals and photobleaching of colored dissolved organic matter in a coastal river of the southeastern United States. *Aquat. Sci*. 65: 402-414.

67. Page, S. E., J. R. Logan, R. M. Cory, and K. McNeill (2014). Evidence for dissolved organic matter as the primary source and sink of photochemically produced hydroxyl radical in arctic surface waters. *Environ. Sci.: Processes Impacts* 16: 807-822.

68. Miles, C., and P. Brezonik (1981). Oxygen consumption in humic-colored waters by a photochemical ferrous-ferric catalytic cycle. *Environ. Sci. Technol.* 15(9): 1089-1095.

69. Xie, H., O. C. Zafiriou, W.-J. Cai, R. G. Zepp, and Y. Wang (2004). Photooxidation and its effects on the carboxyl content of dissolved organic matter in two coastal rivers in the southeastern United States. *Environ. Sci. Technol*. 38(15): 4113-4119.

70. Ward, C. P., and R. M. Cory (2016). Complete and partial photo-oxidation of dissolved organic matter draining permafrost soils. *Environ. Sci. Technol*. 50: 3545-3553.

71. Aeschbacher, M., C. Graf, R. P. Schwarzenbach, and M. Sander (2012). Antioxidant properties of humic substances. *Environ. Sci. Technol*. 46: 4916-4925.

72. Wang, W., M. A. Tarr, T. S. Bianchi, and E. Engelhaupt (2000). Ammonium photoproduction from aquatic humic and colloidal matter. *Aquat. Geochem*. 6: 275-292.

73. Tarr, M. A., W. Wang, T. S. Bianchi, and E. A. Engelhaupt (2001). Mechanisms of ammonia and amino acid photoproduction from aquatic humic and colloidal matter. *Water Res*. 35(15): 3688-3696.

74. Bertilsson, S., and L. J. Tranvik (1998). Photochemically produced carboxylic acids as substrates for freshwater bacterioplankton. *Limnol. Oceanogr*. 43: 885-895.

75. Pullin, M. J., S. Bertilsson, J. V. Goldstone, and B. M. Voelker (2004). Effects of sunlight and hydroxyl radical on dissolved organic matter: Bacterial growth efficiency and production of carboxylic acids and other substrates. *Limnol. Oceanogr*. 49: 2011-2022.

76. Volk, C. J., C. B. Volk, and L. A. Kaplan (1997). Chemical composition of biodegradable dissolved organic matter in streamwater. *Limnol. Oceanogr*. 42: 39-44.

77. Waggoner, D. C., H. Chen, A. S. Willoughby, and P. G. Hatcher (2015). Formation of black carbon-like and alicyclic aliphatic compounds by hydroxyl radical initiated degradation of lignin. *Org. Geochem.* 82: 69-76.

78. Waggoner, D. C., A. S. Wozniak, R. M. Cory, and P. G. Hatcher (2017). The role of reactive oxygen species in the degradation of lignin derived dissolved organic matter. *Geochim. Cosmochim. Acta* 208: 171-184.

79. Ward, C. P., and R. M. Cory (2020). Assessing the prevalence, products, and pathways of dissolved organic matter partial photo-oxidation in arctic surface waters. *Environ. Sci.: Processes Impacts* 22: 1214-1223.

80. McNeill, K., and S. Canonica (2016). Triplet state dissolved organic matter in aquatic photochemistry: Reaction mechanisms, substrate scope, and photophysical properties. *Environ. Sci.: Processes Impacts* 18: 1381-1399.

81. Ossola, R., O. M. Jönsson, K. Moor, and K. McNeill (2021). Singlet oxygen quantum yields in environmental waters. *Chem. Rev*. 121: 4100-4146.

82. Tranvik, L. J., and S. Bertilsson (2001). Contrasting effects of solar UV radiation on dissolved organic sources for bacterial growth. *Ecol. Lett.* 4: 458-463.

83. Amado, A. M., J. B. Cotner, A. L. Suhett, F. D. Assis Esteves, R. L. Bozelli, and V. F. Farjalla (2007). Contrasting interactions mediate dissolved organic matter decomposition in tropical aquatic ecosystems. *Aquat. Microb. Ecol.* 49: 25-34.

84. Judd, K. E., B. C. Crump, and G. W. Kling (2007). Bacterial responses in activity and community composition to photo-oxidation of dissolved organic matter from soil and surface waters. *Aquat. Sci*. 69: 96-107.

85. Nalven, S. G., C. P. Ward, J. P. Payet, R. M. Cory, G. W. Kling, T. J. Sharpton, et al. (2020). Experimental metatranscriptomics reveals the costs and benefits of dissolved organic matter photo-alteration for freshwater microbes. *Environ. Microbiol*. 22(8): 3505-3521.

86. Amado, A. M., J. B. Cotner, R. M. Cory, B. L. Edhlund, and K. McNeill (2015). Disentangling the interactions between photochemical and bacterial degradation of dissolved organic matter: Amino acids play a central role. *Microb. Ecol.* 69: 554-566.

87. Fasching, C., B. Bahounek, G. A. Singer, and T. J. Battin (2014). Microbial degradation of terrigenous dissolved organic matter and potential consequences for carbon cycling in brown-water streams. *Sci. Reports* 4, 4981.

88. Mann, P. J., W. V. Sobczak, M. M. Larue, E. Bulygina, A. Davydova, J. E. Vonk, et al. (2014). Evidence for key enzymatic controls on metabolism of Arctic river organic matter. *Global Change Biol*. 20: 1089-1100.

89. Münster, U., P. Einiö, J. Nurminen, and J. Overbeck (1992). Extracellular enzymes in a polyhumic lake: important regulators in detritus processing. *Hydrobiol.* 229: 225-238.

90. Tranvik, L. J., and N. O. G. Jørgensen (1995). Colloidal and dissolved organic matter in lake water: Carbohydrate and amino acid composition, and ability to support bacterial growth. *Biogeochem*. 30: 77-97.

91. Siuda, W., and R. J. Chróst (2002). Decomposition and utilization of particulate organic matter by bacteria in lakes of different trophic status. *Polish J. Environ. Stud.* 11(1): 53–65.

92. Fellman, J. B., E. Hood, D. V. D. Amore, R. T. Edwards, and D. White (2009). Seasonal changes in the chemical quality and biodegradability of dissolved organic matter exported from soils to streams in coastal temperate rainforest watersheds. *Biogeochem.* 95: 277-293.

93. Balcarczyk, K., J. B. Jones Jr., R. Jaffé, and N. Maie (2009). Stream dissolved organic matter bioavailability and composition in watersheds underlain with discontinuous permafrost. *Biogeochem*. 94: 255-270.

94. Cory, R. M., and L. A. Kaplan (2012). Biological lability of streamwater fluorescent dissolved organic matter. *Limnol. Oceanogr*. 57: 1347-1360.

95. Cory, R. M., K. H. Harrold, B. T. Neilson, and G. W. Kling (2015). Controls on dissolved organic matter (DOM) degradation in a headwater stream: the influence of photochemical and hydrological conditions in determining light-limitation or substrate-limitation of photo-degradation. *Biogeosci.* 12: 6669-6685.

96. Minshall, G. W., R. C. Petersen, K. W. Cummins, T. L. Bott, J. R. Sedell, C. E. Cushing, and R. L. Vannote (1983). Interbiome comparison of stream ecosystem dynamics. *Ecol. Monogr.* 53(1): 1-25.

97. Vähätalo, A. V., M. Salkinoja-Salonen, P. Taalas, and K. Salonen (2000). Spectrum of the quantum yield for photochemical mineralization of dissolved organic carbon in a humic lake. *Limnol. Oceanogr.* 45: 664-676.

98. Ward, C. P., J. C. Bowen, D. H. Freeman, and C. M. Sharpless (2021). Rapid and reproducible characterization of the wavelength dependence of aquatic photochemical reactions using light emitting diodes (LEDs). *Environ. Sci. Technol. Lett.* 8(5): 437-442.

99. Xie, H., S. Bélanger, G. Song, R. Benner, A. Taalba, M. Blais, et al. (2012). Photoproduction of ammonium in the southeastern Beaufort Sea and its biogeochemical implications. *Biogeosci.* 9: 3047-3061.

100. Bélanger, S., H. Xie, N. Krotkov, P. Larouche, W. J. Vincent, and M. Babin (2006). Photomineralization of terrigenous dissolved organic matter in Arctic coastal waters from 1979 to 2003: Interannual variability and implications of climate change. *Global Biogeochem. Cycles* 20, GB4005.

101. Zhang, Y., and H. Xie (2015). Photomineralization and photomethanification of dissolved organic matter in Saguenay River surface water. *Biogeosci.* 12: 6823-6836.

102. Koehler, B., E. Broman, and L. J. Tranvik (2016). Apparent quantum yield of photochemical dissolved organic carbon mineralization in lakes. *Limnol. Oceanogr*. 61: 2207-2221.

103. Kling, G. W., G. W. Kipphut, M. M. Miller, and W. J. O'Brien (2000). Integration of lakes and streams in a landscape perspective: The importance of material processing on spatial patterns and temporal coherence. *Freshw. Biol.* 43: 477-497.

104. Cory, R. M., D. M. McKnight, Y.-P. Chin, P. Miller, and C. L. Jaros (2007). Chemical characteristics of fulvic acids from Arctic surface waters: Microbial contributions and photochemical transformations. *J. Geophys. Res.* 112, G04S51.

105. Hobbie, J. E., and G. W. Kling (Eds.). (2014). *Alaska's Changing Arctic: Ecological Consequences for Tundra, Streams, and Lakes.* Oxford, UK: Oxford University Press.

106. Kalff, J. (1971). Nutrient limiting factors in an arctic tundra pond. *Ecology* 52(4): 655-659.

107. Levine, M. A., and S. C. Whalen (2001). Nutrient limitation of phytoplankton in Alaskan Arctic foothill lakes. *Hydrobiol*. 455: 189-201.

108. Whalen, S. C., and J. C. Cornwell (1985). Nitrogen, phosphorus, and organic carbon cycling in an arctic lake. *Can. J. Fish. Aquat. Sci.* 42: 797-808.

109. Spencer, R. G. M., P. J. Mann, T. Dittmar, E. I. Eglinton, C. McIntyre, R. M. Holmes, et al. (2015). Detecting the signature of permafrost thaw in Arctic rivers. *Geophys. Res. Lett.* 42: 2830-2835.

110. Ward, C. P., and R. M. Cory (2015). Chemical composition of dissolved organic matter draining permafrost soils. *Geochim. Cosmochim. Acta* 167: 63-79.

111. Fujii, M., A. Imaoka, C. Yoshimura, and T. D. Waite (2014). Effects of molecular composition of natural organic matter on ferric iron complexation at circumneutral pH. *Environ. Sci. Technol.* 48: 4414-4424.

112. Xiao, Y.-H., T. Sara-Aho, H. Hartikainen, and A. V. Vähätalo (2013). Contribution of ferric iron to light absorption by chromophoric dissolved organic matter. *Limnol. Oceanogr*. 58: 653-662.

113. Marchisio, A., M. Minella, V. Maurino, C. Minero, and D. Vione (2015). Photogeneration of reactive transient species upon irradiation of natural water samples: Formation quantum yields in different spectral intervals, and implications for the photochemistry of surface waters. *Water Res*. 73: 145-156.

114. Vallino, J. J., C. S. Hopkinson, and J. E. Hobbie (1996). Modeling bacterial utilization of dissolved organic matter: Optimization replaces Monod growth kinetics. *Limnol. Oceanogr.* 41(6): 1591-1609.

115. Kaplan, L. A., and J. D. Newbold (1995). Measurements of streamwater biodegradable dissolved organic carbon with a plug-flow bioreactor. *Water Res.* 29: 2696-2706.

116. Kaplan, L. A., T. N. Wiegner, J. D. Newbold, P. H. Ostrom, and H. Gandhi (2008). Untangling the complex issue of dissolved organic carbon uptake: A stable isotope approach. *Freshw. Biol.* 53: 855-864.

117. Sleighter, R. L., R. M. Cory, L. A. Kaplan, H. A. N. Abdulla, and P. G. Hatcher (2014). A coupled geochemical and biogeochemical approach to characterize the bioreactivity of dissolved organic matter from a headwater stream. *J. Geophys. Res. Biogeosci.* 119: 1520-1537.

Chapter 2

Photochemical Production of NH_4^+ from Dissolved Organic Nitrogen in Arctic Lakes

2.1 Abstract

The photochemical production of ammonium (NH_4^+) from dissolved organic nitrogen (DON) in surface waters is well established, but the extent that photo-produced NH_4^+ provides an important source of inorganic nitrogen (N) to primary producers and creates a strong linkage between the DON exported from soils and surface water nutrient cycling is poorly understood. Here, the photochemical production of NH_4^+ from DON was investigated in arctic surface waters by (1) quantifying apparent quantum yields of NH_4^+ photo-production, (2) identifying the class of DON compounds that is photodegraded to produce NH_4^+, and (3) evaluating whether photodegradation is substrate limited due to its competition with bacterial demand for DON. Waters from ten stream and lake sites across the Alaskan Arctic were exposed to sunlight to quantify the susceptibility of DON to photodegradation and test the chemical controls on NH_4^+ photo-production. Results from this work show that photochemically produced NH_4^+ comes from the degradation of dissolved protein-like compounds. NH_4^+ photo-production depended on the availability of protein-like N, which is also degraded by bacteria to incorporate N into their biomass. In the upper 5 m of an arctic lake, Toolik Lake, NH_4^+ photo-production rates were on average 16% of bacterial N incorporation rates (range 2-87%) and supplied on average 5% of the inorganic N demand by primary producers (range 1-12%) during the ice-free summer. These findings suggest that NH_4^+ photo-production is generally substrate limited due to its competition with bacterial demand for DON, and can support a small portion of the N taken up by primary

producers in arctic lakes. Together, results from this study demonstrate that the DON exported from soils can impact N cycling in arctic lakes by supplying inorganic N to primary producers when the photo-production of NH_4^+ is not limited by available protein-like N to undergo photodegradation.

2.2 Introduction

In the Arctic, the majority of dissolved nitrogen (N) draining from soils to surface waters is in the organic form (> 90%)[1-2] and largely unavailable for uptake by the primary producers in surface waters.[3] As such, the N demand of primary producers in arctic lakes is thought to be supported by fluxes of dissolved inorganic N (DIN) from soils, sediments, and precipitation.[2,4-6] DIN produced during the degradation of terrestrially-derived organic N in arctic surface waters could represent a source of the N taken up by primary producers in arctic lakes,[4,7] increasing the linkage between the N exported from soils and N cycling in lakes.[3] However, the fluxes of DIN produced from terrestrially-derived organic N degradation are unaccounted for in current N budgets.[2]

In sunlit surface waters, light-absorbing chromophoric dissolved organic matter (DOM) initiates photochemical reactions that degrade organic N to ammonium (NH_4^+).[8-11] Because surface water ecosystems are often limited by available inorganic N,[12-14] the photo-production of NH_4^+ has been evaluated as a potential source of N supporting primary producers.[15-17] These prior studies have estimated that the photo-production of NH_4^+ can account for at most 4% of the N taken up by primary producers in surface waters.[15-17] However, photo-produced NH_4^+ could supply a larger portion of the N taken up by primary producers in oligotrophic lakes, like those in the Arctic, where productivity and N demands by primary producers are low, resulting in slower rates of N uptake by primary producers[4,7] compared to other surface waters.[15-17]

The photo-production of NH_4^+ from DOM may also represent an important pathway linking DOM export from soils to N cycling in arctic surface waters. For example, previously reported rates of NH_4^+ photo-production across surface waters[15-18] are comparable to the rates that DIN is exported from arctic soils to streams[2] and arctic streams to lakes,[4] suggesting that the photodegradation of DOM may provide an equally important source of DIN to arctic lakes as other fluxes. In contrast, the photo-production of NH_4^+ from DOM was estimated to supply a negligible portion of the total DIN flux to a coastal lagoon because NH_4^+ photo-production rates were orders of magnitude lower than other fluxes of DIN.[11] Thus, direct comparisons of NH_4^+ photo-production rates to other DIN fluxes and rates of N uptake by primary producers in arctic lakes are needed to determine whether the photodegradation of DOM provides an important source of DIN to these waters.

Water column rates of NH_4^+ photo-production depend on the amount of sunlight reaching the water surface, the amount of light-absorbing chromophoric DOM available to absorb that light in the water column, and the efficiency that NH_4^+ is photo-produced from DOM (i.e., measured as the apparent quantum yield).[15-17] However, NH_4^+ photo-production rates may be limited by the abundance of N-containing compounds susceptible to produce that NH_4^+ (i.e., a substrate limited process).[19] Previous work has shown that no additional NH_4^+ is photo-produced from DOM following longer sunlight exposure times,[8,20] suggesting that the N-containing compounds supplying NH_4^+ become depleted from the DOM pool. It follows that rates of NH_4^+ photo-production in arctic lakes may become substrate limited if the N-containing DOM compounds undergoing photodegradation to produce NH_4^+ are removed more quickly than they are replenished in the water column.[19] Yet, NH_4^+ photo-production rates estimated from laboratory experiments have been applied to surface waters without knowledge of whether there

is enough N-containing compounds to sustain these rates[15-18] because the class(es) of DOM compounds undergoing photodegradation to produce NH_4^+ is poorly known.

The NH_4^+ photo-produced in surface waters likely comes from protein-like compounds within the DOM pool. For instance, NH_4^+ is expected to come from the photochemical removal of primary amine groups from proteins, peptides, and amino acids within DOM (collectively known as protein-like compounds).[21] Consistent with this idea, prior work has shown that NH_4^+ is produced during the photodegradation of free amino acids in the presence of DOM.[22] Given that protein-like compounds can make up 35 to 50% of the N within terrestrially-derived DOM[23-24] and 10 to 30 µM of dissolved organic N is present in arctic surface waters,[1-2] there may be plenty of protein-like N within DOM to support NH_4^+ photo-production over the sunlight exposure times in these waters.

However, the bacterial degradation of protein-like compounds may be a greater cause of substrate limitation for NH_4^+ photo-production rates in arctic lakes if proteins are the class of DOM compounds undergoing photodegradation. It is expected that bacteria primarily obtain N for biomass production from protein-like compounds within DOM in oligotrophic surface waters like those in the Arctic.[25-26] Because free amino acids make up < 5% of the dissolved organic N pool,[25,27-28] bacteria release extracellular enzymes into the water column to break down larger protein-like compounds into free amino acids and small peptides that can be taken up into their cells.[25,27,29] Prior work hypothesized that rates of this degradation by bacteria exceed rates of photodegradation for dissolved organic N in arctic surface waters.[30] This hypothesis is consistent with the higher rates of N incorporation into bacterial biomass previously reported in other surface waters[31] compared to rates of NH_4^+ photo-production from DOM.[15-18] When rates of photodegradation of protein-like compounds are slow compared to degradation rates by

bacteria in the water column, the photo-production of NH_4^+ may become substrate limited. A direct comparison of rates of photodegradation to bacterial degradation is needed to determine whether NH_4^+ photo-production in arctic lakes is substrate limited due to the competition between sunlight and bacteria for protein-like compounds.

Thus, the goals of this study were to: (1) identify the DOM compound class that undergoes photodegradation to produce NH_4^+, (2) compare rates of photodegradation to rates of bacterial degradation of dissolved organic N, and (3) estimate the extent that photochemically produced NH_4^+ can support N demands by primary producers. Results from this study show that photochemically produced NH_4^+ comes from the degradation of protein-like compounds within DOM. Rates of photodegradation were on average 16% of rates of N incorporation into bacterial biomass during the ice-free summer in an arctic lake, Toolik Lake, suggesting that NH_4^+ photo-production rates are substrate limited. The NH_4^+ produced during the photodegradation of protein-like N contributed ~5% of the N taken up by primary producers in arctic lakes. Together, findings from this study demonstrate that the photodegradation of DOM exported from soils creates a strong linkage between the soil and surface water N cycles when the photo-production of NH_4^+ is not limited by available protein-like N to undergo photodegradation.

2.3 Methods

2.3.1 Photochemical DON degradation and NH_4^+ production

Apparent quantum yields of ammonium (NH_4^+) photo-production ($\varphi_{NH4+,\lambda}$) were quantified for arctic surface waters to test chemical controls on the production of NH_4^+ from dissolved organic nitrogen (DON) and quantify daily rates of NH_4^+ photo-produced. Sunlight exposure experiments were conducted using water from arctic lakes, streams, and rivers varying in DON quantity and composition (Section 2.3.1.1; Table 2.1).[2,32] Each surface water sample

was exposed to natural sunlight for ~12 hours, and then some waters had up to two more exposures (Table 2.2, Figure 2.1) to detect a change NH_4^+ concentration relative to dark controls and evaluate whether NH_4^+ photo-production continued after longer exposure times (Section 2.3.1.3). NH_4^+ concentrations and proxies for classes of compounds within the dissolved organic matter (DOM) pool, such as protein-like or aromatic compounds, were measured in the light-exposed and dark-control waters (Section 2.3.1.4; Figure 2.1). When there was a detectable increase in NH_4^+ during sunlight exposure, the concentration of NH_4^+ photo-produced was used to calculate a $\varphi_{NH4+,\lambda}$ (Section 2.3.1.6). The initial composition of DOM and extent of photodegradation for different compound classes were used to test controls on the magnitude of the $\varphi_{NH4+,\lambda}$ and thus, identify the compound class(es) undergoing photodegradation to produce NH_4^+. Daily water column rates of NH_4^+ photo-production in each surface water were then calculated using the measured $\varphi_{NH4+,\lambda}$, the concentration of light-absorbing, chromophoric (aromatic) DOM (CDOM), and the photon flux reaching the water surface throughout the ice-free summer (Section 2.3.1.7).

2.3.1.1 Site description and sampling

Surface water samples were collected near the Toolik Field Station at Toolik Lake, Alaska, USA (68° 38' N, 149° 36' W) from May to July 2018. Toolik Lake is the site of the NSF Arctic LTER, where long-term studies of bacterial production, primary production, and nitrogen cycling have been conducted.[2] Samples were collected from ten surface waters varying in water chemistry and DON quantity and composition:[1,32] Imnavait Creek, Kuparuk River, Sagavanirktok River, Toolik Inlet Stream, Tussock Watershed Lower Stream, Toolik Lake, and four lakes on the Alaskan Coastal Plain (Table 2.1). All water samples were collected at the surface (0.1 m depth), except in Toolik Lake where water was collected at 3 and 16 m below the

water surface. Samples were collected in acid-washed, 2-L amber high-density polyethylene (HDPE) bottles rinsed with deionized water (DI; Barnstead E-Pure and B-Pure system; i.e., hereafter referred to as "clean"). pH and specific conductivity were measured just prior to sample collection in the field (WTW 3210 meters; Figure 2.1). Between one and five water samples were collected from each site during the summer of 2018, resulting in a total of 19 water samples analyzed for this study (Table 2.1).

After collection water samples were immediately brought to the lab at the Toolik Field Station and filtered in a two-step process using pre-combusted (450 °C, 4 hour) GF/F filters followed by sterile, 0.2 μm filters (Sterivex, Millipore) pre-rinsed with DI water into a clean 2-L amber HDPE bottle. Filtered waters were stored at 4 °C in the dark for ≤ 2 months before characterizing the chemical composition of DOM (all analyses except mass spectrometry) and performing the sunlight exposure experiments. An aliquot of each filtered water sample (< 500 mL) was overnight shipped in a clean amber HDPE bottle to the University of Michigan for solid-phase extraction and analysis by mass spectrometry.

2.3.1.2 Characterizing surface water DOM

The chemical composition of DOM in each filtered water sample was characterized using absorbance and fluorescence spectroscopy, and high-resolution mass spectrometry (Figure 2.1). CDOM was measured in triplicate for each water sample using a UV-Vis spectrophotometer (Aqualog, Horiba; 1-cm pathlength) against DI water blanks as previously described.[32] Naperian absorption coefficients of CDOM ($a_{CDOM,\lambda}$; m^{-1}) were calculated by multiplying the absorbance (A) at each wavelength (λ) by 2.303 and dividing by the pathlength (m) (coefficient of variance, CV < 1% on triplicate analyses). The spectral slope ratio (S_R), a proxy for the molecular weight of DOM, was calculated from the $a_{CDOM,\lambda}$ spectrum (CV < 1% on triplicate analyses).[33]

Fluorescent DOM (FDOM) was measured in triplicate using a fluorometer (Aqualog, Horiba) as previously described.[32] Briefly, excitation-emission matrices (EEMs) were collected across excitation wavelengths from 240 to 450 nm (5-nm increments) and emission wavelengths from 320 to 550 nm (2-nm increments) using an integration time of 2, 3, or 4 s. The fluorescence index (FI), a proxy for the aromatic content of DOM,[34] was calculated as the fluorescence intensity at emission wavelength 470 nm divided by the intensity at emission wavelength 520 nm, both at an excitation wavelength of 370 nm (CV < 1% on triplicate analyses).

DOM in each filtered water sample was isolated by solid-phase extraction and then analyzed by high-resolution mass spectrometry as previously described (Figure 2.1).[35] Briefly, DOM was extracted on a PPL solid-phase cartridge (100 mg resin, 1 mL volume; Bond Elut PPL, Agilent) and then eluted by gravity with LC-MS grade MeOH following Dittmar et al. (2008).[36] For every ~ 5 water samples extracted, one PPL cartridge blank was collected by loading LC-MS grade H_2O as the water sample. Previous studies have reported a ~60% extraction efficiency of arctic soil waters onto PPL solid-phase cartridges.[35,37]

Solutions of solid-phase-extracted DOM in MeOH (< 50 mg-C L^{-1}) were injected into the electrospray ionization source (negative mode) of a 12T Bruker SolariX FT-ICR mass spectrometer (located at the Environmental Molecular Sciences Laboratory, Pacific Northwest National Laboratory). Each solid-phase-extracted DOM sample was analyzed alongside a PPL cartridge blank and a MeOH blank to test for contamination during sample preparation and analysis, respectively. Mass spectra were calibrated and molecular formulas were assigned as previously described.[35] Formulas present in the blank spectra were removed from the list of formulas assigned for each solid-phase-extracted DOM sample. Replicate mass spectra were

collected for seven of the solid-phase-extracted DOM samples to assess the reproducibility of acquisitions. On average, 71% of the formulas assigned were common among the replicate spectra (n = 7; Table 2.A.1). Peak magnitudes were also reproducible with average percent relative standard deviations (RSD) for replicate acquisitions of < 13% (n = 7). On average, 66% of the peaks had magnitude ratios within 10% RSD (n = 7).[38]

Protein-like formulas were defined as those with H/C = 1.5 – 2.3, O/C = 0.3 – 0.55, and N ≥ 1.[39-40] The percent of protein-like formulas was calculated as the number of protein-like formulas divided by the total number of molecular formulas assigned multiplied by 100 (CV < 8% on replicate acquisitions, n = 2 or 3; Table 2.A.1). These percentages of protein-like formulas were positively correlated with those calculated from the relative peak magnitude (p < 0.05 when data were fit using a least-squares regression).

2.3.1.3 Sunlight exposure of DOM

Each filtered water sample was exposed to sunlight for 12 hours, except three water samples which were exposed for 10 or 15 hours (Kuparuk River, 18 June; Toolik Inlet Stream, 15 May and 13 July; Table 2.2). Half of the water samples were then exposed up to two more times (Table 2.2, Figure 2.1) to determine the shortest exposure time needed to detect a change in NH_4^+ concentration relative to dark controls and evaluate whether NH_4^+ photo-production continued after longer exposures (see Appendix Section 2.8.1). For each sunlight exposure experiment, filtered waters were brought to room temperature (within 24 hours) and then transferred to six pre-combusted (450 °C, 4 hour) 100-mL quartz tubes with GL-14 caps containing rubber butyl septa. Triplicate quartz tubes were exposed to natural sunlight at the Toolik Field Station on an unshaded black surface alongside triplicate dark-control quartz tubes

wrapped in aluminum foil and kept in a dark storage bin. Sunlight exposure experiments took place on days with average air temperatures ranging from 4 to 14 °C.

Following sunlight exposure, waters from each quartz tube were transferred to three clean 30-mL amber HDPE bottles for analysis of NH_4^+, CDOM and FDOM, and total dissolved nitrogen (TDN) and dissolved organic carbon (DOC), respectively (Figure 2.1). Both the light-exposed and dark-control samples were analyzed for NH_4^+ within 6 hours. Light-exposed and dark-control samples for CDOM and FDOM analyses were stored at 4 °C for < 7 days until subsequent analyses. Light-exposed and dark-control samples for TDN and DOC analyses were immediately preserved with 6 N HCl and stored at 4 °C until shipment to the University of Michigan for subsequent analyses.

2.3.1.4 Analyzing light-exposed and dark-control waters

NH_4^+ concentrations were quantified in the light-exposed and dark-control waters using the salicylate-hypochlorite method.[41] Briefly, the salicylate-nitroprusside, buffer, and hypochlorite stock solutions were prepared volumetrically using reagent grade chemicals and DI water as described in the 2019 Arctic LTER Streams Protocol (https://arc-lter.ecosystems.mbl.edu/streams/arctic-lter-streams-protocol) and then stored in the dark at room temperature until NH_4^+ analyses. NH_4^+ was measured by combining a water sample with the three reagents in a methacrylate cuvette in the dark (0.6 mL water sample + 1.7 mL total reagent volume), capping the cuvette, and then allowing color development for 15-60 minutes before absorbance measurement in the methacrylate cuvette on a spectrophotometer at 660 nm (Aqualog, Horiba; 1-cm pathlength).

Each light-exposed or dark-control water sample was analyzed by standard addition of 0, 1.3, and 2.6 μM NH_4Cl four times, resulting in 12 absorbance measurements per sample. Blanks

were collected within 5 minutes of each sample processed by adding DI water to the three reagents. The average blank absorbance was subtracted from the absorbance of each water sample with and without standard addition. The concentration of NH_4^+ in each water sample was calculated as the absolute value of the intercept divided by the slope of the least-squares regression of all four blank-subtracted standard addition curves, where NH_4^+ concentration is plotted on the x-axis and blank-subtracted absorbance is plotted on the y-axis. The limit of detection of this method was 0.3 μM NH_4^+.

CDOM and FDOM were measured in the light-exposed and dark-control waters as described above (Section 2.3.1.2). TDN concentrations were measured using an auto-analyzer after a potassium persulfate digestion (CV < 5% on duplicate analyses) as previously described.[1] DOC concentrations were measured using a Shimadzu TOC-V analyzer (CV < 5% on duplicate analyses).[1] The molar C/N ratio of DOM was calculated as the molar concentrations of DOC divided by TDN, given that DON makes up > 90% of TDN in arctic surface waters.[1-2] The specific ultraviolet (UV) absorbance at 254 nm ($SUVA_{254}$; L mg^{-1} C m^{-1}) was calculated as the absorbance at 254 nm (A_{254}) divided by the pathlength (m) and the concentration of DOC (mg C L^{-1}).[42]

2.3.1.5 PARAFAC analysis

Parallel factor (PARAFAC) analysis was used to separate the dataset of 598 surface water EEMs (initial, light-exposed, and dark-control waters; Figure 2.1) into mathematically and chemically independent components, where each component represents a single fluorophore or a group of strongly co-varying fluorophores.[43] The PARAFAC model was generated and validated using the drEEM toolbox (version 0.1.0)[44] in MATLAB v9.0. Briefly, the fluorescence intensity was interpolated between wavelengths to achieve 1-nm increments across excitation

and emission wavelengths. Primary and secondary scatter peaks were interpolated or removed to prevent modeling of non-fluorescent peaks, and the range of excitation and emission wavelengths was set to 260-450 nm and 300-600 nm, respectively. Each EEM was then normalized to its total fluorescence intensity to reduce concentration-related co-varying of components, which allows EEMs with lower intensity to influence the model. During the exploratory phase, models were run with three to eight components. For each model run, modeled and residual EEMs were visually examined for model fit and outliers, and five samples were removed as outliers. An eight-component model was validated using a split-half analysis, where the 593 EEMs were split by alternating split style into six different datasets that were modeled independently from one another (Figure 2.A.1). The maximum fluorescence of each component (F_{max}) was used to quantify the relative abundance of each component in a water sample (in Raman units, RU; CV < 4% on triplicate analyses).[43-44]

The fluorescence of the amino acid-like components C7 and C8 overlap with the amino acids tryptophan and tyrosine, respectively,[30,45] whereas the components C1 to C6 correspond to fluorescence of humic-like, terrestrially-derived material (Figure 2.A.1).[30,46-47] The relative abundance of humic-like FDOM was calculated as the sum of F_{max} of C1 to C6 (CV < 1% on triplicate analyses). The percent of amino acid-like FDOM was calculated as the F_{max} of C7 and C8 divided by the total F_{max} of all components in the EEM multiplied by 100 (CV < 4% on triplicate analyses).

The F_{max} of the amino acid-like components C7 and C8 were positively correlated with the fluorescence intensities at excitation / emission wavelengths of 292 / 385 nm and 272 / 318 nm in each EEM, respectively ($p < 0.001$; Figures 2.A.1, 2.A.2). In addition, the sum of F_{max} for the humic-like components were positively correlated with the fluorescence intensity at an

excitation wavelength of 250 nm and emission wavelength of 450 nm in each EEM ($p < 0.001$; Figure 2.A.2), which is the location of the most commonly observed fluorescence peak for humic-like, terrestrially-derived material within DOM.[30,45-47]

2.3.1.6 Quantifying DON photodegradation and NH_4^+ photo-production

The concentration of NH_4^+ photo-produced in each replicate quartz tube was calculated as the light minus dark difference in NH_4^+ concentration. The percent of DON photodegraded was calculated as the concentration of NH_4^+ photo-produced divided by the concentration of TDN in the dark control multiplied by 100. Photodegradation of DOC, CDOM, and FDOM were quantified as the light minus dark differences in DOC, a_{305}, S_R, $SUVA_{254}$, FI, and each FDOM component. NH_4^+ photo-production and each measure of DOM photodegradation are reported as the average ± 1 standard error (SE) of the triplicate quartz tubes in each water sample at each sunlight exposure time.

Apparent quantum yields of NH_4^+ photo-production ($\varphi_{NH4+,\lambda}$) were calculated using the concentration of NH_4^+ photo-produced and the amount of light absorbed by CDOM. The amount of light absorbed by CDOM ($Q_{a\lambda}$; mol photons m^{-2}) was calculated following:

$$Q_{a,\lambda} = \int_{\lambda_{min}}^{\lambda_{max}} E_{0,\lambda}(1 - e^{-a_{CDOM,\lambda} * z}) \frac{a_{CDOM,\lambda}}{a_{tot,\lambda}} d\lambda \quad (1)$$

where λ_{min} and λ_{max} are the minimum and maximum wavelengths of light absorbed by CDOM (280 and 600 nm, respectively), $E_{0,\lambda}$ is the total photon flux spectrum reaching the quartz tubes during the sunlight exposure period (mol photon m^{-2} nm^{-1}), and $a_{CDOM,\lambda}$ is the geometric mean of the light-exposed and dark-control $a_{CDOM,\lambda}$ to account for loss of CDOM during the sunlight exposure period. The pathlength (z) was taken as the depth of each quartz tube (2 cm).

$a_{CDOM,\lambda}/a_{tot,\lambda}$ was set to 1 given that CDOM was the main constituent absorbing light in the filtered surface waters.[32]

Total downward photon flux spectra reaching the quartz tubes during each sunlight exposure period were generated as previously described.[32] Briefly, direct measurements of UV radiation and photosynthetically active radiation (PAR) from 15 May to 26 September 2018 at the Toolik Field Station were apportioned to a modeled solar spectrum and then separated into direct and diffuse spectra. Wavelength-dependent correction factors were applied to those spectra to account for atmospheric turbidity and Rayleigh scattering, and then multiplied by the duration of time between consecutive UV and PAR measurements (5 minutes). The global photon flux spectrum for each 5-minute interval was calculated as the sum of the corrected direct and diffuse spectra. The total photon flux spectrum reaching the quartz tubes during each experiment was calculated as the sum of global photon flux spectra during the sunlight exposure period (mol photon m^{-2} nm^{-1}). The photon dose during the sunlight exposure period (mol photon m^{-2}) was calculated as the sum of the photon flux spectra from 280 to 600 nm.

Values of $\varphi_{NH4+,\lambda}$ were calculated as the concentration of NH_4^+ photo-produced divided by the amount of light absorbed by CDOM at each sunlight exposure time, assuming the spectrum decreased exponentially with increasing wavelength (Figure 2.A.3; see Appendix Section 2.8.1).[48-49] Yields of tryptophan-like C7 and tyrosine-like C8 photodegradation were quantified as the amount of each component photodegraded (light minus dark difference in RU) divided by the total amount of light absorbed by CDOM during the sunlight exposure period (mol photon m^{-2}; Table 2.A.2). The amount of light absorbed by CDOM was calculated as the average ± 1 SE of replicate quartz tubes (n = 3). Yields of NH_4^+ photo-production at 350 nm ($\varphi_{NH4+,350}$), yields of tryptophan-like C7 photodegradation, and yields of tyrosine-like C8 photo-

production are reported as the average ± 1 SE of replicate quartz tubes (n = 3). Values of $\varphi_{NH4+,350}$ were not reported following longer exposure times when there were no significant changes in NH_4^+ photo-production and significant decreases in $\varphi_{NH4+,350}$ between consecutive sunlight exposure times of the same water sample (see Appendix Section 2.8.1).

2.3.1.7 Water column rates of NH_4^+ photo-production

Daily water column rates of NH_4^+ photo-production in each surface water (mmol N m^{-2} d^{-1} nm^{-1}) were calculated as the product of two spectra: the rate of light absorption by CDOM throughout the water column ($Q_{a,\lambda}$; mol photon m^{-2} d^{-1} nm^{-1}) and the average $\varphi_{NH4+,\lambda}$ measured at each site (mmol N mol $photon^{-1}$ nm^{-1}; Table 2.2):

$$\text{Rate of } NH_4^+ \text{photo-production} = \int_{\lambda_{min}}^{\lambda_{max}} Q_{a,\lambda}\,\varphi_{NH4+,\lambda}\,d\lambda \qquad (2)$$

Water column rates of light absorption by CDOM were calculated using daily incoming photon flux spectra (mol photon m^{-2} d^{-1} nm^{-1}) reaching the Toolik Field Station in the summer of 2018, the average $a_{CDOM,\lambda}$ measured in each surface water (m^{-1}; Table 2.1), and the water column depth of each surface water (Table 2.3). The same average $\varphi_{NH4+,\lambda}$ spectrum quantified for each surface water (Table 2.2) was used throughout the summer.

2.3.1.8 Statistical analyses

Two-tailed, paired t-tests were used to determine (1) significant differences in DOM and water chemistry between the lakes versus streams and rivers sampled, (2) significant differences in NH_4^+ concentration and DOM composition between the light-exposed versus dark-control waters, and (3) significant changes in NH_4^+ photo-production and $\varphi_{NH4+,350}$ between two exposure times. T-tests were used to determine whether the slopes and intercepts of least-squares regressions between initial DOM composition, the amount of light absorbed by CDOM,

any measure of DOM photodegradation, or yields of DON photodegradation (e.g., $\varphi_{NH4+,350}$) were significantly different from zero (Figures 2.2, 2.3, 2.A.2). Statistical significance was defined as $p < 0.05$.

2.3.2 Comparing NH_4^+ photo-production to bacterial and algal N uptake in arctic lakes

Daily rates of NH_4^+ photo-production in the arctic lakes on the Alaskan Coastal Plain were compared to average summertime rates of N incorporation into bacterial biomass and N uptake by primary producers estimated from previously reported rates of biomass production. Because long-term studies of bacterial production, primary production, and N cycling have been conducted throughout the water column at Toolik Lake,[2] NH_4^+ photo-production rates were compared to rates of N incorporation into bacterial biomass and N uptake by primary producers over daily timescales, across years, and as a function of water column depth in this lake. Briefly, long-term measurements of UV radiation, PAR, CDOM, and bacterial production by the Arctic LTER were used to estimate daily water column rates of NH_4^+ photo-production and bacterial production in the upper mixing layer of Toolik Lake (0-5 m)[50] in the summers of 2011-2018 (Section 2.3.2.1). Rates of bacterial production were used to estimate daily rates of N incorporation into bacterial biomass in Toolik Lake (Section 2.3.2.2). Lastly, daily rates of N uptake by primary producers in the upper mixing layer of Toolik Lake were calculated from previously reported rates of DIN uptake from two summers in this lake (Section 2.3.2.3).

2.3.2.1 Quantifying rates of NH_4^+ photo-production in Toolik Lake

Daily water column rates of NH_4^+ photo-production in the upper mixing layer of Toolik Lake (0-5 m) were estimated using Eq. (2) for 2011-2018 from the date of ice-off (Table 2.A.3) to the last date that UV and PAR were measured each year. UV radiation and PAR were measured at 5-minute or 1-hour intervals at the Toolik Field Station from 15 May to 1 October

for each year from 2011 to 2018, except in 2013 and 2018 when measurements were collected until 24 August and 26 September, respectively. Global downward photon flux spectra were calculated for each time interval between consecutive measurements as described above (Section 2.3.1.6),[32] and then summed across time intervals to calculate daily downward photon flux spectra (mol photon m^{-2} d^{-1} nm^{-1}). These daily incoming photon flux spectra (mol photon m^{-2} d^{-1} nm^{-1}), along with the average $\varphi_{NH4+,\lambda}$ spectrum measured from water collected from a depth of 3 m (on 9 May 2018; Table 2.2) and average $a_{CDOM,\lambda}$ between 0 and 5 m depths (m^{-1}) were used to calculate NH_4^+ photo-production rates on each day. The same $\varphi_{NH4+,\lambda}$ spectrum quantified for Toolik Lake at a 3 m depth was used throughout the summer and across years.

The average $a_{CDOM,\lambda}$ between 0 and 5 m depths (m^{-1}) in Toolik Lake was estimated for each day using weekly $a_{CDOM,\lambda}$ measurements by the Arctic LTER. Briefly, Toolik Lake water was collected at depths of 0, 1, 3, and 5 m approximately weekly from June to August or September in 2011-2018. The water collected at each depth was then analyzed for CDOM as described above (Section 2.3.1.2; Aqualog, Horiba). Protocols for water sampling and analysis of CDOM has been previously described in the Arctic LTER Landscape Interactions group protocol manual (https://arc-lter.ecosystems.mbl.edu/landwater/lw_protocols). Depth-averaged $a_{CDOM,\lambda}$ (m^{-1}) in the upper mixing layer was calculated as the average $a_{CDOM,\lambda}$ spectra between 0 and 5 m depths on each date of measurement. The average $a_{CDOM,\lambda}$ on each day of the summer season was then calculated by interpolating between two consecutive measurements, assuming that depth-averaged $a_{CDOM,\lambda}$ between the two consecutive dates changed at a constant rate.

2.3.2.2 Estimating rates of N incorporation into bacterial biomass in Toolik Lake

Daily rates of N incorporation into bacterial biomass in Toolik Lake in the summers of 2011-2018 were calculated from depth-integrated rates of bacterial production (mmol C m^{-2} d^{-1})

in the upper mixing layer. Briefly, bacterial production (mmol C L^{-1} d^{-1}) was measured from the weekly water samples collected at 1, 3, and 5 m depths from 2011 to 2018[51-52] by the incorporation of ^{14}C-labeled leucine following Simon and Azam (1989).[53] Depth-integrated rates of bacterial production were calculated in the upper 5 m of the water column on each date measured by first multiplying the average volumetric production (mmol C L^{-1} d^{-1}) between two consecutive depth measurements by the volume of water between those measurements (obtained by lake bathymetry), and then summing across water column depths between 0 and 5 m (mmol C d^{-1}). This total production in the upper mixing layer was then divided by the lake volume (L) between 0 and 5 m and multiplied by the depth of 5 m to get an areal rate of bacterial production at each date of measurement (mmol C m^{-2} d^{-1}). It was assumed that production occurring at a 1 m depth was representative of bacterial production rates between 0 and 1 m below the surface. Daily rates of bacterial production were calculated by interpolating between two consecutive weekly measurements (mmol C m^{-2} d^{-1}), assuming that production between the two consecutive dates changed at a constant rate (slope).

Daily rates of N incorporation into bacterial biomass were calculated by dividing the daily, depth-integrated rates of bacterial production (0-5 m; mmol C m^{-2} d^{-1})[51-52] by the molar ratio of C to N in bacterial biomass. The molar ratio of C to N in bacterial biomass in Toolik Lake was estimated from previously reported molar C/N ratios for native bacteria communities in oligotrophic lakes (see Appendix Section 2.8.2). The same molar C/N ratio of 16 for bacterial biomass was used throughout the summer and across the eight years in Toolik Lake. Thus, it was assumed that the bacteria in Toolik Lake take up and incorporate into biomass 1 mole of N for every 16 moles of C taken up and incorporated, on average, to achieve an average daily molar C/N ratio of 16 in their biomass.

2.3.2.3 Estimating rates of N uptake by primary producers in Toolik Lake

Previously reported rates of DIN uptake by primary producers during two summers in Toolik Lake[54-55] were used to quantify daily rates of N uptake by primary producers in the upper mixing layer of Toolik Lake (see Appendix Section 2.8.2). Briefly, depth-integrated rates of DIN uptake in the upper 5 m of the water column (mmol N m^{-2} d^{-1}) were calculated as described above (Section 2.3.2.1) using previously reported rates of DIN uptake by primary producers (mmol N L^{-1} d^{-1}) measured weekly or biweekly at depths of 0, 1, 3 and 5 m in Toolik Lake.[54] Daily, depth-integrated rates of DIN uptake for each year were calculated by interpolating between two consecutive measurements, assuming that uptake between the two dates changed at a constant rate. The rate of DIN taken up by primary producers on each day of the ice-free summer (mmol N m^{-2} d^{-1}) was then calculated as the average of daily, depth-integrated rates reported for each year (n = 2).[54-55] It was assumed that this average of the daily DIN uptake rates previously reported for Toolik Lake was representative of DIN uptake rates by primary producers in the summers of 2011-2018.

2.4 Results

The DOM in lakes differed in the content and composition of N-containing compounds compared to the DOM in streams and rivers. The molar C/N ratio of DOM varied 3.4-fold across all waters and was significantly lower in the lakes (24 ± 2) than the streams and rivers (35 ± 3; average ± 1 SE; $p < 0.05$; Table 2.1). Likewise, percentages of the amino acid-like components within FDOM and of protein-like formulas varied 3- to 4-fold among the surface waters and were significantly higher in lakes compared to the streams and rivers ($p < 0.05$; e.g., 10 ± 1% and 7 ± 1% protein-like formulas in lakes versus streams and rivers, respectively; average ± 1 SE; Table 2.1). The percentages of amino acid-like components and protein-like

formulas increased linearly with the N content of DOM in all surface waters ($p < 0.001$; as indicated by the decreased C/N ratio of DOM; Figure 2.2a). In addition, the ratio of tryptophan-like C7 to total humic-like FDOM increased linearly with the percentage of protein-like formulas in the mass spectra ($p < 0.05$; Figure 2.2b). There were no significant correlations of the percentage of protein-like formulas with any measure of DOM composition unrelated to the N content of DOM in the surface waters (see Appendix Section 2.8.3).

Absorption of sunlight by CDOM resulted in changes to the chemistry of aromatic and N-containing compounds within DOM (Tables 2.2, 2.A.2). For example, DOC, a_{305}, $SUVA_{254}$, FI, and tryptophan-like C7 decreased following sunlight exposure relative to dark controls, whereas S_R and tyrosine-like C8 increased (Tables 2.2, 2.A.2). Across all the surface waters, DOC, a_{305}, $SUVA_{254}$, and FI decreased linearly with the amount of light absorbed by CDOM ($p < 0.001$; Table 2.A.2). Likewise, the amounts of tryptophan-like C7 photodegraded and tyrosine-like C8 photo-produced increased linearly with the amount of light absorbed by CDOM ($p < 0.05$; Tables 2.2, 2.A.2).

The concentration of NH_4^+ in each surface water increased following sunlight exposure relative to dark controls (Table 2.2). A significant increase in NH_4^+ concentration relative to dark controls was detected following the shortest sunlight exposure for each surface water ($p < 0.05$), except three waters where significant NH_4^+ photo-production was detected after a longer exposure time (Table 2.2). The majority of surface waters showed significant NH_4^+ photo-production after the shortest exposure time and no detectable change in NH_4^+ photo-production following longer exposures ($p < 0.05$; Table 2.2). In only four of the surface waters, the concentration of NH_4^+ photo-produced continued to significantly increase following longer sunlight exposures ($p < 0.05$; Table 2.2). There were no detectable changes in the concentration

of TDN during sunlight exposure relative to dark controls (data not shown), indicating that the light minus dark differences in NH_4^+ concentration were due to the photodegradation of DON. On average, 3.3 ± 0.4% of DON in each surface water was photodegraded to produce NH_4^+ (± 1 SE; Table 2.2).

Photodegradation of DON resulted in an apparent quantum yield spectrum for NH_4^+ photo-production ($\varphi_{NH4+,\lambda}$) that decreased exponentially with increasing wavelength (Figure 2.A.3). Yields of NH_4^+ photo-production at 350 nm ($\varphi_{NH4+,350}$) varied 36-fold in the surface waters (2.8 to 100.8 µmol N mol photon^{-1}; Table 2.2). Similarly, yields of tryptophan-like C7 photodegradation varied 16-fold (-0.02 to 0.31 RU m^2 mol photon^{-1}) and yields of tyrosine-like C8 photo-production varied 8-fold between all the surface waters (-0.01 to 0.12 RU m^2 mol photon^{-1}; Tables 2.2, 2.A.2).

Photo-production yields of N-containing compounds depended on the initial content and composition of DON. NH_4^+ photo-production yields were significantly higher in surface waters with greater percentages of amino acid-like FDOM components and protein-like formulas in the mass spectra ($p < 0.05$). For example, NH_4^+ photo-production yields were on average 2-fold higher in surface waters with > 8% of formulas that were protein-like compared to those with < 8% (Tables 2.1, 2.2). In contrast, photo-production yields for tyrosine-like C8 depended on the initial abundance of the tryptophan-like component relative to the tyrosine-like component, where higher yields were observed when there was more tryptophan-like C7 in the surface water prior to sunlight exposure ($p < 0.05$; Tables 2.1, 2.2). Yields of NH_4^+ and tyrosine-like C8 photo-production increased linearly with the yield of tryptophan-like C7 photodegradation ($p < 0.05$; Figure 2.3).

Water column rates of NH_4^+ photo-production ranged from 3 to 319 μmol N m^{-2} d^{-1} during the ice-free summer (Table 2.3), depending strongly on the NH_4^+ photo-production yield and photon flux. For instance, NH_4^+ photo-production rates increased linearly with the NH_4^+ photo-production yield in each surface water ($p < 0.001$; Eq. 2; Table 2.2), resulting in NH_4^+ photo-production rates that varied 12-fold across the lakes, streams, and rivers on one day in mid-summer (Table 2.3). Changes in the photon flux reaching surface waters throughout the summer resulted in daily NH_4^+ photo-production rates that varied 9- to 14-fold in each surface water (Table 2.3). For example, in Toolik Lake, NH_4^+ photo-production rates decreased throughout the ice-free summer following the decrease in the CDOM concentration and daily photon flux reaching the lake over the summer (Figure 2.4).

2.5 Discussion

2.5.1 Photo-production of NH_4^+ from protein-like compounds

NH_4^+ was photochemically produced in arctic surface waters at rates consistent with values previously reported in other surface waters.[15-17,49,56] For example, water column rates of NH_4^+ photo-production (3 – 319 μmol N m^{-2} d^{-1}; Table 2.3) fell within the range previously reported for boreal lakes[16] and the coastal ocean.[15,17,49,56] Stedmon et al. (2007) reported higher NH_4^+ photo-production rates from DOM with greater N contents,[56] which was consistent with the higher NH_4^+ photo-production rates observed in the Coastal Plain lakes compared to the other surface waters studied (Tables 2.1, 2.2). Rates of NH_4^+ photo-production in these lakes as well as Toolik Lake were similar to previous estimates for a boreal lake (~70 μmol N m^{-2} d^{-1}; Table 2.3).[16] These findings demonstrate that the DON in arctic surface waters has a similar susceptibility to produce NH_4^+ during photodegradation compared to the surface waters previously studied in other geographic regions.

Four lines of evidence suggest that photochemically produced NH_4^+ comes from the degradation of protein-like compounds within DOM. First, NH_4^+ photo-production yields were on average 2-fold higher in surface waters with relatively more protein-like compounds (> 8% of protein-like formulas in the mass spectra) compared to waters with less protein-like compounds (< 8% of protein-like formulas; Tables 2.1, 2.2). Second, photo-production of NH_4^+ increased with the photodegradation of tryptophan-like FDOM (Figure 2.3a), a proxy for protein-like compounds within the DOM pool (Figure 2.2b).[57] Third, there were more than enough protein-like compounds within the DOM pool to account for the NH_4^+ photo-produced (Tables 2.1, 2.2). For example, 35-50% of organic N within terrestrially-derived DOM is classified as protein-like.[23-24] Assuming that the DOM in arctic surface waters is 1% N by mass[30] and 35% of this N is protein-like, there was 2 to 11 µM of protein-like N available to be photodegraded to NH_4^+ in these surface waters. Thus, concentrations of protein-like N were 2- to 15-fold greater than the maximum concentration of NH_4^+ photo-produced in each surface water (Table 2.2).

The fourth line of evidence for the photodegradation of protein-like compounds is that free amino acids were also likely photo-produced alongside the production of NH_4^+.[21-22,31] It is thought that free amino acids are released from proteins residues due to the photochemical cleavage of peptide bonds within peptides and proteins.[22] Similarly, photo-produced NH_4^+ is thought to come from the degradation of primary amines located on the ends of amino acids, peptides, and proteins (i.e., N-terminus).[21] Thus, the photochemical cleavage of peptide bonds within protein-like compounds to form free amino acids and smaller peptides increases the number of primary amines that can undergo photodegradation to NH_4^+.[22,31,58] The photo-production of free amino acids or smaller peptides from larger protein-like compounds is expected to increase the fluorescence intensity of FDOM attributed to the amino acid

tyrosine[56,59-60] because tyrosine fluoresces more in the free form than when it is combined with other amino acids in larger protein structures.[61-62] Consistent with this expectation, there was an increase in tyrosine-like FDOM observed in all surface waters following sunlight exposure (Table 2.2). Thus, together these lines of evidence indicate that NH_4^+ photo-production depends strongly on the abundance of protein-like compounds within the DOM pool.

Changes in the concentration of NH_4^+ photo-produced from DOM with increasing sunlight exposure time suggest that the most photochemically labile protein-like N (i.e., most susceptible to produce NH_4^+) becomes rapidly depleted from the DOM pool. For instance, no additional photo-production of NH_4^+ was observed after longer exposure times for five of the arctic surface water samples (Table 2.2), consistent with previous findings in temperate and boreal surface waters.[8,20] This finding suggests that the most photochemically labile amine groups are degraded to NH_4^+ following smaller photon doses, leaving behind protein-like N that is less susceptible to produce NH_4^+ during photodegradation. The photodegradation of ~3% of the DON pool to NH_4^+ (Table 2.2) further indicates that only a portion of protein-like N within DOM was photochemically labile to produce NH_4^+ because this value is lower than the percentage of DON that may be protein-like in arctic surface waters.[23-24]

The rapid depletion of photo-labile protein-like N from DOM suggests that the photochemical production of NH_4^+ may be substrate limited in arctic surface waters if there is not sufficient replenishment of protein-like compounds to the water column.[19,63] The sunlight exposure times where significant NH_4^+ photo-production was detected relative to the previous time in the sunlight exposure experiments corresponded to 0.5 to 5 hours of sunlight exposure in the water column across the arctic lakes, streams, and rivers (data not shown). This estimate suggests that the most photo-labile protein-like N is removed from the water column within

hours of sunlight exposure. If photo-labile protein-like N in arctic surface waters is replenished from the export of DOM from soils over hourly timescales,[63] then there may be enough protein-like N to sustain rates of NH_4^+ photo-production. However, if DOM is replenished over daily timescales, then NH_4^+ photo-production rates may be limited by available protein-like N to undergo photodegradation.

2.5.2 Competition between sunlight and bacteria for protein-like compounds

Sunlight and bacteria may compete to degrade protein-like compounds in arctic surface waters,[59-60] further contributing to the substrate limitation of NH_4^+ photo-production rates. In oligotrophic waters dominated by terrestrially-derived DOM like those in the Arctic, bacteria obtain N for biomass production from protein-like compounds via extracellular enzymatic degradation.[25,27] If rates of bacterial degradation of protein-like compounds far exceed rates of photodegradation of protein-like compounds, the photo-production of NH_4^+ will be substrate limited (e.g., limited by the abundance of protein-like N).[19] In contrast, if rates of photodegradation exceed rates of bacterial degradation of protein-like compounds, then bacterial degradation of DON may not contribute to the substrate limitation of NH_4^+ photo-production rates in arctic surface waters.

Rates of photodegradation were fast enough to compete with bacterial degradation of protein-like compounds on sunny days in shallow lakes on the Alaskan Coastal Plain (~1 m depth). The Coastal Plain lakes had some of the highest daily rates of NH_4^+ photo-production among the arctic surface waters studied (Table 2.3) and low average summertime rates of bacterial production (~2 mmol C m^{-2} d^{-1}).[64-65] Assuming that bacteria in these lakes take up 1 mole of N for every 16 moles of C incorporated into their biomass (see Appendix Section 2.8.2), daily rates of NH_4^+ photo-production in mid-summer (15 July; Table 2.3) were 0.5- to 2-fold

higher than the average rate of N taken up into bacterial biomass in the Coastal Plain lakes. On average, water column rates of NH_4^+ photo-production exceeded the average rate of N incorporated into bacterial biomass one-fourth of the time in the Coastal Plain lakes (n = 4 lakes), corresponding to sunny days during the ice-free summer.

In the deeper Toolik Lake, NH_4^+ photo-production rates were on average 16% of rates of bacterial N incorporation (range 2-87%; Figure 2.5a). However, the magnitude of photodegradation rates compared to bacterial degradation of protein-like compounds depended strongly on water column depth. Bacterial production rates in the upper 1 m of Toolik Lake were consistently ~50% slower than those between 1-3 and 3-5 m depths throughout the ice-free summer.[51-52] Given that the highest NH_4^+ photo-production rates are observed at shallow depths and decrease as sunlight is absorbed by CDOM with a greater depth in the water column, these findings suggest that photodegradation rates could be fast enough to compete with bacterial degradation of protein-like compounds at the lake surface. Consistent with this idea, rates of NH_4^+ photo-production were on average 1.2-fold slower than rates of N taken up into bacterial biomass in the top 1 m of Toolik Lake throughout the ice-free summer (Figure 2.5a), but orders of magnitude lower between 1 and 5 m depths (data not shown). This comparison of rates suggests that rates of photodegradation become too slow to compete with bacterial degradation of protein-like compounds as photodegradation decreases with a greater depth in the water column, resulting in the substrate limitation of NH_4^+ photo-production below a 1 m depth.

Photodegradation rates were likely fast enough to compete with bacterial degradation of protein-like compounds in the top 1 m of Toolik Lake in the week after ice-off. Peak bacterial production and thus N incorporation into biomass occurred on average 21 days after ice-off (Table 2.A.3), whereas NH_4^+ photo-production peaked just after ice-off (Figure 2.4c). As a

result, NH_4^+ photo-production rates were 1.6-fold higher than rates of bacterial N incorporation in the week after ice-off on Toolik Lake (Figure 2.5a). This comparison of rates suggests that photodegradation rates are fast enough to compete with bacterial degradation of protein-like compounds and thus, produce NH_4^+ in the upper 1 m of Toolik Lake just following ice-off. However, NH_4^+ photo-production rates are likely substrate limited during the rest of the ice-free summer in Toolik Lake due to the competition for protein-like compounds between sunlight and bacteria.

There are several untested assumptions in these NH_4^+ photo-production and bacterial N incorporation rate comparisons that could impact the relative importance of photochemical versus bacterial degradation of protein-like compounds in the arctic lakes. First, it was assumed that NH_4^+ was the only product formed during the photodegradation of protein-like compounds. Free amino acids or smaller peptides were also produced during their photodegradation in arctic surface waters (e.g., tyrosine-like compounds; discussed above; Table 2.2, Figure 2.3b). Prior work has reported rates of amino acid photo-production that are comparable to NH_4^+ photo-production rates in surface waters.[17] Thus, measuring only NH_4^+ photo-production rates could underestimate photodegradation rates for protein-like compounds by 2-fold. Second, the average molar C/N ratio of bacterial biomass was assumed to be 16, resulting in a relatively low N demand by bacteria in the water column (see Appendix Section 2.8.2). If bacterial biomass in arctic lakes had a molar C/N ratio closer to 9, which was the average value reported for bacteria across lakes of different trophic status (see Appendix Section 2.8.2), then rates of N incorporation into bacterial biomass would be twice as high. Third, it was assumed that bacteria took up and incorporated all of the protein-like N that they degraded extracellularly into cells. Previous studies showed that bacteria do not take up all of the amino acids produced during

enzymatic hydrolysis of protein-like compounds, especially during periods of high primary productivity.[66-68] Lastly, it was assumed that bacteria only obtain N from the DON pool, even though bacteria may take up DIN in place of DON when it is available.[26,69-70] If any of the N taken up by bacteria was inorganic, then calculated rates of N incorporation into bacterial biomass would overestimate rates of bacterial degradation for protein-like compounds.

It is likely that the relative importance of photochemical versus bacterial degradation of protein-like compounds is least sensitive to the assumptions that bacteria take up all the protein-like N that they degrade and only take up protein-like N into their biomass. Primary production rates are low in arctic lakes,[1-2,13,71] indicating that bacteria likely take up all of the protein-like N that they degrade extracellularly into their biomass. Likewise, the low concentrations of inorganic N in arctic lakes[1-2,72] suggest that bacteria likely obtain the majority of N for biomass production from the DON pool. Thus, our estimates of the extent that NH_4^+ photo-production rates are substrate limited in arctic lakes are likely most sensitive to the assumption that NH_4^+ is the only product of photodegradation of protein-like compounds and the assumed molar C/N ratio of bacterial biomass.

2.5.3 Contribution of photo-produced NH_4^+ to the N demand by primary producers

NH_4^+ produced during the photodegradation of protein-like compounds can account for 4.6 ± 0.1% of the N required by primary producers in the upper mixing layer of Toolik Lake during the ice-free summer (average ± 1 SE; Figure 2.5c). However, there were times when photo-produced NH_4^+ contributed up to 12% of the N taken up by primary producers in the upper mixing layer (Figure 2.5c). During those times, the contribution of photo-produced NH_4^+ to primary production varied 3- to 10-fold, depending on the variability in primary production (Figure 2.A.4), and on daily photon fluxes reaching the lake surface (Figure 2.4c). Both the

average and range of the contribution of photo-produced NH_4^+ to primary production in Toolik Lake is similar to previous estimates in other surface waters (~5%).[15-17] For example, Vähätalo et al. (2003) estimated that on average 4% of the N taken up by primary producers in a boreal lake could come from the photo-production of NH_4^+ throughout the summer.[16]

However, the contribution of photo-produced NH_4^+ to N uptake by primary producers in Toolik Lake also depended most strongly on the depth that NH_4^+ was produced in the water column (Figure 2.5). The primary producers in the upper 1 m of Toolik Lake consistently take up DIN at a rate ~50% slower than those between 1-3 and 3-5 m depths throughout the ice-free summer.[54-55] These findings suggest that NH_4^+ photo-produced at the surface of Toolik Lake could supply more of the N needed by primary producers than that estimated from depth-integrated rates. Consistent with this idea, photo-produced NH_4^+ accounted for on average 22% of the N taken up by primary producers in this surface layer throughout the ice-free summer season (± 1, SE; Figure 2.5b). In contrast, the NH_4^+ photo-produced between 1-3 and 3-5 m depths in Toolik Lake accounted for on average 0.5% and 0.1% of the N taken up by primary producers in the summer, respectively. Together, these findings demonstrate that photo-produced NH_4^+ can contribute one-fifth of the N required by primary producers at the water surface, and negligible amounts at greater depths in the water column.

The photodegradation of protein-like compounds may provide a more important source of DIN to primary producers in shallow lakes on the Alaskan Coastal Plain, where NH_4^+ photo-production rates are higher than Toolik Lake near the Brooks Range foothills (Table 2.3). Rates of DIN uptake by primary producers were estimated in lakes on the Coastal Plain using the range of previously reported primary production rates in these lakes (2 to 66 mmol C m^{-2} d^{-1}) and the average molar ratio of C to N in algal biomass in arctic lakes (molar C/N ratio of 9; see

Appendix Section 2.8.4). Based on these estimates, NH_4^+ photo-produced in the top 1 m of Coastal Plain lakes can account for on average 7% of the N taken up by primary producers throughout the ice-free summer season. However, this estimated contribution of photo-produced NH_4^+ to primary production depended strongly on the rate of primary production. For instance, the NH_4^+ photo-produced could account for 44% of the N required by primary producers when primary production rates were low (2 mmol C m^{-2} d^{-1}) or 1% when primary production rates were high (66 mmol C m^{-2} d^{-1}).

The molar ratio of C to N in the biomass of primary producers in arctic lakes can also strongly impact the extent that photo-produced NH_4^+ supports the N demands of primary producers (Figure 2.6). Algal biomass can have molar C/N ratios ranging from 4 to 13, depending on the lake and the date during the ice-free summer (see Appendix Section 2.8.2). A higher molar ratio of C/N indicates that primary producers demand lower amounts of N for biomass production. Thus, the contribution of photo-produced NH_4^+ to N uptake by primary producers increases with the molar C/N ratio of algal biomass (Figure 2.6). The impact of this relative N demand on the extent that photo-produced NH_4^+ provides a source of DIN to primary producers is greater in lakes with low productivity. For instance, NH_4^+ production can supply 5 to 15% of the N required by primary producers in low productivity lakes, depending on the molar C/N ratio of algal biomass. In contrast, photo-produced NH_4^+ can only contribute 1 to 2% of the N taken up in lakes with high primary productivity, regardless of the relative N demand by primary producers (Figure 2.6). Together, these findings demonstrate that the extent that photo-produced NH_4^+ contributes to N uptake by primary producers in arctic lakes depends on the rate at which primary producers demand N, with the greatest contribution occurring at the surface of lakes with low primary productivity.

2.6 Conclusions and implications

This study is the first to demonstrate that photochemically produced NH_4^+ comes from the degradation of protein-like compounds within the DOM pool in natural waters. The photodegradation of protein-like compounds within arctic stream and lake DOM to NH_4^+ indicates that photodegradation can facilitate the use of DON exported from inlet streams by primary producers in arctic lakes. The majority of N entering arctic lakes is in the organic form and the conversion of a small fraction (~3%) of this organic pool to NH_4^+ can supply DIN to arctic lakes at rates comparable to DIN export from arctic soils to streams[2] and inlet streams to lakes.[4] This finding indicates that primary production in arctic lakes may depend on sources of DON exported from soils and inlet streams in addition to the fluxes of DIN.[2,4-5]

Although estimates of the extent and importance of NH_4^+ photo-production was limited to arctic surface waters in this study, our assessment of the factors impacting the photo-production of NH_4^+ and its contribution to N uptake by primary producers indicate when and where photo-produced NH_4^+ can contribute an important source of DIN to primary production across surface waters. For instance, our results show that NH_4^+ photo-production rates may be overestimated if they are limited by the amount of protein-like N available to undergo photodegradation (i.e., substrate limited) due to the competition between sunlight and bacteria for protein-like N or the low replenishment of photochemically labile protein-like N in the water column. The photo-production of NH_4^+ is likely substrate limited in surface waters, such as eutrophic lakes, where bacteria have higher rates of biomass production and N demands compared to the oligotrophic waters in this study. The findings from this study also demonstrate that the contribution of photo-produced NH_4^+ to N uptake by primary producers will be highest in surface waters with low primary productivity, such as oligotrophic lakes at other latitudes.

2.7 Acknowledgements

We thank L. Treibergs, C. Polik, C. Cook, M. Harris, J. Dobkowski, J. Albrigtsen, and colleagues of the NSF Arctic LTER and Toolik Lake Field Station for field and laboratory assistance. We thank R. Chu and staff at the Environmental Molecular Science Laboratory (EMSL) for help with FT-ICR mass spectrometry measurements. Special thanks to C. Ward (WHOI) for access to the light emitting diode (LED) reactor[73] and to A. Giblin (MBL) for providing Toolik Lake water needed to characterize the apparent quantum yield spectrum for NH_4^+ photo-production. Research was supported by NSF CAREER 1351745 (R.M.C.), DEB 1753731, DEB 1637459, OPP 1936769 (G.W.K.), and the Scott Turner Research Award at the University of Michigan (J.C.B.).

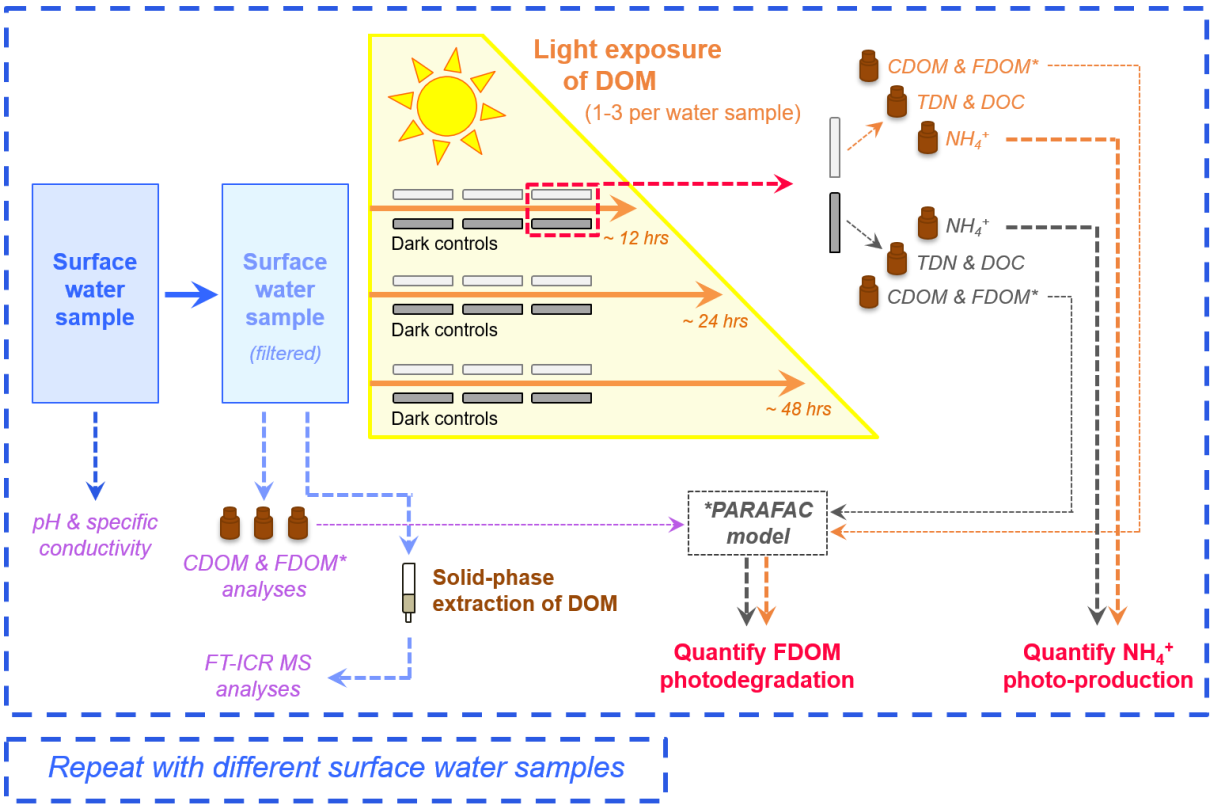

Figure 2.1. Experimental design for the sunlight exposure experiments conducted with each surface water sample. Each initial water sample was analyzed by absorbance spectroscopy (CDOM), fluorescence spectroscopy (FDOM), and mass spectrometry (FT-ICR MS) and then exposed to natural sunlight for up to three exposure times ranging from 10 to 48 hours in triplicate quartz tubes alongside dark controls. Each light-exposed and dark control water was analyzed for CDOM, FDOM, TDN, DOC, and NH_4^+. Light minus dark differences were used to quantify DOM photodegradation and NH_4^+ photo-production.

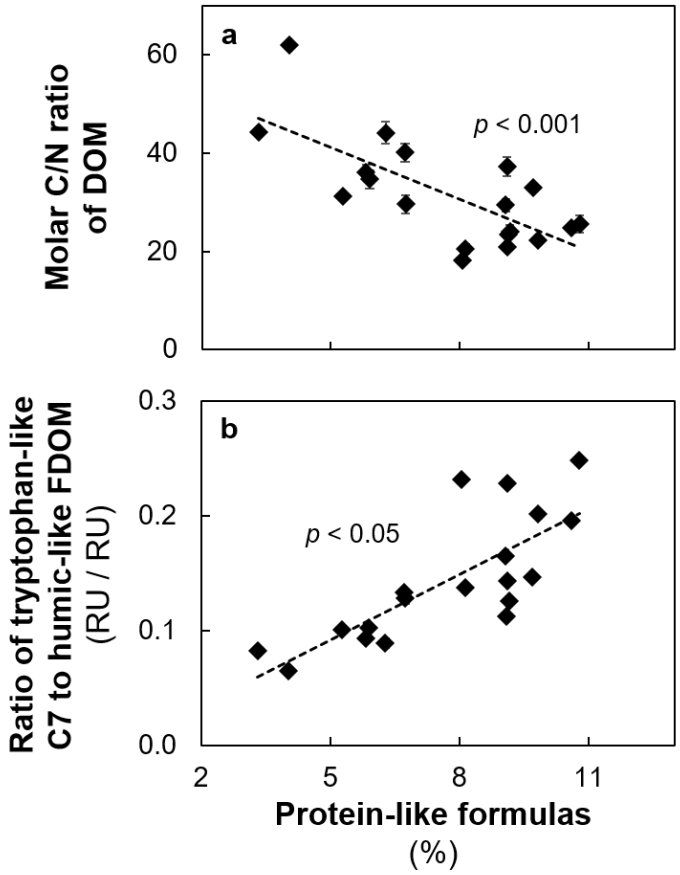

Figure 2.2. The molar C/N ratio of DOM and abundance of tryptophan-like FDOM changed with the percentage of protein-like formulas in the mass spectra. The (a) molar C/N ratio of DOM and the (b) abundance of tryptophan-like C7 relative to humic-like FDOM are plotted versus the percentage of protein-like formulas in the mass spectra for DOM in the surface waters prior to sunlight exposure. Protein-like formulas were defined as those with H/C = 1.5 – 2.3, O/C = 0.3 – 0.55, and N ≥ 1.[39-40] Values on the y-axis are shown as the average ± 1 standard error of experimental replicates (n = 3).

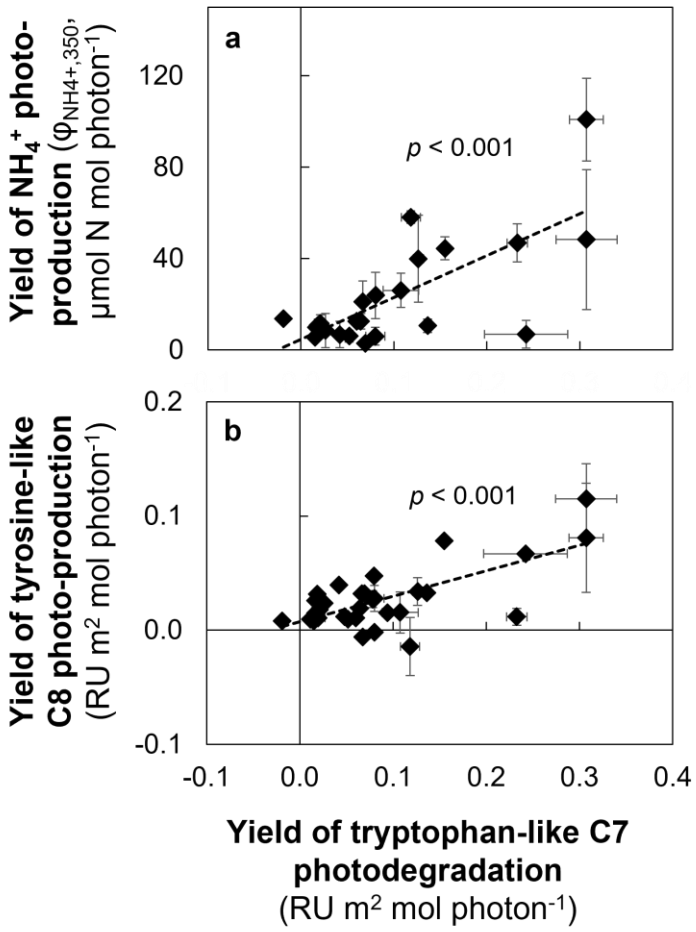

Figure 2.3. Yields of NH_4^+ and tyrosine-like FDOM photo-production increased with the yield of tryptophan-like FDOM photodegradation. Yields of (a) NH_4^+ photo-production at 350 nm ($\varphi_{NH4+,350}$) and (b) tyrosine-like C8 photo-production are plotted versus the yield of tryptophan-like C7 photodegradation. Values are shown as the average ± 1 standard error of experimental replicates (n = 3).

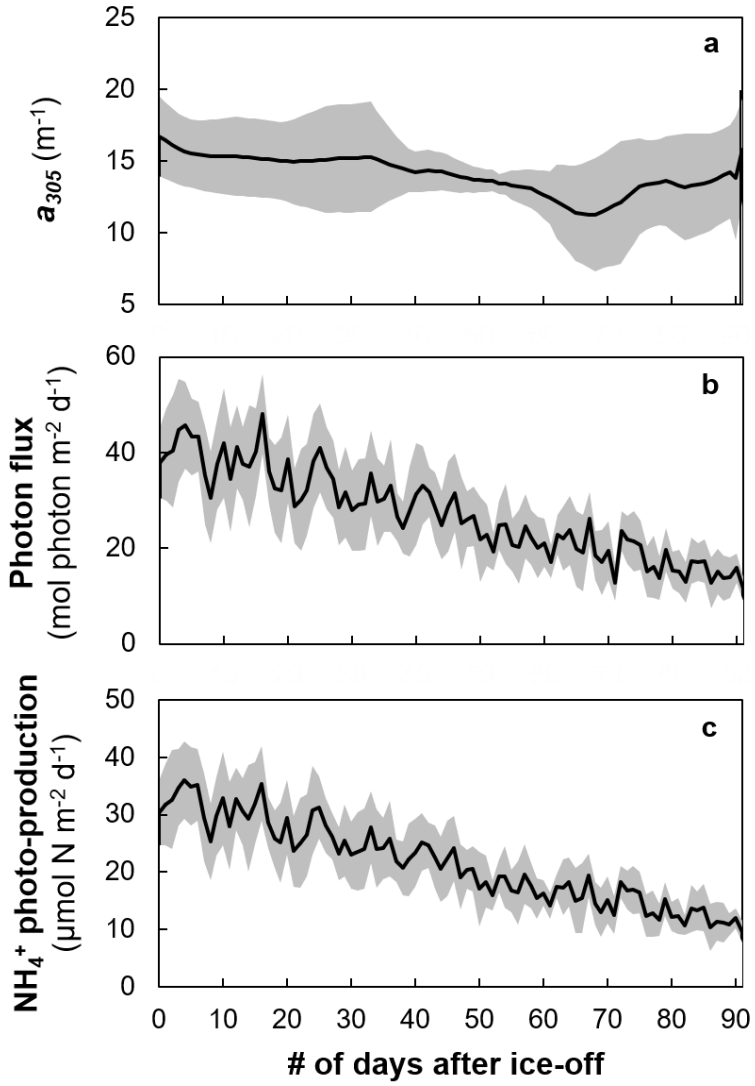

Figure 2.4. CDOM, photon dose, and NH_4^+ photo-production rates in Toolik Lake. Average (a) Naperian absorption coefficient at 305 nm (a_{305}) in the upper mixing layer of Toolik Lake (0-5 m),[50] (b) daily photon flux reaching the lake surface, and (c) rate of NH_4^+ photo-produced in the upper 5 m of the lake on each day after ice-off. Solid lines show the average value on each date in 2011-2018 and shading shows the upper and lower 95% confidence intervals.

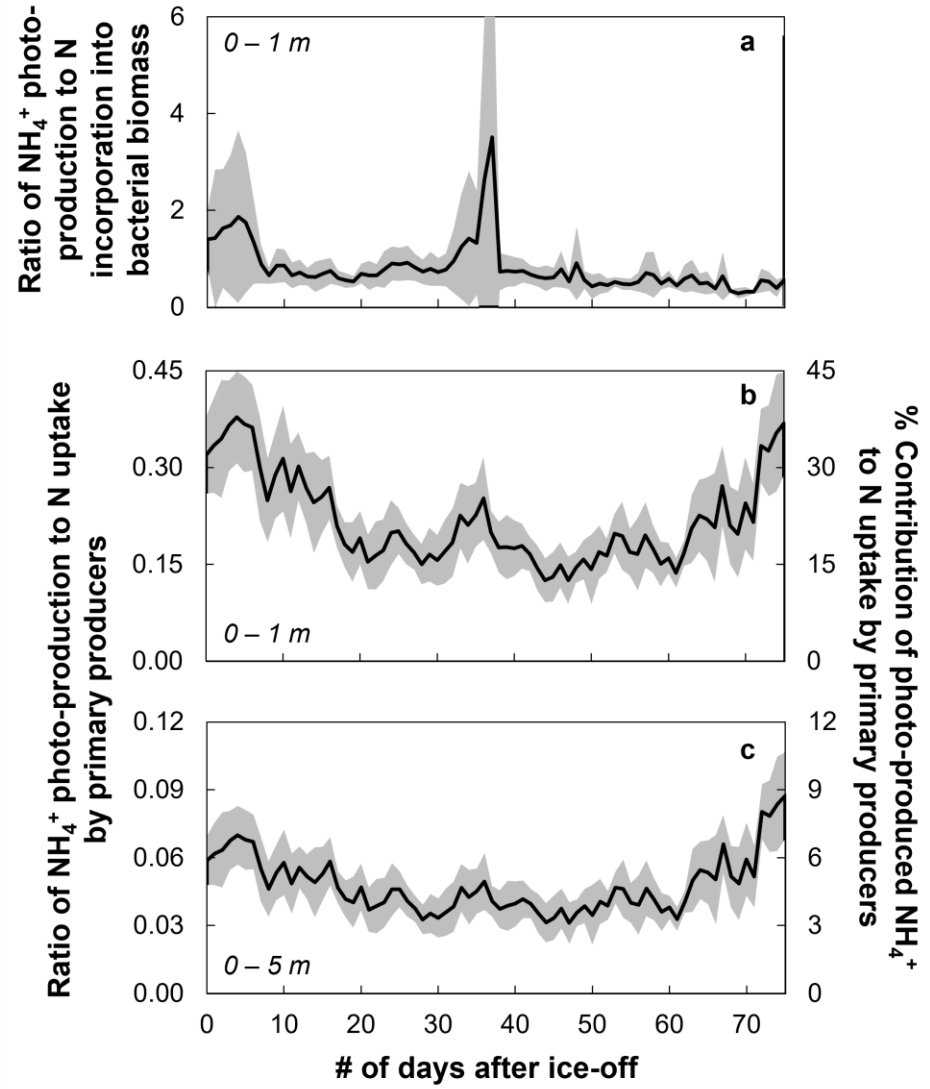

Figure 2.5. Ratios of NH_4^+ photo-production rates to N uptake by bacteria and primary producers in Toolik Lake. The ratios of daily water column rates of NH_4^+ photo-production (µmol N m^{-2} d^{-1}) to daily rates of (a) N incorporation into bacterial biomass (µmol N m^{-2} d^{-1}) and (b, c) N uptake by primary producers (µmol N m^{-2} d^{-1}) in the upper 1 m (a, b) and 5 m (c) of Toolik Lake are plotted versus the number of days after ice-off. Solid lines show the average ratio from 2011 to 2018 and shading shows the upper and lower 95% confidence intervals. A value of 1 on the primary y-axis indicates that NH_4^+ photo-production rates were equal to rates of N incorporation or uptake by microbes, whereas values close to 0.1 indicate that NH_4^+ photo-production rates were 10% of microbial N incorporation or uptake rates. The percent that photo-produced NH_4^+ could contribute to the N taken up by primary producers in the upper mixing layer of Toolik Lake is shown on the secondary y-axis in (b, c).

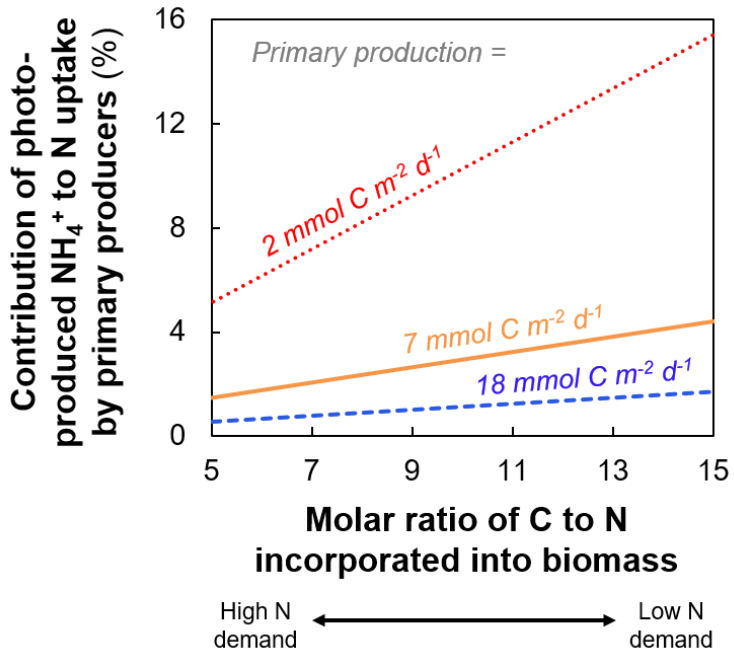

Figure 2.6. The contribution of photo-produced NH_4^+ to N uptake by primary producers depends on the molar ratio of C to N incorporated into their biomass and the rate of primary production. The percent that photo-produced NH_4^+ could contribute to N uptake by primary producers was calculated as the average daily rate of NH_4^+ photo-production during the ice-free summer in Toolik Lake (20 mmol N m^{-2} d^{-1}; Figure 2.4c) divided by the daily rate of N taken up by primary producers in the upper 5 m of the water column and multiplied by 100. The daily rate of N uptake was calculated using the minimum (2 mmol C m^{-2} d^{-1}; red dotted line), average (7 mmol C m^{-2} d^{-1}; orange solid line), and maximum (18 mmol C m^{-2} d^{-1}; blue dashed line) rates of primary production in the upper mixing layer of Toolik Lake (0-5 m; Figure 2.A.4)[50,71] and the range of potential molar ratios of C to N in the biomass of primary producers in arctic lakes (see Appendix Section 2.8.2).

Site	Date of collection	TDN (μM)	Molar C/N of DOM	Tryptophan -like C7 (RU)	Tyrosine -like C8 (RU)	Humic -like FDOM (RU)	Protein -like formulas* (%)
Imnavait Creek	28-May-18	29.7	62	0.39	0.23	5.98	4
	22-Jun-18	24.3	36	0.31	0.14	3.34	6
Kuparuk River	26-May-18	32.5	44	0.37	0.20	4.54	3
	30-May-18	22.3	44	0.29	0.13	3.26	6
	18-Jun-18	17.7	31	0.20	0.07	2.00	5
Sagavanirktok River	26-May-18	17.1	24	0.16	0.09	1.26	9
	30-May-18	14.1	21	0.13	0.08	0.96	8
Toolik Inlet Stream	15-May-18	27.7	24	0.28	0.18	1.95	9
	26-May-18	28.0	35	0.31	0.16	3.02	6
	8-Jun-18	13.1	30	0.18	0.09	1.44	7
	22-Jun-18	12.2	37	0.19	0.06	1.66	9
	13-Jul-18	12.6	29	0.20	0.06	1.21	9
Tussock Watershed Lower Stream	14-Jul-18	17.6	40	0.37	0.04	2.79	7
Toolik Lake (3 m)	9-May-18	16.9	25	0.23	0.08	1.15	11
Toolik Lake (16 m)	9-May-18	17.7	22	0.23	0.07	1.14	10
Coastal Plain Lake LS 1-05	27-Jun-18	16.3	18	0.10	0.12	0.41	8
Coastal Plain Lake LS 1-28	29-Jun-18	25.3	21	0.30	0.17	1.30	9
Coastal Plain Lake LHS 2-01	27-Jun-18	16.9	33	0.26	0.15	1.80	10
Coastal Plain Lake LHS 2-02	27-Jun-18	29.6	26	0.30	0.28	1.19	11

* Protein-like formulas were defined as those with H/C = 1.5 – 2.3, O/C = 0.3 – 0.55, and N ≥ 1.[39-40]

Table 2.1. Content and composition of DON in the surface waters used to test chemical controls on NH_4^+ photo-production. The abundance of tryptophan-like C7, tyrosine-like C8, and total humic-like FDOM are reported as the average of triplicate analyses in Raman Units (RU). The percent of protein-like formulas in the mass spectra are reported as the average of replicate acquisitions (n = 2 or 3) when replicate mass spectra were collected (Table 2.A.1). The concentration of TDN and molar C/N ratio of DOM are reported as the average of experimental replicate dark control waters (n = 3, 6 or 9; Table 2.2). DOC and TDN concentrations changed < 2% and < 6% in the dark control waters between sunlight exposure times, respectively (n = 17).

Site	Date of collection	Sunlight exposure time (hr)	Tryptophan -like C7 photo-degraded (%)	Tyrosine -like C8 photo-produced (%)	NH_4^+ photo-produced (μM)	DON photo-degraded (%)	$\varphi_{NH4+,350}$ (μmol N mol photon^{-1})
Imnavait Creek	28-May-18	12	25 ± 1	37 ± 4	1.37 ± 0.46	4.5 ± 1.2	11.5 ± 3.8
		24	35 ± 8	44 ± 15	0.96 ± 0.21	3.2 ± 0.8	-
		48	23 ± 2	20 ± 1	0.87 ± 0.23	2.9 ± 0.7	-
	22-Jun-18	12	-17 ± 2	11 ± 1	0.79 ± 0.01	3.3 ± 0.2	13.6 ± 0.2
Kuparuk River	26-May-18	12	16 ± 1	50 ± 1	0.67 ± 0.16	2.1 ± 0.5	10.8 ± 2.7
		24	29 ± 5	47 ± 16	0.76 ± 0.17	2.3 ± 0.5	-
		48	37 ± 1	56 ± 2	0.64 ± 0.07	2.0 ± 0.2	-
	30-May-18	12	16 ± 4	40 ± 8	0.62 ± 0.08	2.8 ± 0.3	9.8 ± 1.4
	18-Jun-18	10	27 ± 2	66 ± 4	0.22 ± 0.19	1.3 ± 1.1	6.7 ± 5.8
Sagavanirktok River	26-May-18	12	51 ± 5	12 ± 13	0.75 ± 0.22	3.4 ± 0.4	26.0 ± 7.5
		48	66 ± 1	24 ± 2	0.62 ± 0.04	3.5 ± 0.1	-
	30-May-18	12	39 ± 4	22 ± 10	0.11 ± 0.08	0.8 ± 0.5	5.9 ± 3.9
		23	51 ± 1	15 ± 6	0.41 ± 0.07	2.9 ± 0.5	12.6 ± 2.0
Toolik Inlet Stream	15-May-18	10	29 ± 2	21 ± 1	0.09 ± 0.06	0.3 ± 0.2	2.8 ± 1.8
		22	43 ± 1	13 ± 1	0.39 ± 0.16	1.5 ± 0.7	6.0 ± 2.5
	26-May-18	12	19 ± 3	29 ± 2	ND	ND	-
		24	31 ± 1	33 ± 1	0.61 ± 0.21	2.5 ± 0.9	6.6 ± 2.3
		48	42 ± 2	35 ± 7	0.93 ± 0.19	3.3 ± 0.7	5.4 ± 1.1
	8-Jun-18	12	39 ± 1	21 ± 6	ND	ND	-
		24	52 ± 1	24 ± 1	0.55 ± 0.15	4.5 ± 1.2	12.4 ± 3.4
	22-Jun-18	12	38 ± 1	62 ± 6	ND	ND	-
		20	44 ± 1	55 ± 5	0.85 ± 0.37	7.2 ± 2.8	21.0 ± 9.1
	13-Jul-18	15	39 ± 2	32 ± 12	0.76 ± 0.36	5.7 ± 2.5	39.9 ± 19.1
		26	50 ± 1	24 ± 4	0.97 ± 0.66	7.6 ± 5.2	-
Tussock Watershed Lower Stream	14-Jul-18	12	32 ± 1	128 ± 9	1.04 ± 0.12	5.9 ± 1.4	44.4 ± 5.0
Toolik Lake (3 m)	9-May-18	12	41 ± 4	29 ± 2	0.08 ± 0.07	0.5 ± 0.4	6.8 ± 6.0
		29	48 ± 1	32 ± 7	0.25 ± 0.07	1.5 ± 03	10.5 ± 3.0
Toolik Lake (16 m)	9-May-18	12	27 ± 1	24 ± 7	0.31 ± 0.20	1.8 ± 1.1	48.2 ± 30.7
Coastal Plain Lake LS 1-05	27-Jun-18	12	56 ± 1	ND	0.55 ± 0.02	3.4 ± 0.2	58.0 ± 2.7
Coastal Plain Lake LS 1-28	29-Jun-18	12	24 ± 1	11 ± 7	0.78 ± 0.14	3.1 ± 0.6	100.8 ± 18.2
Coastal Plain Lake LHS 2-01	27-Jun-18	12	40 ± 1	ND	0.98 ± 0.42	5.7 ± 2.3	23.8 ± 10.2
		20	43 ± 2	-6 ± 1	0.67 ± 0.15	4.0 ± 0.9	-
Coastal Plain Lake LHS 2-02	27-Jun-18	12	28 ± 1	2 ± 1	0.56 ± 0.10	1.9 ± 0.2	46.7 ± 8.3

Table 2.2. DON photodegradation and NH_4^+ photo-production following each sunlight exposure of surface waters. All values are reported as the average ± 1 standard error of experimental replicates (n = 3). Apparent quantum yields of NH_4^+ photo-production at 350 nm ($\varphi_{NH4+,350}$) were reported for waters when there were significant changes in NH_4^+ concentration relative to dark controls ($p < 0.05$). ND = not detectable.

Site	Integration depth (m)	Mid-summer NH_4^+ photo-production (μmol N m^{-2} d^{-1})	Ice-free summer average (μmol N m^{-2} d^{-1})	Ice-free summer range (μmol N m^{-2} d^{-1})
Imnavait Creek	0.5	31	29	4 – 61
Kuparuk River	0.5	22	20	3 – 43
Saganvanirktok River	0.5	33	31	5 – 66
Toolik Inlet Stream	0.5	31	29	4 – 62
Tussock Watershed Lower Stream	0.1	66	61	10 – 133
Toolik Lake	5	21	16	3 – 39
Coastal Plain Lake LS 1-05	1	116	75	17 – 148
Coastal Plain Lake LS 1-28	1	246	161	35 – 319
Coastal Plain Lake LHS 2-01	1	59	38	8 – 76
Coastal Plain Lake LHS 2-02	1	111	73	16 – 144

Table 2.3. Water column rates of NH_4^+ photo-production in each surface water in the summer of 2018. NH_4^+ photo-production was integrated over the water column depth of each surface water, except Toolik Lake where the average depth of the upper mixing layer was used (5 m).[50] The estimated rate of NH_4^+ photo-production (μmol N m^{-2} d^{-1}) was compared across all sites using mid-summer solar conditions on 15 July 2018. The ice-free summer average and range of estimated NH_4^+ photo-production rates (μmol N m^{-2} d^{-1}) are reported between a conservative estimate of ice-off in each surface water and the last date of photon flux measurements (26 September 2018). For instance, it was assumed that ice-off occurred on 15 July 2018 for the four Coastal Plain Lakes because prior work has reported ice-off dates between early- to late-July for lakes on the Alaskan Coastal Plain with depths > 1 m.[64,74-77] In 2018, ice-off on Toolik Lake occurred on 27 June (Table 2.A.3).

2.8 Appendix

2.8.1 Apparent quantum yields of NH_4^+ photo-production

2.8.1.1 Sunlight exposure times used to quantify NH_4^+ photo-production yields

NH_4^+ photo-production was quantified following up to three sunlight exposure times for two reasons. First, a minimum amount of light absorption by CDOM was needed to produce enough NH_4^+ to detect a change in its concentration. Second, NH_4^+ photo-production was also quantified using longer exposure times to estimate the maximum concentration of NH_4^+ that could be photo-produced from DON. Previous studies have showed that concentrations of photo-produced NH_4^+ increase with the amount of light exposure.[8,11,18,20] However, longer exposure times can result in no detectable changes in the concentration of NH_4^+ photo-produced.[8,20] This has been interpreted to mean that the most photo-labile components of the DON pool are degraded or altered after short exposure times, leaving behind less labile moieties with a lower capacity to form NH_4^+ per mole photon absorbed by CDOM.[78]

The change in photo-produced NH_4^+ with increasing sunlight exposure time was also used to identify which exposure times should not have a reported apparent quantum yield for NH_4^+ photo-production ($\varphi_{NH4+,\lambda}$). At longer exposure times where no additional NH_4^+ was photo-produced relative to the previous exposure time (yet more photons of light were absorbed), the values of $\varphi_{NH4+,\lambda}$ would decrease because they are calculated as the amount of NH_4^+ produced divided by more photons than were needed to produce that NH_4^+. Thus, values of $\varphi_{NH4+,\lambda}$ were not reported following longer exposure times when there were no detectable changes to the concentration of NH_4^+ photo-produced and a significant decrease in $\varphi_{NH4+,350}$ between consecutive sunlight exposure times of the same water sample.

2.8.1.2 The wavelength dependence of the NH_4^+ photo-production yield

Values of $\varphi_{NH4+,\lambda}$ were calculated from each sunlight exposure experiment in broadband sunlight (Figure 2.1) by modeling the spectral shape of the $\varphi_{NH4+,\lambda}$ (i.e., the magnitude of φ_{NH4+} at each wavelength of light) following Vähätalo et al. (2000).[48] The spectral shape used to model these $\varphi_{NH4+,\lambda}$ for each surface water was verified by directly measuring $\varphi_{NH4+,\lambda}$ at specific wavelengths of light emitted by light-emitting diodes (LED) for Toolik Lake water. Spectra were characterized at the Woods Hole Oceanographic Institution (WHOI) using Toolik Lake water that was collected in the summer of 2018. Briefly, Toolik Lake water collected at 3 and 16 m depths in this study (~1 L total, 0.2 μm filtered; Table 2.1) was shipped overnight to the WHOI and then stored at 4 ºC. To achieve a total starting volume > 2 L, leftover GF/F filtered water (~10 mL) from weekly nitrate analyses of Toolik Lake water at 0, 1, 3, 5, 8, 12, 16, and 20 m depths from June to October 2018 (n = 127)[72] was also used in the experiment. This water was stored frozen in low-density polyethylene bottles at the Marine Biological Laboratory before and after nitrate analysis.[72] At WHOI the frozen water in each bottle was thawed to room temperature, combined in a pre-combusted (450 ºC; 4 h) 2.5-L glass amber bottle, and then filtered through a sterile, 0.2 μm filter (Sterivex, Millipore) pre-rinsed with MilliQ water (Millipore Simplicity ultraviolet, UV, system) into a new, pre-combusted 2.5-L glass amber bottle. The leftover Toolik Lake water from the current study was added to the same glass bottle and then the pooled water was stored at 4 ºC until the $\varphi_{NH4+,\lambda}$ experiments.

Two $\varphi_{NH4+,\lambda}$ spectra were measured at individual wavelengths using custom-built high-powered (≥100 mW), narrow-banded (±10 nm) light-emitting diode (LED) reactors.[73] For each spectrum, the pooled Toolik Lake water was brought to room temperature (within 24 hours) and then 170 mL were placed in 6 pre-combusted (450 °C; 4 hour) 250-mL glass beakers. A quartz

plate was placed over the top of each beaker, where rolled up polytetrafluoroethylene (PTFE) tape was used to create a ~20 mm gap between the beaker and the plate to prevent condensation under the plate. The water was then exposed to LEDs at 278, 309, 348, 369, and 406 nm (LG Innotek 6060 Series) alongside a dark control for 12 or 40 hours, where one beaker was placed under each LED or dark-control reactor.[73] Immediately after exposure, water from each beaker was analyzed in triplicate for NH_4^+, CDOM, and FDOM (see Method Sections 2.3.1.2 and 2.3.1.4). Triplicate aliquots from each beaker were also immediately preserved with 6 N HCl and stored at 4 °C in three clean 30-mL amber HDPE bottles until shipment to the University of Michigan for triplicate total dissolved nitrogen (TDN) analyses (see Method Section 2.3.1.4). There were no statistically significant changes in TDN concentration during light exposure relative to dark controls ($p > 0.05$; data not shown).

The $\varphi_{NH4+,\lambda}$ at each wavelength was calculated as the concentration of NH_4^+ photo-produced multiplied by the pathlength of water in the beaker (6.5 cm) and divided by the amount of light absorbed by CDOM in each beaker. The amount of light absorbed by CDOM ($Q_{a\lambda}$; mol photons m^{-2}) was calculated using the total photon flux spectrum reaching the water surface, the $a_{CDOM,\lambda}$ of the light-exposed and dark-control waters, and the pathlength of water in the beaker following Eq. (1). The photon flux spectrum was calculated from the solar irradiance measured from each LED following Bowen et al. (2020),[79] which was validated by chemical actinometry.[73] Briefly, the solar irradiance spectrum (W m^{-2} nm^{-1}) was measured in triplicate at the same height as the water surface in the 250-mL beaker in four positions within the outer aluminum housing with a radiometer over wavelengths from 250 to 500 nm (NIST-Calibrated Black Comet Spectral Radiometer, StellarNet, Inc.). Each spectrum (W m^{-2} nm^{-1}) was converted to a photon flux spectrum (mol photon m^{-2} s^{-1} nm^{-1}). Replicate photon flux spectra for the light exposure period

($E_{0,\lambda}$; mol photon m^{-2} nm^{-1}) were calculated as the average of all 12 measurements multiplied by the light exposure time. There was a < 5% CV in the photon flux spectrum across space within the outer aluminum housing.[79] Values of $\varphi_{NH4+,\lambda}$ are reported as the average ± 1 SE of replicate measurements (n = 3).

The irradiances received by the Toolik Lake water at each wavelength were selected to achieve similar amounts of light absorbed by CDOM in each beaker.[79] For example, photon doses ranged from 0.5 mol photon m^{-2} at 278 nm to 3 mol photon m^{-2} at 406 nm, resulting in an average of 0.37 ± 0.01 mol photon m^{-2} of light absorbed by CDOM in the water across the five wavelengths during the 12-hour exposure (± 1 SE; n = 5). In addition, photon doses ranged from 2 mol photon m^{-2} at 278 nm to 10 mol photon m^{-2} at 406 nm, resulting in an average of 1.62 ± 0.10 mol photon m^{-2} of light absorbed by CDOM in the water across all wavelengths during the 40-hour exposure (± 1 SE; n = 5).

2.8.2 N uptake and incorporation into bacterial and algal biomass in Toolik Lake

2.8.2.1 Molar C/N ratio used to calculate rates of N incorporation into bacterial biomass

The biomass of native bacterial communities in lakes can have molar C/N ratios ranging from 5 to 16.[80-85] However, two lines of evidence suggest that bacteria demand lower amounts of N relative to C in Toolik Lake, resulting in higher C/N ratios incorporated in their biomass. First, previous studies report higher molar C/N ratios of bacterial biomass in oligotrophic lakes than in mesotrophic and eutrophic lakes.[80-81,83] Second, laboratory studies with cultures of P-limited lake bacteria show that molar C/N ratios of bacterial biomass can increase up to 2-fold under conditions with low P availability (i.e., molar ratios of DOC to total dissolved P, or C/P, > 1000) compared to those with high P availability (C/P < 200).[85-86] Given that Toolik Lake is ultra-oligotrophic, is typically P limited and sometimes P and N co-limited,[13,87] and has molar

ratios of DOC to total dissolved P exceeding 1500 throughout the summer season,[72] it is likely that the molar C/N ratios of bacterial biomass in Toolik Lake fall in the upper range of values reported in the literature (closer to ~16).[83] Thus, it was assumed that bacterial biomass had a molar C/N ratio of 16 in Toolik Lake.

2.8.2.2 Rates of N uptake into algal biomass

Daily rates of DIN uptake by primary producers in Toolik Lake in the summers of 2011-2018 were estimated using rates previously reported for other years in Toolik Lake[54-55] instead of using the depth-integrated primary production rates for 2011-2018[71] and previously reported molar C/N ratios of algal biomass in other arctic lakes. DIN uptake rates were used for two reasons. First, previously reported C/N ratios for algal biomass in arctic lakes have been estimated from the C and N contents of the seston pool (>1 μm size fraction),[88-90] which can include algal cells as well as non-algal particulate organic matter. In oligotrophic lakes like Toolik Lake, the abundance of non-algal particulate organic matter can exceed that of algal biomass.[82,91-92] For example, Dodds and Priscu (1990) estimated that 60-70% of C and N in the > 1 μm size fraction comes from non-algal material in an oligotrophic lake.[91] As a result, molar C/N ratios of the seston pool in oligotrophic lakes may reflect the stoichiometry of the non-algal particulate pool, not the biomass of primary producers.

Second, previously reported C/N ratios for algal biomass in arctic lakes were estimated from a handful of measurements made during the middle of the ice-free season (1-3 measurements in July),[4,7,88-90,93] which can bias the molar C/N ratios. For instance, the molar ratios of C/N in algal biomass in arctic lakes from this prior work range from 4 to 13.[4,7,88-90,93] Yet, it has been shown that C/N ratios of algal biomass in oligotrophic lakes are highest in early summer (molar C/N ratio of 20) and decrease throughout the summer.[91] Thus, previously

reported C/N ratios for algal biomass in arctic lakes could overestimate rates of N incorporation into biomass at the beginning and end of the ice-free season because the molar C/N ratios have only been measured in the middle of the ice-free season. The algal biomass in arctic lakes could have molar C/N ratios ranging from 4 to 20 during the ice-free summer season.

2.8.3 Surface water DOM chemistry prior to sunlight exposure

2.8.3.1 The chemical properties of formulas in the mass spectra

The chemical properties of formulas in the solid-phase extracted DOM from surface waters in this study were consistent with those observed from proxies for the N-content and aromaticity of DOM. For example, there were significant, negative linear relationships between the molar C/N ratio of DOM and the percentages of N-containing and protein-like formulas ($p < 0.05$). In contrast, there were no significant correlations between the molar C/N ratio of DOM and the other measures of DOM composition in the mass spectra (Tables 2.1, 2.A.4). In addition, $SUVA_{254}$ had a significant, positive correlation with the percentage of aromatic formulas ($p < 0.05$), significant negative correlations with the percentages of unsaturated hydrocarbon-like and protein-like formulas ($p < 0.05$), and no significant correlations with any other measure of DOM composition in the mass spectra (Tables 2.1, 2.A.4, 2.A.5).

The compound class assignments for formulas in the mass spectra were also consistent with proxies for protein-like compounds and the molecular weight of DOM. For example, the percentage of amino acid-like FDOM and the S_R both had significant, positive correlations with the percentage of protein-like formulas ($p < 0.001$), significant negative correlations with the percentage of aromatic formulas ($p < 0.05$), and no significant correlations with any other measure of DOM composition in the mass spectra (Tables 2.1, 2.A.4, 2.A.5). These findings are consistent with protein-like compounds being made up of amino acids that are mostly aliphatic[94]

and having a lower molecular weight compared to terrestrially-derived compounds that make up the rest of the DOM pool.[95-96]

2.8.3.2 Patterns in DOM chemistry across sites

The surface waters sampled ranged in DOM concentration and composition consistent with patterns previously observed across the Arctic.[1,30,32] For example, there were significant, negative linear relationships between the molar C/N ratio of DOM versus S_R, the percentage of amino acid-like FDOM, and the ratio of tryptophan-like C7 to humic-like FDOM ($p < 0.05$; Tables 2.1, 2.A.5). In addition, there were significant, positive linear relationships between the molar C/N ratio of DOM versus a_{305}, humic-like FDOM, and tryptophan-like C7 ($p < 0.05$; Tables 2.1, 2.A.5). DOC, a_{305}, and humic-like FDOM each had significant positive correlations with the percentage of lipid-like formulas ($p < 0.05$), significant negative correlations with the percentages of N-containing, protein-like, amino sugar-like, and unsaturated hydrocarbon-like formulas ($p < 0.05$), and no significant correlations with any other measure of DOM composition in the mass spectra (Tables 2.1, 2.A.4, 2.A.5). Together, these findings are consistent with more N-rich, low molecular weight DOM being observed in arctic lakes with lower concentrations of DOC compared to arctic streams and rivers.[1,30,32]

2.8.4 Contribution of photo-produced NH_4^+ to the N demand by primary producers in Coastal Plain lakes

Because direct measures of DIN uptake rates by primary producers have only been reported for Toolik Lake, DIN uptake rates for lakes on the Alaskan Coastal Plain were estimated from previously reported primary production rates and molar C/N ratios for algal biomass in other arctic lakes. Briefly, the range of daily rates of primary production previously reported for Coastal Plain lakes with depths > 1 m (2 to 66 mmol C m^{-2} d^{-1})[74] were used to

estimate DIN uptake rates because the four lakes on the Alaskan Coastal Plain sampled in this study had depths > 1 m (Table 2.1). This range of primary production rates was consistent with those previously reported in more shallow ponds on the Alaskan Coastal Plain (from 0.2 to 62 mmol C m^{-2} d^{-1}).[7,65,74,97-99] A molar C/N ratio of 9 for algal biomass, which is the average of literature values reported for arctic lakes (see Appendix Section 2.8.2), was used to convert primary production rates to N uptake rates. The range of daily rates of N uptake by primary producers in Coastal Plain lakes was calculated by dividing the minimum, average, and maximum daily primary production rates from prior work (mmol C m^{-2} d^{-1}) by the average molar ratio of C to N in algal biomass.

The potential contribution of photo-produced NH_4^+ to N uptake by primary producers in these lakes was estimated using this range of daily N uptake rates and the range of daily NH_4^+ photo-production rates estimated in this study (Table 2.3). Using the average daily rate of NH_4^+ photo-production in the Coastal Plain lakes during the ice-free summer of 2018 (87 µmol N m^{-2} d^{-1}; Table 2.3) and the maximum and minimum rates of primary production, photo-produced NH_4^+ could account for 1 to 44% of the N required by primary producers in these lakes. Using the average daily rate of primary production (11 mmol C m^{-2} d^{-1}; n = 3 lakes)[74] and the maximum and minimum rates of NH_4^+ photo-production, photo-produced NH_4^+ could account for 1 to 25% of the N required by primary producers. On average, NH_4^+ photo-production may contribute 7% of the N taken up by primary producers in lakes on the Alaskan Coastal Plain.

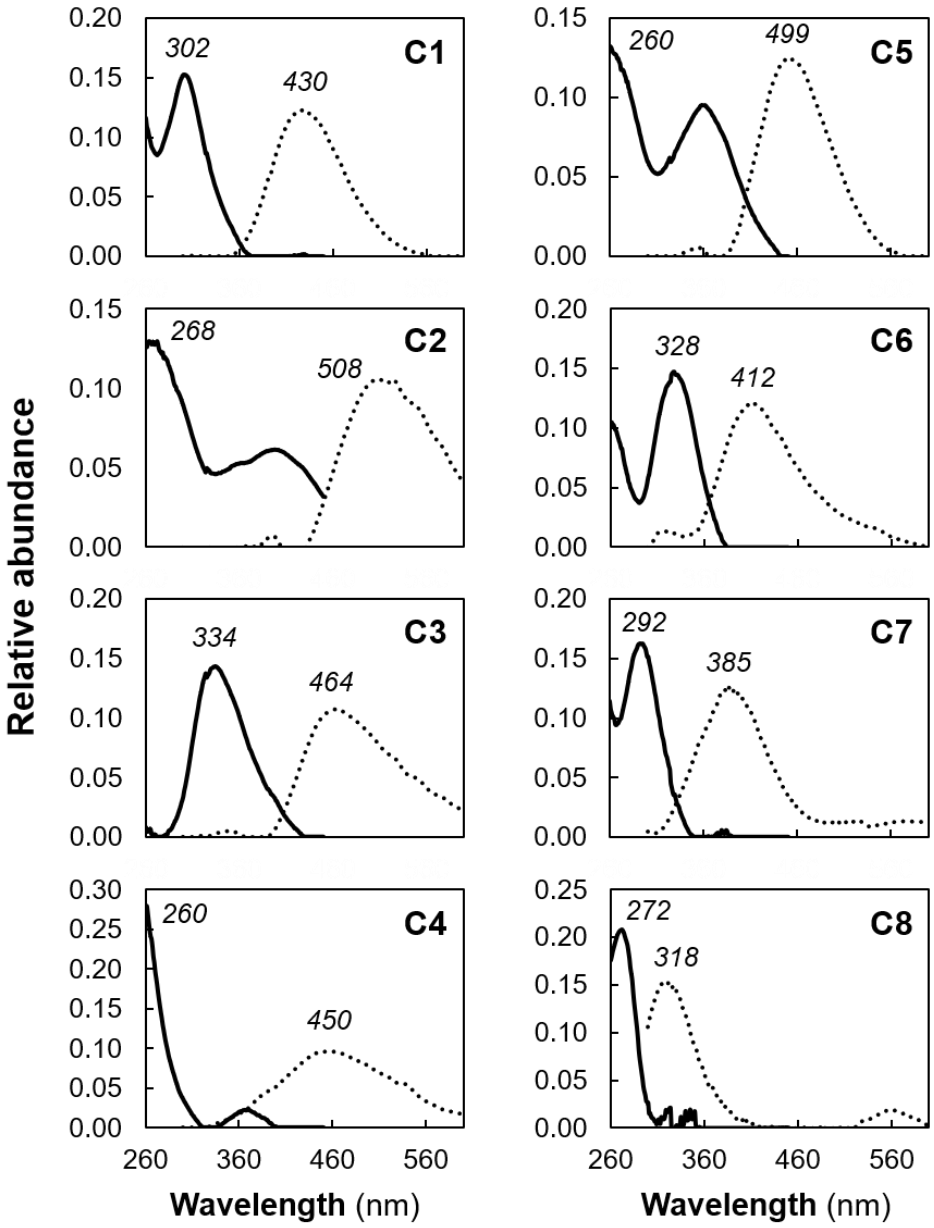

Figure 2.A.1. Fluorescence signatures of the eight PARAFAC components identified in the data set of surface water EEMs in this study. The excitation (solid line) and emission (dotted line) spectra for each component were validated using split-half analysis and then compared to the entire data set. The relative abundance of each component is plotted on the y-axis versus the excitation or emission wavelength on the x-axis. The wavelength at which primary excitation and emission maxima were observed for each component are reported in each panel in nanometers.

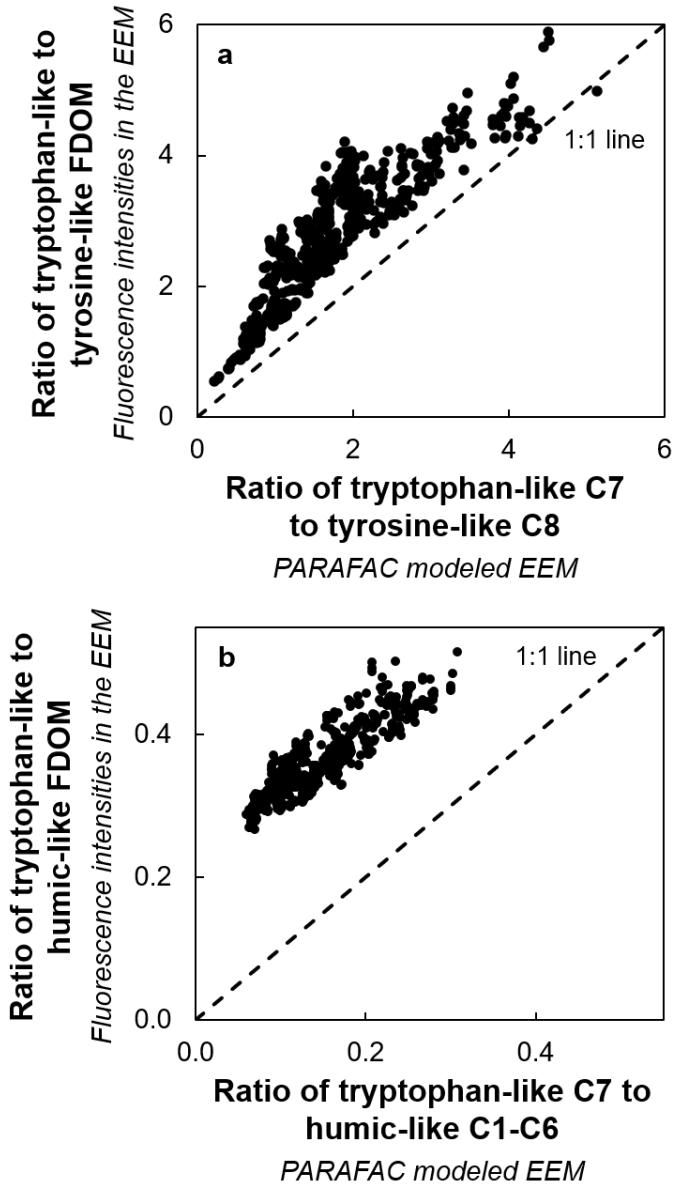

Figure 2.A.2. Ratios of tryptophan-like FDOM to tyrosine-like and humic-like FDOM estimated from original versus PARAFAC-modelled EEMs. Ratios of tryptophan-like FDOM to (a) tyrosine-like and (b) humic-like FDOM in the initial, light-exposed, and dark control surface waters estimated from PARAFAC-modeled excitation-emission matrices (EEM; x-axis) plotted versus the original EEM (y-axis) with a 1:1 line. Relative abundances of tryptophan-like, tyrosine-like, and humic-like FDOM in the PARAFAC-modeled EEM were estimated from the maximum fluorescence of C7, C8, and C1-C6, respectively, in Raman Units (RU). Fluorescence intensities of tryptophan-like, tyrosine-like, and humic-like FDOM in the original EEM were obtained at excitation / emission wavelengths of 292 / 385 nm, 272 / 318 nm, and 250 / 450 nm respectively (in RU; Figure 2.A.1). When the data in each panel are fit using a least-squares regression, $R^2 > 0.73$, $p < 0.001$.

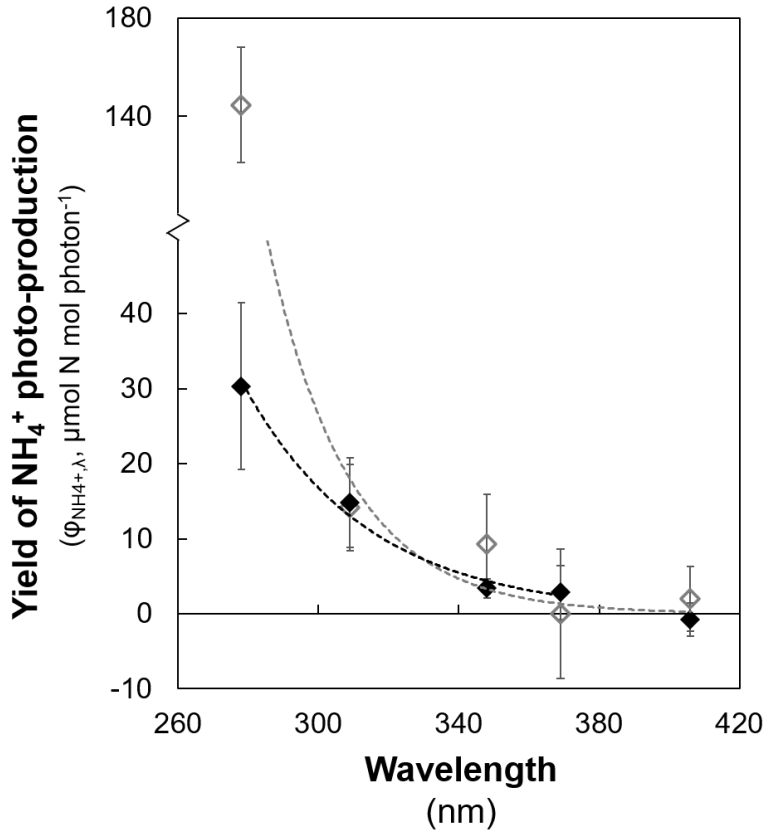

Figure 2.A.3. Wavelength-dependent apparent quantum yield spectra for NH_4^+ photo-production in Toolik Lake water. The apparent quantum yields for NH_4^+ photo-production ($\varphi_{NH4+,\lambda}$) are shown following 12 (gray symbols) and 40 (black symbols) hour exposures to light-emitting diodes (LEDs) at 278, 309, 348, 369, and 406 nm. The data in each series were fit with a least-squares exponential model, where $p < 0.001$. All values are the average ± 1 standard error of replicate measurements ($n = 3$).

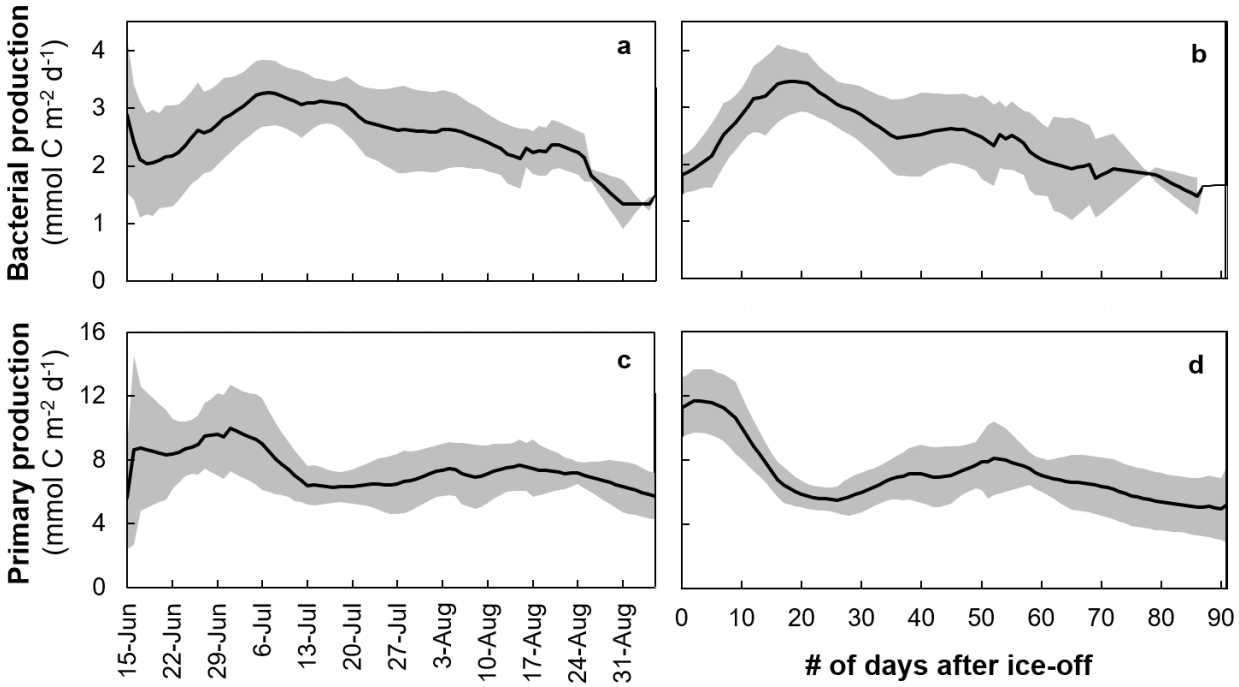

Figure 2.A.4. Bacterial and primary production rates in the upper mixing layer of Toolik Lake. Daily water column rates of (a, b) bacterial production and (c, d) primary production in the top 5 m of Toolik Lake are plotted versus the (a, c) date and (b, d) number of days after ice-off. Depth-integrated primary production rates in the top 5 m of Toolik Lake were calculated from weekly measures of primary production using the ^{14}C method[13] at 0, 1, 3, and 5 m depths from 2011 to 2018 by the Arctic LTER[71] as described in the Methods (Section 2.3.2.2). Solid lines show the average ratio from 2011 to 2018 and shading shows the upper and lower 95% confidence intervals.

Site	Date of collection	n	Total formulas (#)	MW	O/C ratio	H/C ratio	Protein-like formulas* (%)	Common formulas (%)
Kuparuk River	26-May-18	2	1721 ± 10	439 ± 2	0.33 ± 0.01	1.33 ± 0.01	3.3 ± 0.2	85 ± 1
	18-Jun-18	2	3265 ± 18	478 ± 1	0.43 ± 0.01	1.22 ± 0.01	5.3 ± 0.2	72 ± 1
Sagavanirktok River	26-May-18	3	2104 ± 181	472 ± 2	0.38 ± 0.01	1.27 ± 0.01	9.2 ± 0.1	74 ± 7
Toolik Inlet Stream	15-May-18	2	2553 ± 38	471 ± 4	0.36 ± 0.01	1.31 ± 0.01	9.1 ± 0.3	79 ± 1
	26-May-18	3	1607 ± 71	446 ± 3	0.34 ± 0.01	1.30 ± 0.01	5.9 ± 0.2	46 ± 2
Toolik Lake (3 m)	9-May-18	3	2426 ± 100	503 ± 2	0.34 ± 0.01	1.34 ± 0.01	10.6 ± 0.4	67 ± 3
Coastal Plain Lake LHS 2-01	27-Jun-18	3	2105 ± 55	476 ± 2	0.34 ± 0.01	1.33 ± 0.01	9.7 ± 0.2	76 ± 2

MW = molecular weight.
*Protein-like formulas were defined as those with H/C = 1.5 – 2.3, O/C = 0.3 – 0.55, and N ≥ 1.[39-40]

Table 2.A.1. Reproducibility of FT-ICR MS data for seven of the surface water samples used to test chemical controls on NH_4^+ photo-production. All values are reported as the average ± 1 standard error of replicate acquisitions (n = 2 or 3). The percent of common formulas was calculated as the number of formulas present in all replicate acquisitions divided by the total number of formulas assigned in each acquisition multiplied by 100.

Site	Date of collection	Sunlight exposure time (hr)	Photon dose (mol photon m^{-2})	Light absorbed by CDOM (mol photon m^{-2})	Photodegraded (%)				
					DOC	*a305*	S_R	$SUVA_{254}$	*FI*
Imnavait Creek	28-May-18	12	52	4.72 ± 0.01	13 ± 1	27 ± 1	-36 ± 1	7 ± 1	18 ± 1
		24	97	8.38 ± 0.05	17 ± 1	39 ± 1	-49 ± 1	14 ± 1	21 ± 1
		48	184	13.95 ± 0.19	22 ± 1	56 ± 1	-68 ± 1	30 ± 1	20 ± 1
	22-Jun-18	12	41	2.33 ± 0.04	12 ± 3	25 ± 1	-22 ± 1	8 ± 3	12 ± 1
Kuparuk River	26-May-18	12	31	3.18 ± 0.04	8 ± 1	13 ± 1	-28 ± 1	ND	14 ± 1
		24	67	6.44 ± 0.01	11 ± 1	24 ± 1	-42 ± 1	2 ± 1	19 ± 1
		48	132	12.04 ± 0.04	15 ± 2	37 ± 1	-60 ± 1	10 ± 2	24 ± 1
	30-May-18	12	41	2.56 ± 0.02	8 ± 1	23 ± 1	-31 ± 2	6 ± 1	17 ± 1
	18-Jun-18	10	35	1.22 ± 0.01	8 ± 1	21 ± 1	-38 ± 1	2 ± 1	16 ± 1
Sagavanirktok River	26-May-18	12	52	0.89 ± 0.03	9 ± 2	25 ± 1	-25 ± 1	2 ± 1	11 ± 1
		48	184	2.25 ± 0.14	11 ± 1	50 ± 1	-52 ± 4	17 ± 1	13 ± 1
	30-May-18	12	41	0.64 ± 0.01	6 ± 2	23 ± 1	-27 ± 2	5 ± 3	12 ± 1
		23	77	1.07 ± 0.01	7 ± 1	35 ± 1	-41 ± 1	10 ± 2	13 ± 1
Toolik Inlet Stream	15-May-18	10	35	1.18 ± 0.01	5 ± 1	20 ± 1	-23 ± 1	4 ± 1	14 ± 1
		22	79	2.40 ± 0.03	6 ± 1	33 ± 1	-34 ± 1	11 ± 1	15 ± 1
	26-May-18	12	31	2.19 ± 0.02	8 ± 2	14 ± 1	-20 ± 1	ND	12 ± 1
		24	67	4.48 ± 0.06	9 ± 1	23 ± 1	-29 ± 1	3 ± 1	16 ± 1
		48	132	8.14 ± 0.02	13 ± 1	35 ± 1	-44 ± 1	9 ± 1	18 ± 1
	8-Jun-18	12	55	0.88 ± 0.02	6 ± 1	25 ± 1	-25 ± 2	7 ± 1	10 ± 1
		24	99	1.39 ± 0.02	8 ± 1	37 ± 1	-35 ± 1	13 ± 1	12 ± 1
	22-Jun-18	12	52	1.04 ± 0.01	7 ± 1	24 ± 1	-30 ± 1	5 ± 2	12 ± 1
		20	70	1.42 ± 0.01	9 ± 1	30 ± 1	-33 ± 1	8 ± 1	15 ± 1
	13-Jul-18	15	42	0.59 ± 0.01	4 ± 1	18 ± 1	-28 ± 2	4 ± 2	8 ± 1
		26	76	1.02 ± 0.03	8 ± 1	28 ± 1	-38 ± 3	6 ± 1	10 ± 1
Tussock Watershed Lower Stream	14-Jul-18	10	33	0.73 ± 0.01	7 ± 1	20 ± 1	-40 ± 1	2 ± 1	14 ± 1
Toolik Lake (3 m)	9-May-18	12	26	0.39 ± 0.01	ND	12 ± 1	-22 ± 2	3 ± 1	8 ± 1
		29	54	0.74 ± 0.01	4 ± 1	20 ± 1	-28 ± 1	6 ± 1	12 ± 1
Toolik Lake (16 m)	9-May-18	12	22	0.20 ± 0.02	2 ± 1	10 ± 2	-26 ± 5	2 ± 1	7 ± 2
Coastal Plain Lake LS 1-05	27-Jun-18	12	55	0.35 ± 0.03	2 ± 2	22 ± 1	-10 ± 5	9 ± 1	ND
Coastal Plain Lake LS 1-28	29-Jun-18	12	22	0.24 ± 0.01	3 ± 1	9 ± 1	-12 ± 1	ND	5 ± 1
Coastal Plain Lake LHS 2-01	27-Jun-18	12	52	1.59 ± 0.02	5 ± 1	22 ± 1	-20 ± 1	8 ± 1	12 ± 1
		20	69	2.03 ± 0.01	6 ± 1	26 ± 1	-24 ± 1	11 ± 1	14 ± 1
Coastal Plain Lake LHS 2-02	27-Jun-18	12	31	0.36 ± 0.01	ND	11 ± 1	-8 ± 2	4 ± 1	6 ± 1

Table 2.A.2. The total photon dose, amount of light absorbed by CDOM in the quartz tubes, and percentages of DOM photodegraded during each sunlight exposure experiment. Photodegradation of DOC, the Naperian absorption coefficient at 305 nm (a_{305}), the spectral slope ratio (S_R), the specific UV absorbance at 254 nm ($SUVA_{254}$), and the fluorescence index (FI) were calculated as the percent removed during sunlight exposure relative to dark controls. Values are reported as the average ± 1 standard error of experimental replicates (n = 3).

Year	Ice-off	Ice-on	Ice-free days (#)	Peak bacterial production (0 – 5 m)	Average bacterial production (0 – 16 m; mmol C m^{-2} d^{-1})	Peak primary production (0 – 5 m)	Average primary production (0 – 12 m; mmol C m^{-2} d^{-1})
2011	16-Jun	15-Oct	121	8-Jul	9	24-Jun	15
2012	17-Jun	15-Oct	120	20-Jul	5	22-Jun	17
2013	28-Jun	2-Oct	96	19-Jul	8	6-Jul	15
2014	24-Jun	4-Oct	102	18-Jul	6	27-Jun	12
2015	10-Jun	27-Sep	109	26-Jun	9	24-Jul	10
2016	26-Jun	14-Oct	110	8-Jul	7	1-Jul	17
2017	18-Jun	29-Sep	103	7-Jul	9	18-Jun	17
2018	27-Jun	15-Oct	110	13-Jul	9	6-Jul	21

Table 2.A.3. Date of peak production and average daily rate for bacterial and primary production in Toolik Lake during the ice-free summers of 2011-2018. Ice-off is reported as the date of ice thaw on Toolik Lake and ice-on is reported as the date when the lake became 100% iced over (reported by the Toolik Field Station Environmental Data Center; https://toolik.alaska.edu/edc/journal/annual_summaries.php). The date of peak production in the upper mixing layer of Toolik Lake (0-5 m)[50] is reported for each year. Daily, depth-integrated rates of bacterial and primary production in the upper 16 and 12 m of Toolik Lake, respectively, were estimated from weekly production measurements at depths of 0, 1, 3, 5, 8, 12, or 16 m from 2011 to 2018 by the Arctic LTER[51-52,71] as described in the Methods Section 2.3.2.2. The average daily rates for bacterial and primary production are reported for the first 20 days following ice-off each year.

Site	Date of collection	MW	O/C	H/C	Aromatic* (%)	N-containing† (%)	Lignin (%)	Cond. aromatic (%)	Unsat HC (%)	Lipid (%)	Amino sugar (%)
Imnavait Creek	28-May-18	420	0.32	1.33	16	9	58	3	1	20	1
	22-Jun-18	442	0.40	1.25	19	22	62	4	1	8	2
Kuparuk River	26-May-18	439	0.33	1.33	16	10	57	3	1	19	1
	30-May-18	452	0.38	1.27	19	18	58	4	1	10	1
	18-Jun-18	478	0.43	1.22	21	33	57	5	3	4	3
Sagavanirktok River	26-May-18	472	0.38	1.27	17	25	58	4	3	8	2
	30-May-18	479	0.42	1.27	16	27	59	3	3	5	3
Toolik Inlet Stream	15-May-18	471	0.36	1.31	17	24	55	4	3	13	1
	26-May-18	446	0.34	1.30	18	16	58	3	3	14	1
	8-Jun-18	467	0.40	1.26	19	29	58	5	3	7	3
	22-Jun-18	484	0.36	1.28	17	24	59	4	3	9	1
	13-Jul-18	493	0.36	1.29	17	27	60	3	3	9	2
Tussock Watershed Lower Stream	14-Jul-18	509	0.43	1.25	15	38	59	2	4	3	3
Toolik Lake (3 m)	9-May-18	503	0.34	1.34	13	27	60	2	3	11	1
Toolik Lake (16 m)	9-May-18	494	0.37	1.31	13	28	64	2	3	7	2
Coastal Plain Lake LS 1-05	27-Jun-18	456	0.35	1.31	17	23	55	4	2	14	1
Coastal Plain Lake LS 1-28	29-Jun-18	480	0.38	1.29	16	31	60	3	3	8	2
Coastal Plain Lake LHS 2-01	27-Jun-18	476	0.34	1.33	14	21	61	2	2	12	1
Coastal Plain Lake LHS 2-02	27-Jun-18	496	0.34	1.37	13	28	54	2	4	15	2

MW = molecular weight; Cond. aromatic = condensed aromatic; Unsat. HC = unsaturated hydrocarbon.
* Aromatic formulas were identified from the modified aromaticity index (AI_{MOD}) following Koch and Dittmar (2006).[100]
† N-containing formulas were defined as any formula with $N \geq 1$.

Compound classes were assigned to formulas as follows: Lignin-like formulas, $H/C = 0.8 – 1.5$, $O/C = 0.13 – 0.65$, $AI_{MOD} < 0.67$; Condensed aromatic-like, $H/C = 0.2 – 0.8$, $O/C = 0 – 1.0$, $AI_{MOD} \geq 0.67$; Unsaturated hydrocarbon-like, $H/C = 0.8 – 1.5$, $O/C = 0 – 0.13$; Lipid-like formulas, $H/C = 1.5 – 2.5$, $O/C = 0 – 0.3$; Amino sugar-like, $H/C = 1.5 – 2.3$, $O/C = 0.55 – 0.7$.[39-40]
Percentages of carbohydrate-like ($H/C = 1.5 – 2.2$, $O/C = 0.7 – 1.2$) and tannin-like formulas ($H/C = 0.8 – 1.5$, $O/C = 0.65 – 1.2$)[39-40] are not shown.
Percentages of protein-like formulas are reported in Table 2.1.

Table 2.A.4. Chemical properties of formulas assigned in the mass spectra for surface water DOM used to test chemical controls on NH_4^+ photo-production. Values are reported as the average of replicate measurements (n = 2 or 3) when replicate mass spectra were collected (Table 2.A.1).

Site	Date of collection	pH	SC (µS cm^{-1})	a_{305} (m^{-1})	S_R	$SUVA_{254}$ (L mg^{-1} C m^{-1})	FI
Imnavait Creek	28-May-18	4.95	14.3	98.5	0.73	3.67	1.46
	22-Jun-18	5.33	9.7	51.6	0.75	3.89	1.52
Kuparuk River	26-May-18	7.04	35.9	72.4	0.75	3.36	1.49
	30-May-18	6.76	25.7	54.7	0.74	3.55	1.46
	18-Jun-18	6.91	32.8	30.4	0.75	3.73	1.50
Sagavanirktok River	26-May-18	8.26	204.0	18.6	0.89	3.06	1.49
	30-May-18	8.24	183.0	13.7	0.87	3.17	1.50
Toolik Inlet Stream	15-May-18	7.51	98.4	27.9	0.86	2.99	1.55
	26-May-18	7.69	59.5	46.5	0.81	3.25	1.49
	8-Jun-18	7.49	46.9	17.2	0.84	3.19	1.46
	22-Jun-18	7.43	54.3	20.8	0.85	3.44	1.49
	13-Jul-18	7.02	88.7	13.5	0.93	2.85	1.50
Tussock Watershed Lower Stream	14-Jul-18	6.66	39.2	26.5	0.77	3.00	1.59
Toolik Lake (3 m)	9-May-18	7.07	109.0	11.5	0.99	2.53	1.52
Toolik Lake (16 m)	9-May-18	6.85	112.6	10.1	0.96	2.42	1.53
Coastal Plain Lake LS 1-05	27-Jun-18	7.64	92.3	5.3	1.11	1.65	1.46
Coastal Plain Lake LS 1-28	29-Jun-18	7.54	125.6	12.3	1.17	2.16	1.52
Coastal Plain Lake LHS 2-01	27-Jun-18	7.41	56.9	26.6	0.86	3.46	1.49
Coastal Plain Lake LHS 2-02	27-Jun-18	7.77	90.3	13.2	1.17	1.82	1.46

Table 2.A.5. Water and aromatic DOM chemistry in the surface waters used to test chemical controls on NH_4^+ photo-production. The Naperian absorption coefficient at 305 nm (a_{305}), spectral slope ratio (S_R), and the fluorescence index (FI) are reported as the average of triplicate analyses. The specific UV absorbance at 254 nm ($SUVA_{254}$) are reported as the average of experimental replicate dark control waters (n = 3, 6 or 9; Table 2.A.2). The absorbance at 254 nm (A_{254}) and DOC concentration changed < 1% and < 2% in the dark control waters between sunlight exposure times, respectively (n = 17).

2.9 References

1. Kling, G. W., G. W. Kipphut, M. M. Miller, and W. J. O'Brien (2000). Integration of lakes and streams in a landscape perspective: The importance of material processing on spatial patterns and temporal coherence. *Freshw. Biol.* 43: 477-497.

2. Hobbie, J. E., and G. W. Kling (Eds.). (2014). *Alaska's Changing Arctic: Ecological Consequences for Tundra, Streams, and Lakes.* Oxford, UK: Oxford University Press.

3. Kling, G. W. (1995). Land-Water Interactions: The Influence of Terrestrial Diversity on Aquatic Ecosystems. In F. S. Chapin and C. Körner (Eds.), *Arctic and Alpine Biodiversity: Patterns, Causes and Ecosystems* (pp. 297-310). Berlin, Germany: Springer.

4. Whalen, S. C., and J. C. Cornwell (1985). Nitrogen, phosphorus, and organic carbon cycling in an arctic lake. *Can. J. Fish. Aquat. Sci.* 42: 797-808.

5. Gettel, G. M. (2006). Rates, importance, and controls of nitrogen fixation in oligotrophic arctic lakes, Toolik, Alaska. Cornell University. Ithaca, New York.

6. Luecke, C., A. E. Giblin, N. D. Bettez, G. A. Burkart, B. C. Crump, M. A. Evans, et al. (2014). The Response of Lakes Near the Arctic LTER to Environmental Change. In J. E. Hobbie and G. W. Kling (Eds.), *Alaska's Changing Arctic: Ecological Consequences for Tundra, Streams, and Lakes* (pp. 238-286). Oxford, UK: Oxford University Press.

7. Alexander, V., S. C. Whalen, and K. M. Klingensmith (1989). Nitrogen cycling in arctic lakes and ponds. *Hydrobiol.* 172: 165-172.

8. Bushaw, K. L., R. G. Zepp, M. A. Tarr, D. Schulz-Jander, R. A. Bourbonniere, R. E. Hodson, et al. (1996). Photochemical release of biologically available nitrogen from aquatic dissolved organic matter. *Nature* 381: 404-407.

9. Smith, E. M., and R. Benner (2005). Photochemical transformation of riverine dissolved organic matter: effects on estuarine bacterial metabolism and nutrient demand. *Aquat. Microb. Ecol.* 40: 37-50.

10. Jeff, S., K. Hunter, D. Vandergucht, and J. Hudson (2012). Photochemical mineralization of dissolved organic nitrogen to ammonia in prairie lakes. *Hydrobiol.* 693: 71-80.

11. Porcal, P., J. Kopáček, and I. Tomkova (2014). Seasonal photochemical transformations of nitrogen species in a forest stream and lake. *PLoS ONE* 9(12), e116364.

12. Vincent, W. F., W. Wurtsbaugh, C. L. Vincent, and P. J. Richerson (1984). Seasonal dynamics of nutrient limitation in a tropical high-altitude lake (Lake Titicaca, Peru-Bolivia): Application of physiological bioassays. *Limnol. Oceanogr*. 29(3): 540-552.

13. Miller, M. C., G. R. Hatter, P. Spatt, P. Westlake, and D. Yeakel (1986). Primary

production and its control in Toolik Lake, Alaska. *Arch. Hydrobiol.* 74: 97-131.

14. Elser, J. J., E. R. Marzolf, and C. R. Goldman (1990). Phosphorous and nitrogen limitation of phytoplankton growth in the freshwaters of North America: a review and critique of experimental enrichments. *Can. J. Fish. Aquat. Sci.* 47: 1468-1477.

15. Buffam, I., and K. J. McGlathery (2003). Effect of ultraviolet light on dissolved nitrogen transformations in coastal lagoon water. *Limnol. Oceanogr.* 48(2): 723-734.

16. Vähätalo, A. V., K. Salonen, U. Münster, M. Järvinen, and R. G. Wetzel (2003). Photochemical transformation of allochthonous organic matter provides bioavailable nutrients in a humic lake. *Arch. Hydrobiol.* 156(3): 287-314.

17. Vähätalo A. V. and M. Järvinen (2007). Photochemically produced bioavailable nitrogen from biologically recalcitrant dissolved organic matter stimulates production of a nitrogen-limited microbial food web in the Baltic Sea. *Limnol. Oceanogr.* 52(1): 132-143.

18. Vähätalo, A. V., and R. G. Zepp (2005). Photochemical mineralization of dissolved organic nitrogen to ammonium in the Baltic Sea. *Environ. Sci. Technol*. 39: 6985-6992.

19. Cory, R. M., K. H. Harrold, B. T. Neilson, and G. W. Kling (2015). Controls on dissolved organic matter (DOM) degradation in a headwater stream: the influence of photochemical and hydrological conditions in determining light-limitation or substrate-limitation of photo-degradation. *Biogeosci.* 12: 6669-6685.

20. Mesfioui, R., H. A. N. Abdulla, and P. G. Hatcher (2014). Photochemical alterations of natural and anthropogenic dissolved organic nitrogen in the York River. *Environ. Sci. Technol*. 49: 159-167.

21. Wang, W., M. A. Tarr, T. S. Bianchi, and E. Engelhaupt (2000). Ammonium photoproduction from aquatic humic and colloidal matter. *Aquat. Geochem.* 6: 275-292.

22. Tarr, M. A., W. Wang, T. S. Bianchi, and E. A. Engelhaupt (2001). Mechanisms of ammonia and amino acid photoproduction from aquatic humic and colloidal matter. *Water Res.* 35(15): 3688-3696.

23. Schmidt-Rohr, K., J.-D. Mao, and D. C. Olk (2004). Nitrogen-bonded aromatics in soil organic matter and their implications for a yield decline in intensive rice cropping. *Proc. Natl. Acad. Sci. USA* 101(17): 6351-6354.

24. Mao, J.-D., L. Tremblay, J.-P. Gagné, S. Kohl, and K. Schmidt-Rohr (2007). Humic acids from particulate organic matter in the Saguenay Fjord and the St. Lawrence Estuary investigated by advanced solid-state NMR. *Geochim. Cosmochim. Acta* 71(22): 5483-5499.

25. Münster, U., P. Einiö, J. Nurminen, and J. Overbeck (1992). Extracellular enzymes in a polyhumic lake: important regulators in detritus processing. *Hydrobiol.* 229: 225-238.

26. Kirchman, D. L. (1994). The uptake of inorganic nutrients by heterotrophic bacteria. *Microb. Ecol.* 28: 255-271.

27. Tranvik, L. J., and N. O. G. Jørgensen (1995). Colloidal and dissolved organic matter in lake water: Carbohydrate and amino acid composition, and ability to support bacterial growth. *Biogeochem*. 30: 77-97.

28. Weintraub, M. N., and J. P. Schimel (2005). The seasonal dynamics of amino acids and other nutrients in Alaskan Arctic tundra soils. *Biogeochem*. 73: 359-380.

29. Siuda, W., and R. J. Chróst (2002). Decomposition and utilization of particulate organic matter by bacteria in lakes of different trophic status. *Polish J. Environ. Stud.* 11(1): 53-65.

30. Cory, R. M., D. M. McKnight, Y.-P. Chin, P. Miller, and C. L. Jaros (2007). Chemical characteristics of fulvic acids from Arctic surface waters: Microbial contributions and photochemical transformations. *J. Geophys. Res.* 112, G04S51.

31. Jørgensen, N. O. G., L. Tranvik, H. Edling, W. Granèli, and M. Lindell (1998). Effects of sunlight on occurrence and bacterial turnover of specific carbon and nitrogen compounds in lake water. *FEMS Microbiol. Ecol.* 25: 217–227.

32. Cory, R. M., C. P. Ward, B. C. Crump, and G. W. Kling (2014). Sunlight controls water column processing of carbon in arctic fresh waters. *Science* 345: 925-928.

33. Helms, J. R., A. Stubbins, J. D. Ritchie, E. C. Minor, D. J. Kieber, and K. Mopper (2008). Absorption spectral slopes and slope ratios as indicators of molecular weight, source, and photobleaching of chromophoric dissolved organic matter. *Limnol. Oceanogr.* 53: 955-969.

34. McKnight, D. M., E. W. Boyer, P. K. Westerhoff, P. T. Doran, T. Kulbe, and D. T. Andersen (2001). Spectrofluorometric characterization of dissolved organic matter for indication of precursor organic material and aromaticity. *Limnol. Oceanogr.* 46(1): 38-48.

35. Ward, C. P., and R. M. Cory (2015). Chemical composition of dissolved organic matter draining permafrost soils. *Geochim. Cosmochim. Acta* 167: 63-79.

36. Dittmar, T., B. Koch, N. Hertkorn, and G. Kattner (2008). A simple and efficient method for the solid-phase extraction of dissolved organic matter (SPE-DOM) from seawater. *Limnol. Oceanogr.: Methods* 6: 230-235.

37. Ward, C. P., S. G. Nalven, B. C. Crump, G. W. Kling, and R. M. Cory (2017). Photochemical alteration of organic carbon draining permafrost soils shifts microbial

metabolic pathways and stimulates respiration. *Nat. Commun.* 8, 772.

38. Sleighter, R. L., H. Chen, A. S. Wozniak, A. S. Willoughby, P. Caricasole, and P. G. Hatcher (2012). Establishing a measure of reproducibility of ultrahigh-resolution mass spectra for complex mixtures of natural organic matter. *Anal. Chem.* 84: 9184-9191.

39. Hockaday, W. C., J. M. Purcell, A. G. Marshall, J. A. Baldock, and P. G. Hatcher (2009). Electrospray and photoionization mass spectrometry for the characterization of organic matter in natural waters: A qualitative assessment. *Limnol. Oceanogr.: Methods* 7: 81-95.

40. Sleighter, R., and P. G. Hatcher (2011). Fourier transform mass spectrometry for the molecular level characterization of natural organic matter: Instrument capabilities, applications, and limitations. In G. S. Nikolic (Ed.), *Fourier Transforms: Approach to Scientific Principles* (pp. 295-320). Rijeka, Croatia: InTech.

41. Bower, C. E., and T. Holm-Hansen (1980). A salicylate-hypochlorite method for determining ammonia in seawater. *Can. J. Fish. Aquat. Sci.* 37: 794-798.

42. Weishaar, J. L., G. R. Aiken, B. A. Bergamaschi, M. S. Fram, R. Fujii, and K. Mopper (2003). Evaluation of specific ultraviolet absorbance as an indicator of the chemical composition and reactivity of dissolved organic carbon. *Environ. Sci. Technol.* 37: 4702-4708.

43. Stedmon, C. A., S. Markager, and R. Bro (2003). Tracing dissolved organic matter in aquatic environments using a new approach to fluorescence spectroscopy. *Mar. Chem.* 82: 239-254.

44. Murphy, K. R., C. A. Stedmon, D. Graeber, and R. Bro (2013). Fluorescence spectroscopy and multi-way techniques: PARAFAC. *Anal. Methods* 5: 6557-6566.

45. Stedmon, C. A., and S. Markager (2005). Tracing the production and degradation of autochthonous fractions of dissolved organic matter by fluorescence analysis. *Limnol. Oceanogr.* 50(5): 1415-1426.

46. Hernes, P. J., B. A. Bergamaschi, R. S. Eckard, and R. G. M. Spencer (2009). Fluorescence-based proxies for lignin in freshwater dissolved organic matter. *J. Geophys. Res.* 114, G00F03.

47. Cory, R. M., T. W. Davis, G. J. Dick, T. Johengen, V. J. Denef, M. A. Berry, et al. (2016). Seasonal dynamics in dissolved organic matter, hydrogen peroxide, and cyanobacterial blooms in Lake Erie. *Front. Mar. Sci*. 3(54): 1-17.

48. Vähätalo, A. V., M. Salkinoja-Salonen, P. Taalas, and K. Salonen (2000). Spectrum of the quantum yield for photochemical mineralization of dissolved organic carbon in a humic lake. *Limnol. Oceanogr.* 45: 664-676.

49. Xie, H., S. Bélanger, G. Song, R. Benner, A. Taalba, M. Blais, et al. (2012). Photoproduction of ammonium in the southeastern Beaufort Sea and its biogeochemical implications. *Biogeosci.* 9: 3047-3061.

50. Cornwell, C. J. (1983). The geochemistry of manganese, iron, and phosphorus in an arctic lake. University of Alaska. Fairbanks, Alaska.

51. Kling, G. (2013). Bacterial production data for lakes and lake inlets/outlets samples collected summer 2011, Arctic LTER, Toolik Research Station, Alaska. Environmental Data Initiative. http://dx.doi.org/10.6073/pasta/e173d6777edde2174fe5a065508ac0fa

52. Kling, G. (2019). Bacterial production data for lake and stream samples collected in summer 2012 through 2018, Arctic LTER, Toolik Lake Field Station, Alaska Environmental Data Initiative. http://dx.doi.org/10.6073/pasta/308b10a7626734082e9d3e43195b8853

53. Simon, M., and F. Azam (1989). Protein content and protein synthesis rates of planktonic marine bacteria. *Mar. Ecol. Prog. Ser.* 51: 201-213.

54. Whalen, S. C. (1986). Pelagic nitrogen cycle in an arctic lake. University of Alaska. Fairbanks, Alaska.

55. Whalen, S. C., and V. Alexander (1986). Seasonal inorganic carbon and nitrogen transport by phytoplankton in an arctic lake. *Can. J. Fish. Aquat. Sci.* 43: 1177-1186.

56. Stedmon, C. A., S. Markager, L. Tranvik, L. Kronberg, T. Slätis, and W. Martinsen (2007). Photochemical production of ammonium and transformation of dissolved organic matter in the Baltic Sea. *Mar. Chem.* 104: 227-240.

57. Sleighter, R. L., R. M. Cory, L. A. Kaplan, H. A. N. Abdulla, and P. G. Hatcher (2014). A coupled geochemical and biogeochemical approach to characterize the bioreactivity of dissolved organic matter from a headwater stream. *J. Geophys. Res. Biogeosci*. 119: 1520-1537.

58. Zhang, Y., R. Zhang, S.-L. Li, K. M. G. Mostofa, X. Fu, H. Ji, et al. (2021). Photo-ammonification of low molecular weight dissolved organic nitrogen by direct and indirect photolysis. *Sci. Total Environ.* 764, 142930.

59. Amado, A. M., J. B. Cotner, R. M. Cory, B. L. Edhlund, and K. McNeill (2015). Disentangling the interactions between photochemical and bacterial degradation of dissolved organic matter: Amino acids play a central role. *Microb. Ecol.* 69: 554-566.

60. Bowen, J. C., L. A. Kaplan, and R. M. Cory (2020). Photodegradation disproportionately impacts biodegradation of semi-labile DOM in streams. *Limnol. Oceanogr.* 65: 13-26.

61. Wolfbeis, O. S. (1985). The fluorescence of organic natural products. In S.G. Schulman

(Ed.), *Molecular Luminescence Spectroscopy – Methods and Applications; Part 1* (pp. 167-370). New York, USA: John Wiley & Sons.

62. Permyakov, E. A. (Ed.) (1993). *Luminescence Spectroscopy of Proteins*. Boca Raton, USA: CRC Press.

63. Li, A., A. F. Aubeneau, T. King, R. M. Cory, B. T. Neilson, D. Bolster, and A. I. Packman (2019). Effects of vertical hydrodynamic mixing on photomineralization of dissolved organic carbon in arctic surface waters. *Environ. Sci.: Processes Impacts* 21: 748-760.

64. Boyd, W. L., and J. W. Boyd (1963). A bacteriological study of an arctic coastal lake. *Ecology* 44(4): 705-710.

65. Hobbie, J. E., and P. Rublee (1975). Bacterial production in an arctic pond. *Verhandlungen der Internationalen Vereinigung fur Theoretische und Angewandte Limnologie* 19: 466-471.

66. Hoppe, H.-G., S.-J. Kim, and K. Gocke (1988). Microbial decomposition in aquatic environments: Combined process of extracellular enzyme activity and substrate uptake. *Appl. Environ. Microbiol.* 54(3): 784-790.

67. Murrell, M. C., J. T. Hollibaugh, M. W. Silver, and P. S. Wong (1999). Bacterioplankton dynamics in northern San Francisco Bay: Role of particle association and seasonal freshwater flow. *Limnol. Oceanogr.* 44(2): 295-308.

68. Kiersztyn, B., W. Siuda, and R. J. Chróst (2012). Persistence of bacterial proteolytic enzymes in lake ecosystems. *FEMS Microbiol. Ecol.* 80: 124-134.

69. Zweifel, U. L., B. Norman, and Å. Hagström (1993). Consumption of dissolved organic carbon by marine bacteria and demand for inorganic nutrients. *Mar. Ecol. Prog. Ser.* 101: 23-32.

70. Joint, I., P. Henriksen, G. A. Fonnes, D. Bourne, T. F. Thingstad, and B. Riemann (2002). Competition for inorganic nutrients between phytoplankton and bacterioplankton in nutrient manipulated mesocosms. *Aquat. Microb. Ecol.* 29: 145-159.

71. Giblin, A., and G. Kling (2019a). Chlorophyll a and primary productivity data for various lakes near Toolik Research Station, Alaska, Arctic LTER. Summer 2010 to 2018 Environmental Data Initiative. http://dx.doi.org/10.6073/pasta/3cee97b0c9d36cbdd67dd853b176e164

72. Giblin, A., and G. Kling (2019b). Water chemistry data for various lakes near Toolik Research Station, Arctic LTER. Summer 2010 to 2018 ver 4. Environmental Data Initiative. https://doi.org/10.6073/pasta/33fa3f6a43f9231678e6ee3c3357265e

73. Ward, C. P., J. C. Bowen, D. H. Freeman, and C. M. Sharpless (2021). Rapid and reproducible characterization of the wavelength dependence of aquatic photochemical reactions using light emitting diodes (LEDs). *Environ. Sci. Technol. Lett.* 8(5): 437-442.

74. Howard, H. H., and G. W. Prescott (1971). Primary production in arctic tundra lakes. *American Midland Naturalist* 85(1): 108-123.

75. Jeffries, M. O., K. Morris, and G. E. Liston (1996). A method to determine lake depth and water availability on the North Slope of Alaska with spaceborne imaging radar and numerical ice growth modelling. *Arctic* 49(4): 357-374.

76. Arp, C. D., B. M. Jones, F. E. Urban, and G. Grosse (2011). Hydrogeomorphic processes of thermokarst lakes with grounded-ice and floating-ice regimes on the Arctic coastal plain, Alaska. *Hydrol. Process.* 25: 2422-2438.

77. Surdu, M., C. R. Duguay, L. C. Brown, and D. F. Prieto (2014). Response of ice cover on shallow lakes of the North Slope of Alaska to contemporary climate conditions (1950–2011): Radar remote-sensing and numerical modeling data analysis. *Cryosphere* 8: 167-180.

78. Miller, W. L., and R. G. Zepp (1995). Photochemical production of dissolved inorganic carbon from terrestrial organic matter: Significance to the oceanic organic carbon cycle. *Geophys. Res. Lett.* 22: 417-420.

79. Bowen, J. C., C. P. Ward, G. W. Kling, and R. M. Cory (2020). Arctic amplification of warming strengthened by sunlight oxidation of permafrost carbon to CO_2. *Geophys. Res. Lett.* 47, e2020GL087085.

80. Nagata, T. (1986). Carbon and nitrogen content of natural planktonic bacteria. *Appl. Environ. Microbiol.* 52(1): 28-32.

81. Vadstein, O., and Y. Olsen (1989). Chemical composition and phosphate uptake kinetics of limnetic bacterial communities cultured in chemostats under phosphorus limitation. *Limnol. Oceanogr.* 34(5): 939-946.

82. Elser, J. J., T. H. Chrzanowski, R. W. Sterner, J. H. Schampel, and D. K. Foster (1995). Elemental ratios and the uptake and release of nutrients by phytoplankton and bacteria in three lakes of the Canadian Shield. *Microb. Ecol.* 29: 145-162.

83. Biddanda, B., M. Ogdahl, and J. Cotner (2001). Dominance of bacterial metabolism in oligotrophic relative to eutrophic lakes. *Limnol. Oceanogr.* 46(3): 730-739.

84. Cotner, J. B., E. K. Hall, J. T. Scott, and M. Heldal (2010). Freshwater bacteria are stoichiometrically flexible with a nutrient composition similar to seston. *Front. Microbiol.* 1(132): 1-11.

85. Manzella, M., R. Geiss, and E. K. Hall (2019). Evaluating the stoichiometric trait distributions of cultured bacterial populations and uncultured microbial communities. *Environ. Microbiol.* 21(10): 3613-3626.

86. Godwin, C. M., and J. B. Cotner (2015). Stoichiometric flexibility in diverse aquatic heterotrophic bacteria is coupled to differences in cellular phosphorus quotas. *Front. Microbiol.* 6(159): 1-15.

87. Whalen, S. C., and V. Alexander (1986). Chemical influences on ^{14}C and ^{15}N primary production in an arctic lake. *Polar Biol.* 5: 211-219.

88. Hecky, R. E., P. Campbell, and L. L. Hendzel (1993). The stoichiometry of carbon, nitrogen, and phosphorus in particulate matter of lakes and oceans. *Limnol. Oceanogr.* 38(4): 709-724.

89. Dobberfuhl, D. R., and J. J. Elser (2000). Elemental stoichiometry of lower food web components in arctic and temperate lakes. *J. Plankton Res*. 22(7): 1341-1354.

90. Bergström, A.-K., D. Karlsson, J. Karlsson, and T. Vrede (2015). N-limited consumer growth and low nutrient regeneration N:P ratios in lakes with low N deposition. *Ecosphere* 6(9): 1-13.

91. Dodds, W. K., and J. C. Priscu (1990). A comparison of methods for assessment of nutrient deficiency of phytoplankton in a large oligotrophic lake. *Can. J. Fish. Aquat. Sci.* 47: 2328-2338.

92. Hessen, D. O., T. Andersen, P. Brettum, and B. A. Faafeng (2003). Phytoplankton contribution to sestonic mass and elemental ratios in lakes: Implications for zooplankton nutrition. *Limnol. Oceanogr.* 48(4): 1289-1296.

93. Schindler, D. W., H. E. Welch, J. Kalff, G. J. Brunskill, and N. Kritsch (1976). Physical and chemical limnology of Char Lake, Cornwallis Island (75º N Lat.). *J. Fish. Res. Board. Can*. 31: 585-607.

94. Lundeen, R. A., E. M.-L. Janssen, C. Chu, and K. McNeill (2014). Environmental photochemistry of amino acids, peptides, and proteins. *Chimia* 68(11): 812-817.

95. Chin, Y.-P., G. Aiken, and E. O'Loughlin (1994). Molecular weight, polydispersity, and spectroscopic properties of aquatic humic substances. *Environ. Sci. Technol.* 28: 1853-1858.

96. Brown, A., D. M. McKnight, Y.-P. Chin, E. C. Roberts, and M. Uhle (2004). Chemical characterization of dissolved organic material in Pony Lake, a saline costal pond in Antarctica. *Mar. Chem.* 89: 327-337.

97. Kalff, J. (1967). Phytoplankton abundance and primary production rates in two arctic

ponds. *Ecology* 48(4): 558-565.

98. Stanley, D. W., and R. J. Daley (1976). Environmental control of primary productivity in Alaskan tundra ponds. *Ecology* 57: 1025-1033.

99. Sheath, R. G. (1986). Seasonality of phytoplankton in northern tundra ponds. *Hydrobiol.* 138: 75-83.

100. Koch, B. P., and T. Dittmar (2006). From mass to structure: an aromaticity index for high-resolution mass data of natural organic matter. *Rapid Commun. Mass Spectrom.* 20: 926-932.

Chapter 3

Arctic Amplification of Global Warming Strengthened by Sunlight Oxidation of Permafrost Carbon to CO_2[1]

3.1 Abstract

Once thawed, up to 15% of the ~1,000 Pg of organic carbon (C) in arctic permafrost soils may be oxidized to carbon dioxide (CO_2) by 2100, amplifying climate change. However, predictions of this amplification strength ignore the oxidation of permafrost C to CO_2 in surface waters (photomineralization). We characterized the wavelength dependence of permafrost dissolved organic carbon (DOC) photomineralization and demonstrate that iron catalyzes the photomineralization of old DOC (4,000-6,300 a BP) derived from soil lignin and tannin. Rates of CO_2 production from photomineralization of permafrost DOC are two-fold higher than for modern DOC. Given that model predictions of future net loss of ecosystem C from thawing permafrost do not include the loss of CO_2 to the atmosphere from DOC photomineralization, current predictions of an average of 208 Pg C loss by 2299 may be too low by ~14%.

3.2 Introduction

Current estimates are that 5 to 15% of the ~1,000 Pg of the soil organic carbon (C) stored in surface permafrost soils could be emitted as greenhouse gases by 2100 given the current trajectory of global warming,[1-2] with additional C lost in lateral transfer from soils to surface

[1] Bowen, J. C., C. P. Ward, G. W. Kling, and R. M. Cory, *Geophys. Res. Lett.*, 2020.

waters.[2] Models assessing the sensitivity of the climate system to thawing permafrost soils estimate that decomposition of organic C in these soils could result in 0.3 °C to 0.4 °C additional global warming (i.e., arctic amplification) by 2100 to 2299, respectively.[3] However, none of these predictions include the oxidation of organic C upon export to sunlit surface waters.

Oxidation of dissolved organic carbon (DOC) to carbon dioxide (CO_2) by sunlight (photomineralization) currently accounts for up to 30% of the CO_2 emitted to the atmosphere from arctic surface waters.[4] As permafrost DOC is exported to sunlit waters, its oxidation to CO_2 will depend on whether permafrost DOC is labile to photomineralization, which is currently debated.[5-8] The lability of terrestrially-derived DOC to photomineralization is hypothesized to depend on iron and DOC chemical composition.[6,9-12] To test these hypothesized controls, we made the first direct measurements of the amount, source, and age of CO_2 produced from photomineralization of permafrost DOC collected on younger and older glacial surfaces, and from two common vegetation types in the Arctic (Table 2.1).[13-14] Here we show that (1) the lability of permafrost DOC to photomineralization depends on sunlight wavelength, (2) iron controls the lability of permafrost DOC to photomineralization, and (3) old carboxylic acid C (4,000 to 6,300 a BP) derived from lignin and tannin is mineralized to CO_2 by sunlight. Collectively, our results support the inclusion of photomineralization in model predictions and experimental studies of arctic amplification of climate change.

3.3 Methods

3.3.1 Experimental design

Light exposure experiments were conducted to (i) characterize the spectral (wavelength) dependence of the photomineralization yield ($\varphi_{PM,\lambda}$) for permafrost DOC, (ii) quantify the radiocarbon (^{14}C) and stable carbon (^{13}C) isotopic compositions of CO_2 produced from

photomineralization of permafrost DOC, and (iii) quantify changes in the chemical composition of permafrost DOC from light exposure. To test for controls on the $\varphi_{PM,\lambda}$ and the chemical composition of DOC photomineralized to CO_2, each light exposure experiment was conducted using DOC leached from five permafrost soils varying in DOC composition and iron concentration (Table 3.1, Figure 3.1).[13-14] The study objectives required exposing permafrost DOC to different sources and doses of light. For objectives (i) and (ii), DOC from permafrost soils collected in 2018 were exposed to light using custom-built high-powered (≥ 100 mW), narrow-banded (± 10 nm) light-emitting diodes (LED). The $\varphi_{PM,\lambda}$ (objective (i)) was measured upon exposure of permafrost DOC to LEDs with peak emissions at 278, 309, 348, 369, and 406 nm (Figure 3.1). For objective (ii), the ^{14}C and ^{13}C compositions of dissolved inorganic carbon (DIC) in the permafrost leachates were measured upon exposure to LEDs at 309 and 406 nm alongside dark controls, and compared to the ^{14}C and ^{13}C compositions of DOC leached from the permafrost soil (Figure 3.1). For objective (iii), we used permafrost soils collected in 2013 and 2015 from the same sites as in 2018 to quantify shifts in major functional groups of permafrost DOC by ^{13}C nuclear magnetic resonance (NMR) upon exposure to broadband light relative to dark controls (Figure 3.1). We also quantified $\varphi_{PM,\lambda}$ following the same exposure of these permafrost DOC samples to broadband light (Figure 3.1). Directly measured $\varphi_{PM,\lambda}$ spectra for permafrost DOC from objective (i) were used to calculate surface water rates of photomineralization as a function of increasing permafrost DOC in the DOC pool in surface waters.

3.3.2 Permafrost soil collection

Soils were collected from the frozen permafrost layer (> 60 cm below the surface) at five sites underlying moist acidic tussock or wet sedge vegetation, and on three glacial surfaces on

the North Slope of Alaska during summer 2018 (Table 3.1).[15-17] See the Appendix Section 3.7.1 for soil collection protocols, including precautions to minimize ^{14}C contamination. DOC was leached from each permafrost soil (leachate) at the Woods Hole Oceanographic Institution (WHOI) as described in the Appendix Section 3.7.1.

3.3.3 $\Delta^{14}C$ and $\delta^{13}C$ analyses of DOC

The ^{14}C and ^{13}C isotopic compositions of DOC were analyzed from each permafrost leachate at the National Ocean Sciences Accelerator Mass Spectrometry (NOSAMS) facility at WHOI (Table 3.A.1) following Beaupré et al. (2007).[18] Each permafrost leachate was diluted with UVC-oxidized MilliQ water (Millipore Simplicity ultraviolet, UV, system; 1.5 hr; 1200 W medium pressure mercury arc lamp) to achieve a total C mass between 800 and 2000 μg. The diluted permafrost leachate was acidified with UVC-oxidized trace-metal grade phosphoric acid (85%) to pH < 2 in a precombusted quartz reactor (450 °C; 4 hr) and the DIC was purged with high-purity helium gas in the dark. The DOC was then oxidized with UVC light to DIC for 4 hr (1200 W medium pressure mercury arc lamp), and the resultant CO_2 was extracted cryogenically. On average, 1370 ± 240 μg of C were extracted from each permafrost leachate (± 1 standard error, SE; n = 6; Table 3.A.1). A subsample of the CO_2 was analyzed for ^{13}C using a VG Prism-II or Optima stable isotope ratio mass spectrometer (instrumental precision of 0.1‰),[19] and the $\delta^{13}C$ (‰) was calculated as follows:

$$\delta^{13}C = ({}^{13}R_{sample}/{}^{13}R_{standard} - 1) \quad (1)$$

where ^{13}R is the isotope ratio of a sample or standard (VPDB), as defined by:

$$^{13}R = ({}^{13}C/{}^{12}C) \quad (2)$$

The remaining CO_2 was reduced to graphite with H_2 and an iron catalyst, and then analyzed for ^{14}C isotopic composition using an accelerator mass spectrometer at the NOSAMS facility.[20] The $\Delta^{14}C$ (‰) and radiocarbon age of DOC were calculated from the fraction modern[21-22] using the oxalic acid I standard (NIST-SRM 4990). $\Delta^{14}C$ analyses of DOC had an instrumental precision of 2-6‰.[20,22]

DOC leached from one permafrost soil (Toolik moist acidic tundra) was prepared and analyzed for ^{14}C and ^{13}C twice to quantify the standard error of duplicate analyses (Table 3.A.1). $\Delta^{14}C$ and $\delta^{13}C$ analyses of DOC had standard errors of 1‰ and 0.1‰, respectively (1 SE; $n = 2$; Table 3.2). A procedural blank was quantified manometrically by oxidizing MilliQ water with UVC light in a precombusted quartz reactor (450 °C; 4 hr) for 1.5 hr, acidifying to pH < 2, and purging the DIC as described above. The procedural blank was 4 μg of C, which was < 0.5% of the total C masses extracted from the permafrost leachates.

3.3.4 Apparent quantum yield spectra

The CO_2 produced from photomineralization of permafrost DOC was measured as a function of sunlight wavelength. The lability of DOC to photomineralization is defined as the apparent quantum yield spectrum (CO_2 produced per mol photon absorbed by DOC; hereafter called the yield spectrum, $\varphi_{PM,\lambda}$). Yield spectra of permafrost DOC were directly measured for the first time with a custom-built high-powered (≥ 100 mW), narrow-banded (± 10 nm) LED system from soils collected in 2018 (Figure 3.1). Each permafrost leachate was equilibrated to room temperature (~24 hr) and then placed in 20 gas-tight, flat-bottomed precombusted (450 °C; 4 hr) 12 mL quartz vials with butyl rubber septa and GL-18 caps (light-exposed vials) and four gas-tight precombusted (450 °C; 4 hr) 12 mL borosilicate exetainer vials (dark control vials; Labco, Inc.). Vials were placed in an inner aluminum housing (painted black matte to minimize

light scattering), with the flat bottom facing upward toward the light source, and then exposed to ≥ 100 mW, narrow-banded (± 10 nm) LEDs at 278, 309, 348, 369, and 406 nm alongside the dark controls for 12 or 30 hr (Table 3.A.2). The LEDs were tuned such that each permafrost leachate absorbed the same about of light at each wavelength. After LED exposure, light-exposed and dark control waters were immediately analyzed for DIC (Apollo SciTech, Inc.) and for chromophoric dissolved organic matter (CDOM).[4] The experiment above was then repeated for the analysis of photochemical oxygen (O_2) consumption to quantify the apparent quantum yield spectra of photo-oxidation ($\varphi_{PO,\lambda}$) from each permafrost DOC. Dissolved O_2 was measured in each light-exposed and dark control vial on a membrane inlet mass spectrometer (Bay Instruments).[23]

At each LED wavelength, $\varphi_{PM,\lambda}$ and $\varphi_{PO,\lambda}$ were calculated as the concentration of DIC produced and O_2 consumed, respectively, divided by the light absorbed by CDOM. The amount of light absorbed by CDOM (mol photon m^{-2} nm^{-1}) was quantified for each vial exposed to a LED using absorption coefficients of CDOM ($a_{CDOM,\lambda}$) and the photon flux spectrum.[4] The photon flux spectrum was quantified from the solar irradiance spectrum from each LED source, which was measured by radiometry and chemical actinometry (see Appendix Section 3.7.2). $\varphi_{PM,\lambda}$ and $\varphi_{PO,\lambda}$ are reported as the average ± 1 SE of experimental replicate vials (n = 4).

3.3.5 $\Delta^{14}C$ and $\delta^{13}C$ of CO_2 produced from light

The $\Delta^{14}C$ and $\delta^{13}C$ of DIC produced following exposure of DOC to UV and visible light were quantified from permafrost leachates prepared from each permafrost soil collected in 2018, except for Sagwon moist acidic tundra (Figure 3.1). Each permafrost leachate was equilibrated to room temperature and then placed in up to four precombusted (450 °C; 4 hr) 600 mL quartz flasks with ground glass stoppers and no headspace. The flasks were exposed to custom-built

LED arrays consisting of ten ≥ 100 mW, narrow-banded (± 10 nm) 309 or 406 nm chips alongside one or two foil-wrapped dark control flasks (Table 3.A.1). Exposure times ranged from 8 to 25 hr to achieve similar concentrations of DIC produced from each permafrost DOC sample and at each wavelength (Table 3.A.3).

After LED exposure, foil-wrapped light-exposed and dark control flasks were immediately transferred to foil-wrapped, precombusted 500 mL borosilicate glass bottles (450 °C; 4 hr) in a N_2-filled glove bag, preserved with saturated mercuric chloride, and plugged with gas-tight ground glass stoppers.[24] Those bottles were stored in the dark at room temperature for ≤ 1 week until preparation for carbon isotope analyses at the NOSAMS facility. Bottles were kept foil-wrapped while each water sample was acidified with trace-metal grade phosphoric acid (85%) to pH < 2 and stripped of DIC with high-purity N_2 gas. The resultant CO_2 was trapped and purified cryogenically and its concentration was quantified manometrically. The ^{14}C and ^{13}C of the CO_2 were analyzed at the NOSAMS facility (Table 3.A.1) and converted to $\Delta^{14}C$ and $\delta^{13}C$ values as described above. $\Delta^{14}C$ analyses of DIC had an instrumental precision of 1-2‰.[20,22] The reported precision of $\delta^{13}C$ is 0.1‰.[19]

The $\Delta^{14}C$ and $\delta^{13}C$ of CO_2 produced from the photomineralization of DOC were calculated as follows:

$$\Delta^{14}C\text{-}CO_{2_\lambda} = \frac{(\Delta^{14}C\text{-}DIC_{Light,\lambda} * [DIC]_{Light,\lambda}) - (\Delta^{14}C\text{-}DIC_{Dark} * [DIC]_{Dark})}{([DIC]_{Light,\lambda} - [DIC]_{Dark})} \quad (3)$$

$$\delta^{13}C\text{-}CO_{2_\lambda} = \frac{(\delta^{13}C\text{-}DIC_{Light,\lambda} * [DIC]_{Light,\lambda}) - (\delta^{13}C\text{-}DIC_{Dark} * [DIC]_{Dark})}{([DIC]_{Light,\lambda} - [DIC]_{Dark})} \quad (4)$$

The $\Delta^{14}C$ and $\delta^{13}C$ of CO_2 produced in each light-exposed flask were calculated relative to one or two dark controls (Tables 3.A.1, 3.A.3) and are reported as the average ± 1 SE of replicate

values for the experiments conducted alongside two dark controls (Table 3.2). The concentration, $\Delta^{14}C$, and $\delta^{13}C$ of DIC in the dark controls are reported as the average ± 1 SE of replicate flasks (n = 2; Table 3.A.3). The ^{14}C age of CO_2 produced was calculated from the $\Delta^{14}C$ of CO_2 produced in each light-exposed flask relative to dark controls.[21-22] This approach to quantify the $\Delta^{14}C$ and $\delta^{13}C$ of CO_2 produced from photomineralization of organic C was previously described in detail for polystyrene.[25] In this previous study, experimental reproducibility of $\Delta^{14}C$ and $\delta^{13}C$ of CO_2 produced from photomineralization was 5‰ and 0.1‰, respectively (± 1 SE; n = 3).

3.3.6 Photochemical changes in DOC composition

Permafrost soils collected in 2013 and 2015 were used to evaluate changes in DOC chemical composition by ^{13}C-NMR following light exposure and to quantify $\varphi_{PM,\lambda}$ (Figure 3.1). Sampling and preparation of the permafrost leachates from soils collected in 2013 and 2015 were previously described[26-27] and similar to the methods described for soils collected in 2018 (see Appendix Section 3.7.1). All information on samples collected in 2013 were previously published.[26] Here we describe methods used in this study to quantify photochemical changes in DOC chemical composition and the $\varphi_{PM,\lambda}$ for DOC leached from permafrost soils collected in 2015.

Each permafrost leachate was exposed to 18 hours of simulated sunlight at 20 °C (Atlas Suntest XLS+) in Whirl-Pak bags (Nasco, Inc.) alongside dark controls (Figure 3.1). Dissolved organic matter in the light-exposed and dark control waters was isolated by solid-phase extraction, freeze-dried, and analyzed by solid-state ^{13}C-NMR as previously described.[6,26] The percentages of aromatic and carboxyl C within the DOC pool[28] are reported as the average ± 1 SE of the experimental replicate leachates (n = 2), except for Toolik moist acidic tundra, which

did not have an experimental replicate. The percent loss of carboxyl C was calculated as previously described[6] and reported as the average ± 1 SE of the experimental replicate leachates (n = 2).

From these same broadband light exposure experiments used to determine changes in DOC composition by ^{13}C-NMR, we determined $\varphi_{PM,\lambda}$ by measuring DIC and CDOM in triplicate gas-tight, precombusted 12 mL borosilicate exetainer vials (450 °C; 4 hrs; Labco, Inc.) alongside dark controls (Table 3.A.2, Figure 3.1).[4] The solar irradiance spectrum (W m^{-2} nm^{-1}) was measured in duplicate at the surface of the Suntest XLS+ with a radiometer over wavelengths from 280 to 700 nm (USB4000 Spectrometer, Ocean Optics). The amount of light absorbed by CDOM (mol photon m^{-2} nm^{-1}) was calculated as previously described.[4] $\varphi_{PM,\lambda}$ was calculated as the light minus dark difference in DIC concentration divided by the light absorbed by CDOM during the light exposure period, assuming the $\varphi_{PM,\lambda}$ spectrum decreased exponentially with increasing wavelength.[4] The $\varphi_{PM,\lambda}$ for each permafrost leachate is reported as the average ± 1 SE of replicate experiments (n = 2), except for Toolik moist acidic tundra, which only had one experiment conducted.

3.3.7 Statistical analyses

Statistical tests were used to determine whether light exposure of permafrost DOC resulted in significant changes in DOC concentration and chemical composition, and whether light minus dark differences in DOC concentration and chemical composition changed significantly as a function of light wavelength or dissolved iron concentration. Two-tailed, paired t-tests were conducted to determine significant differences in DIC concentrations, O_2 concentrations, Δ^{14}C and δ^{13}C of DIC, and percentages of carboxyl C within DOC in the light-exposed versus dark control leachates. Statistical significance was defined as $p < 0.05$. T-tests

were used to determine whether the slopes and intercepts of each regression in Figures 3.2, 3.3, 3.5, 3.6, and 3.A.2 were significantly different from zero. T-tests were used to determine whether the slopes and intercepts of least-squares regressions between cation, DOC composition, or $\varphi_{PM,\lambda}$ data were significantly different from zero (see Appendix Sections 3.7.5 and 3.7.6). The open symbols for Toolik moist acidic tundra permafrost DOC in Figures 3.2b and 3.3 were identified as outliers because the value for this permafrost DOC was more than ± 5 standard deviations from the slope of the least-squares regression (see Appendix Section 3.7.6).

Statistical analyses were conducted to determine whether the $\varphi_{PM,\lambda}$ and $\varphi_{PO,\lambda}$ spectral slopes of permafrost and surface water DOC were significantly different from one another. Two-tailed, unpaired t-tests or analysis of variance were used to determine significant differences between the slopes of the $\varphi_{PM,\lambda}$ or $\varphi_{PO,\lambda}$ spectra among permafrost DOC in Figures 3.2a or 3.A.2, and between permafrost and surface water DOC in Figures 3.2a and 3.A.1.

3.4 Results and discussion

All permafrost DOC was labile to photomineralization at all wavelengths measured (Figure 3.2a), and the yield spectrum always decreased exponentially with increasing wavelength from the UV to the visible ($p < 0.05$; Figure 3.2a). The magnitude of the photomineralization yield varied up to 8-fold among permafrost DOC samples (Figure 3.2a) and was significantly, positively correlated with the concentration of dissolved iron ($p < 0.001$ as shown at 309 nm in Figure 3.2b; see Appendix Section 3.7.6). There were no significant correlations of the photomineralization yield with dissolved cations other than iron or with any measure of DOC concentration or composition (see Appendix Section 3.7.6).

Our results are the first to demonstrate in natural samples that the lability of permafrost DOC to photomineralization is controlled by dissolved iron. Although photomineralization of

terrestrially-derived DOC has been shown to increase with addition or decrease with removal of iron in the laboratory,[9-12] evidence is lacking for a mechanism by which iron enhances photomineralization. Here we present new experimental evidence and a synthesis of literature results that collectively support a mechanism of iron-catalyzed photo-decarboxylation of lignin- and tannin-derived carboxylic acids within old permafrost DOC.

Iron is hypothesized to catalyze the photo-decarboxylation of organic acids by a Ligand-Metal-Charge-Transfer reaction[29] where Fe(III) is a cyclic catalyst that is photo-reduced to Fe(II) while the C in carboxylic acids (hereafter "carboxyl C") is oxidized to CO_2.[9-11] Two lines of evidence from our study strongly support iron-catalyzed photo-decarboxylation of permafrost DOC to CO_2. First, loss of carboxyl C (quantified by ^{13}C-NMR) upon exposure of permafrost DOC to sunlight was significantly, positively correlated with the dissolved iron concentration ($p < 0.05$; Figure 3.3), as expected if photo-decarboxylation is the mechanism of CO_2 production. The only other study that quantified photochemical loss of carboxyl C from permafrost DOC concluded that it accounted for up to 90% of the CO_2 produced from photomineralization.[6] However, this prior study used DOC from one site (with only one iron concentration) and thus was unable to link iron abundance to DOC photo-decarboxylation. Second, the ratio of photochemical CO_2 production per dissolved O_2 consumption by DOC was ≥ 1 for all permafrost DOC that also contained > 1 μM total dissolved iron (Figure 3.4). A ratio ≥ 1 for photochemical CO_2 produced per O_2 consumed is considered evidence for photo-decarboxylation because this reaction is expected to proceed with a stoichiometry of $\geq$ 2:1 mol CO_2 produced per mol O_2 consumed.[9,11] While ratios ≥ 1 for photochemical CO_2 produced per O_2 consumed have previously been observed in high-iron waters,[9,11,30] here we show ratios ≥ 1 for DOC from various permafrost soils concurrent with photochemical loss of carboxyl C.

Isotopic signatures of the CO_2 produced by sunlight indicate that iron is catalyzing the oxidation of carboxyl C attached to organic matter derived from lignin and tannin. Photochemical production of ^{13}C-depleted CO_2 (Table 3.2) increased significantly with the ratio of photochemical CO_2 produced per mol of O_2 consumed ($p < 0.05$; Figure 3.5). Therefore, as photo-decarboxylation accounts for more of the total CO_2 produced (as indicated by increasing CO_2/O_2; Figure 3.5), the source of the CO_2 is increasingly ^{13}C-depleted carboxyl C, such as that derived from lignin and tannin.[31] Photochemical production of ^{13}C-depleted CO_2 is interpreted as resulting from photomineralization of lignin- or tannin-derived DOC[32-33] because lignin and tannin are relatively more depleted in ^{13}C compared to other fractions of DOC (see Appendix Section 3.7.7).[34] In addition, the ^{13}C enrichment of DOC remaining after photomineralization has been correlated with photochemical loss of lignin,[32] and high-resolution mass spectrometry revealed that lignin- and tannin-derived compounds within permafrost DOC are preferentially degraded by sunlight compared to other fractions of DOC.[6,27] Thus, our results indicate that iron-catalyzed photo-decarboxylation of lignin and tannin in permafrost DOC is producing CO_2 (Table 3.2, Figures 3.3, 3.5).

The carboxyl C derived from lignin and tannin that was photomineralized to CO_2 was old, from 4,000 to 6,300 a BP (Table 3.2, Figure 3.6). The $\Delta^{14}C$ composition of CO_2 produced from photomineralization of permafrost DOC (-546‰ to -397‰) was always ≤ 70‰ different from the initial, bulk $\Delta^{14}C$-DOC signature (-585‰ to -411‰; Table 3.2, Figure 3.6). The linear relationship between the initial, bulk permafrost $\Delta^{14}C$-DOC and the $\Delta^{14}C$-CO_2 produced by photomineralization ($p < 0.05$; Figure 3.6) indicates that the bulk age of permafrost DOC was a strong predictor of the age of DOC photomineralized to CO_2. Collectively, our results

demonstrate that old carboxyl C (4,000 to 6,300 a BP) derived from lignin and tannin and associated with iron is photomineralized to CO_2.

The presence of iron may explain contrasting literature results from high[6-8] to little or no[5,8] lability of permafrost DOC to photomineralization. For example, undetectable photomineralization of permafrost DOC from Russian arctic thaw slumps[5] may have been due to the 100-fold dilution of the DOC with deionized water. Although dissolved iron was not reported,[5] dilution likely also resulted in the precipitation of iron (oxy)hydroxides and thus lower dissolved iron concentrations.[35] In a study of Russian arctic surface waters that likely contained permafrost DOC,[8] up to 13% of the DOC pool was photomineralized to CO_2, consistent with the presence of dissolved iron (3-7 μM). Provided that all permafrost DOC contains carboxyl C[6,27,36] and that permafrost soils generally contain high levels of leachable iron,[13-14,37-38] arctic permafrost DOC is labile to photomineralization in proportion to the iron present. Given that the export of iron is currently strongly, positively correlated with DOC export from arctic soils to surface waters,[14] we expect that iron and DOC export may continue to co-vary as permafrost soils thaw. Therefore, we predict that the yield spectrum of permafrost DOC will be within the range reported here in the future (Figure 3.2a).

The photomineralization yield spectra of permafrost DOC directly measured in this study have significantly shallower spectral slopes compared to those quantified indirectly for arctic surface water DOC (two-tailed, unpaired t-test; $p < 0.001$; Figure 3.A.1). Thus, permafrost DOC has relatively lower lability to photomineralization at UV wavelengths and higher lability at visible wavelengths (different at 95% confidence interval; Figure 3.A.1). If permafrost DOC comprises 100% of the DOC in surface water, photomineralization rates will increase by two-fold compared to current rates (Figure 3.7a) due to the higher lability of permafrost DOC at

visible wavelengths multiplied by the ~10-fold greater photon flux in the visible versus the UV light region (Table 3.A.4). It follows that photomineralization rates increase in proportion to the permafrost DOC exported to surface waters (Figure 3.7b).

3.5 Implications

The uncertainty in model predictions of future ecosystem C gain or loss crosses zero.[3] For example, under the RCP8.5 scenario a net ecosystem loss of C of 208 ± 307 Pg C is predicted by 2299 (average ± 1 SD). The large uncertainty in model predictions of permafrost C storage in this scenario includes a 20% probability that the net C storage is between +100 (gain) or -100 (loss) Pg C (see Appendix Section 3.7.8). Photomineralization of DOC to CO_2 is always a loss to the atmosphere, and as the net C gain or loss for any particular year or over time nears zero, the relative importance of photomineralization increases. Given that photomineralization rates of permafrost DOC are nearly two-fold higher than for modern DOC in arctic surface waters (Figure 3.7a), and assuming from 2010 to 2299 75% of DOC in surface waters was delivered from permafrost soils, then the photomineralization rates of 20 g C m^{-2} y^{-1} reported in Cory et al. (2014) would increase to 39 g C m^{-2} y^{-1}. Using a surface area of water in permafrost regions of 6%,[39] ~9 Pg CO_2 could be produced from the photomineralization of permafrost DOC by 2299 (see Appendix Section 3.7.8). In addition, if potentially more than half of future terrestrial C losses are lateral in hydrologic flow,[2] a pathway missing from models used in McGuire et al. (2018), photomineralization of that C would occur upon exposure to sunlight. For example, taking the predicted net ecosystem loss of 208 Pg C by 2299 under RCP8.5,[3] potentially another ~100 Pg C could be lost laterally and produce ~21 Pg C as CO_2 from photomineralization in surface waters (see Appendix Section 3.7.8).[4] CO_2 from photodegradation of permafrost DOC is conservative because it does not account for (a)

increased lability of permafrost DOC to microbial respiration following exposure to sunlight,[27,40] and (b) increased annual sunlight exposure due to more ice-free days for surface waters in a warmer Arctic.[41] Therefore, reducing the uncertainty on whether permafrost thaw will be a net sink or source of C to the atmosphere requires representing processes such as photochemistry in models of the future arctic C balance.

3.6 Acknowledgements

We thank N. Jeliniski, L. Treibergs, J. Dobkowski, K. Romanowicz, C. Armstrong, C. Cook, J. Albrigtsen, J. Jastrow, R. Matamala, T. Vugteveen, J. Lederhouse, and colleagues of the NSF Arctic LTER and Toolik Lake Field Station for assistance. We thank L. Xu, J. Burton, and staff at the WHOI NOSAMS facility for help with C isotope measurements. We thank J. Johnson and E. Kujawinski for feedback on the manuscript, and X. Yang, S. Cooley, and T. Pavelsky for determining water surface area in permafrost regions. Research was supported by NSF CAREER 1351745 (R.M.C.), DEB 1637459 and 1754835 (G.W.K.), the Camille and Henry Dreyfus Postdoctoral Program in Environmental Chemistry (R.M.C. and C.P.W.), the Frank and Lisina Hock Endowed Fund (C.P.W.), and the NOSAMS Graduate Student Internship Program (J.C.B.). All authors contributed to the study design, sample collection, laboratory experiments, data analysis, and manuscript preparation. The authors declare no competing financial interests. Data can be found at the Arctic LTER (https://arc-lter.ecosystems.mbl.edu/data-catalog).

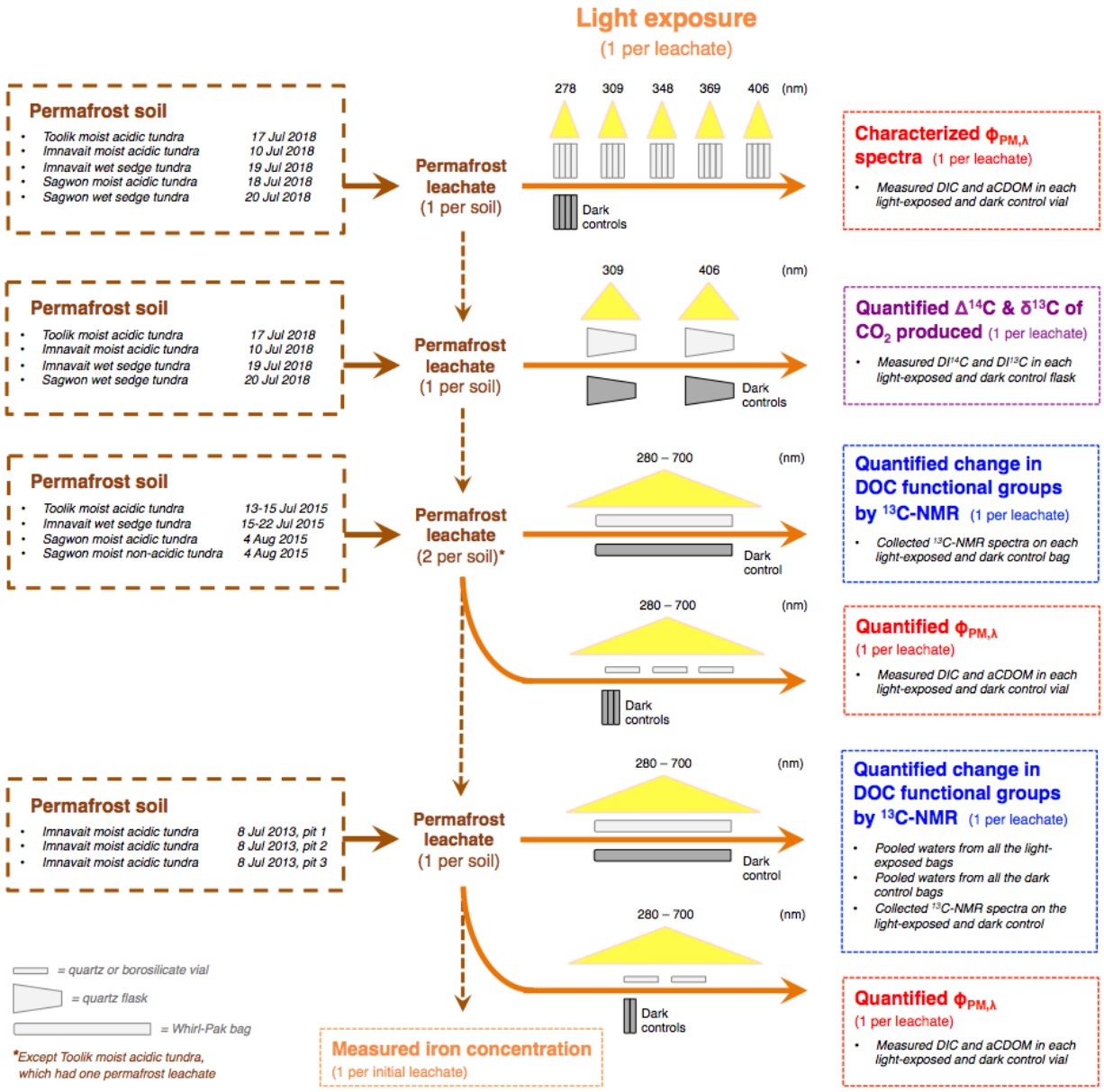

Figure 3.1. Experimental design for the light exposure experiments of permafrost DOC. Permafrost soils were collected at six different sites from two dominant vegetation types of the low Arctic and three glacial surfaces[15-17] on the dates indicated in the figure. One or two permafrost leachates were prepared from each permafrost soil. The concentration of total dissolved iron was measured in each permafrost leachate prior to light exposure following Stookey (1970).[43] Each permafrost leachate was exposed to either high-powered (≥ 100 mW), narrow-banded (± 10 nm) LEDs (at 278, 309, 348, 369, or 406 nm) or broadband light (280 – 700 nm; Tables 3.A.2, 3.A.3). Details from the light exposure of DOC leached from Imnavait moist acidic tundra permafrost soil collected in 2013 were previously reported.[6]

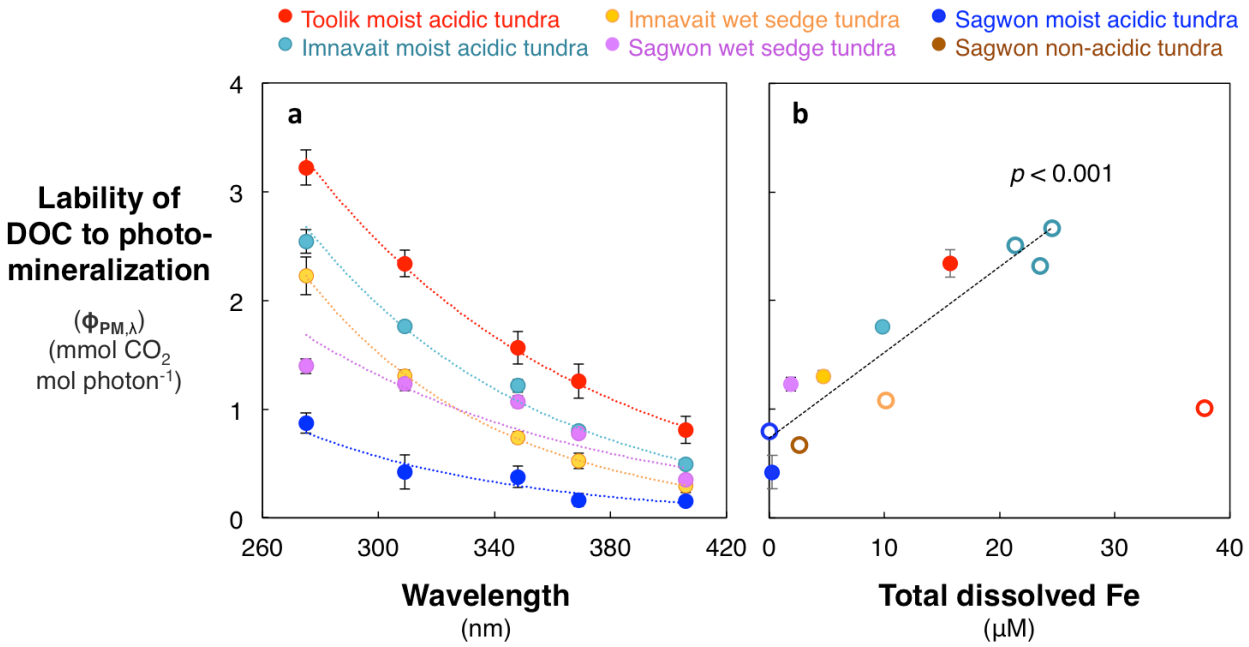

Figure 3.2. Controls on the lability of permafrost DOC to photomineralization. (a) Wavelength-dependent apparent quantum yield spectrum for photomineralization ($\varphi_{PM,\lambda}$) of permafrost DOC. Each data series was fit with a least-squares exponential model where $R^2 > 0.83$, $p < 0.05$. (b) Apparent quantum yield for photomineralization at 309 nm ($\varphi_{PM,309}$) versus total dissolved iron concentration in permafrost leachates prior to light exposure. Closed symbols indicate $\varphi_{PM,309}$ measured following LED exposure at 309 nm. Open symbols indicate $\varphi_{PM,309}$ estimated from an exponential fit following exposure to broadband light (see Methods Section 3.3.6). Data in (b) were fit using a least-squares regression where $R^2 = 0.87$, t-statistic = 7.8, $p < 0.001$, excluding the open red symbol (see Appendix Section 3.7.6). Open symbols for Imnavait moist acidic tundra were previously reported.[6] All values are the average ± 1 standard error of experimental replicates ($n = 2$ and 4 for open and closed symbols, respectively). $\varphi_{PM,\lambda}$ at other wavelengths versus dissolved iron are reported in the Appendix Section 3.7.5.

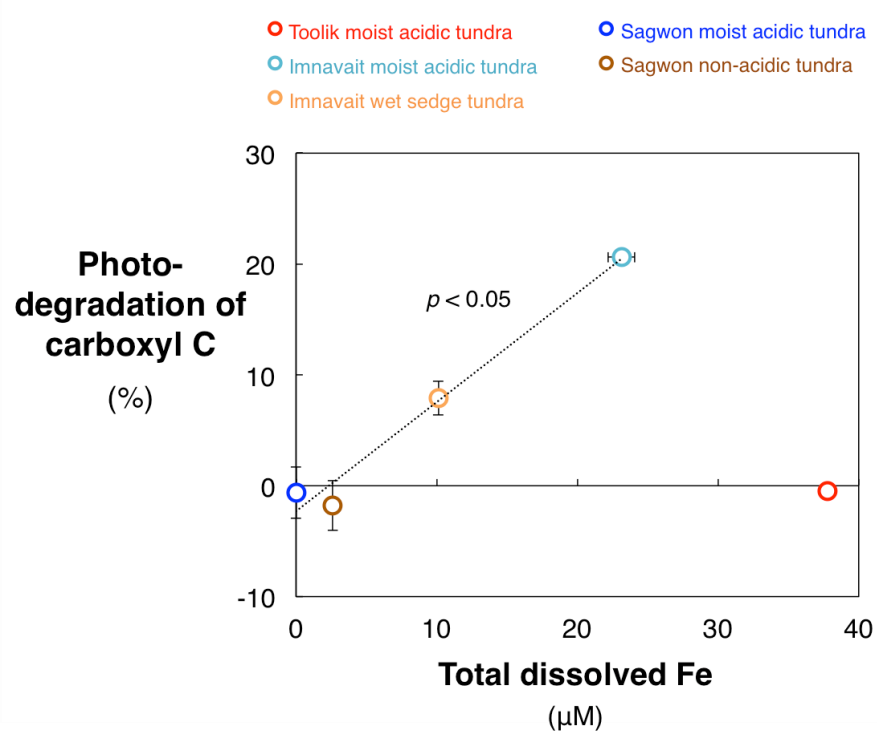

Figure 3.3. Photochemical degradation of carboxyl C increased with increasing dissolved iron. Percentage of carboxyl C degraded after exposure of permafrost DOC to broadband light relative to dark controls (quantified by ^{13}C-NMR) versus the total dissolved iron concentration in permafrost leachates prior to light exposure. Data were fit using a least-squares regression where $R^2 = 0.98$, t-statistic = 9.4, $p < 0.05$, excluding the red symbol (see Appendix Section 3.7.6). Data for Imnavait moist acidic tundra permafrost DOC were previously reported.[6] All values on the x-axis are shown as the average ± 1 SE of replicate permafrost leachates ($n = 2$, except Imnavait moist acidic tundra, which had $n = 3$). All values on the y-axis are shown as the average ± 1 standard error of replicate experiments ($n = 2$), except Toolik moist acidic tundra and Imnavait moist acidic tundra, which only had one experiment conducted (see Methods Section 3.3.6).[6]

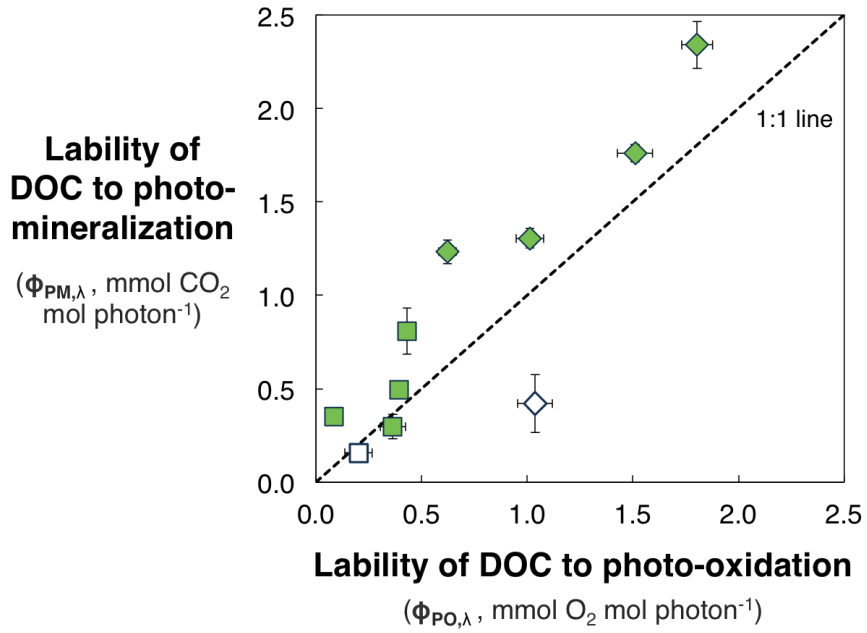

Figure 3.4. Apparent quantum yields for photomineralization and photo-oxidation of permafrost DOC. Apparent quantum yield (lability) for photomineralization ($\varphi_{PM,\lambda}$) versus the apparent quantum yield (lability) for photo-oxidation ($\varphi_{PO,\lambda}$) at UV (309 nm, diamond symbols) and visible (406 nm, square symbols) light plotted with the 1:1 line (dashed). Open symbols indicate the permafrost leachate with < 1 μM total dissolved iron. All values are shown as the average ± 1 standard error of experimental replicate vials (n = 4).

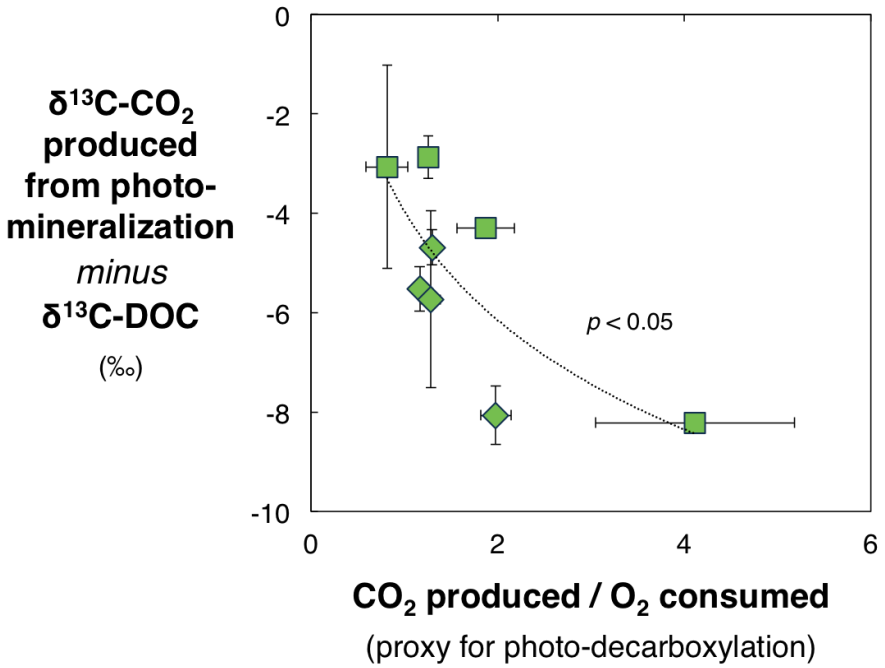

Figure 3.5. Photochemical production of ^{13}C-depleted CO_2 increased with the extent of photo-decarboxylation. δ^{13}C-CO_2 produced from photomineralization of permafrost DOC minus the δ^{13}C of initial, bulk DOC plotted versus the molar ratio of photochemical CO_2 production per O_2 consumed by permafrost DOC at UV (309 nm, diamond symbols) and visible (406 nm, square symbols) wavelengths of light. The molar ratio of photochemical CO_2 production to O_2 consumption is a proxy for the extent of photo-decarboxylation. Data were fit with a least-squares exponential model where $R^2 = 0.65$, t-statistic = 3.4, $p < 0.05$. Values on the x- and y-axes are shown as the average ± 1 standard error of experimental replicates (n = 4 and 2, respectively).

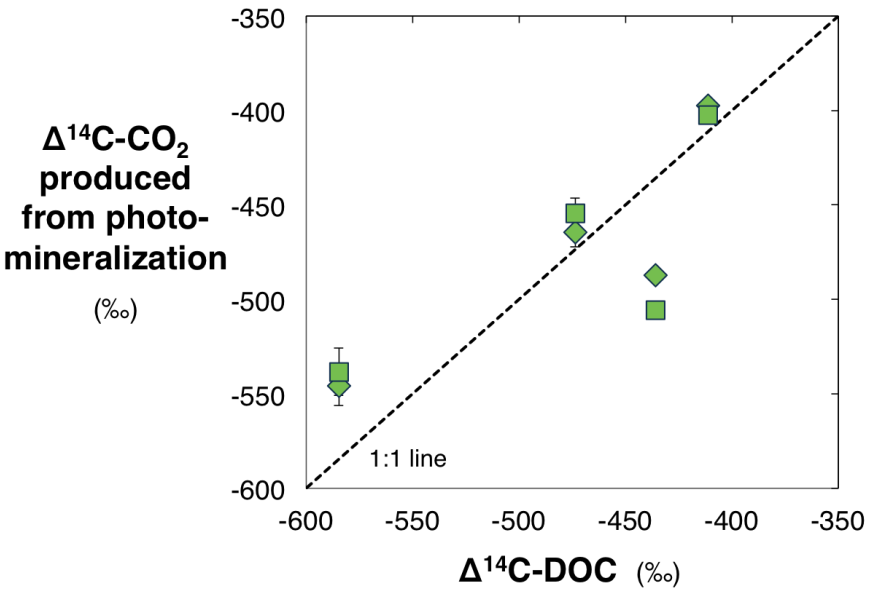

Figure 3.6. $\Delta^{14}C$ of bulk permafrost DOC was a strong predictor of the $\Delta^{14}C$-CO_2 produced from photomineralization of DOC. $\Delta^{14}C$-CO_2 produced from exposure of permafrost DOC to UV (309 nm, diamond symbols) and visible (406 nm, square symbols) wavelengths of light versus the $\Delta^{14}C$ of initial, bulk permafrost DOC plotted with the 1:1 line (dashed). When all data are fit using a least-squares regression, $R^2 = 0.66$, t-statistic = 3.4, $p < 0.05$. Values for photochemically produced $\Delta^{14}C$-CO_2 are shown as the average ± 1 standard error of experimental replicates ($n = 2$).

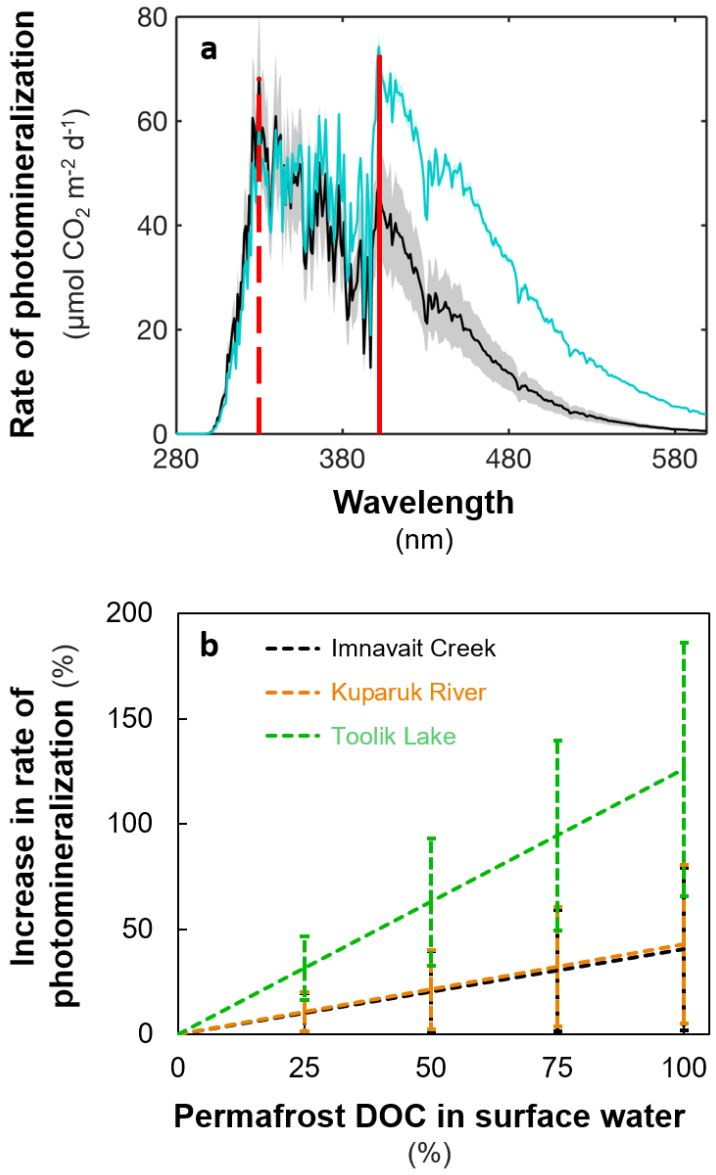

Figure 3.7. Photomineralization rates were higher for permafrost DOC than for surface water DOC due to higher lability in the visible light region. (a) Wavelength-dependent water column rates of photomineralization for Imnavait moist acidic tundra permafrost DOC and Imnavait Creek DOC (turquoise versus black line, respectively). Solid lines show the average photomineralization rate spectrum and the similar color shading shows the upper and lower 95% confidence intervals. Rates of photomineralization were calculated using the different wavelength-dependent apparent quantum yields for photomineralization ($\varphi_{PM,\lambda}$) for Imnavait moist acidic tundra permafrost DOC or Imnavait Creek DOC (Figure 3.A.1; see Appendix Section 3.7.3). The red dashed and solid lines mark the wavelength of peak photomineralization rates (330 nm versus 402 nm) for Imnavait Creek and Imnavait moist acidic tundra permafrost DOC, respectively. (b) Calculated photomineralization rates increased with an increasing fraction of permafrost DOC in the surface water DOC pool. Percent increase in photomineralization rates as permafrost DOC comprises 0-100% of the DOC pool in Imnavait

Creek, Kuparuk River, and Toolik Lake (compared to no permafrost DOC in the DOC pool). Only the $\varphi_{PM,\lambda}$ was varied in the water column rate calculations, using a 'mixed' $\varphi_{PM,\lambda}$ calculated as a mixture of the $\varphi_{PM,\lambda}$ for permafrost DOC with the $\varphi_{PM,\lambda}$ for the surface water DOC (see Appendix Section 3.7.3). All values are shown as the average ± 1 standard error of calculated rates for surface water DOC mixed with each of the five permafrost DOCs in this study (n = 5).

Permafrost soil	Landscape age (k a BP)	Glaciation	Date of soil collection	Location	Depth of soil collection (cm)	Thaw depth (cm)
Toolik moist acidic tundra	14	Itkillik I	13 Jul 2015	68°37'46.97"N, 149°34'49.29"W	95 – 110	--
			17 Jul 2018	68°37'16.18"N, 149°36'54.17"W	75 – 90	24
Imnavait moist acidic tundra	250	Sagavanirktok	8 Jul 2013	68°36'51.86"N, 149°18'30.87"W	90 – 105	20
			8 Jul 2013	68°36'51.86"N, 149°18'30.87"W	90 – 105	17
			8 Jul 2013	68°36'51.86"N, 149°18'30.87"W	90 – 105	21
			10 Jul 2018	68°36'35.36"N, 149°18'29.80"W	70 – 85	15
Imnavait wet sedge tundra	250	Sagavanirktok	22 Jul 2015	68°36'33.89"N, 149°18'52.58"W	90 – 130	--
			19 Jul 2018	68°36'31.90"N, 149°18'47.90"W	100 – 130	50
Sagwon wet sedge tundra	> 2,500	Gunsight Mountain	20 Jul 2018	69°20'38.66"N, 148°45'21.87"W	60 – 80	25
Sagwon moist acidic tundra	> 2,500	Gunsight Mountain	4 Aug 2015	69°25'28.70"N, 148°41'39.05"W	90 – 100	--
			18 Jul 2018	69°20'36.81"N, 148°45'31.75"W	75 – 90	40
Sagwon non-acidic tundra	> 2,500	Gunsight Mountain	4 Aug 2015	69°26'52.77"N, 148°36'42.21"W	90 – 100	--

Table 3.1. Date, location, and depth of permafrost soil collection. Permafrost soils were collected on three glacial surfaces and from the two dominant vegetation types of the low Arctic (upland moist acidic tussock tundra and lowland wet sedge tundra).[42-44] Thaw depth was not recorded during soil collection in 2015.

	Light source	Toolik moist acidic tundra	Imnavait moist acidic tundra	Imnavait wet sedge tundra	Sagwon wet sedge tundra	Sagwon moist acidic tundra
Δ^{14}C-DOC (‰)		– 436 ± 1	– 474	– 585	– 411	– 519
^{14}C age of DOC (a BP)		4,520 ± 5	5,080	6,990	4,300	5,890
δ^{13}C-DOC (‰)		– 25.5 ± 0.1	– 25.4	– 26.1	– 27.8	– 26.9
Δ^{14}C-CO_2 produced (‰)	UV	– 487 ± 4	– 465 ± 8	– 546 ± 11	– 397 ± 1	N/A
	Visible	– 506	– 454 ± 8	– 538 ± 13	– 402	N/A
^{14}C age of CO_2 produced (a BP)	UV	5,300 ± 55	4,950 ± 110	6,270 ± 190	4,000 ± 5	N/A
	Visible	5,600	4,800 ± 120	6,150 ± 220	4,070	N/A
δ^{13}C-CO_2 produced (‰)	UV	– 30.2 ± 0.4	– 31.0 ± 0.4	– 31.8 ± 1.8	– 35.8 ± 0.6	N/A
	Visible	– 29.8	– 28.3 ± 0.4	– 29.2 ± 2.0	– 36.0	N/A

Table 3.2. Δ^{14}C and δ^{13}C of initial, bulk permafrost DOC and the CO_2 produced by UV and visible light. The Δ^{14}C and δ^{13}C of the CO_2 produced from photomineralization of permafrost DOC are reported following exposure to LEDs at 309 (UV) or 406 nm (visible). When available, all values are reported as the average ± 1 standard error of experimental replicates (*n* = 2).

3.7 Appendix

3.7.1 Preparation and characterization of permafrost leachates from soils

Here we describe how permafrost leachates were prepared from soils collected in the summer of 2018 (Figure 3.1), including the precautions taken to minimize ^{14}C contamination during soil collection and while leaching DOC from those soils. We also describe the methodology for each chemical analysis conducted on the permafrost leachates prepared from soils collected in 2018.

3.7.1.1 Field and laboratory precautions to minimize ^{14}C contamination

Personnel digging soil pits and collecting soil samples wore new Tyvek protective coveralls (DuPont) and powder-free nitrile gloves (Kimberly-Clark) that were rinsed with deionized water (Barnstead E-Pure and B-Pure system) prior to soil collection. Soil samples were collected using a chisel that was rinsed with deionized water. Soil samples were quintuple-bagged using two Ziploc bags and three clear plastic bags so that a bag layer could be shed each time a sample was transferred to a new storage container (e.g., from a cooler to a freezer). Between shipments and experiments, soil samples were stored in freezers in ^{14}C-free facilities.

In the laboratory, the frozen soils were broken up into smaller pieces using a chisel that was rinsed with MilliQ water in between each use. New 5 gallon high-density polyethylene (HDPE) buckets with lids (Uline, Inc.) were used to leach the permafrost DOC. Those buckets were cleaned in between each use by rinsing 30 times with MilliQ water, soaking overnight in MilliQ water, and then rinsing again 30 times with MilliQ water. Each permafrost leachate was filtered through a sieve that was rinsed 30 times with MilliQ water in between use, and through new, MilliQ-rinsed high-capacity cartridge filters.

A leach test was conducted to quantify potential DOC contamination from the HDPE buckets by filling two HDPE buckets with five liters of MilliQ water covered with a HDPE lid. Buckets were leached at 25 °C for 24 hours. DOC was analyzed on the initial MilliQ water added to the buckets and on the water in each bucket after 24 hours using a Shimadzu TOC-V analyzer. The HDPE buckets leached on average 4.8 ± 2.2 μM DOC into solution during the 24-hour leaching (± 1 SE; n = 2; leaching rate of 58 ± 26 μg DOC L^{-1} per day). If each permafrost leachate was in a HDPE bucket for 2 days, and the DOC leached from plastic buckets were fossil (i.e., $\Delta^{14}C$ = -1000‰), then DOC leached from the HDPE buckets would result in ^{14}C-depletion of the permafrost DOC by -3.6 ± 1.1‰ (± 1 SE; n = 5 permafrost leachates). Thus, any ^{14}C contamination from using the 5 gallon HDPE buckets to leach DOC from the permafrost soil was within the instrumental precision of the radiocarbon analyses (≤ 6‰; see Methods Section 3.3.3).

3.7.1.2 Permafrost soil collection

Soil cores were collected at Imnavait wet sedge tundra using a SIPRE corer, and the permafrost layer (1.0 – 1.3 m below the surface) was separated from the soil core using a knife (Table 3.1). At the other four sites, 1 m x 1 m x 1 m soil pits were excavated using a jack hammer, shovels, and pickaxe (Table 3.1). Soil sampling at each site took place over the course of one day. From each site, an equal mass of soil (~2.5 kg) was placed in four Ziploc bags (1 gallon) and then each soil sample was quintuple-bagged. Following collection, soil samples were immediately transferred to coolers in the field and then stored in freezers at the Toolik Lake Field Station for ≤ 4 weeks until overnight shipment on dry ice to WHOI. All soil samples were frozen upon arrival at WHOI and immediately placed into ^{14}C-free freezers until further use.

3.7.1.3 Permafrost leachate preparation and characterization

DOC was leached from each permafrost soil at WHOI as described in the following five steps. First, frozen soil in one or two Ziploc bags was broken into smaller pieces inside the bag using a clean chisel. Second, 0.8 to 3.3 kg of frozen soil was transferred to a new Ziploc bag (1 gallon) and then thawed in a chest cooler at 4 °C for up to 20 hours (Table 3.A.5). Third, the thawed permafrost soil was added to five liters of MilliQ water in a MilliQ-rinsed HDPE bucket (5 gallon). Each bucket was covered with a HDPE lid and allowed to leach at 4 °C for 24 hours. Fourth, the permafrost leachate was filtered through a sieve with 60 μm nylon mesh screening (Component Supply) into a new, MilliQ-rinsed 5 gallon HDPE bucket and then placed in the chest cooler at 4 °C for ≤ 1 day to allow suspended particles to settle before additional filtration. Fifth, the 60-μm filtered leachate was filtered through 10 μm (Geotech Environmental Equipment, Inc.) and then finally through 0.2 μm (Whatman), MilliQ-rinsed high-capacity cartridge filters. Four liters of the final 0.2-μm filtered permafrost leachate (now referred to as permafrost leachate) were then transferred to a precombusted (450 °C; 4 h) 4 L glass amber bottle and kept at 4 °C prior to ^{14}C and ^{13}C analyses and the light exposure experiments. The remaining one liter of the permafrost leachate was transferred to amber HDPE bottles for water chemistry analyses (excluding ^{14}C and ^{13}C analyses).

Water chemistry analyses (pH, specific conductivity, iron, DOC, and cations) were performed on each of the permafrost leachates, as previously described.[40,42] Dissolved total and reduced iron concentrations were quantified using the Ferrozine method[43] immediately after permafrost leachate preparation (detection limit = 1 μM; coefficient of variance, CV, < 2% on triplicate analyses).[30] DOC concentrations were measured using a Shimadzu TOC-V analyzer (CV < 5% on duplicate analyses).[42] Water samples were analyzed for cations on a Thermo

Scientific 2 High-Resolution inductively coupled plasma mass spectrometer (ICP-MS; CV < 2% on triplicate analyses).[44] Chromophoric and fluorescent dissolved organic matter (CDOM and FDOM, respectively) were measured for each permafrost leachate,[4] and then the spectral slope ratio (S_R), specific UV absorbance at 254 nm ($SUVA_{254}$), and fluorescence index were calculated as previously described.[4]

3.7.2 Photon fluxes and rates of light absorption during LED experiments to characterize apparent quantum yield spectra

Solar irradiance spectra were measured from each ≥ 100 mW, narrow-banded (± 10 nm) LED (LG Innotek 6060 Series) at 278, 309, 348, 369, and 406 nm. The solar irradiance spectrum (W m^{-2} nm^{-1}) was measured in triplicate at the same height as the flat bottom of the 12 mL quartz vial and in each of the four positions of the inner aluminum housing with a radiometer over wavelengths from 250 to 500 nm (NIST-Calibrated Black Comet Spectral Radiometer, StellarNet, Inc.). Each spectrum (W m^{-2} nm^{-1}) was converted to a photon flux spectrum (mol photon m^{-2} s^{-1} nm^{-1}). The total photon flux spectrum during the light exposure period ($E_{0,\lambda}$; mol photon m^{-2} nm^{-1}) was calculated as the average of triplicate measurements multiplied by the light exposure time. The photon dose was calculated as the sum of the total photon flux spectrum across all wavelengths (mol photon m^{-2}).

A cross-validation of the photon flux estimated by radiometry was conducted using nitrite actinometry.[45] There was a < 10% difference in the photon flux of the 348-nm LED determined by actinometry versus radiometry (described above). Thus, the photon flux spectra from radiometry measurements were used to calculate the amount of light absorbed by CDOM in the quartz vials during each light exposure period.

For each vial exposed to a LED, the amount of light absorbed by CDOM ($Q_{a\lambda}$; mol photons m^{-2}) was calculated following:

$$Q_{a,\lambda} = \int_{\lambda_{min}}^{\lambda_{max}} E_{0,\lambda}(1 - e^{-a_{CDOM,\lambda} * z}) \frac{a_{CDOM,\lambda}}{a_{tot,\lambda}} d\lambda \quad (5)$$

where λ_{min} and λ_{max} are the minimum and maximum wavelengths of light absorbed by CDOM and $E_{0,\lambda}$ is the total photon flux spectrum reaching the quartz vial from an LED during the light exposure period (± 10 nm; n = 3; mol photon m^{-2} nm^{-1}). $a_{CDOM,\lambda}$ was calculated as the geometric mean of the light-exposed and dark control absorption coefficients of CDOM to account for loss of light-absorbing DOC (i.e., photobleaching of CDOM) during the light exposure period. We assumed that the pathlength (z) was equivalent to the height of each quartz vial (10 cm) and that $a_{CDOM,\lambda}/a_{tot,\lambda}$ was equal to 1 given that CDOM was the main constituent absorbing light at UV and visible wavelengths in the filtered permafrost leachates.[4] The amount of light absorbed by CDOM at each wavelength was calculated as the average ± 1 SE of experimental replicate vials (n = 4). There was < 5% CV in the amount of light absorbed by CDOM between the experimental replicate vials (n = 4).

The irradiances received by permafrost DOC were chosen to achieve similar amounts of light absorbed by CDOM during the light exposure period at each wavelength and between all permafrost leachates. Thus, irradiances were chosen by taking into account that concentrations of a_{CDOM} decrease with increasing wavelength and permafrost leachates had different a_{CDOM} concentrations (Table 3.A.5). Photon doses ranged from 2 mol photon m^{-2} at 278 nm to 6 mol photon m^{-2} at 406 nm, resulting in an average of 2.40 ± 0.04 mol photon m^{-2} of light absorbed by CDOM at all wavelengths for four of the five permafrost leachates (± 1 SE; n = 20). The exception was the Sagwon moist acidic tundra permafrost leachate, which had no detectable CO_2

production at any wavelengths after CDOM absorbed 2.40 ± 0.04 mol photon m^{-2} of light. Thus, the Sagwon moist acidic tundra permafrost leachate was exposed to the LEDs for 30 hours with photon doses ranging from 5 to 28 mol photon m^{-2}, which resulted in an average of 4.04 ± 0.22 mol photon m^{-2} of light absorbed by CDOM at all wavelengths (± 1 SE; n = 5). The photon doses received by each permafrost leachate and amounts of light absorbed by CDOM in each permafrost leachate during LED exposure at 309 nm are reported in Table 3.A.2.

3.7.3 Photomineralization rate calculations

First, to quantify the effect of the shallower slope of the $\varphi_{PM,\lambda}$ spectrum on photomineralization rates, we calculated photomineralization rates in Imnavait Creek using the average $\varphi_{PM,\lambda}$ spectrum of the DOC in this surface water (Figure 3.A.1)[4,30] versus the $\varphi_{PM,\lambda}$ spectrum of Imnavait moist acidic tundra permafrost DOC (Figure 3.2a). Water column rates of photomineralization (mmol C m^{-2} d^{-1} nm^{-1}) were calculated in Imnavait Creek as the product of two spectra: the rate of light absorption by CDOM throughout the water column ($Q_{a,\lambda}$; mol photon m^{-2} d^{-1} nm^{-1}) and the apparent quantum yield for photomineralization ($\varphi_{PM,\lambda}$; mmol C mol $photon^{-1}$ nm^{-1}):

$$\text{Rate of DOC photomineralization} = \int_{\lambda_{min}}^{\lambda_{max}} Q_{a,\lambda}\varphi_{PM,\lambda}\, d\lambda \qquad (6)$$

Water column rates of light absorption by CDOM were calculated using the average $a_{CDOM,\lambda}$ in Imnavait Creek (m^{-1}),[4,30] the average depth of Imnavait Creek (0.5 m), and the daily incoming photon flux spectrum (mol photon m^{-2} d^{-1} nm^{-1}) measured on 21 June 2018 at the nearby Toolik Lake Field Station. Thus, differences in water column rates of photomineralization were due only to the $\varphi_{PM,\lambda}$ spectrum (Figure 3.7a).

Second, to estimate the effect of permafrost DOC on photomineralization rates in arctic surface waters, we quantified photomineralization rates in Imnavait Creek, Kuparuk River, and Toolik Lake (representative surface waters in the Arctic)[4] if permafrost DOC made up 0, 5, 10, 15, 20, and 25% of the total DOC pool. Photomineralization rates were estimated by 'mixing' (in the stated proportions of 0-25%) the $\varphi_{PM,\lambda}$ spectra for each of the five permafrost DOC samples in this study (Figure 3.2a) with the $\varphi_{PM,\lambda}$ spectra for DOC in each of the three surface waters (Figure 3.A.1).[4] For each calculation, a 'mixed' $\varphi_{PM,\lambda}$ spectrum was generated using a mixing equation ($\varphi_{PM\text{-}mixture,\lambda}$), where X is the fraction of permafrost DOC comprising the DOC pool (0-25%):

$$\varphi_{PM\text{-}mixture,\lambda} = (\varphi_{PM\text{-}permafrost,\lambda} * X) + (\varphi_{PM\text{-}surface\ water,\lambda} * (1 - X)) \quad (7)$$

Water column rates of photomineralization (mmol C m^{-2} d^{-1} nm^{-1}) were calculated as described above in the example for Imnavait Creek using the respective water column depth and average $a_{CDOM,\lambda}$ for each surface water,[4,30] and the daily incoming photon flux spectrum measured on 21 June 2018 at the Toolik Lake Field Station; described below). There were 90 photomineralization rates calculated: 5 permafrost $\varphi_{PM,\lambda}$ spectra x 3 surface water $\varphi_{PM,\lambda}$ spectra x 6 fractions of permafrost DOC in the DOC pool. The percent change in water column rates of photomineralization relative to no permafrost DOC is shown for each surface water DOC in Figure 3.7b as the average ± 1 SE of the calculated rates (n = 5 for each fraction of permafrost DOC in the DOC pool). The percent change in water column rates of photomineralization relative to no permafrost DOC in the surface water DOC pool is reported as the average ± 1 SE of the calculated rates in all three surface waters (n = 15 for each fraction of permafrost DOC in the DOC pool). The variance of each estimate represents the difference in the magnitude of the photomineralization yield spectra between each permafrost DOC and the DOC from each of

three arctic surface waters.[4] When reporting the results of these calculations, we assumed that all controls on DOC photomineralization aside from the $\varphi_{PM,\lambda}$ spectrum remain the same as previously described; i.e., DOC photomineralization will remain light-limited[30] and independent of rates of water column mixing,[46] and that any DOC photomineralized to CO_2 is rapidly replenished by new DOC exported from the riparian zone.[47-48]

3.7.4 Daily photon flux spectra reaching the Toolik Field Station

Daily downward photon flux spectra were generated from 15 May to 1 Oct for 2012, 2015, 2016, 2017, and 2018 as previously described.[4] Briefly, direct measurements of UV and photosynthetically active radiation (PAR) at the Toolik Lake Field Station (68.62° N, 149.29° W) were apportioned to a modeled solar spectrum and separated into direct and diffuse spectra. Wavelength-dependent correction factors were then applied to those spectra to account for atmospheric turbidity and Rayleigh scattering. The global photon flux spectra (mol photon m^{-2} s^{-1} nm^{-1}) were calculated as the sum of the corrected direct and diffuse photon flux spectra multiplied by the duration of time between consecutive UV and PAR measurements (5 minutes and hourly, respectively). Daily downward photon flux spectra were calculated as the sum of photon flux spectra for each time interval during each day (mol photon m^{-2} d^{-1} nm^{-1}).

Daily photon flux spectra were summed from 280 to 400 nm and 401 to 700 nm to calculate daily UV and PAR photon doses, respectively. Total summertime UV and PAR photon doses were then calculated as the sum of daily UV and PAR photon doses from 15 May to 1 Oct for each year (Table 3.A.4). There was on average 11-fold more visible light than UV light reaching the Toolik Lake Field Station for the 2012, 2015, 2016, and 2017 summer seasons (Table 3.A.4).

3.7.5 Total dissolved iron concentrations

There was a significant, positive linear relationship between the total dissolved iron concentration quantified using the Ferrozine method[43] versus by ICP-MS[44] for permafrost leachates prepared from soils collected in 2018 (t-statistic = 57.4, $p < 0.001$; Table 3.A.5). Because the Ferrozine method was used to quantify total dissolved iron in all permafrost leachates in this study (prepared from soils collected in 2013, 2015, and 2018), we report the results from this method in Figures 3.2b and 3.3.

3.7.6 Lability of permafrost DOC to photomineralization

There were significant, positive linear relationships between the $\varphi_{PM,\lambda}$ for permafrost DOC at 278, 309, 348, and 406 nm (in Figure 2.2a) versus the total dissolved iron concentration in permafrost leachates prior to light exposure ($p < 0.05$; quantified either using the Ferrozine method or by ICP-MS).[43-44] In contrast, there were no significant correlations of the $\varphi_{PM,\lambda}$ at any wavelength (Figure 3.2a) with concentrations of other dissolved cations in the permafrost leachates (Na, Ca, K, Mg, Ba, Mn, Zn, Al, or Si as quantified by ICP-MS; Table 3.A.5).[44] There were no significant correlations of the $\varphi_{PM,\lambda}$ at any wavelength (Figure 3.2a) with any proxy for the aromatic content of DOC (e.g., a_{305}, $SUVA_{254}$, or the fluorescence index) or a proxy for the average molecular weight of DOC (S_R; Table 3.A.5).

Photomineralization yields at 309 nm ($\varphi_{PM,309}$) for permafrost DOC exposed to either broadband light or a ≥ 100 mW, narrow-banded (± 10 nm) LED were significantly, positively correlated with total dissolved iron concentration in the permafrost leachates prior to light exposure (t-statistic = 8.2 or 5.0, respectively; $p < 0.05$; Figure 3.2b). There were no significant correlations of these $\varphi_{PM,309}$ values (Figure 3.2b) with any proxy for DOC chemical composition, such as a_{305}, $SUVA_{254}$, S_R, or fluorescence index (Tables 3.A.5, 3.A.6). There were no

significant correlations of $\varphi_{PM,309}$ obtained from exposure of permafrost DOC to broadband light (Figure 3.2b) with the % of aromatic or carboxyl C in the initial permafrost DOC quantified by ^{13}C-NMR (Table 3.A.6).

The Toolik moist acidic tundra permafrost leachate that was exposed to broadband light (Figure 3.1) was an outlier in the relationships shown in Figures 3.2b and 3.3. In Figure 3.2b, Toolik moist acidic tundra permafrost DOC showed a significantly lower $\varphi_{PM,309}$ than expected based on the initial iron concentration in the leachate (open red symbol). A lower photomineralization yield than expected may be due to the 2.6-fold higher light absorption of this permafrost DOC compared to the average amount of light absorbed by CDOM in the other permafrost leachates shown in Figure 3.2b (Table 3.A.2). As photon dose increases, the most photo-labile components of the DOC pool are consumed or altered, leaving behind less labile moieties with a lower capacity to form CO_2 per mol photon absorbed by DOC.[49] It is likely that most of the CO_2 was produced from Toolik moist acidic tundra permafrost DOC after relatively less light was absorbed by CDOM (i.e., after a shorter light exposure time). As CDOM continued to absorb light over the course of the experiment, less and less CO_2 was produced. Assuming that was the case, then $\varphi_{PM,309}$ is lower than expected based on the amount of iron present initially because it was calculated as the amount of CO_2 produced divided by more photons than were needed to produce that CO_2.

The relatively higher amount of light absorbed by CDOM in the Toolik moist acidic tundra permafrost leachate (Table 3.A.2) is consistent with this permafrost DOC as an outlier in Figure 3.3, showing no detectable loss of carboxyl C despite having the highest total dissolved iron concentration. Photodegradation of DOC is thought to both produce and remove carboxyl C.[11] Thus, no detectable loss of carboxyl C after exposure to a relatively higher photon dose

compared to the other permafrost DOC samples may be due to concurrent photochemical production and loss of carboxyl C, such that production of carboxyl C masks the loss of labile carboxyl C from photo-decarboxylation.[11]

Photomineralization rates averaged across all sites (lake and river) increased by 7 ± 3% (10% permafrost DOC addition) to 52 ± 20% (75% permafrost DOC addition, compared to no permafrost DOC in the DOC pool; ± 1 SE; n = 15; Figure 2.7b). For only lakes, the photomineralization rates increased by 94.5 ± 45% at 75% permafrost DOC addition (average ± 1 SE; n = 5; Figure 3.7b). The increase in photomineralization rates as permafrost DOC is exported to surface waters is due to significantly shallower spectral slopes directly measured in this study using LEDs compared to those quantified indirectly for arctic surface water DOC (two-tailed, unpaired t-test; $p < 0.001$; Figure 3.A.1). A shallower spectral slope for permafrost compared to surface water DOC indicates relatively lower lability to photomineralization at UV wavelengths and higher lability at visible wavelengths (different at 95% confidence interval; Figure 3.A.1). For example, higher lability of Imnavait moist acidic tundra permafrost DOC at visible wavelengths increased photomineralization rates in sunlit waters by nearly two-fold (6 ± 0.7 mmol CO_2 m^{-2} d^{-1} for Imnavait Creek DOC versus 10 ± 0.1 mmol CO_2 m^{-2} d^{-1} for Imnavait moist acidic tundra permafrost DOC; average ± 1 SE; n = 5 and 4, respectively; Figure 3.7a).

3.7.7 Photochemical production of ^{13}C-depleted CO_2

Photochemical production of ^{13}C-depleted CO_2 (Figure 3.5) was interpreted as the preferential photomineralization of DOC compounds that were ^{13}C-depleted. An alternative explanation is that photochemical isotope fractionation is taking place and resulting in an offset of the $\delta^{13}C$ of CO_2 relative to the $\delta^{13}C$ of initial DOC. Such fractionation has been reported for organic pollutants,[50-51] but not for DOC. However, there is no current method to our knowledge

to determine the effect of $\delta^{13}C$ source versus fractionation on the net offset of the $\delta^{13}C$ of CO_2 relative to the $\delta^{13}C$ of initial DOC. Given that lignin and tannin are commonly more depleted in ^{13}C compared to other fractions of DOC,[34,52] and lignin and tannin are preferentially removed during light exposure of permafrost DOC,[6,27] the most robust and simple interpretation is that ^{13}C-depleted DOC is photomineralized.

Together our results strongly suggest that iron catalyzes the oxidation of carboxylic acids attached to organic matter derived from lignin and tannin (Figures 3.2b, 3.3, 3.4, and 3.5). Given the evidence for iron-catalyzed photo-decarboxylation, we suggest that iron was likely closely associated (i.e., complexed) with the carboxylic acids that were photomineralized to CO_2.[53]

3.7.8 Comparative photochemical strengthening of arctic amplification

Determining the relative importance of photochemical conversion of permafrost C to CO_2 compared to net ecosystem storage (gain or loss) of C depends in part on the variability of model-predicted storage. As the net ecosystem storage term approaches zero, the photochemical term, which is always a loss of C to the atmosphere, will increase in importance. This is analogous to the current situation for the arctic terrestrial C balance, where aquatic losses of CO_2 to the atmosphere can be ~40-100% of net ecosystem exchange depending on the net terrestrial balance in any one year.[54-55] That is, for either the current arctic C balance or predicted C balance given permafrost degradation, if the estimated or predicted net ecosystem C storage is zero then up to 100% of C loss to the atmosphere comes from photomineralization in surface waters. To estimate the probability that model predictions in McGuire et al. (2018) fell within any given range, say -100 to +100 Pg C storage, we fit the data from McGuire et al. Figure 3 to a normal distribution. This fitting included results from all five models used at both scenarios (RCP4.5 and RCP8.5) and both time points (2100 and 2299). For the RCP8.5 scenario at 2299,

there was a cumulative probability of 0.40 (40%) that the average model predictions fell between -200 (loss to atm) to +200 Pg C (gain to land), and a 20% probability that the model predictions fell between -100 to +100 Pg C. The probabilities (percentages) that all other combinations of scenarios and time points (RCP4.5, RCP8.5, 2100, 2299) had model predictions between -100 to +100 Pg C ranged from 57% to 74%.

DOC from permafrost is more labile to photomineralization than DOC from currently thawed soils (Figures 3.7a, 3.A.1; Appendix Section 3.7.6). We calculated the impact of this lability on future rates of photomineralization assuming that from 2010 to 2299 75% of the DOC in surface waters was leached from thawed permafrost soils (Figure 3.7b), and we used the area of permafrost lost by 2299 in the RCP8.5 scenario from McGuire et al. (2018). For this area of permafrost lost we assumed a surface water fraction of 6% (S. Cooley, X. Yang, T. Pavelsky personal communication).[39] We used a rate of surface water photomineralization corresponding to the Toolik Lake value when 75% of the DOC is from permafrost of 39 g C m^{-2} y^{-1}, which is 94.5% higher (Figure 3.7b) than the 20 g C m^{-2} y^{-1} photomineralization reported in Cory et al. (2014). This rate applied to the area of surface water in the area thawed by permafrost results in ~9 Pg C photomineralized to CO_2.

As described in Plaza et al. (2019), potentially more than half of the C loss from thawing permafrost soils could be in lateral water flow rather than directly to the atmosphere. That means of the 208 Pg C predicted average ecosystem loss from thawing permafrost by 2299 (RCP8.5),[3] another ~100 Pg C may move from thawing permafrost soils to surface waters. We assume that this 100 Pg C exported from permafrost soils to surface waters in headwater catchments is primarily DOC.[56-57] To calculate the amount of this C that could be photomineralized, we used the ratio of DOC exported from the Kuparuk River basin each year[55]

to the photomineralization of DOC in the Kuparuk basin per year.[4] This ratio shows that ~ 11% of the C moved from land to surface waters would be photomineralized using the photomineralization rate of 20 g C m^{-2} y^{-1}, and if the higher rate for permafrost DOC of 39 g C m^{-2} y^{-1} is used, then ~ 21% or 21 Pg of the 100 Pg C from land could be mineralized in surface waters. Combining the photomineralization of ~ 9 Pg C with the additional photomineralization of 21 Pg C from the lateral loss of C gives a value of 30 Pg C from photomineralization, or ~14% of the 208 Pg C lost from permafrost by 2299.[3]

These predictions are likely conservative for several reasons. First, we are not including the photo-stimulated respiration of bacteria that is at least an additional 20% CO_2 produced in surface waters.[4,40] Second, we are using ecosystem C losses and not soil C losses (which are higher)[3] to estimate the lateral hydrologic loss. Third, we are not considering the photodegradation of permafrost DOC and particulate organic carbon laterally transported to surface waters during thermo-erosional failures.[40,58] Fourth, we are not accounting for earlier ice-off on lakes that would increase the time of open water and thus the annual surface water photomineralization of DOC.[41] Finally, we are not accounting for any photomineralization once river DOC enters oceans.

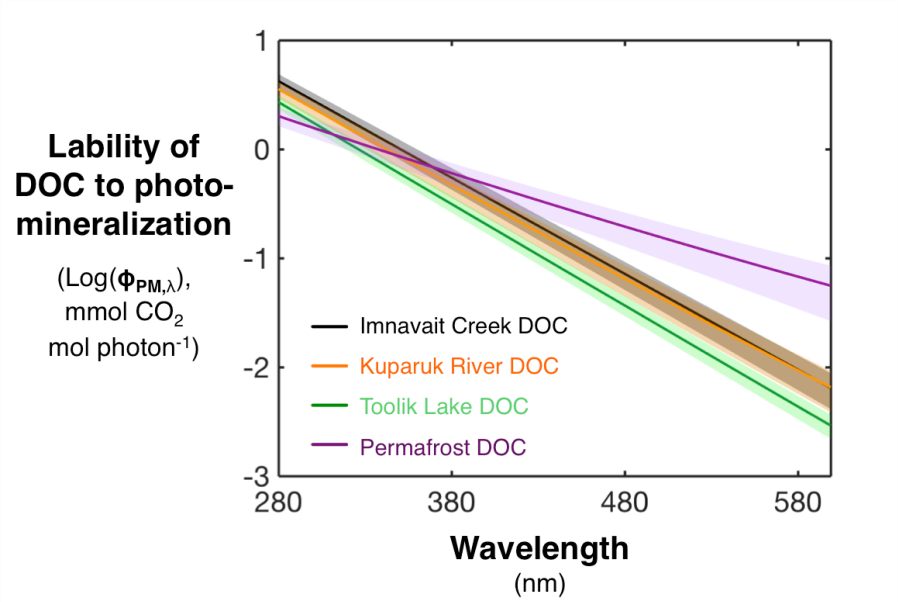

Figure 3.A.1. Photomineralization yield spectra for permafrost DOC were significantly shallower than for surface water DOC. Average wavelength-dependent apparent quantum yields (lability) for photomineralization ($\varphi_{PM,\lambda}$) of DOC in arctic surface waters compared to permafrost DOC measured in this study (Figure 3.2a). Data are plotted on the y-axis as log10 values of $\varphi_{PM,\lambda}$. Solid lines show the average $\varphi_{PM,\lambda}$ spectrum and the similar color shading shows the upper and lower 95% confidence intervals. $\varphi_{PM,\lambda}$ spectra were previously reported for DOC in Imnavait Creek, Kuparuk River, and Toolik Lake assuming an exponentially decaying spectrum.[4] The $\varphi_{PM,\lambda}$ spectral slopes directly measured for permafrost DOC in this study (-0.005 ± 0.0004 log10(mmol CO_2) mol photon^{-1} nm^{-1}; average ± 1 standard error; n = 5) were significantly shallower than those previously estimated indirectly for surface water DOC (-0.009 ± 0.0002 log10(mmol CO_2) mol photon^{-1} nm^{-1}; average ± 1 standard error; n = 3; two-tailed, unpaired t-test; t-statistic = 7.4, $p < 0.001$).

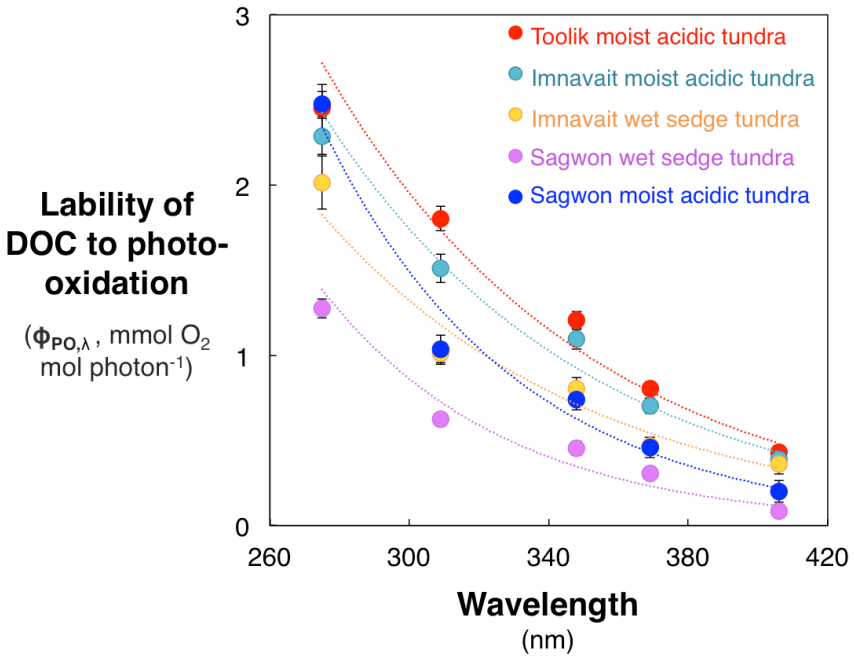

Figure 3.A.2. Wavelength-dependent apparent quantum yield spectra for photo-oxidation of permafrost DOC. Each data series was fit to an exponential model using a least-squares regression where $R^2 > 0.93$, $p < 0.05$. All values are shown as the average ± 1 standard error of experimental replicate vials ($n = 4$).

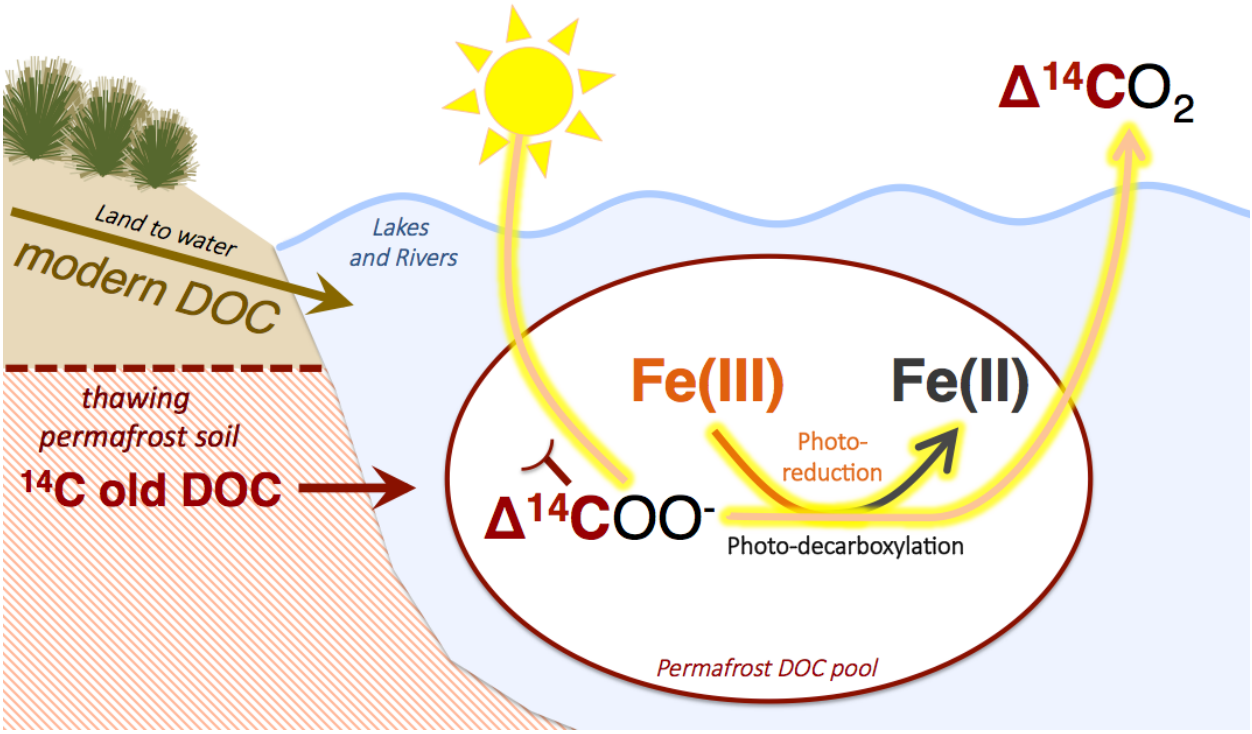

Figure 3.A.3. Sunlight and iron convert millennia-aged permafrost DOC to CO_2 in arctic surface waters.

Accession #	Permafrost soil	DOC or DIC analyzed for ^{14}C and ^{13}C	Light exposure experiment #	Treatment
OS-146256	Sagwon wet sedge tundra	DOC	N/A	N/A
OS-146257	Sagwon moist acidic tundra	DOC	N/A	N/A
OS-147265	Toolik moist acidic tundra	DOC	N/A	N/A
OS-147266	Toolik moist acidic tundra	DOC	N/A	N/A
OS-147267	Imnavait moist acidic tundra	DOC	N/A	N/A
OS-147268	Imnavait wet sedge tundra	DOC	N/A	N/A
OS-147595	Toolik moist acidic tundra	DIC	1	Dark control
OS-147596	Toolik moist acidic tundra	DIC	1	Dark control
OS-147597	Toolik moist acidic tundra	DIC	1	LED-exposed, 309 nm
OS-147598	Imnavait moist acidic tundra	DIC	2	Dark control
OS-147599	Imnavait moist acidic tundra	DIC	2	Dark control
OS-147600	Imnavait moist acidic tundra	DIC	2	LED-exposed, 309 nm
OS-147601	Imnavait moist acidic tundra	DIC	2	LED-exposed, 406 nm
OS-147602	Imnavait wet sedge tundra	DIC	3	Dark control
OS-147603	Imnavait wet sedge tundra	DIC	3	Dark control
OS-147604	Imnavait wet sedge tundra	DIC	3	LED-exposed, 309 nm
OS-147605	Imnavait wet sedge tundra	DIC	3	LED-exposed, 406 nm
OS-147606	Sagwon wet sedge tundra	DIC	4	Dark control
OS-147607	Sagwon wet sedge tundra	DIC	4	Dark control
OS-147608	Sagwon wet sedge tundra	DIC	4	LED-exposed, 309 nm
OS-147655	Toolik moist acidic tundra	DIC	5	Dark control
OS-147656	Toolik moist acidic tundra	DIC	5	LED-exposed, 406 nm
OS-147941	Sagwon wet sedge tundra	DIC	6	Dark control
OS-147942	Sagwon wet sedge tundra	DIC	6	LED-exposed, 406 nm

Table 3.A.1. Accession numbers for the permafrost leachates analyzed for carbon isotopes of DOC or DIC at the National Ocean Sciences Accelerator Mass Spectrometry facility. Permafrost leachates were prepared from soils collected in 2018 and the initial, bulk DOC was analyzed for ^{14}C and ^{13}C. DOC leached from the Toolik moist acidic tundra permafrost soil was analyzed in duplicate. Permafrost leachates were exposed to ≥ 100 mW narrow-banded (± 10 nm) LEDs at either 309 or 406 nm alongside one or two dark controls, and then the DIC in those waters was analyzed for ^{14}C and ^{13}C. Exposure of the Toolik moist acidic and Sagwon wet sedge tundra permafrost leachates to LEDs at 309 and 406 nm took place on separate days.

Permafrost leachate	Light source	Light exposure time (hr)	Photon dose (mol photon m^{-2})	Light absorbed by CDOM (mol photon m^{-2})
Toolik moist acidic tundra	LED	12	2.42	2.35
	Suntest XLS+	18	73.3	7.46
Imnavait moist acidic tundra	LED	12	2.83	2.53
	Natural sunlight	16	52.0	0.87 ± 0.12
Imnavait wet sedge tundra	LED	12	2.70	2.52
	Suntest XLS+	18	73.3	5.03 ± 0.26
Sagwon wet sedge tundra	LED	12	2.66	2.38
Sagwon moist acidic tundra	LED	30	6.81	3.65
	Suntest XLS+	18	73.3	1.61 ± 0.11
Sagwon moist non-acidic tundra	Suntest XLS+	18	73.3	4.20 ± 0.12

Table 3.A.2. Summary of the light exposure time, photon dose, and amount of light absorbed by CDOM during the light exposure experiments to quantify photomineralization yields of permafrost DOC at 309 nm. DOC leached from permafrost soils was exposed to ≥ 100 mW, narrow-banded (± 10 nm) LEDs at 309 nm, simulated sunlight (Atlas Suntest XLS+), or natural sunlight. Details from the natural sunlight exposure of Imnavait moist acidic tundra permafrost DOC were previously reported.[6] Light absorption by CDOM is reported as the average ± 1 standard error of replicate experiments with the permafrost leachates (n = 2, except Imnavait moist acidic tundra, which had n = 3).

Permafrost leachate	LED wave-length (nm)	Light exposure time (hr)	DIC_{dark} (μM)	$\Delta^{14}C$-DIC_{dark} (‰)	$\delta^{13}C$-DIC_{dark} (‰)	DIC_{light} (μM)	$\Delta^{14}C$-DIC_{light} (‰)	$\delta^{13}C$-DIC_{light} (‰)
Toolik moist acidic tundra	309	8	61 ± 2	– 245 ± 1	– 6.0 ± 0.1	161	– 395	– 21.0
	406	10	41	– 189	– 9.6	113	– 391	– 22.5
Imnavait moist acidic tundra	309	14	45 ± 2	– 159 ± 2	– 9.8 ± 0.1	118	– 348	– 22.9
	406	14	45 ± 2	– 159 ± 2	– 9.8 ± 0.1	111	– 335	– 20.8
Imnavait wet sedge tundra	309	24	227 ± 4	– 406 ± 3	5.8 ± 0.1	325	– 448	– 5.4
	406	24	227 ± 4	– 406 ± 3	5.8 ± 0.1	307	– 440	– 3.2
Sagwon wet sedge tundra	309	20	177 ± 1	– 235 ± 1	– 1.0 ± 0.1	232	– 273	– 9.1
	406	24.6	225	– 176	– 2.0	272	– 216	– 8.0

Table 3.A.3. Concentrations, $\Delta^{14}C$, and $\delta^{13}C$ of DIC in the light-exposed and dark control permafrost leachates following exposure to LEDs at 309 or 406 nm. Dark control water values are reported as the average ± 1 standard error of replicate flasks (n = 2). For the Imnavait moist acidic and wet sedge tundra permafrost leachates, the dark controls were the same for the LED exposures at 309 and 406 nm.

	Total summertime photon dose (mol photon m^{-2})	
Year	UV 280 – 400 nm	Visible 401 – 700 nm
2012	359	3,501
2015	366	3,575
2016	359	3,932
2017	321	4,007

Table 3.A.4. Total summertime UV and visible photon doses at the Toolik Lake Field Station from 15 May to 1 October for 2012, 2015, 2016, and 2017.

Objective:	(i) Characterize the photomineralization yield spectra for permafrost DOC					(ii) Quantify the ^{14}C and ^{13}C compositions of CO_2 produced by sunlight			
	Toolik moist acidic tundra	Imnavait moist acidic tundra	Imnavait wet sedge tundra	Sagwon wet sedge tundra	Sagwon moist acidic tundra	Toolik moist acidic tundra	Imnavait moist acidic tundra	Imnavait wet sedge tundra	Sagwon wet sedge tundra
Frozen soil weight (g)	800	812	803	800	803	2,292	3,261	1,448	2,391
Thaw time (hr)	13	12.5	18	13	12.5	12.5	12.5	19.5	12.5
DOC leaching rate (μmol C g-soil^{-1} d^{-1})	15.2	3.9	9.4	6.4	4.6	12.7	2.1	10.5	4.1
pH	6.5	5.8	7.0	6.5	8.0	5.8	6.0	7.0	7.2
Specific conductivity (μS cm^{-1})	17	9	28	18	146	29	12	51	34
Total Fe* (μM)	15.7	9.8	4.7	1.9	ND	30.0	31.0	8.8	1.7
Fe(II)* (μM)	8.4	5.6	ND	ND	ND	17.6	23.7	1.3	ND
Total Fe† (μM)	17.3	11.6	4.8	1.4	0.2	31.8	32.2	9.7	2.1
Total Mn† (μM)	0.3	0.1	0.1	0.5	0.4	0.7	0.3	0.2	0.8
DOC (μM)	2,435	643	1,520	1,019	718	5,820	1,340	3,017	1,931
a_{305} (m^{-1})	39	21	30	24	10	70	46	52	42
$SUVA_{254}$ (L mg^{-1} C m^{-1})	1.13	2.17	1.47	1.63	1.16	0.87	2.28	1.25	1.56
S_R (unitless)	0.87	0.92	1.09	0.94	1.00	0.88	0.81	0.94	0.93
Fluorescence index (unitless)	1.68	1.49	1.63	1.58	1.73	1.73	1.61	1.63	1.72

*Quantified using the colorometric Ferrozine method.[43]
†Quantified using inductively coupled plasma mass spectrometry.[44]

Table 3.A.5. Leaching conditions and chemical attributes of the permafrost leachates prepared from soils collected in 2018. Two different permafrost leachates were prepared from each permafrost soil to achieve objectives (i) and (ii) of this study (see Methods Section 3.3.1). The exception was Sagwon moist acidic tundra permafrost soil, which was not used for study objective (ii).

	Toolik moist acidic tundra	Imnavait moist acidic tundra	Imnavait wet sedge tundra	Sagwon moist acidic tundra	Sagwon moist non-acidic tundra
pH	7.0	5.8 ± 0.1	5.5 ± 0.1	7.7 ± 0.1	7.3 ± 0.1
Specific conductivity (μS cm^{-1})	30	9 ± 1	15 ± 1	177 ± 1	133 ± 3
Total Fe (μM)	37.8	23.1 ± 0.9	10.1 ± 0.1	ND	2.6 ± 0.2
Fe(II) (μM)	20.8	--	3.2 ± 0.5	ND	ND
DOC (μM)	2,356	998 ± 18	1,595 ± 20	2,077 ± 29	1,550 ± 68
a_{305} (m^{-1})	66	17 ± 3	55 ± 3	32 ± 1	63 ± 1
$SUVA_{254}$ (L mg^{-1} C m^{-1})	1.92	1.23 ± 0.15	2.27 ± 0.07	1.32 ± 0.01	2.91 ± 0.12
S_R (unitless)	0.85	0.96 ± 0.04	0.85 ± 0.01	0.88 ± 0.01	0.96 ± 0.1
Fluorescence index (unitless)	1.66	1.55 ± 0.01	1.53 ± 0.01	1.79 ± 0.01	1.61 ± 0.01
Aromatic C (%)	13	12	19 ± 1	11 ± 1	21 ± 1
Carboxyl C (%)	11	15	11 ± 1	12 ± 1	14 ± 1

Table 3.A.6. Chemical attributes of permafrost leachates prepared from soils collected in 2013 and 2015. All values are reported as the average ± 1 standard error of replicate experiments (n = 2, except Imnavait moist acidic tundra, which had n = 3, and Toolik moist acidic tundra, which did not have an experimental replicate). The pH, specific conductivity, DOC, and $SUVA_{254}$ for these permafrost leachates were previously reported.[26-27] Dissolved Fe(II) was not measured for the Imnavait moist acidic tundra permafrost leachate.[26] ND = not detectable.

3.8 References

1. Schuur, E. A. G., A. D. McGuire, C. Schädel, G. Grosse, J. W. Harden, D. J. Hayes, et al. (2015). Climate change and the permafrost carbon feedback. *Nature* 520: 171-179.

2. Plaza, C., E. Pegoraro, R. Bracho, G. Celis, K. G. Crummer, J. A. Hutchings, et al. (2019). Direct observation of permafrost degradation and rapid soil carbon loss in tundra. *Nat. Geosci.* 12: 627-631.

3. McGuire, A. D., D. M. Lawrence, C. Koven, J. S. Clein, E. Burke, G. Chen, et al. (2018). Dependence of the evolution of carbon dynamics in the northern permafrost region on the trajectory of climate change. *Proc. Natl. Acad. Sci. USA* 115: 3882-3887.

4. Cory, R. M., C. P. Ward, B. C. Crump, and G. W. Kling (2014). Sunlight controls water column processing of carbon in arctic fresh waters. *Science* 345: 925-928.

5. Stubbins, A., P. J. Mann, L. Powers, T. B. Bittar, T. Dittmar, C. P. McIntyre, et al. (2016). Low photolability of yedoma permafrost dissolved organic carbon. *J. Geophys. Res. Biogeosci.* 122: 200-211.

6. Ward, C. P., and R. M. Cory (2016). Complete and partial photo-oxidation of dissolved organic matter draining permafrost soils. *Environ. Sci. Technol.* 50: 3545-3553.

7. Selvam, B. P., J.-F. Lapierre, G. Guillemette, C. Voigt, R. E. Lamprecht, C. Biasi, et al. (2017). Degradation potentials of dissolved organic carbon (DOC) from thawed permafrost peat. *Nature Sci. Reports* 7, 45811.

8. Shirokova, L. S., A. V. Chupakov, S. A. Zabelina, N. V. Neverova, D. Payandi-Rolland, C. Causseraund, et al. (2019). Humic surface waters of frozen peat bogs (permafrost zone) are highly resistant to bio- and photodegradation. *Biogeosci.* 16: 2511-2526.

9. Miles, C., and P. Brezonik (1981). Oxygen consumption in humic-colored waters by a photochemical ferrous-ferric catalytic cycle. *Environ. Sci. Technol.* 15(9): 1089-1095.

10. Gao, H., and R. G. Zepp (1998). Factors influencing photoreactions of dissolved organic matter in a coastal river of the southeastern United States. *Environ. Sci. Technol.* 32: 2940-2946.

11. Xie, H., O. C. Zafiriou, W.-J. Cai, R. G. Zepp, and Y. Wang (2004). Photooxidation and its effects on the carboxyl content of dissolved organic matter in two coastal rivers in the southeastern United States. *Environ. Sci. Technol.* 38(15): 4113-4119.

12. Gu, Y., A. Lensu, S. Perämäki, A. Ojala, and A. V. Vähätalo (2017). Iron and pH regulating the photochemical mineralization of dissolved organic carbon. *ACS Omega* 2: 1905-1914.

13. Ping, C. L., J. G. Bockheim, J. M. Kimble, G. J. Michaelson, and D. A. Walker (1998). Characteristics of cryogenic soils along a latitudinal transect in Arctic Alaska. *J. Geophys. Res.* 103: 28917-28928.

14. Trusiak, A., L. A. Treibergs, G. W. Kling, and R. M. Cory (2019). The controls of iron and oxygen on hydroxyl radical (•OH) production in soils. *Soil Syst.* 3(1): 1-23.

15. Mull, C. G., and K. E. Adams (Eds.). (1989). *Bedrock Geology of the Eastern Koyukuk Basin, Central Brooks Range, and Eastcentral Arctic Slope Along the Dalton Highway, Yukon River to Prudhoe Bay, Alaska* (guidebook 7, vol. 1). Anchorage, AK: Department of Natural Resources, Division of Geological and Geophysical Surveys.

16. Walker, D. A., M. K. Raynolds, F. J. A. Daniëls, E. Einarsson, A. Elvebakk, W. A. Gould, et al. (2005). The Circumpolar Arctic vegetation map. *J. Veg. Sci.* 16: 267-282.

17. Hobbie, J. E., and G. W. Kling (Eds.). (2014). *Alaska's Changing Arctic: Ecological Consequences for Tundra, Streams, and Lakes.* Oxford, UK: Oxford University Press.

18. Beaupré, S. R., E. R. M. Druffel, and S. Griffin (2007). A low-blank photochemical extraction system for concentration and isotopic analyses of marine dissolved organic carbon. *Limnol. Oceanogr.: Methods* 5: 174-184.

19. Coplen, T. B., W. A. Brand, M. Gehre, M. Gröning, H. A. J. Meijer, B. Toman, and R. M. Verkouteren (2006). New guidelines for $\delta^{13}C$ measurements. *Anal. Chem.* 78: 2439-2441.

20. Longworth, B. E., K. F. von Reden, P. Long, and M. L. Roberts (2015). A high output, large acceptance injector for the NOSAMS Tandetron AMS system. *Nucl. Instr. Meth. Phys. Res. B* 361: 211-216.

21. Stuiver, M., and H. A. Polach (1977). Discussion: Reporting of ^{14}C data. *Radiocarbon* 19(3): 355-363.

22. McNichol, A. P., A. J. T. Jull, and G. S. Burr (2001). Converting AMS data to radiocarbon values: Considerations and conventions. *Radiocarbon* 43: 313-320.

23. Kana, T. M., C. Darkangelo, M. D. Hunt, J. B. Oldham, G. E. Bennett, and J. C. Cornwell (1994). Membrane inlet mass spectrometer for rapid high-precision determination of N2, O2, and Ar in environmental water samples. *Anal. Chem*. 66(23): 4166-4170.

24. McNichol, A. P., G. A. Jones, D. L. Hutton, and A. R. Gagon (1994). The rapid preparation of seawater ΣCO_2 for radiocarbon analysis at the National Ocean Sciences AMS facility. *Radiocarbon* 36(2): 237-246.

25. Ward, C. P., C. J. Armstrong, A. N. Walsh, J. J. Jackson, and C. M. Reddy (2019). Sunlight converts polystyrene into carbon dioxide and dissolved organic carbon. *Environ. Sci. Technol. Lett*. 6: 669-674.

26. Ward, C. P., and R. M. Cory (2015). Chemical composition of dissolved organic matter draining permafrost soils. *Geochim. Cosmochim. Acta* 167: 63-79.

27. Ward, C. P., S. G. Nalven, B. C. Crump, G. W. Kling, and R. M. Cory (2017). Photochemical alteration of organic carbon draining permafrost soils shifts microbial metabolic pathways and stimulates respiration. *Nat. Commun.* 8, 722.

28. Cory, R. M., D. M. McKnight, Y.-P. Chin, P. Miller, and C. L. Jaros (2007). Chemical characteristics of fulvic acids from Arctic surface waters: Microbial contributions and photochemical transformations. *J. Geophys. Res.* 112, G04S51.

29. Mangiante, D. M., R. D. Schaller, P. Zarzycki, J. F. Banfield, and B. Gilbert (2017). Mechanism of ferric oxalate photolysis. *ACS Earth Space Chem.* 1: 270-276.

30. Cory, R. M., K. H. Harrold, B. T. Neilson, and G. W. Kling (2015). Controls on dissolved organic matter (DOM) degradation in a headwater stream: the influence of photochemical and hydrological conditions in determining light-limitation or substrate-limitation of photo-degradation. *Biogeosci.* 12: 6669-6685.

31. Ball, G. I., and L. I. Aluwihare (2014). CuO-oxidized dissolved organic matter (DOM) investigated with comprehensive two dimensional gas chromatography-time of flight-mass spectrometry (GC x GC-TOF-MS). *Org. Geochem.* 75: 87-98.

32. Spencer, R. G. M., A. Stubbins, P. J. Hernes, A. Baker, K. Mopper, A. K. Aufdenkampe, et al. (2009). Photochemical degradation of dissolved organic matter and dissolved lignin phenols from the Congo River. *J. Geophys. Res.* 114, G03010.

33. Franke, D., M. W. Hamilton, and S. E. Ziegler (2012). Variation in the photochemical lability of dissolved organic matter in a large boreal watershed. *Aquat. Sci.* 74: 751-768.

34. Benner, R., M. L. Fogel, E. K. Sprague, and R. E. Hodson (1987). Depletion of ^{13}C in lignin and its implications for stable carbon isotope studies. *Nature* 329: 708-710.

35. Miller, C. J., A. L. Rose, and T. D. Waite (2009). Impact of natural organic matter on H_2O_2-mediated oxidation of Fe(II) in a simulated freshwater system. *Geochim. Cosmochim. Acta* 73: 2758-2768.

36. Feng, X., J. E. Vonk, C. Griffin, N. Zimov, D. B. Montluçon, L. Wacker, and T. I. Eglinton (2017). ^{14}C variation of dissolved lignin in arctic river systems. *ACS Earth Space Chem.* 1: 334-344.

37. Herndon, E. M., Z. Yang, J. Bargar, N. Janot, T. Z. Regier, D. E. Graham, et al. (2015). Geochemical drivers of organic matter decomposition in arctic tundra soils. *Biogeochem.* 126: 397-414.

38. Heslop, J. K., M. Winkel, K. M. Walter Anthony, R. G. M. Spencer, D. C. Podgorski, P. Zito, et al. (2019). Increasing organic carbon biolability with depth in yedoma permafrost: Ramifications for future climate change. *J. Geophys. Res. Biogeosci.* 124: 1-18.

39. Cooley, S. W., L. C. Smith, J. C. Ryan, L. H. Pitcher, and T. M. Pavelsky (2019). Arctic-Boreal lake dynamics revealed using CubeSat imagery. *Geophys. Res. Lett.* 46: 2111-2120.

40. Cory, R. M., B. C. Crump, J. A. Dobkowski, and G. W. Kling (2013). Surface exposure to sunlight stimulates CO_2 release from permafrost soil carbon in the Arctic. *Proc. Natl. Acad. Sci. USA* 110: 3429-3434.

41. Šmejkalová, T., M. E. Edwards, and J. Dash (2016). Arctic lakes show strong decadal trends in earlier spring ice-out. *Nature Sci. Reports,* 6, 38449.

42. Kling, G. W., G. W. Kipphut, M. M. Miller, and J. W. O'Brien (2000). Integration of lakes and streams in a landscape perspective: the importance of material processing on spatial patterns and temporal coherence. *Freshw. Biol.* 43: 477-497.

43. Stookey, L. L. (1970). Ferrozine—A new spectrophotometric reagent for iron. *Anal. Chem.* 42: 779-781.

44. Linge, K. L., and K. E. Jarvis (2009). Quadrupole ICP-MS: Introduction to instrumentation, measurement techniques and analytical capabilities. *Geostand, Geoanal. Res.* 33(4): 445-467.

45. Jankowski, J. J., D. J. Kieber, and K. Mopper (1999). Nitrate and nitrite ultraviolet actinometers. *Photochem. Photobiol. Sci.* 70(3): 319-328.

46. Li, A., A. F. Aubeneau, T. King, R. M. Cory, B. T. Neilson, D. Bolster, and A. I. Packman (2019). Effects of vertical hydrodynamic mixing on photomineralization of dissolved organic carbon in arctic surface waters. *Environ. Sci.: Processes Impacts* 21: 748-760.

47. Merck, M. F., B. T. Neilson, R. M. Cory, and G. W. Kling (2012). Variability of in-stream and riparian storage in a beaded arctic stream. *Hydrol. Process.* 26: 2938-2950.

48. Neilson, B. T., M. B. Cardenas, M. T. O'Connor, M. T. Rasmussen, T. V. King, and G. W. Kling (2018). Groundwater flow and exchange across the land surface explain carbon export patterns in continuous permafrost watersheds. *Geophys. Res. Lett.* 45: 7596-7605.

49. Miller, W. L., and R. G. Zepp (1995). Photochemical production of dissolved inorganic carbon from terrestrial organic matter: Significance to the oceanic organic carbon cycle. *Geophys. Res. Lett.* 22: 417-420.

50. Ratti, M., S. Canonica, K. McNeill, P. R. Erickson, J. Bolotin, and T. B. Hofstetter (2015). Isotope fractionation associated with the direct photolysis of 4-chloroaniline. *Environ. Sci. Technol.* 49(7): 4263-4273.

51. Willach, S., H. V. Lutze, K. Eckey, K. Löppenberg, M. Lüling, J. B. Wolbert, et al. (2018). Direct photolysis of sulfamethoxazole using various irradiation sources and wavelength ranges - Insights from degradation product analysis and compound-specific stable isotope analysis. *Environ. Sci. Technol.* 52(3): 1225-1233.

52. Bertoldi, D., A. Santato, M. Paolini, A. Barbero, F. Camin, G. Nicolini, and R. Larcher (2014). Botanical traceability of commercial tannins using the mineral profile and stable isotopes. *J. Mass Spectrom.* 49: 792-801.

53. Fujii, M., A. Imaoka, C. Yoshimura, and T. D. Waite (2014). Effects of molecular composition of natural organic matter on ferric iron complexation at circumneutral pH. *Environ. Sci. Technol.* 48: 4414-4424.

54. Kling, G. W., G. W. Kipphut, and M. C. Miller (1991). Arctic Lakes and Streams as Gas Conduits to the Atmosphere: Implications for Tundra Carbon Budgets. *Science* 251: 298-301.

55. McGuire, A. D., L. G. Anderson, T. R. Christensen, S. Dallimore, L. Guo, D. J. Hayes, et al. (2009). Sensitivity of the carbon cycle in the Arctic to climate change. *Ecol. Monogr.* 79: 523-555.

56. Judd, K. E., and G. W. Kling (2002). Production and export of dissolved C in arctic tundra mesocosms: the roles of vegetation and water flow. *Biogeochem.* 60: 213-234.

57. Kling, G. W., H. E. Adams, N. D. Bettez, W. B. Bowden, B. C. Crump, A. E. Giblin, et al. (2014). Land-Water Interactions. In J. E. Hobbie and G. W. Kling (Eds.), *Alaska's Changing Arctic: Ecological Consequences for Tundra, Streams, and Lakes* (pp. 143-172). Oxford, UK: Oxford University Press.

58. Turetsky, M. R., B. W. Abbott, M. C. Jones, K. W. Anthony, D. Olefeldt, E. A. G. Schuur, et al. (2019). Permafrost collapse is accelerating carbon release. *Nature* 569: 32-34.

Chapter 4

Iron and the Aromatic Content Control Photochemical Changes to the Oxidation State of Permafrost Dissolved Organic Matter at UV and Visible Wavelengths

4.1 Abstract

Sunlight exposure can impact the susceptibility of permafrost dissolved organic matter (DOM) to bacterial respiration by increasing or decreasing the oxidation state of DOM. Yet, controls on photochemical changes to the oxidation state of permafrost DOM remain too poorly understood to predict how much permafrost DOM will be respired to carbon dioxide by bacteria once it reaches sunlit freshwaters in the Arctic. Here, (1) changes to the oxidation state of DOM leached from four permafrost soils following exposure to ultraviolet (UV) and visible wavelengths of light were measured using high-resolution mass spectrometry and (2) chemical controls on the photochemical production (photo-production) of more versus less oxidized DOM compounds were tested. Following exposure to UV light, the DOM compounds photo-produced had a higher oxidation state compared to the initial permafrost DOM. This high oxidation state of DOM compounds photo-produced at UV wavelengths indicates that the amount of oxygen incorporated into DOM during partial photo-oxidation exceeded the amount lost from permafrost DOM. In contrast, the DOM compounds photo-produced at visible light were more oxidized or less oxidized than the initial DOM depending on the permafrost leachate. The generally lower oxidation state of DOM compounds photo-produced at visible light was likely due to a greater extent of iron-catalyzed photo-decarboxylation taking place at longer wavelengths compared to the UV, which converted carboxylic acids associated with permafrost DOM to carbon dioxide.

The photo-production of more oxidized DOM compounds at visible wavelengths increased with the aromatic content of DOM because these conjugated structures were likely needed to initiate the partial photo-oxidation of permafrost DOM. Findings from this study demonstrate that sunlight exposure of permafrost DOM can increase or decrease its oxidation state depending on the aromatic content of DOM draining from thawing permafrost soils and the amount of dissolved iron present to catalyze the photo-decarboxylation of DOM in neighboring freshwaters.

4.2 Introduction

Tremendous stores of organic matter in permanently frozen permafrost soils are thawing as the Arctic warms.[1-3] The dissolved organic matter (DOM) draining from thawing permafrost to freshwaters can be converted to CO_2 by sunlight and bacteria,[4-8] resulting in the amplification of global warming. For instance, recent work estimated that the sunlight-driven or photochemical degradation (photodegradation) of permafrost DOM to CO_2 can contribute an additional ~30 Pg of carbon to the atmosphere in the next 200 years[8] in addition to model predictions of future net ecosystem carbon loss from thawing permafrost soils.[2-3] The coupled photodegradation and bacterial respiration of permafrost DOM to CO_2 is expected to also become an increasingly important component of the arctic carbon budget as permafrost soils thaw.[5,9-10] However, the extent that bacterial respiration of sunlight-exposed permafrost DOM in arctic freshwaters amplifies global warming remains poorly constrained in part because photodegradation has contrasting effects on the susceptibility of DOM compounds to bacterial respiration.[5,10-11]

The effect of photodegradation on bacterial respiration of permafrost DOM is expected to depend partly on the chemical properties of DOM compounds produced during sunlight exposure. For example, it has been shown that the photo-production of smaller (i.e., lower

molecular weight) and more aliphatic DOM compounds increases bacterial respiration of DOM.[12-14] In addition, recent work showed that less oxidized compounds produced during the photodegradation of terrestrially-derived DOM are labile to bacterial respiration.[11] Findings from Ward et al. (2017) suggest that the oxidation state of DOM compounds photo-produced from permafrost DOM impacts its susceptibility to bacterial respiration.[12] Thus, photochemical changes to the oxidation state of permafrost DOM could impact how much will be respired to CO_2 by bacteria once it reaches sunlit freshwaters in the Arctic.

The oxidation state of sunlight-exposed DOM depends on the balance of two processes: photo-decarboxylation and partial photo-oxidation. Photo-decarboxylation involves the removal of carboxylic acids from DOM compounds,[8,15-16] resulting in a decrease to the average oxidation state of DOM. In contrast, partial photo-oxidation involves the incorporation of oxygen into DOM compounds likely by reactive oxygen species (ROS),[17-18] which increases the oxidation state of the DOM pool. It follows that a change to the oxidation state of permafrost DOM should come from the balance of more oxidized versus less oxidized compounds photochemically produced (photo-produced) during sunlight exposure. However, chemical controls on the photo-production of these DOM compounds remain too poorly understood to predict how the oxidation state of permafrost DOM will change as it is exposed to sunlight in arctic freshwaters.

One major challenge to investigating chemical controls on the photo-production of DOM compounds that are more oxidized versus less oxidized is that photo-decarboxylation and partial photo-oxidation can only be measured independently through analyses by ^{13}C-NMR[8,16] and the use of ^{18}O-labelled isotopic tracers,[17-18] respectively. Recent work used ^{13}C-NMR analyses to demonstrate that the amount of carboxylic acids removed from permafrost DOM during photo-decarboxylation increases with the concentration of dissolved iron,[8] suggesting that less oxidized

compounds should be photo-produced in proportion to the amount of dissolved iron present in arctic freshwaters. In contrast, chemical controls on the amount of ^{18}O-labelled oxygen incorporated into DOM from different ROS cannot be tested quantitatively.[17-18] As a result, the extent of partial photo-oxidation is often inferred from the molar ratio of photochemical CO_2 production to O_2 consumption (i.e., CO_2/O_2 ratio),[16,19-21] where low CO_2/O_2 ratios indicate that more oxygen was incorporated into DOM than removed as CO_2. However, a recent study estimated that this approach can underestimate partial photo-oxidation up to 4-fold because the photo-decarboxylation of DOM also impacts the CO_2/O_2 ratio.[18] Thus, measurements of the CO_2/O_2 ratio alone cannot be used to estimate the extent of partial photo-oxidation.

The extent of partial photo-oxidation likely depends on the quantity and quality of aromatic compounds within DOM. The absorption of sunlight by aromatic compounds within terrestrially-derived DOM produces ROS,[22-25] which can react with DOM to form more oxidized compounds.[18] For example, previous work showed that more oxidized, saturated compounds are photo-produced from terrestrially-derived DOM during the partial photo-oxidation of unsaturated compounds by ROS.[26] The amount of ROS available to partially oxidize DOM may also be limited by the abundance of phenolics associated with lignin-like compounds because they can quench ROS before the ROS partially oxidize DOM.[16,27] For instance, a lower phenolic content of permafrost DOM compared to the DOM currently draining to freshwaters from the active soil layer could explain the higher partial photo-oxidation observed for permafrost DOM in prior work.[16] Given that the aromatic content of DOM leached from different arctic permafrost soils can vary ~2-fold,[10,28-29] the amount of oxygen incorporated into permafrost DOM during partial photo-oxidation may increase with its total aromatic content, but decrease as phenolic moieties make up more of the aromatic carbon pool.

Recent work suggests that controls on the photo-production of more versus less oxidized DOM compounds may be tested at ultraviolet (UV) versus visible wavelengths of light, respectively. For instance, apparent quantum yields of photochemical ROS production from terrestrially-derived DOM have been shown to be higher at UV wavelengths than visible wavelengths,[20,30-32] suggesting that more partial photo-oxidation of DOM may take place at UV wavelengths of light. In addition, previous studies showed that dissolved iron absorbs more light at longer wavelengths,[33-34] suggesting that iron may catalyze the photo-decarboxylation of more lignin-like compounds within DOM at visible wavelengths of light. Consistent with these expectations, a recent study showed that the molar ratio of CO_2/O_2 for permafrost DOM was lower at UV wavelengths compared to the visible,[8] indicative of more oxygen being incorporated into DOM during partial photo-oxidation compared to the amount lost during photo-decarboxylation at UV wavelengths of light.

Thus, the goals of this study were to (1) measure changes to the oxidation state of permafrost DOM at UV versus visible wavelengths of light using high-resolution mass spectrometry and (2) investigate chemical controls on the photo-production of DOM compounds that are more versus less oxidized. DOM leached from four permafrost soils varying in DOM chemical composition and water chemistry[8] were used to investigate chemical controls on the oxidation state of photodegraded DOM. DOM compounds with a lower oxidation state were generally photo-produced at visible wavelengths than UV wavelengths of light, likely due to the greater extent of iron-catalyzed photo-decarboxylation at longer wavelengths. The incorporation of oxygen into DOM during partial photo-oxidation was controlled by the quality and quantity of aromatic compounds within permafrost DOM. Together, findings from this study suggest that the decreased oxidation state of permafrost DOM previously observed following sunlight

exposure[10,16] is due to the photo-decarboxylation taking place at longer wavelengths of light, but that the magnitude of this decrease depends strongly on the aromatic content of the permafrost DOM draining to sunlit freshwaters in the Arctic.

4.3 Methods

4.3.1 LED exposure of permafrost DOM

DOM leached from four permafrost soils collected on the North Slope of Alaska (leachate) was exposed to UV and visible wavelengths of light as previously described.[8] Briefly, soils were collected from the permafrost layer (> 60 cm below the surface) at four sites underlying moist acidic tussock or wet sedge vegetation, and on three glacial surfaces with different ages on the North Slope of Alaska during the summer of 2018. The frozen soils were shipped overnight to the Woods Hole Oceanographic Institution (WHOI), where DOM was leached from each permafrost soil. The water and DOM chemistry of each permafrost leachate can be found in Bowen et al. (2020).[8]

For each permafrost soil sample, the leachate was brought to room temperature (within 24 hours) and then placed in up to four precombusted (450 °C; 4 hr) 600 mL quartz flasks with ground glass stoppers and no headspace. The flasks were exposed to custom-built light-emitting diode (LED) arrays consisting of ten ≥ 100 mW, narrow-banded (± 10 nm) chips at 309 or 406 nm alongside one or two foil-wrapped dark-control flasks for exposure times ranging from 8 to 25 hr. After LED exposure, water in each LED-exposed and dark-control flask was acidified with trace-metal grade phosphoric acid (85%) to pH < 2, stripped of dissolved inorganic carbon with high-purity N_2 gas to analyze the isotopic content of the dissolved inorganic carbon pool[8] and then shipped overnight to the University of Michigan for solid-phase extraction of the DOM.

4.3.2 Characterizing DOM compounds in the LED-exposed and dark-control waters

DOM in each LED-exposed and dark-control water was isolated by solid-phase extraction 18-40 days after the LED exposure experiments to analyze its chemical composition by high-resolution mass spectrometry. Briefly, DOM was extracted on a PPL solid-phase cartridge (100 mg resin, 1 mL volume; Bond Elut PPL, Agilent) and then eluted by gravity with LC-MS grade MeOH following Dittmar et al. (2008).[35] One PPL cartridge blank was collected by loading LC-MS grade H_2O as the water sample. Although the extraction efficiency was not quantified, previous studies have reported a ~60% extraction efficiency of arctic permafrost DOM onto PPL solid-phase cartridges.[10,36] Solutions of solid-phase-extracted DOM in MeOH (< 50 mg-C L^{-1}) were injected in triplicate into the electrospray ionization source (negative mode) of a 12T Bruker SolariX FT-ICR mass spectrometer (located at the Environmental Molecular Sciences Laboratory, Pacific Northwest National Laboratory). Each solid-phase-extracted DOM sample was analyzed alongside the PPL cartridge blank and a MeOH blank to test for contamination during sample preparation and analysis, respectively. Mass spectra were calibrated and formulas were assigned as previously described.[36] Formulas present in the mass spectra for each blank were removed from the list of formulas assigned for each replicate spectra for solid-phase-extracted DOM.

Two of the three replicate mass spectra for each of the solid-phase-extracted DOM samples were collected on the same date to assess the reproducibility of acquisitions. On average, 85% of the formulas assigned were common among the replicate spectra (n = 19). Peak magnitudes were also reproducible with average percent relative standard deviations (RSD) for replicate acquisitions of 13% (n = 19). On average, 51% of the peaks had magnitude ratios within 10% RSD (n = 19).

The third replicate mass spectrum for each solid-phase-extracted DOM sample was collected on a different date from the other two replicate acquisitions. There were no significant differences in any measure of the chemical properties of DOM between the first, second, and third replicate acquisitions ($p > 0.05$). There was < 3% coefficient of variance (CV) for the average molecular weight (m/z), oxygen to carbon (O/C) ratio, and hydrogen to carbon (H/C) ratio across the formulas assigned in each replicate acquisition (n = 19 DOM samples). The formulas present in each LED-exposed and dark-control DOM sample were selected among the formulas common to the triplicate acquisitions.

4.3.3 Identifying the DOM compounds photochemically removed and produced

Differences between LED-exposed and dark-control mass spectra for each permafrost DOM were analyzed to identify formulas completely removed during LED exposure and the formulas that simply decreased in intensity. The formulas completely removed during LED exposure were defined as the formulas present in the dark-control DOM and absent in the LED-exposed DOM. The formulas that decreased in intensity following LED exposure were identified as the formulas in the LED-exposed DOM sample that decreased in their relative peak intensity by > 20% relative to the respective dark-control DOM. The 95% confidence interval of the mean of replicate acquisitions for each DOM sample was used to determine if a decrease in relative peak intensity was significantly different from zero. The formulas completely removed and with decreased intensity in the LED-exposed DOM were identified relative to each dark-control DOM sample for the LED exposure experiment (n = 1 or 2).

Differences between LED-exposed and dark-control mass spectra were also analyzed to identify new formulas produced and the formulas that increased in intensity during LED exposure. The formulas newly formed during LED exposure were defined as the formulas

present in the LED-exposed DOM and absent in the dark-control DOM. The formulas that increased in intensity following LED exposure were identified as the formulas in the LED-exposed DOM sample that increased in their relative peak intensity by > 20% relative to the respective dark-control DOM, where the 95% confidence interval of the mean of replicate acquisitions was used to determine if an increase in relative peak intensity was significantly different from zero. The formulas newly formed and with increased intensity in the LED-exposed DOM were identified relative to each dark-control DOM sample for the LED exposure experiment (n = 1 or 2).

The formulas removed during LED exposure were defined as the formulas that were completely removed and decreased in intensity relative to dark-controls, whereas the formulas produced were defined as the formulas that were newly formed and increased in intensity relative to dark-controls. The average chemical properties of formulas that decreased in intensity were similar to those for the DOM formulas completely removed at both wavelengths (plotting along the 1:1 line; Figure 4.A.1). Likewise, the average chemical properties of formulas that increased in intensity were similar to those for the formulas produced at both wavelengths (plotting along the 1:1 line; Figure 4.A.2).

4.3.4 Chemical composition of the initial, photo-removed, and photo-produced DOM

Formulas in the dark-control DOM and those removed or produced were classified as aromatic or other compound classes as previously described.[37-39] Briefly, aromatic formulas were defined as those with a modified aromaticity index (AI_{MOD}) greater than or equal to 0.5.[37] Condensed aromatic-like formulas were defined as those with H/C = 0.2 – 0.8, O/C = 0 – 1.0, and $AI_{MOD} \geq 0.67$. Unsaturated hydrocarbon-like formulas were defined as those with H/C = 0.8 – 1.5 and O/C = 0 – 0.13. Lignin-like formulas were defined as those with H/C = 0.8 – 1.5, O/C

= 0.13 – 0.65, and AI_{MOD} < 0.67. Unsaturated hydrocarbon-like and lignin-like formulas were identified as aromatic if they also had $AI_{MOD} \geq 0.5$ (i.e., $0.5 \geq AI_{MOD} < 0.67$ for lignin-like formulas). Lipid-like formulas were defined as those with H/C = 1.5 – 2.5 and O/C = 0 – 0.3.[38-39]

The percentage that condensed aromatic-like, unsaturated hydrocarbon-like, lignin-like, and lipid-like formulas made up the total formulas assigned had a CV < 20, 11, 3, and 30% across replicate acquisitions. The percentages of total formulas that were aromatic, condensed aromatic-like, unsaturated hydrocarbon-like, lignin-like, and lipid-like formulas were positively correlated with the percentage that each compound class made up from the total peak intensity ($p < 0.001$ when data were fit using a least-squares regression).

The double bond equivalence (DBE) of each formula was also calculated.[37] The average chemical properties (O/C, H/C, or DBE) and chemical composition for the DOM formulas removed or produced are reported as the average ± 1 standard error (SE) of replicate values for the exposure experiments conducted alongside two dark-controls.

4.3.5 Statistical analyses

Two-tailed, paired t-tests were used to determine significant differences in DOM chemical properties and composition between the permafrost leachates and between the two wavelengths (309 versus 406 nm). T-tests were used to determine whether the slopes and intercepts of least-squares regressions between the DOM chemical properties and composition for the dark-control DOM, photo-removed compounds, and photo-produced compounds were significantly different from zero. Statistical significance was defined as $p < 0.05$.

4.4 Results

DOM leached from the permafrost soils had similar average chemical properties but varied in the composition of compound classes. The average ratios of O/C and H/C in the formulas assigned for each permafrost DOM varied < 10% and averaged 0.33 ± 0.01 and 1.25 ± 0.03, respectively (± 1 SE; n = 4; Table 4.1). There were no significant differences in the DBE of formulas between the permafrost DOM ($p > 0.05$), which had an average value of 9.8 ± 0.3 (± 1 SE; n = 4; Table 4.1). However, the DOM leached from the Sagwon wet sedge permafrost soil had significantly lower percentages of unsaturated aromatics and lignin-like formulas ($p < 0.05$) and a significantly higher percentage of lipid-like formulas compared to the other permafrost DOM ($p < 0.001$; Table 4.1). In addition, Toolik moist acidic permafrost DOM had a significantly lower percentage of condensed aromatics compared to the other DOM ($p < 0.05$; Table 4.1). DOM from the Imnavait permafrost soils had significantly higher percentages of aromatic formulas and lignin-like aromatics compared to the other soils ($p < 0.05$), consistent with the lower fluorescence indices of DOM for these soils (Table 4.1, Figure 4.A.3).

4.4.1 DOM formulas photo-removed at UV and visible wavelengths

In general, less oxidized, aliphatic lignin-like and aromatic formulas were removed during LED exposure of the permafrost DOM. The average O/C ratio of DOM formulas removed during LED exposure at 309 or 406 nm (Figure 4.1a) was generally lower than the average O/C ratio of formulas in the dark-control DOM (Table 4.1). Aliphatic lignin-like formulas were the main class of compounds photo-removed, making up 35 ± 2% of the DOM removed during LED exposure (average ± 1 SE; n = 9; Table 4.2). On average, 17 ± 5% of the formulas photo-removed were aromatic (± 1 SE; n = 9). Unsaturated hydrocarbon-like and lipid-like formulas each made up 13% of the DOM photo-removed on average (Table 4.2).

The average O/C and H/C ratios of DOM formulas photo-removed varied more across the permafrost leachates than the wavelength of light (Figure 4.1). For example, there were no significant differences in the average O/C or H/C ratios of formulas removed at 309 versus 406 nm. Instead, the average O/C and H/C ratios of DOM formulas photo-removed differed between the permafrost leachates at 406 nm. The formulas photo-removed from Toolik moist acidic permafrost at 406 nm had significantly higher average O/C and H/C ratios compared to the other leachates (Figure 4.1). In addition, the formulas photo-removed from the Imnavait permafrost DOM at 406 nm had significantly lower average O/C and H/C ratios compared to the other two leachates (Figure 4.1). The average O/C of formulas photo-removed at 406 nm increased linearly with the percent of lignin-like formulas that were aliphatic ($p < 0.05$; Figure 4.2a; see Appendix Section 4.8.1). At 309 nm, there were no significant differences between the average O/C or H/C ratio of formulas photo-removed between permafrost leachates (Figure 4.1).

As a result, the composition of compound classes comprising the DOM pool removed during LED exposure varied more across the permafrost leachates than the wavelength of light. For instance, there were no significant differences in the percentages of aromatic formulas or compound classes comprising the pool of DOM removed at 309 versus 406 nm in any permafrost leachate, except Sagwon wet sedge permafrost which had 1.1-fold less aliphatic lignin-like formulas photo-removed at 406 nm and Toolik moist acidic permafrost which had 8-fold more protein-like formulas photo-removed at 406 nm compared to at 309 nm. In contrast, the aromatic, lignin-like aromatics, condensed aromatics, and unsaturated hydrocarbon-like formulas all made up significantly lower abundances of the total formulas removed in the Sagwon wet sedge permafrost DOM compared to the other permafrost leachates ($p < 0.05$; Table 4.2). The formulas photo-removed from the Imnavait permafrost DOM had a significantly

higher percentage of condensed aromatics compared to the other permafrost DOM, and the Imnavait wet sedge permafrost had significantly less lipid-like formulas making up the DOM photo-removed ($p < 0.05$; Table 4.2).

4.4.2 DOM formulas photo-produced at UV and visible wavelengths

Less saturated and more conjugated, aliphatic lignin-like and aromatic formulas were primarily produced during LED exposure of the permafrost DOM. The average H/C ratios of DOM formulas photo-produced during LED exposure (Figure 4.1b) were generally lower than the average H/C ratio of formulas in the dark-control DOM (Table 4.1). In addition, the average DBE of DOM formulas produced was significantly higher than the average DBE of formulas in the dark-control ($p < 0.05$; Table 4.1, Figure 4.1c). Aromatic formulas made up the highest portion of the DOM produced during LED exposure at 44 ± 3% (average ± 1 SE; $n = 9$; Table 4.3), followed by aliphatic lignin-like and unsaturated hydrocarbon-like formulas. On average, aliphatic lignin-like and unsaturated hydrocarbon-like formulas made up 29 ± 2% and 18 ± 5% of the DOM photo-produced, respectively (± 1 SE; $n = 9$; Table 4.3).

The chemical properties and composition of DOM formulas photo-produced at each wavelength were similar for the Imnavait permafrost leachates, but differed for the other two leachates. For instance, the DOM formulas produced at 406 nm had significantly lower average O/C ratios than the formulas produced at 309 nm for the Toolik moist acidic and Sagwon wet sedge permafrost leachates (Figure 4.1a). In the Toolik moist acidic permafrost DOM, aromatic and condensed aromatic-like formulas made up 1.4- and 2.4-fold more of the DOM pool produced at 406 nm, respectively, compared to at 309 nm ($p < 0.05$; Table 4.3). The DOM photo-produced in the Sagwon wet sedge permafrost leachate at 406 nm had significantly less aromatic and lignin-like aromatics and more unsaturated hydrocarbon-like formulas compared to

the DOM photo-produced at 309 nm ($p < 0.05$; Table 4.3). There were no significant differences between the average O/C ratio, average H/C ratio, or the percentage of any compound class making up the pool of DOM photo-produced at 309 versus 406 nm for the Imnavait permafrost leachates (Table 4.3, Figure 4.1).

At 309 nm, less oxidized and more conjugated aromatic formulas were photo-produced in the Sagwon wet sedge permafrost DOM compared to the other permafrost DOM. The average O/C ratio of DOM formulas photo-produced at 309 nm in the Sagwon wet sedge permafrost leachate was significantly lower than that for the other permafrost leachates ($p < 0.05$; Figure 4.1a). The DBE of DOM formulas produced at 309 nm in this Sagwon permafrost was also significantly higher than that for the other leachates (Figure 4.1c). Condensed and unsaturated aromatics made up significantly more of the DOM photo-produced in the Sagwon wet sedge permafrost leachate than the other permafrost leachates, whereas aliphatic lignin-like formulas made up significantly less ($p < 0.05$; Table 4.3).

At 406 nm, the chemical properties and composition of DOM formulas photo-produced varied across the permafrost leachates. For instance, less oxidized and more conjugated formulas were produced at 406 nm in the Toolik moist acidic permafrost leachate, as shown by the significantly lower average O/C ratio and higher DBE for the formulas photo-produced in this leachate compared to the other leachates ($p < 0.05$; Figure 4.1). In contrast, significantly more oxidized (higher O/C) and less conjugated (lower DBE) formulas were produced at this wavelength in the Imnavait permafrost leachate compared to the other leachates ($p < 0.05$; Figure 4.1). The DOM formulas photo-produced at 406 nm in the Toolik moist acidic permafrost were made up of a significantly higher abundance of unsaturated aromatics and lower abundance of protein-like formulas compared to the other leachates ($p < 0.05$; Table 4.3). For the Imnavait

permafrost leachates, unsaturated aromatics made up significantly less of the DOM formulas photo-produced at 406 nm, whereas lipid-like formulas made up significantly more compared to the other leachates ($p < 0.05$; Table 4.3). The average O/C of formulas photo-produced at 406 nm increased linearly with the percent of aromatic formulas in the mass spectra ($p < 0.05$; Figure 4.2b; see Appendix Section 4.8.1).

4.5 Discussion

4.5.1 Partial photo-oxidation limited by unsaturated aromatics at UV wavelengths

The bulk chemical properties of DOM compounds produced relative to those removed during UV exposure of permafrost DOM demonstrate that partial photo-oxidation dominates over photo-decarboxylation at UV wavelengths of light. For example, the DOM compounds produced in three of the four permafrost leachates had a higher oxidation state, higher degree of saturation, and lower degree of conjugation as indicated by the higher average O/C and H/C ratios and lower average DBE compared to the compounds removed at UV light (Figure 4.1). The higher oxidation state of photo-produced compounds in these leachates indicates that more oxygen was incorporated into DOM than the amount of oxygen lost from DOM during photo-decarboxylation at UV light, even though there were high concentrations of dissolved iron present and lignin-like compounds available to undergo photo-decarboxylation (Table 4.1). Recent work showed that more oxidized, saturated compounds are produced during the partial photo-oxidation of unsaturated compounds within terrestrially-derived DOM by reactive oxygen species (ROS), including singlet oxygen ($^1O_2$) and superoxide ($O_2^{-\bullet}$).[26] Thus, the photo-production of more saturated, partially oxidized compounds in the permafrost leachates suggests that unsaturated hydrocarbons were a major compound class within DOM undergoing partial photo-oxidation at UV wavelengths.[40]

However, findings from this study suggest the extent that permafrost DOM gets partially oxidized at UV light is limited by the abundance of unsaturated aromatics needed to produce ROS. It is expected that the two ROS that partially oxidize unsaturated compounds ($^1O_2$ and $O_2^{-\bullet}$) are produced photochemically from unsaturated aromatic compounds within the DOM pool.[21-25] It follows that a lower abundance of unsaturated aromatics would lower ROS production and thus, their ability to partially oxidize permafrost DOM. Consistent with this idea, the one permafrost DOM that showed no detectable change in its oxidation state during UV exposure (Sagwon wet sedge tundra; Figure 4.1) also had a significantly lower abundance of unsaturated aromatics compared to the permafrost DOM where oxidized products were formed (Table 4.1). The absence of unsaturated hydrocarbons from the pool of DOM photo-removed from the Sagwon wet sedge permafrost at UV light (Table 4.2) further suggests that ROS production was too low for these compounds to undergo partial photo-oxidation. In contrast, unsaturated hydrocarbons made up ~20% of the DOM compounds photo-removed at UV light for the three permafrost leachates where more oxidized, saturated compounds were produced (Table 4.2).

An alternative explanation for the minimal change in oxidation state of the Sagwon wet sedge permafrost DOM at UV light is that the photo-decarboxylation of lignin-like compounds offset an increased oxidation state of DOM from partial photo-oxidation. Lignin-like compounds made up ~40% of the DOM pool removed from this permafrost leachate at UV light (Table 4.2), some of which could have undergone photo-decarboxylation. However, the low concentration of dissolved iron present in this permafrost leachate (~2 µM; Table 4.1) indicates that only a small portion of lignin-like compounds could undergo the iron-catalyzed photo-decarboxylation mechanism.[8] Thus, the lack of a detectable change to the oxidation state of the

Sagwon wet sedge permafrost DOM during UV light exposure was likely due to the low extent of partial photo-oxidation caused by the lower abundance of unsaturated aromatics.

4.5.2 The balance of photo-decarboxylation and partial photo-oxidation at visible wavelengths depended on the aromatic content of DOM

The bulk chemical properties of compounds produced and removed from permafrost DOM at visible light indicate that either partial photo-oxidation or photo-decarboxylation can drive the oxidation state of DOM at this waveband. For example, in the Imnavait permafrost leachates, the DOM compounds produced at visible light had a higher oxidation state and lower degree of conjugation compared to the compounds removed (plotting above and below the 1:1 line, respectively; Figure 4.1), suggesting that the extent that oxygen was incorporated into unsaturated compounds exceeded oxygen loss from DOM during photo-decarboxylation. In contrast, more oxidized compounds were photo-removed from the Toolik moist acidic and Sagwon wet sedge permafrost DOM at visible light followed by the formation of less oxidized products (Figure 4.1a). The significantly higher oxidation state of DOM compounds photo-removed in these two permafrost leachates at visible light compared to those removed in the Imnavait permafrost at either wavelength demonstrates that oxidized compounds were preferentially removed from the Toolik moist acidic and Sagwon wet sedge permafrost DOM. Furthermore, the low oxidation state of compounds photo-produced in the Toolik moist acidic and Sagwon wet sedge permafrost leachates indicates that more oxygen was lost from DOM during the photo-decarboxylation of lignin-like compounds than the amount of oxygen incorporated into DOM during partial photo-oxidation at visible light.

The extent that permafrost DOM underwent photo-decarboxylation at visible light likely depended on the quality of lignin-like compounds present to undergo this mechanism. For

instance, more compounds with a high oxidation state were photo-removed from permafrost DOM as a greater portion of lignin-like compounds were aliphatic (Figure 4.2a). More carboxyl groups are located on the aliphatic components of lignin-like compounds than aromatic ring structures.[41] Thus, a higher abundance of aliphatic lignin-like compounds within DOM would result in more carboxyl groups available to undergo the photo-decarboxylation mechanism in the presence of dissolved iron.

In contrast, the abundance of all aromatic-containing compounds within DOM determined whether the compounds produced at visible light were more versus less oxidized on average, where compounds with a higher oxidation state were produced at visible light when permafrost DOM had a higher aromatic carbon content (Figure 4.2b). For example, between the two permafrost leachates that had similarly high concentrations of total dissolved iron (~30 μM; Toolik and Imnavait moist acidic tundra; Table 4.1) that could initiate the photo-decarboxylation of DOM, the one with the higher aromatic content of DOM had more oxidized compounds formed, and the permafrost DOM with a lower aromatic content had compounds photo-produced with a lower oxidation state (Figure 4.1a). Aromatic compounds are the main light-absorbing constituent needed for DOM to produce ROS and undergo photochemical degradation.[22-24,42] It follows that a higher aromatic content of DOM would result in greater production of ROS[42] that can go on to partially oxidize DOM compounds, such as unsaturated compounds (see Section 4.5.1 above). Consistent with this idea, unsaturated hydrocarbons made up significantly less of the total DOM compounds photo-produced in the two permafrost leachates with the highest aromatic contents of DOM (Imnavait moist acidic and wet sedge tundra) compared to the permafrost DOM with lower aromatic contents (Table 4.3).

However, aromatics compounds can also limit partial photo-oxidation by quenching ROS before they partially oxidize DOM compounds. Phenolics associated with lignin-like aromatic compounds are expected to primarily quench ROS within terrestrially-derived DOM by acting as antioxidants.[27] Across the permafrost leachates, lignin-like compounds contained 31 ± 1% of the aromatic moieties within DOM (average ± 1 SE; n = 6; Table 4.1), suggesting that the majority of aromatic compounds present could contribute to ROS production rather than quenching. This low abundance of lignin-like aromatics within the permafrost DOM in this study is consistent with previous estimates that permafrost DOM has less lignin-like aromatics compared to the DOM currently draining to arctic freshwaters.[16] Thus, together the low abundance of lignin-like aromatics and greater removal of unsaturated hydrocarbons in the aromatic-rich permafrost DOM suggest that the aromatic compounds present within the DOM pool produced more ROS than quenching them at visible light, resulting in a higher extent of partial photo-oxidation by ROS as the aromatic content of DOM increased.

4.5.3 Evidence supporting the photo-decarboxylation of DOM at visible wavelengths

The oxidation state of DOM compounds photo-produced from the Sagwon wet sedge permafrost at each wavelength demonstrates that more photo-decarboxylation of lignin-like compounds takes place at visible light than the UV. This permafrost DOM had the lowest extent of oxygen incorporated into DOM during partial photo-oxidation as shown by the decreased oxidation state of DOM compounds photo-produced (Figure 4.1a) and the high molar ratio of photochemical CO_2 production to O_2 consumption at both wavelengths (Figure 4.3b).[8] These findings indicate that changes to the oxidation state of DOM during exposure to UV and visible light were mainly due to photo-decarboxylation. Thus, the larger decrease in oxidation state between the DOM compounds removed and produced at visible light compared to UV (plotting

lower than and on the 1:1 line in Figure 4.1a, respectively) suggests that more oxygen was lost during the photo-decarboxylation of carboxylic acids associated with lignin-like compounds at visible wavelengths.

A higher extent of the iron-catalyzed photo-decarboxylation of lignin-like compounds at visible than UV light is consistent with prior evidence suggesting that the complexation of iron with DOM compounds increases its light absorption at longer wavelengths. For instance, previous studies have showed that dissolved iron absorbs more light at longer wavelengths compared to the UV,[33-34] accounting for up to ~50% of the light absorption taking place by DOM at visible wavelengths.[34] It is expected that dissolved iron absorbs more light in the visible waveband because of its complexation with DOM compounds.[34] Given that dissolved iron has been shown to complex with carboxylic acids within DOM,[43] it is possible that the light absorption of iron complexed with carboxylic acids can initiate the ligand-metal-charge-transfer reaction where Fe(III) is photo-reduced to Fe(II) and DOM is oxidized to CO_2.[44] Thus, the complexation of dissolved iron with carboxylic acids that are associated with lignin-like compounds may initiate the photo-decarboxylation of permafrost DOM at visible wavelengths of light.

4.6 Conclusions and implications

The results of this study suggest that the quantity and quality of aromatic compounds within the DOM draining from thawing permafrost soils and the concentration of dissolved iron present in sunlit freshwaters will be major controls on the oxidation state of DOM compounds photo-produced. The exposure of permafrost DOM to UV and visible light generally resulted in an increase to the oxidation state of DOM compounds photo-produced (Figure 4.1a), unless the partial photo-oxidation of DOM was limited by a low abundance of aromatic compounds or the

portion of aromatics that were unsaturated. The greater iron-catalyzed photo-decarboxylation of DOM taking place at visible wavelengths of light compared to the UV meant that an increased oxidation state due to partial photo-oxidation could be increasingly offset by the removal of oxygen in carboxylic acids at longer wavelengths as dissolved iron concentrations increase. The low oxidation state of DOM compounds photo-produced in the Sagwon wet sedge permafrost at visible light (purple square in Figure 4.1a) further demonstrates that a small amount of dissolved iron (~2 μM; Table 4.1) can initiate photo-decarboxylation of DOM and thus, decrease the oxidation state of DOM compounds photo-produced when partial photo-oxidation is low.

An increased oxidation state of DOM compounds photo-produced with the aromatic content of DOM was observed following the broadband sunlight exposure of permafrost DOM in prior work[10,16] similar to that observed at visible light (circle and square symbols, respectively; Figure 4.3a). The one permafrost leachate that had a greater increase in the oxidation state of DOM compounds photo-produced than expected based on the DOM aromatic content had no detectable amounts of dissolved iron present (open circle in Figure 4.3a), suggesting that photo-decarboxylation reactions did not impact the oxidation state of compounds photo-produced. This comparison of findings in the current study to prior work suggests that the oxidation state of compounds photo-produced from permafrost DOM in sunlit freshwaters may increase in proportion to the aromatic content of DOM draining from thawing permafrost soils as long as dissolved iron is present at concentrations > 1 μM in arctic freshwaters.[42,45-46]

Findings from this study improve our ability to estimate the oxidation state of DOM compounds photo-produced from molar ratios of photochemical CO_2 production to O_2 consumption measured (i.e., CO_2/O_2 ratio). For instance, there were more oxidized DOM compounds photo-produced at UV and visible wavelengths of light when the molar ratio of

CO_2/O_2 was lower, and less oxidized DOM compounds photo-produced when the CO_2/O_2 ratio was higher (Figure 4.3b). These findings suggest that when the molar ratio of CO_2/O_2 is greater than ~1.5 for permafrost DOM, the amount of oxygen lost from DOM during photo-decarboxylation exceeds the amount incorporated into DOM compounds during partial photo-oxidation (Figure 4.3b). Moreover, CO_2/O_2 ratios as high as 4 for permafrost DOM may indicate that partial photo-oxidation is negligible and thus, photo-decarboxylation controls the oxidation state of DOM compounds photo-produced (Figure 4.3b).

4.7 Acknowledgments

We thank N. Jeliniski, L. Treibergs, J. Dobkowski, K. Romanowicz, C. Armstrong, C. Cook, J. Albrigtsen, J. Jastrow, R. Matamala, T. Vugteveen, J. Lederhouse, and colleagues of the NSF Arctic LTER and Toolik Lake Field Station for assistance. We thank R. Chu and staff at the Environmental Molecular Science Laboratory (EMSL) for help with FT-ICR mass spectrometry measurements. Research was supported by NSF CAREER 1351745 (R.M.C.), DEB 1637459 and 1754835 (G.W.K.), the Frank and Lisina Hock Endowed Fund (C.P.W.), and the Scott Turner Research Award at the University of Michigan (J.C.B.).

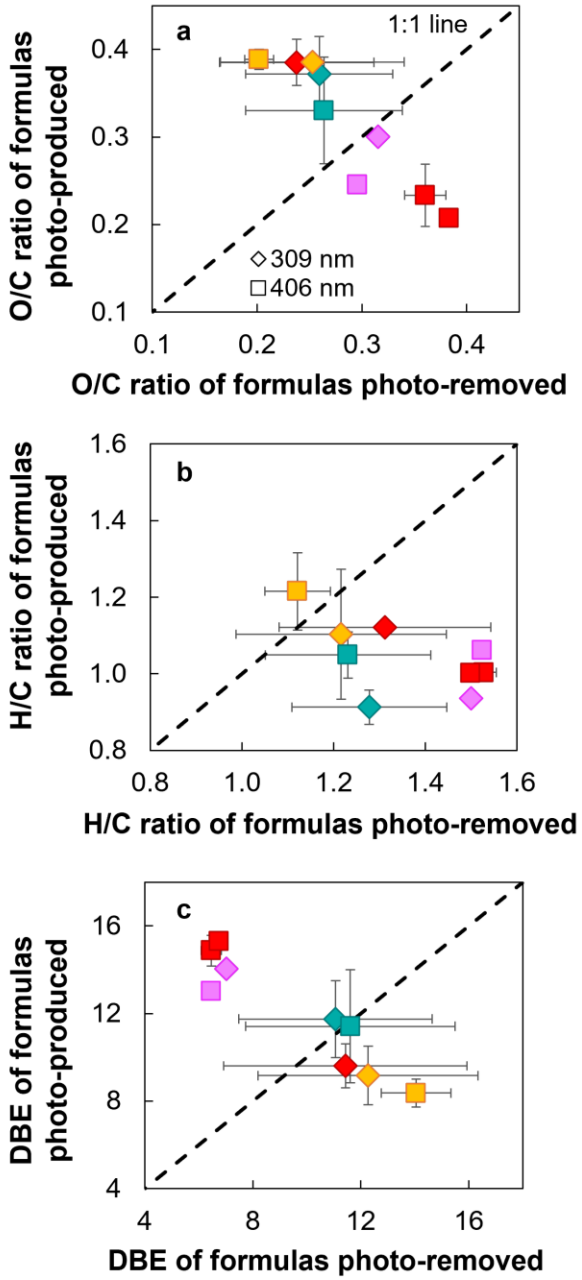

Figure 4.1. Oxidation state of DOM formulas produced and removed during the exposure of permafrost leachates to UV and visible light. Average (a) ratio of oxygen to carbon (O/C), (b) ratio of hydrogen to carbon (H/C), and (c) double bond equivalence (DBE) for the DOM formulas photo-removed versus the DOM formulas photo-produced at UV (309 nm; diamond symbols) and visible (406 nm; square symbols) wavelengths of light plotted along a 1:1 line for: Toolik moist acidic tundra (red symbol), Imnavait moist acidic tundra (teal symbol), Imnavait wet sedge tundra (yellow symbol), and Sagwon wet sedge tundra (purple symbol). Values on the x- and y-axes are shown as the average ± 1 standard error of experimental replicates (n = 2). When data in (a) are fit using a least-squares regression, y = [-1.14 ± 0.18]*x + [0.64 ± 0.05], R^2 = 0.85, p < 0.001 (± 1 standard error). When data in (c) are fit using a least-squares regression, y = [-0.80 ± 0.12]*x + [19.68 ± 1.17], R^2 = 0.87, p < 0.001 (± 1 standard error).

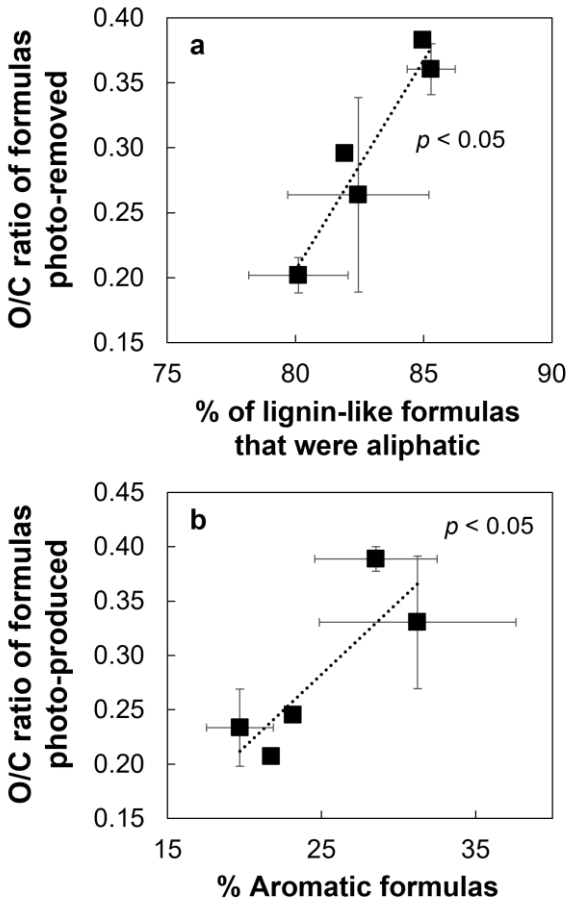

Figure 4.2. Impact of DOM chemical composition on the oxidation state of formulas produced and removed during the exposure of permafrost leachates to visible light. (a) The ratio of oxygen to carbon (O/C) of DOM formulas photo-removed at 406 nm increased with the percentage of lignin-like formulas that were aliphatic. (b) The O/C ratio of DOM formulas photo-produced at 406 nm increased with the percentage of aromatic formulas present in the mass spectra. The number of aliphatic, lignin-like and aromatic formulas identified in the mass spectra were not impacted by the ratios of O/C in the DOM formulas removed and produced during LED exposure (see Appendix Section 4.8.1). Values on the x- and y-axes are shown as the average ± 1 standard error of experimental replicates (n = 2).

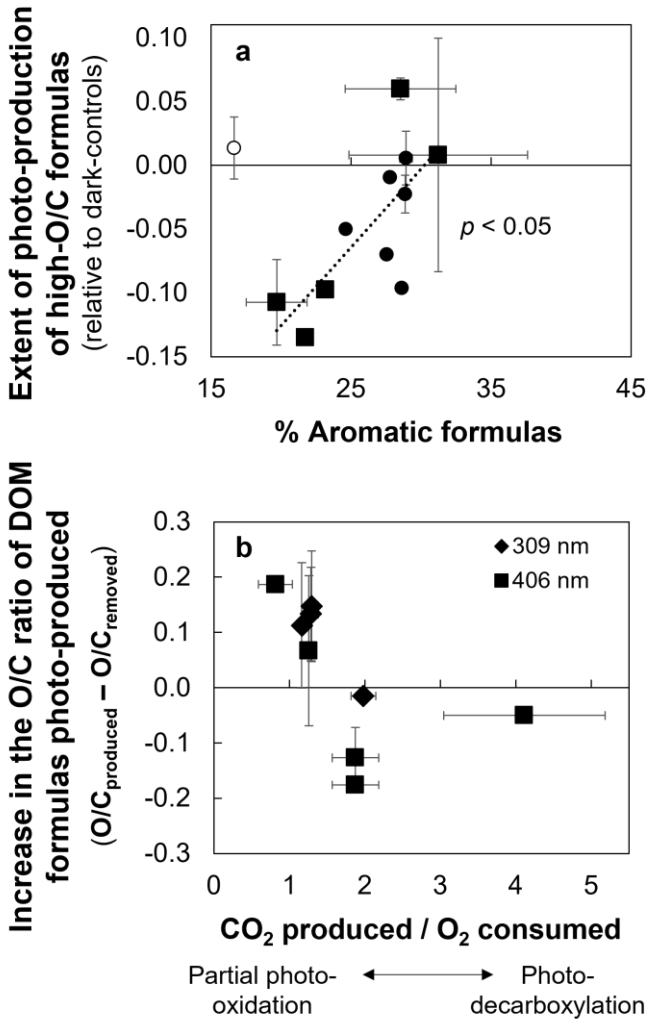

Figure 4.3. The oxidation state of DOM formulas photo-produced in the permafrost leachates were consistent with previous estimates from high-resolution mass spectrometry and molar ratios of photochemical CO_2 production to O_2 consumption. (a) The increased ratio of oxygen to carbon (O/C) in the DOM formulas produced following exposure to visible (406 nm; square symbols) and broadband (circle symbols) light relative to dark controls increased with the percentage of aromatic formulas present in the mass spectra. Changes to the oxidation state of permafrost DOM following broadband light were previously reported.[10,16] The O/C ratios of DOM formulas photo-produced are shown relative to dark controls to account for differences in the instrumental error between the three studies (see Appendix Section 4.8.1). (b) The increased O/C ratio of DOM formulas produced following exposure to UV (309 nm; diamond symbols) and visible (406 nm; square symbols) light relative to those photo-removed decreased with the molar ratio of photochemical CO_2 production to O_2 consumption. The molar ratios of CO_2 production to O_2 consumption were previously reported.[8] Values on the x- and y-axes are shown as the average ± 1 standard error of experimental replicates (n = 2). When all data points in (a), except the open circle, are fit to least-squares regression, $R^2 = 0.52$, $p < 0.05$. When all data points in (b), except the one with a CO_2 production to O_2 consumption ratio of 4, are fit to a least-squares regression, $R^2 = 0.77$, $p < 0.05$.

	Toolik moist acidic tundra	Imnavait moist acidic tundra	Imnavait wet sedge tundra	Sagwon wet sedge tundra
pH	5.84	5.99	7.05	7.22
Total dissolved Fe (μM)	30.0	31.0	8.8	1.7
$\delta^{13}C$ of DOC (‰)	-25.5	-25.4	-26.1	-27.8
Fluorescence index	1.73	1.61	1.63	1.72
$SUVA_{254}$ (L mg^{-1} C m^{-1})	0.87	2.28	1.25	1.56
O/C ratio	0.34 ± 0.01	0.32 ± 0.03	0.33 ± 0.02	0.34 ± 0.01
H/C ratio	1.31 ± 0.02	1.18 ± 0.07	1.24 ± 0.04	1.29 ± 0.01
DBE	9.4 ± 0.3	10.6 ± 1.4	10.0 ± 0.6	9.2 ± 0.1
Aromatic formulas (%)	20.4 ± 1.4	31.2 ± 6.4	28.5 ± 4.0	23.4 ± 0.3
Condensed aromatics (%)	2.1 ± 0.3	5.4 ± 1.4	4.7 ± 1.3	3.9 ± 0.1
Unsaturated hydrocarbons (%)	10.6 ± 1.0	11.3 ± 5.7	11.5 ± 3.0	8.1 ± 0.6
Unsaturated aromatics (%)	5.2 ± 0.4	6.6 ± 2.3	5.7 ± 1.4	3.4 ± 0.2
Lignin-like formulas (%)	44.7 ± 0.5	49.5 ± 2.8	42.6 ± 2.2	41.7 ± 0.7
Lignin-like aromatics (%)	6.6 ± 0.2	8.6 ± 0.9	8.4 ± 0.4	7.2 ± 0.1
Lipid-like formulas (%)	6.7 ± 0.9	6.8 ± 1.4	7.5 ± 0.7	12.3 ± 0.2

Table 4.1. Average water and DOM chemistry in the permafrost leachates. The ratios of oxygen to carbon (O/C) and hydrogen to carbon (H/C), double bond equivalence (DBE), and percentages of formulas in the mass spectra making up each compound class are listed as the average ± 1 standard error of experimental replicate dark controls (n = 2 or 3). The pH, concentration of total dissolved iron, the stable isotopic composition ($\delta^{13}C$) of DOC, fluorescence index, and specific ultraviolet absorbance at 254 ($SUVA_{254}$) for each permafrost leachate were previously reported.[8]

	Toolik moist acidic tundra	Imnavait moist acidic tundra	Imnavait wet sedge tundra	Sagwon wet sedge tundra
UV light (309 nm)				
% of formulas photo-removed	23 ± 4	35 ± 6	19 ± 5	39 ± 3
Composition of formulas photo-removed				
Aromatic (%)	21 ± 20	24 ± 20	28 ± 24	4 ± 1
Condensed aromatic (%)	1 ± 1	3 ± 2	7 ± 5	0.3 ± 0.1
Unsaturated hydrocarbon-like (%)	20 ± 20	20 ± 19	23 ± 21	0.5 ± 0.1
Unsaturated aromatic (%)	10 ± 10	10 ± 10	11 ± 10	0.3 ± 0.1
Lignin-like formula (%)	36 ± 1	41 ± 14	37 ± 16	43 ± 1
Lignin-like aromatic (%)	5 ± 4	5 ± 3	4 ± 3	3 ± 1
Lipid-like (%)	12 ± 8	7 ± 4	4 ± 1	22 ± 1
Visible light (406 nm)				
% of formulas photo-removed	44 ± 3	36 ± 11	18 ± 9	12
Composition of formulas photo-removed				
Aromatic (%)	2 ± 1	26 ± 20	41 ± 9	4
Condensed aromatic (%)	0.3 ± 0.1	5 ± 4	8 ± 6	0.5
Unsaturated hydrocarbon-like (%)	0.3 ± 0.1	17 ± 16	39 ± 1	0
Unsaturated aromatic (%)	0 ± 0	7 ± 6	19 ± 1	0
Lignin-like formula (%)	42 ± 3	45 ± 14	28 ± 8	38
Lignin-like aromatic (%)	1 ± 1	8 ± 4	8 ± 1	2
Lipid-like (%)	10 ± 2	7 ± 4	6 ± 1	39

Table 4.2. Extent and composition of DOM formulas photo-removed during the exposure of permafrost leachates to UV versus visible wavelengths of light. The percentages of total formulas removed and of compound classes comprising the total formulas removed are listed as the average ± 1 standard error of experimental replicates at each wavelength (n = 2).

	Toolik moist acidic tundra	Imnavait moist acidic tundra	Imnavait wet sedge tundra	Sagwon wet sedge tundra
UV light (309 nm)				
% of formulas photo-produced	37 ± 7	42 ± 1	66 ± 40	39 ± 0
Composition of formulas photo-produced				
Aromatic (%)	35 ± 2	54 ± 7	40 ± 16	52 ± 0
Condensed aromatic (%)	3 ± 0	13 ± 3	7 ± 1	14 ± 1
Unsaturated hydrocarbon-like (%)	10 ± 8	9 ± 8	2 ± 2	23 ± 0
Unsaturated aromatic (%)	5 ± 4	5 ± 5	1 ± 1	9 ± 1
Lignin-like formula (%)	48 ± 6	43 ± 10	43 ± 1	31 ± 1
Lignin-like aromatic (%)	9 ± 1	9 ± 1	10 ± 3	7 ± 1
Lipid-like (%)	3 ± 1	4 ± 2	7 ± 2	2 ± 1
Visible light (406 nm)				
% of formulas photo-produced	32 ± 4	36 ± 2	69 ± 42	21
Composition of formulas photo-produced				
Aromatic (%)	50 ± 1	45 ± 9	30 ± 11	37
Condensed aromatic (%)	7 ± 1	13 ± 4	4 ± 1	8
Unsaturated hydrocarbon-like (%)	33 ± 3	13 ± 10	2 ± 1	40
Unsaturated aromatic (%)	15 ± 1	6 ± 5	1 ± 1	15
Lignin-like formula (%)	31 ± 1	37 ± 12	45 ± 1	29
Lignin-like aromatic (%)	10 ± 1	8 ± 1	10 ± 3	5
Lipid-like (%)	3 ± 1	7 ± 2	6 ± 1	2

Table 4.3. Extent and composition of DOM formulas photo-produced during the exposure of permafrost leachates to UV versus visible wavelengths of light. The percentages of total formulas produced and of compound classes comprising the total formulas produced are listed as the average ± 1 standard error of experimental replicates at each wavelength (n = 2).

4.8 Appendix

4.8.1 Evaluating chemical controls on the oxidation state of DOM compounds removed and produced

Impacts of the initial chemical composition of DOM formulas on the average O/C ratio of DOM formulas photo-removed and photo-produced were evaluated to test chemical controls on the oxidation state of compounds removed and produced from permafrost DOM (Figure 4.2). The impacts of DOM chemical composition on the change in the average O/C ratio of DOM formulas removed or produced relative to dark-controls were not evaluated to test chemical controls because the O/C ratios of formulas in the dark-control DOM samples were used to identify the chemical composition of DOM formulas. For instance, aromaticity and compound classes are assigned using the elemental composition of each DOM formula in the mass spectra.[37-39] It follows that the percentage of DOM formulas with each chemical composition should be significantly correlated with ratios of O/C or H/C. Consistent with this idea, the percentage of aromatic formulas in the mass spectra significantly decreased with the average ratio of O/C in the replicate dark-control permafrost DOM samples ($p < 0.05$; $n = 9$; Table 4.1). In addition, the percentage of lignin-like formulas that were aliphatic generally increased with the average O/C ratio in the replicate dark-control permafrost DOM samples ($p > 0.05$; $n = 9$; Table 4.1).

However, there are two reasons why the impacts of the aromatic content of permafrost DOM on the change in the average O/C ratio of DOM formulas photo-produced relative to dark-controls were assessed when comparing results from the current study to those previously reported (Figure 4.3a). First, the average O/C ratios of formulas assigned in the mass spectra of dark-control DOM samples in these previous studies were significantly higher than those for the

dark-control samples in this study ($p < 0.05$; Table 4.1). For example, the average O/C ratios of formulas in the dark-control DOM leached from permafrost soils collected in 2013 and 2015 were 0.42 ± 0.01 and 0.49 ± 0.01, respectively (average ± 1 SE).[10,36] Thus, the photochemical production of DOM formulas with high versus low O/C ratios could only be interpreted relative to the initial O/C ratios of DOM formulas in the respective dark-control(s). Second, there were much larger differences in the average O/C ratio of DOM formulas produced between the permafrost leachates compared to the average O/C ratio of formulas in the dark-controls for each study. For example, the average O/C ratio of DOM formulas in the dark-control DOM samples varied < 6% in the current study (Table 4.1) and < 2% in prior work.[10,36] In contrast, the average O/C ratio of DOM formulas photo-produced varied 90% at visible light (Figure 4.1a) and 13-23% at broadband light in prior work.[10,16] Thus, the range of values shown on the y-axis of Figure 4.3a represent the average O/C ratios of DOM formulas photo-produced, not those in the dark-control DOM samples.

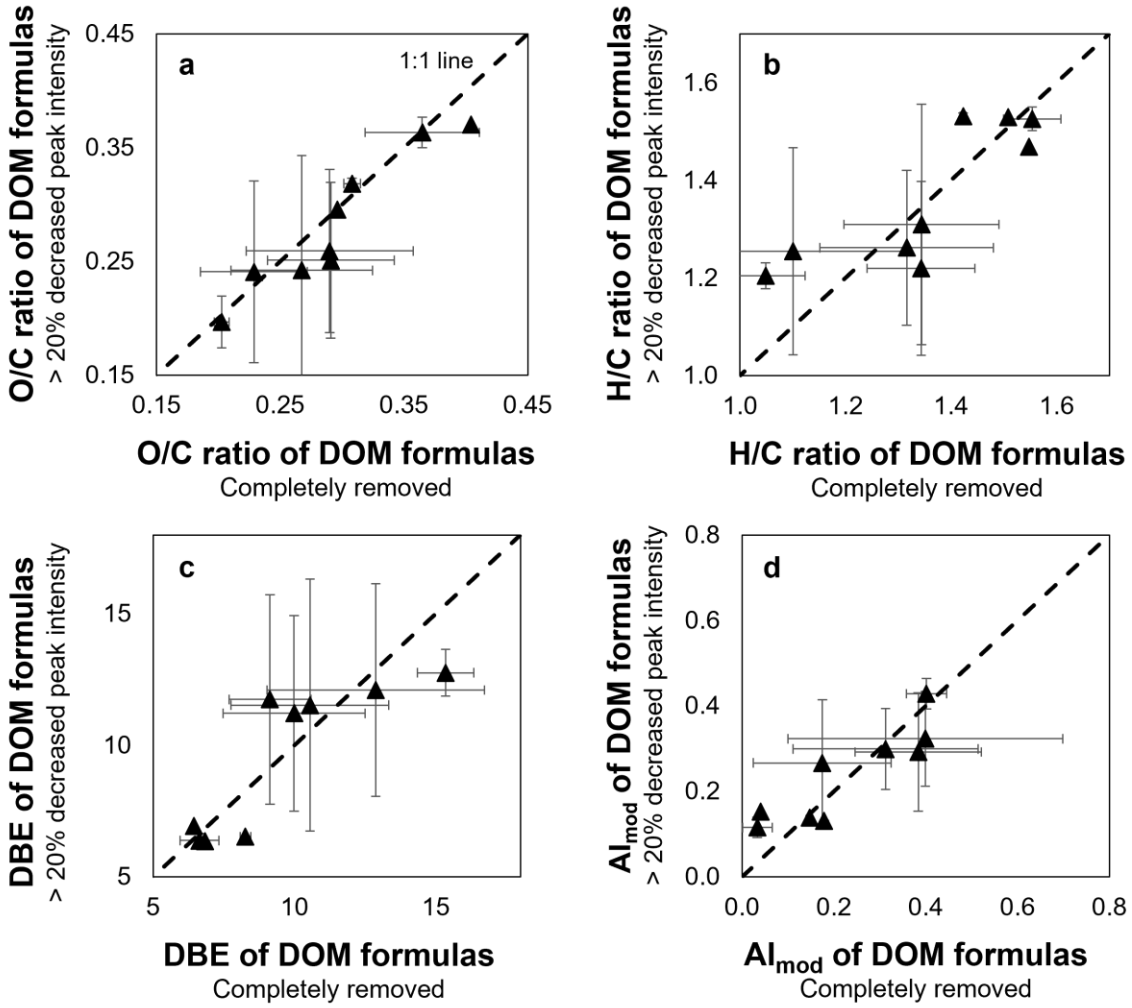

Figure 4.A.1. The average chemical properties for DOM formulas that decreased in relative peak intensity by > 20% during LED exposure were similar to those for the formulas completely removed. The average (a) ratio of oxygen to carbon (O/C), (b) hydrogen to carbon (H/C), (c) double bond equivalence (DBE), and (d) modified aromaticity index (AI_{mod}) for the DOM formulas completely removed during LED exposure (x-axis) versus the DOM formulas that decreased > 20% in relative peak intensity (y-axis) along a 1:1 line. Values on the x- and y-axes are shown as the average ± 1 standard error of experimental replicates (n = 2). When data in each panel are fit using a least-squares regression, $p < 0.05$ and the slope is not significantly different from 1.

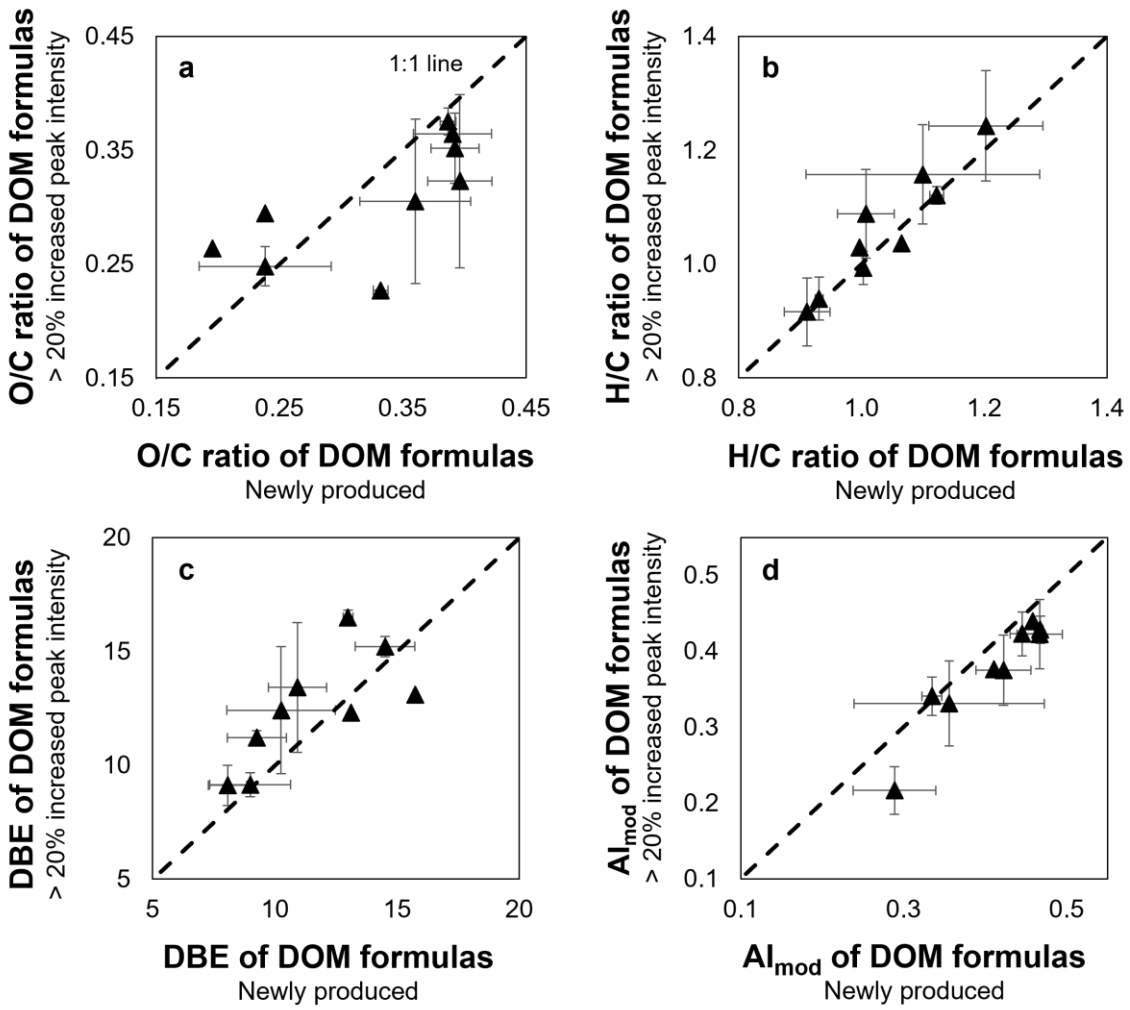

Figure 4.A.2. The average chemical properties for DOM formulas that increased in relative peak intensity by > 20% during LED exposure were similar to those for the new formulas produced. The average (a) ratio of oxygen to carbon (O/C), (b) hydrogen to carbon (H/C), (c) double bond equivalence (DBE), and (d) modified aromaticity index (AI_{mod}) for the DOM new formulas produced during LED exposure (x-axis) versus the DOM formulas that increased > 20% in relative peak intensity (y-axis) along a 1:1 line. Values on the x- and y-axes are shown as the average ± 1 standard error of experimental replicates (n = 2). When data in each panel are fit using a least-squares regression, $p < 0.05$ and the slope is not significantly different from 1.

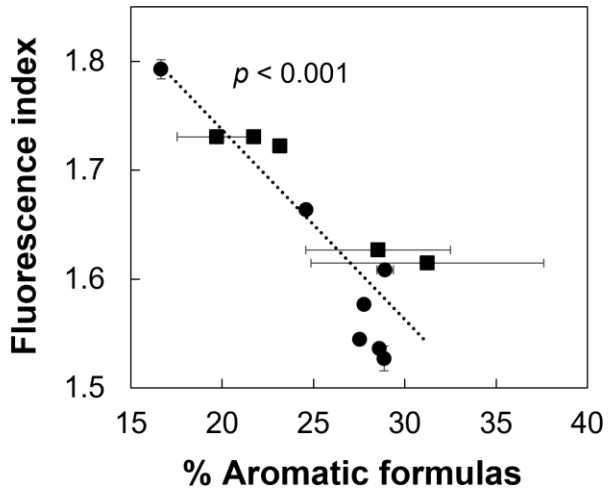

Figure 4.A.3. The fluorescence index decreased with the aromatic content of permafrost DOM, consistent with previous findings for other DOM samples.[47] Square symbols indicate the DOM leached from permafrost soils collected from the Alaskan Arctic in 2018 (this study).[8] Circle symbols indicate the DOM leached from permafrost soils collected from the Alaskan Arctic in 2013 and 2015.[10,36] Values indicate average ± 1 standard error of experimental replicates.

4.9 References

1. Tarnocai, C., J. G. Canadell, E. A. G. Schuur, P. Kuhry, G. Mazhitova, and S. Zimov (2009). Soil organic carbon pools in the northern circumpolar permafrost region. *Global Biogeochem. Cycles* 23, GB2023.

2. Schuur, E. A. G., A. D. McGuire, C. Schädel, G. Grosse, J. W. Harden, D. J. Hayes, et al. (2015). Climate change and the permafrost carbon feedback. *Nature* 520: 171-179.

3. Plaza, C., E. Pegoraro, R. Bracho, G. Celis, K. G. Crummer, J. A. Hutchings, et al. (2019). Direct observation of permafrost degradation and rapid soil carbon loss in tundra. *Nat. Geosci.* 12: 627-631.

4. Laurion, I., and N. Mladenov (2013). Dissolved organic matter photolysis in Canadian arctic thaw ponds. *Environ. Res. Lett*. 8, 035026.

5. Cory, R. M., B. C. Crump, J. A. Dobkowski, and G. W. Kling (2013). Surface exposure to sunlight stimulates CO_2 release from permafrost soil carbon in the Arctic. *Proc. Natl. Acad. Sci. USA* 110: 3429-3434.

6. Abbott, B. W., J. R. Larouche, J. B. Jones Jr., W. B. Bowden, and A. W. Balser (2014). Elevated dissolved organic carbon biodegradability from thawing and collapsing permafrost. *J. Geophys. Res. Biogeosci.* 119: 2049-2063.

7. Selvam, B. P., J.-F. Lapierre, G. Guillemette, C. Voigt, R. E. Lamprecht, C. Biasi, et al. (2017). Degradation potentials of dissolved organic carbon (DOC) from thawed permafrost peat. *Nature Sci. Reports* 7, 45811.

8. Bowen, J. C., C. P. Ward, G. W. Kling, and R. M. Cory (2020). Arctic amplification of warming strengthened by sunlight oxidation of permafrost carbon to CO_2. *Geophys. Res. Lett.* 47, e2020GL087085.

9. Vonk, J. E., S. E. Tank, W. B. Bowden, I. Laurion, W. F. Vincent, P. Alekseychik, et al. (2015). Reviews and synthesis: Effects of permafrost thaw on Arctic aquatic ecosystems. *Biogeosci*. 12(23): 7129-7167.

10. Ward, C. P., S. G. Nalven, B. C. Crump, G. W. Kling, and R. M. Cory (2017). Photochemical alteration of organic carbon draining permafrost soils shifts microbial metabolic pathways and stimulates respiration. *Nat. Commun.* 8, 772.

11. Nalven, S. G., C. P. Ward, J. P. Payet, R. M. Cory, G. W. Kling, T. J. Sharpton, et al. (2020). Experimental metatranscriptomics reveals the costs and benefits of dissolved organic matter photo-alteration for freshwater microbes. *Environ. Microbiol*. 22(8): 3505-3521.

12. Wetzel, R. G., P. G. Hatcher, and T. S. Bianchi (1995). Natural photolysis by ultraviolet irradiance of recalcitrant dissolved organic matter to simple substrates for rapid bacterial

metabolism. *Limnol. Oceanogr*. 40: 1369-1380.

13. Bertilsson, S., and L. J. Tranvik (1998). Photochemically produced carboxylic acids as substrates for freshwater bacterioplankton. *Limnol. Oceanogr*. 43: 885-895.

14. Bowen, J. C., L. A. Kaplan, and R. M. Cory (2020). Photodegradation disproportionately impacts biodegradation of semi-labile DOM in streams. *Limnol. Oceanogr.* 65: 13-26.

15. Xie, H., O. C. Zafiriou, W.-J. Cai, R. G. Zepp, and Y. Wang (2004). Photooxidation and its effects on the carboxyl content of dissolved organic matter in two coastal rivers in the southeastern United States. *Environ. Sci. Technol*. 38(15): 4113-4119.

16. Ward, C. P., and R. M. Cory (2016). Complete and partial photo-oxidation of dissolved organic matter draining permafrost soils. *Environ. Sci. Technol*. 50: 3545-3553.

17. Cory, R. M., K. McNeill, J. P. Cotner, A. Amado, J. M. Purcell, and A. G. Marshall (2010). Singlet oxygen in the coupled photochemical and biochemical oxidation of dissolved organic matter. *Environ. Sci. Technol*. 44: 3683-3689.

18. Ward, C. P., and R. M. Cory (2020). Assessing the prevalence, products, and pathways of dissolved organic matter partial photo-oxidation in arctic surface waters. *Environ. Sci.: Processes Impacts* 22: 1214-1223.

19. Amon, R. M. W., and R. Benner (1996). Photochemical and microbial consumption of dissolved organic carbon and dissolved oxygen in the Amazon River. *Geochim. Cosmochim. Acta* 60(10): 1783-1792.

20. Andrews, S. S., S. Caron, and O. C. Zafiriou (2000). Photochemical oxygen consumption in marine waters: A major sink for colored dissolved organic matter? *Limnol. Oceanogr*. 45: 267-277.

21. Cory, R. M., C. P. Ward, B. C. Crump, and G. W. Kling (2014). Sunlight controls water column processing of carbon in arctic freshwaters. *Science* 345: 925-928.

22. Blough, N. V., and R. G. Zepp (1995). Reactive oxygen species in natural waters. In C. S. Foote, J. S. Valentine, A. Greenberg, and J. F. Liebman (Eds.), *Active Oxygen in Chemistry* (pg. 280-333). The Netherlands: Springer.

23. Latch, D. E., and K. McNeill (2006). Microheterogeneity of singlet oxygen distributions in irradiated humic acid solutions. *Science* 311(4981): 1743-1747.

24. McNeill, K., and S. Canonica (2016). Triplet state dissolved organic matter in aquatic photochemistry: Reaction mechanisms, substrate scope, and photophysical properties. *Environ. Sci.: Processes Impacts* 18: 1381-1399.

25. Ossola, R., O. M. Jönsson, K. Moor, and K. McNeill (2021). Singlet oxygen quantum yields

in environmental waters. *Chem. Rev*. 121: 4100-4146.

26. Waggoner, D. C., A. S. Wozniak, R. M. Cory, and P. G. Hatcher (2017). The role of reactive oxygen species in the degradation of lignin derived dissolved organic matter. *Geochim. Cosmochim. Acta* 208: 171-184.

27. Aeschbacher, M., C. Graf, R. P. Schwarzenbach, and M. Sander (2012). Antioxidant properties of humic substances. *Environ. Sci. Technol*. 46: 4916-4925.

28. Spencer, R. G. M., P. J. Mann, T. Dittmar, T. I. Eglinton, C. McIntyre, R. M. Holmes, et al. (2015). Detecting the signature of permafrost thaw in Arctic rivers. *Geophys. Res. Lett.* 42: 2830-2835.

29. Hodgkins, S. B., M. M. Tfaily, D. C. Podgorski, C. K. McCalley, S. R. Saleska, P. M. Crill, et al. (2016). Elemental composition and optical properties reveal changes in dissolved organic matter along a permafrost thaw chronosequence in a subarctic peatland. *Geochim. Cosmochim. Acta* 187: 123-140.

30. Haag, W. R., and J. Hoigné (1984). Singlet oxygen in surface waters. 3. Photochemical formation and steady-state concentrations in various types of water. *Environ. Sci. Technol*. 20: 341-348.

31. Kieber, D. J., G. W. Miller, P. J. Neale, and K. Mopper (2014). Wavelength and teimperature-dependent apparent quantum yields for photochemical formation of hydrogen peroxide in seawater. *Environ. Sci.: Processes Impacts* 16: 777-791.

32. Marchisio, A., M. Minella, V. Maurino, C. Minero, and D. Vione (2015). Photogeneration of reactive transient species upon irradiation of natural water samples: Formation quantum yields in different spectral intervals, and implications for the photochemistry of surface waters. *Water Res*. 73: 145-156.

33. Gao, H., and R. G. Zepp (1998). Factors influencing photoreactions of dissolved organic matter in a coastal river of the southeastern United States. *Environ. Sci. Technol.* 32: 2940-2946.

34. Xiao, Y.-H., T. Sara-Aho, H. Hartikainen, and A. V. Vähätalo (2013). Contribution of ferric iron to light absorption by chromophoric dissolved organic matter. *Limnol. Oceanogr*. 58: 653-662.

35. Dittmar, T., B. Koch, N. Hertkorn, and G. Kattner (2008). A simple and efficient method for the solid-phase extraction of dissolved organic matter (SPE-DOM) from seawater. *Limnol. Oceanogr.: Methods* 6: 230-235.

36. Ward, C. P., and R. M. Cory (2015). Chemical composition of dissolved organic matter draining permafrost soils. *Geochim. Cosmochim. Acta* 167: 63-79.

37. Koch, B. P., and T. Dittmar (2006). From mass to structure: an aromaticity index for high-resolution mass data of natural organic matter. *Rapid Commun. Mass Spectrom.* 20: 926-932.

38. Hockaday, W. C., J. M. Purcell, A. G. Marshall, J. A. Baldock, and P. G. Hatcher (2009). Electrospray and photoionization mass spectrometry for the characterization of organic matter in natural waters: A qualitative assessment. *Limnol. Oceanogr.: Methods* 7: 81-95.

39. Sleighter, R., and P. G. Hatcher (2011). Fourier transform mass spectrometry for the molecular level characterization of natural organic matter: Instrument capabilities, applications, and limitations. In G. S. Nikolic (Ed.), *Fourier Transforms: Approach to Scientific Principles* (pp. 295-320). Rijeka, Croatia: InTech.

40. Gonsoir, M., B. M. Peake, W. T. Cooper, D. Podgorski, J. D'Andrilli, and W. J. Cooper (2009). Photochemically induced changes in dissolved organic matter identified by ultrahigh resolution Fourier transform ion cyclotron resonance mass spectrometry. *Environ. Sci. Technol.* 43: 698-703.

41. Ball, G. I., and L. I. Aluwihare (2014). CuO-oxidized dissolved organic matter (DOM) investigated with comprehensive two dimensional gas chromatography-time of flight-mass spectrometry (GC x GC-TOF-MS). *Org. Geochem.* 75: 87-98.

42. Page, S. E., J. R. Logan, R. M. Cory, and K. McNeill (2014). Evidence for dissolved organic matter as the primary source and sink of photochemically produced hydroxyl radical in arctic surface waters. *Environ. Sci.: Processes Impacts* 16: 807-822.

43. Fujii, M., A. Imaoka, C. Yoshimura, and T. D. Waite (2014). Effects of molecular composition of natural organic matter on ferric iron complexation at circumneutral pH. *Environ. Sci. Technol.* 48: 4414-4424.

44. Mangiante, D. M., R. D. Schaller, P. Zarzycki, J. F. Banfield, and B. Gilbert (2017). Mechanism of ferric oxalate photolysis. *ACS Earth Space Chem.* 1: 270-276.

45. Pokrovsky, O. S., and J. Schott (2002). Iron colloids/organic matter associated transport of major and trace elements in small boreal rivers and their estuaries (NW Russia). *Chem. Geol.* 190: 141-179.

46. Cory, R. M., K. H. Harrold, B. T. Neilson, and G. W. Kling (2015). Controls on dissolved organic matter (DOM) degradation in a headwater stream: the influence of photochemical and hydrological conditions in determining light-limitation or substrate-limitation of photo-degradation. *Biogeosci.* 12: 6669-6685.

47. McKnight, D. M., E. W. Boyer, P. K. Westerhoff, P. T. Doran, T. Kulbe, and D. T. Andersen (2001). Spectrofluorometric characterization of dissolved organic matter for indication of precursor organic material and aromaticity. *Limnol. Oceanogr.* 46(1): 38-48.

Chapter 5

Photodegradation Disproportionately Impacts Biodegradation of Semi-labile DOM in Streams[1]

5.1 Abstract

Exposure of dissolved organic matter (DOM) to sunlight can increase or decrease the fraction that is biodegradable (BDOM), but conceptual models fail to explain this dichotomy. We investigated the effect of sunlight exposure on BDOM, addressing three knowledge gaps: (1) how fractions of DOM overlap in their susceptibility to degradation by sunlight and microbes, (2) how the net effect of sunlight on BDOM changes with photon dose, and (3) how rates of DOM photodegradation and biodegradation compare in a stream. Stream waters were exposed to sunlight, and then fed through bioreactors designed to separate labile and semi-labile pools within BDOM. The net effects of photodegradation on DOM biodegradability, while generally positive, represented the balance between photochemical production and removal of BDOM that was mediated by photon dose. By using sunlight exposure times representative of sunlight exposures in a headwater stream and bioreactors colonized with natural communities and scaled to whole-stream dynamics, we were able to relate our laboratory findings to the stream. The impact of sunlight exposure on rates of DOM biodegradation in streams was calculated using rates of light absorption by chromophoric DOM, apparent quantum yields for

[1] Bowen, J. C., L. A. Kaplan, and R. M. Cory, *Limnol. Oceanogr.*, 2020

photomineralization and photochemical alteration of BDOM, and mass transfer coefficients for labile and semi-labile DOM. Rates of photochemical alteration of labile DOM were an order of magnitude lower than rates of biodegradation of labile DOM, but for semi-labile DOM these rates were similar, suggesting that sunlight plays a substantial role in the fate of semi-labile DOM in streams.

5.2 Introduction

Terrestrially-derived dissolved organic matter (DOM) sourced from decaying plant and soil organic matter fuels heterotrophic microbial degradation in streams.[1] Export of terrestrially-derived DOM to streams in many regions has increased in response to changes in climate, land-use, or other processes.[2-4] However, controls on the biodegradation of DOM to CO_2 remain too poorly understood to predict changes in CO_2 emissions from streams in response to increasing DOM export from watersheds.[5-6]

Following export of terrestrially-derived DOM to sunlit streams, photodegradation of DOM may be a major control on its biodegradation.[7] In sunlit waters, the chromophoric fraction of DOM (CDOM) absorbs sunlight, initiating photochemical reactions that can photomineralize DOM to CO_2[8-9] or photo-alter the chemical composition of DOM by producing different DOM compounds.[10-12] Evidence suggests that some of the DOM compounds that are photomineralized or photo-altered are also biodegradable (BDOM).[13-16] This potential overlap between photo- and biodegradation of DOM creates a range of scenarios in which sunlight and microbes may both cooperate and compete to degrade DOM. Sunlight and microbes cooperate to degrade DOM when sunlight photo-alters relatively recalcitrant, high molecular weight (HMW) DOM to produce biodegradable low molecular weight (LMW) acids or aldehydes.[17-18] On the other hand,

sunlight and microbes compete to degrade DOM when sunlight photomineralizes BDOM, or photo-alters BDOM to compounds no longer biodegradable.[14,16]

The presence of these cooperative and competitive interactions, as well as the balance between them, may help reconcile widespread observations of both positive and negative effects of sunlight on DOM biodegradability.[19-20] However, we cannot predict the net effect of sunlight on DOM biodegradability because the fractions of DOM accounting for increases and decreases in BDOM on a mass basis are not well known. For example, photochemical production of compounds thought to contribute to increased BDOM, such as acetate and amino acids, can only account for small changes in BDOM on a mass basis following photodegradation of terrestrially-derived DOM.[17,18,21] Likewise, fractions of DOM removed by sunlight are not well constrained on a mass basis, but may include a range of aliphatic,[16] aromatic,[14] and nitrogen-rich protein-like DOM.[15]

The photochemical production and removal of BDOM that account for cooperative and competitive interactions between sunlight and microbes to degrade DOM may be inferred by examining changes in CDOM and the fluorescent fraction of DOM (FDOM) following photo- and biodegradation.[13,15,22-23] CDOM and FDOM are proxies for sources and compositions of carbon within the DOM pool, such as HMW, aromatic carbon associated with terrestrially-derived DOM or carbon associated with free or combined fluorescent amino acids (e.g., tryptophan, tyrosine, and phenylalanine).[24] CDOM and FDOM are fractions of DOM most susceptible to photodegradation[9,13] and that are also biodegradable.[25-26] Thus, many studies have made inferences on cooperative and competitive interactions between sunlight and microbes to degrade DOM by analyzing the overlap (or lack thereof) between CDOM and FDOM degraded by sunlight or microbes alone.[13,15,22-23] However, what is missing from these studies, but needed

to quantify how sunlight impacts biodegradation of DOM in streams, is the connection between the fractions of DOM degraded by sunlight and microbes and the rates of each process, photo- and biodegradation, in streams.

The few studies that have directly compared rates of DOM photo- and biodegradation in streams have showed that photodegradation can be as fast as or faster than biodegradation of DOM in the water column.[27-28] However, it is not known how rates of DOM photodegradation compare to rates of biodegradation of DOM in the benthic zone of the streambed, the habitat where most microbial activity occurs in streams. For example, the DOM fractions accounting for increases or decreases in BDOM after sunlight exposure on a mass basis may not impact organic matter processing in streams if rates of their photochemical production or removal are too slow compared to rates of their biodegradation in the streambed. Thus, knowing how sunlight impacts DOM biodegradability in a stream reach requires a comparison of the rates of photodegradation of DOM fractions in the water column to rates of their biodegradation in the streambed.

The balance of photochemical production and removal of BDOM, and thus the net effect of sunlight on DOM biodegradability, should depend strongly on the amount of light received by DOM as it travels downstream. This is because the extent of DOM photodegradation increases as CDOM absorbs more light with increasing photon dose.[8-9,13] The only study that has quantified the effect of photon dose on DOM biodegradability showed diminished enhancement of DOM biodegradability with increasing photon dose.[29] Those findings have been interpreted to mean that photochemical production of BDOM becomes increasingly offset by the removal of BDOM with increasing photon dose. However, in that study, waters were exposed to high doses of light comparable to sunlight exposures in coastal waters not streams.[29] Quantifying the net

effect of sunlight on DOM biodegradability following photon doses representative of those in streams is thus needed to determine the effects of photon dose on stream water DOM biodegradability and estimate rates of DOM photodegradation in streams.

Here we address three knowledge gaps on the effect of sunlight exposure on BDOM: (1) how fractions of DOM overlap in their susceptibility to degradation by sunlight and microbes, (2) how the net effect of sunlight on BDOM changes with photon dose, and (3) how rates of photodegradation and biodegradation of DOM compare in a stream. Stream water was exposed to sunlight alongside dark controls to mimic sunlight exposure times in streams and then fed through bioreactors designed to separate labile and semi-labile pools within BDOM. We evaluated overlap between CDOM and FDOM fractions that were photo- and biodegraded to qualitatively interpret changes in BDOM following photodegradation. By using short-term sunlight exposure times representative of sunlight exposures in streams and short-term biodegradation experiments with bioreactors colonized with natural communities and scaled to whole-stream dynamics, we related our laboratory findings to in situ rates in the stream reach. Photodegradation rates were calculated using light absorption by CDOM throughout the stream water column and apparent quantum yields for photomineralization and for photochemical alteration of labile or semi-labile DOM. Biodegradation rates were calculated using prior instream measures of mass transfer coefficients for labile and semi-labile DOM. The net effect of photodegradation on DOM biodegradability was generally positive and resulted from the photo-alteration of DOM to produce and remove BDOM. Photon dose impacted photochemical production and removal of BDOM, and in doing so, impacted the net effect of sunlight on the biodegradability of DOM. Finally, rates of photochemical alteration of labile DOM (i.e., net production or removal) were much less than rates of biodegradation of labile DOM, but were

similar for semi-labile DOM, suggesting that sunlight may be particularly important in controlling the fate of the semi-labile DOM pool in stream ecosystems.

5.3 Methods

5.3.1 Site description and sampling

A total of five stream water samples were collected from a third-order reach of White Clay Creek (WCC; 39°51'N, 75°47'W) in persulfate-cleaned 20-L carboys during August 2016 and May 2017 (Table 5.1). This temperate stream in the southeastern Pennsylvania Piedmont flows through intact riparian woodlands.[30] All stream waters were collected at 06:00, within 0.5 h of sunrise, with four collected under baseflow conditions and one collected on the receding limb of a storm hydrograph. Stream waters were filtered immediately in a two-step process using organic-C free GF/F filters followed by sterile, 0.2 μm filters (Pall Corporation), and stored at 4 °C in a separate, persulfate-cleaned carboy in the dark for ≤ 9 days before a sunlight exposure experiment.

5.3.2 Sunlight exposure of DOM

Aliquots of each filtered stream water sample were used in 1 to 4 separate sunlight exposures ranging from 3 to 17 hours (Table 5.1). Sunlight exposures were performed by equilibrating 2 L of a sample to room temperature, distributing 1 L into 10 precombusted (450 °C, 5h) 100-mL quartz tubes with ground glass stoppers, and exposing the tubes to natural sunlight on a black surface alongside a dark control kept in a foil-wrapped, precombusted 1-L borosilicate glass bottle (Figure 5.1). Exposures took place on cloudy and sunny days, during which the temperature of waters in the quartz tubes ranged from 27 to 32 °C compared to 25 to 26 °C in the dark controls. Following sunlight exposure, waters from the quartz tubes were

composited into a precombusted 1-L borosilicate glass bottle (Figure 4.1), and both the light-exposed and dark control samples were stored in the dark at 4 °C for < 1 day until bioreactor experiments. In total, 15 sunlight exposure experiments took place on separate days, generating 15 sets of light-exposed and dark control samples (Table 5.1).

5.3.3 Bioreactor approach to quantify BDOM

Plug-flow biofilm reactors (i.e., bioreactors) are chromatography columns filled with sintered glass beads that are maintained by continuous inputs of WCC waters that are filtered to remove larger particles but allow suspended bacteria to pass. Over time the bioreactors, covered to eliminate light and maintained in a room kept at 20 °C, were colonized and fed by a unidirectional flow of WCC water and suspended bacteria which generated gradients of bacterial densities, species composition, and activity.[31] Bioreactors were constructed with different volumes to vary the empty bed contact times (EBCT), or the amount of time that BDOM is available for uptake, such that EBCT could be used as a surrogate for the relative biodegradability of DOM. For example, the most biologically labile compounds are rapidly degraded over short bioreactor contact times and semi-labile compounds are degraded following longer contact times.[32] Bioreactors facilitate the measurements of BDOM without the confounding issues of groundwater and tributary inputs, disturbances from elevated storm flows, phototrophs, and seasonal and diel temperature variations. Prior work comparing the behavior of a ^{13}C-DOC tracer in bioreactors and in WCC scaled DOM biodegradation in the bioreactors to the stream, where the uptake of BDOM occurring in the bioreactors over minutes and centimeters occurred in the stream over hours to days and hundreds of meters to kilometers.[32]

We used bioreactors to quantify BDOM in the light-exposed or dark control water samples[26,31] and to separate the BDOM into operationally defined labile and semi-labile pools.[32]

Samples were individually fed through a bioreactor with an EBCT of either 1.5 or 37 minutes, and the bioreactor influent and effluent waters were collected in triplicate in precombusted borosilicate glass vials for DOC, CDOM, and FDOM analyses (Figure 5.1). The bioreactor with an EBCT of 1.5 minutes was used to quantify the labile pool within BDOM and the bioreactor with an EBCT of 37 minutes was used to quantify total BDOM, which includes both the labile and semi-labile pools.[32] Of the 15 sets of light-exposed and dark control samples, three were used to quantify only the labile pool and 12 were used to quantify total BDOM (Table 5.1).

Prior studies have quantified total BDOM using a bioreactor with an EBCT of 150 minutes.[33] As such, BDOM quantified in the 37-min EBCT bioreactor, used here because of volume constraints associated with the quartz tubes, underestimates total BDOM by approximately 20% (see Appendix Section 5.8.1). For simplicity of presentation, hereafter we refer to the data from the 37-min EBCT bioreactor as total BDOM (Table 5.A.1).

5.3.4 DOC, CDOM, and FDOM analyses

DOC samples were refrigerated at 4°C and analyzed within < 1 day of collection. CDOM and FDOM samples were made biologically stable by a modification of the Tyndallization procedure[34] involving 3 cycles of heating in a water bath to 60 °C for 5 minutes, followed by 30 minutes at 25 °C (Kaplan et al. unpubl.); samples were analyzed within < 3 weeks of Tyndallization. DOC concentrations were measured by UV-catalyzed persulfate oxidation with conductimetric detection (Sievers 900 analyzer). Optical properties of CDOM were analyzed using a UV-Vis spectrophotometer with a 10-cm (Cary Varian 300) or 1-cm pathlength cuvette (Aqualog, Horiba) against laboratory-grade deionized water blanks. CDOM absorption coefficients were calculated as follows:

$$a_{\mathrm{CDOM},\lambda} = \frac{A_\lambda}{l} 2.303 \qquad (1)$$

where A is the absorbance at wavelength λ and l is the pathlength in meters.

The specific UV absorbance at 254 nm ($SUVA_{254}$), a proxy for aromatic content of DOM, was calculated as the ratio of the absorbance at 254 nm divided by the pathlength (m) and by the concentration of DOC (mg C L^{-1}).[35] The spectral slope ratio (S_R), a proxy for the molecular weight of DOM, was calculated from the CDOM absorbance spectrum following Helms et al. (2008).[36]

Excitation emission matrices (EEM) were measured using an Aqualog fluorometer (Horiba). EEMs were collected across excitation wavelengths 240 – 450 nm with 5 nm increments and emission wavelengths 320 – 550 nm with 2 nm increments using integration times of 4 or 5 seconds. EEMs were corrected for inner-filter effects and for instrument-specific excitation and emission corrections in MATLAB v8.5 as previously described.[26,37] EEMs of laboratory-grade deionized water blanks were subtracted from the sample EEMs and the fluorescence intensities were converted to Raman units (RU).[38]

Parallel factor analysis (PARAFAC) was used to separate a dataset of EEMs of WCC water into mathematically- and chemically-independent components, as previously described.[26] Briefly, all five FDOM components in WCC water were validated by PARAFAC analysis.[26] The humic-like C2 and C3 correspond to peaks A and C, respectively,[24] which have been associated with terrestrially-derived material, such as products of lignin degradation[39-40] and aromatic carbon content of DOM.[10,41] The humic-like C1 has been associated with recent autochthonous production (peak M).[42] The amino acid-like C4 and C5 overlap with the fluorescence of the amino acids tryptophan and tyrosine, respectively,[41,43] and their fluorescence has been shown to increase with the percentage of protein-like compounds within the DOM pool

in WCC water.[33] The F_{max} value of each component was quantified to estimate its relative abundance within an EEM (in RU).[26]

5.3.5 Amount of light absorbed by CDOM

The photon dose (mol photon m^{-2}) during each light exposure period was calculated from measurements of the global solar irradiance spectra at WCC. That spectrum, including direct and diffuse irradiance, was measured approximately hourly with a radiometer over wavelengths from 280 to 600 nm (USB4000 Spectrometer, Ocean Optics). Every global solar irradiance spectrum (μW cm^{-1} nm^{-1}) was converted to a photon flux spectrum (mol photon m^{-2} s^{-1} nm^{-1}) assuming that the photon flux spectra during each time interval were equal to the average photon flux spectrum bracketed by two consecutive measurements. The average photon flux spectrum between any two consecutive measurements was multiplied by the duration of the time interval to calculate the photon flux spectrum for that interval (mol photon m^{-2} nm^{-1}). The photon flux spectra during each time interval were summed to calculate the total photon flux spectrum during the light exposure period ($E_{0,\lambda}$; mol photon m^{-2} nm^{-1}), and across all wavelengths to calculate the photon dose.

The extent of DOM photodegradation depends on the amount of light absorbed by CDOM, which is a product of photon dose and the concentration of CDOM available to absorb the light. Thus, we calculated the amount of light absorbed by CDOM during each light exposure period ($Q_{a\lambda}$; mol photons m^{-2}) as follows:

$$Q_{a,\lambda} = \int_{\lambda_{min}}^{\lambda_{max}} E_{0,\lambda}(1 - e^{-a_{CDOM,\lambda} * z}) \frac{a_{CDOM,\lambda}}{a_{tot,\lambda}} d\lambda \quad (2)$$

where λ_{min} and λ_{max} are the minimum and maximum wavelengths of light absorbed by CDOM (280 and 600 nm, respectively). $E_{0,\lambda}$ is the total photon flux spectrum during the light exposure

period (mol photon m^{-2} nm^{-1}). We assumed that the pathlength of light (z) was equivalent to the diameter of the quartz tubes (3 cm) and that the fraction of light absorbed by CDOM relative to other light-absorbing constituents, $a_{CDOM,\lambda}/a_{tot,\lambda}$, was equal to 1 at all wavelengths in the filtered stream water.[27]

5.3.6 Concentration versus composition of DOM and BDOM

Our approach to understand the impact of sunlight exposure on DOM biodegradability involves the quantification of different operationally defined fractions of DOM (Table 4.A.1). We use dissolved organic carbon (DOC) and biodegradable DOC (BDOC) for carbon concentrations of DOM amenable to mass balance analyses, and CDOM, FDOM, and BDOM for compositions of chromophoric, fluorescent, and biodegradable DOM, respectively, that are not quantifiable on a mass basis. The expected relationships and overlap among these operational fractions of DOM, including CDOM, FDOM, and BDOM, are shown in Figure 5.A.1.

Photomineralization was quantified as the difference in DOC concentrations between the light-exposed and dark control samples. Photodegradation of DOM was quantified as the light-exposed minus dark control differences in CDOM and FDOM (Table 5.A.1). BDOC concentration and BDOM composition were quantified as differences in DOC concentration and CDOM or FDOM between the influent and effluent waters from a bioreactor (Table 5.A.1).[26,32] The effects of sunlight exposure on DOM biodegradation were calculated as differences between BDOC concentrations or BDOM compositions in the light-exposed waters and the respective dark controls.

For the purpose of calculating rates of biodegradation in the stream, concentrations of labile and semi-labile DOC were estimated from the total BDOC concentration (Table 5.A.2) based on prior work showing that 39% of the BDOC concentration degraded within a 37-min

EBCT was in the labile pool, with the remaining 61% of BDOC in the semi-labile pool (see Appendix Section 5.8.1). Thus, concentrations of labile DOC were both quantified using the 1.5-min EBCT bioreactor (n = 3) and estimated as a percentage of total BDOC degraded in the 37-min EBCT bioreactor (n = 12), whereas concentrations of semi-labile DOC were only estimated as a percentage of total BDOC (n = 12).

5.3.7 Sunlight exposure times in the stream

Sunlight exposure times in the quartz tubes were converted to sunlight exposure times in WCC by a two-step process. First, we calculated hourly water column rates of light absorption by CDOM in WCC (Eq. 2) using 0.145 m as the average depth of WCC (based on 29 separate salt injections; J. D. Newbold unpubl.), the initial CDOM in the stream water (Table 5.2), and the average hourly incoming photon flux spectrum (mol photon m^{-2} h^{-1} nm^{-1}) measured on each date of stream water collection. Second, the amount of light absorbed by CDOM in the quartz tubes during each light exposure period (mol photons m^{-2}) was divided by the hourly water column rate (mol photons m^{-2} h^{-1}) to calculate the sunlight exposure time in the stream (Table 5.1).

5.3.8 Rates of photo- and biodegradation of DOM in the stream

We compared rates of DOM biodegradation in the streambed of WCC to rates of photodegradation in the water column of WCC on a mass basis. Areal rates of biodegradation (mg C m^{-2} d^{-1}) of labile and semi-labile DOC in the streambed were calculated by multiplying mass transfer coefficients (μm s^{-1}), previously determined for labile and semi-labile DOC pools in WCC,[32] by the concentrations of labile and semi-labile DOC in the dark control waters in this study, respectively (n = 15 and 12).

Areal rates of DOM photodegradation (mg C m^{-2} d^{-1}) are the product of two spectra: the rate of light absorption by CDOM throughout the water column in WCC ($Q_{a\lambda}$) and the apparent quantum yield (AQY; φ_λ):

$$\text{Rate of DOM photodegradation} = \int_{\lambda_{min}}^{\lambda_{max}} Q_{a,\lambda}\varphi_\lambda \, d\lambda \quad (3)$$

The AQY is a measure of the susceptibility of DOM to photodegradation defined as the moles of product formed per mole of photons absorbed by CDOM at each wavelength. For example, the AQY for photomineralization was calculated as the light minus dark difference in DOC concentration divided by the light absorbed by CDOM during the light exposure period that resulted in detectable loss of DOC in each stream water sample (n = 5; Table 5.A.2), assuming the AQY spectra decreased exponentially with increasing wavelength.[7,27,44-45] Daily water column rates of light absorption by CDOM were calculated as described above (Eq. 2) using the average depth of WCC (0.145 m), the initial CDOM in the stream water (Table 5.2), and the daily incoming photon flux spectrum (mol photon m^{-2} d^{-1} nm^{-1}) measured on each date of stream water collection.

Quantifying areal rates of DOM photodegradation on a mass basis (mg C m^{-2} d^{-1}) is limited to processes that form a product quantified on a per carbon basis. Because the products of DOM photo-alteration are not well known or quantifiable on a per carbon basis (e.g., photobleaching that leads to removal of CDOM and FDOM), we used two conservative assumptions to quantify AQYs on a mass basis for photochemical production and removal of BDOM. First, we used the light minus dark difference in BDOC concentration (Table 5.A.2) to quantify the net effect of DOM photodegradation on BDOM. Second, we assumed that the AQY spectra for photochemical production and removal of BDOM decreased exponentially with

increasing wavelength.[7,27,44-45] AQYs for the photo-production of BDOM were calculated for waters that showed a net increase in BDOC concentration (e.g., 0.03 to 0.12 mg C L^{-1} BDOC produced after 0.08 to 0.28 mol photon m^{-2} of light was absorbed by CDOM; Table 4.A.2, Figure 4.5; labile DOC (n = 3) and total BDOC (n = 6)). AQYs for the photo-removal of BDOM were calculated for waters that showed a net decrease in BDOC concentration (e.g., 0.05 to 0.14 mg C L^{-1} BDOC removed after 0.22 to 0.29 mol photon m^{-2} of light was absorbed by CDOM; Table 4.A.2, Figure 4.5, total BDOC (n = 6)). Rates of photochemical production or removal of total BDOC were separated into labile and semi-labile pools assuming that 39% and 61% of the total BDOC photo-produced or photo-removed were labile and semi-labile, respectively.

5.3.9 Statistical analyses

DOC, CDOM, and FDOM are reported as the average value ± 1 standard error (SE) of the triplicate measurements (Figure 5.1), unless otherwise noted. DOC, CDOM, and FDOM were compared among the five stream waters collected using analysis of variance (ANOVA). Paired t-tests were used to determine significant differences between percentages of photodegraded DOM and total biodegradable DOM in the dark control, and between percentages of total biodegradable DOM in the light-exposed and dark control waters. Statistical significance was defined as $p < 0.05$.

5.4 Results

Stream waters collected for the sunlight exposure experiments exhibited a range of DOC, CDOM, and FDOM concentrations, with the greatest differences driven by hydrology. The stream water sample collected on 27 May, as the stream hydrograph receded from a storm 24 hours earlier that had increased discharge by approximately 15-fold over baseflow, was distinguished by concentrations of DOM fractions that were 40% to 70% greater than the

average for the four stream waters collected under baseflow conditions (Table 5.2). In contrast, under baseflow conditions the average concentrations of DOM fractions varied by < 15% and averaged as follows (average ± SE): DOC, 1.58 ± 0.16 mg C L^{-1}; a_{305}, 5.53 ± 0.58 m^{-1}; humic-like C1, 0.42 ± 0.05 RU; tryptophan-like C4, 0.13 ± 0.02 RU; and tyrosine-like C5, 0.05 ± 0.01 RU (n = 4; Table 5.2). DOM compositions as measured by $SUVA_{254}$ and S_R were similar across all five stream waters collected (Table 5.3).

Sunlight exposures of the quartz tubes ranged from 3 to 17 hours, which were equivalent to exposure times of 0.4 to 3.8 hours in the stream water column (Table 5.1). During the sunlight exposure experiments, the extent of DOM photodegradation increased as the amount of light absorbed by CDOM increased over a range of 0.03 to 0.29 mol photon m^{-2} (Figure 5.2), or over photon doses ranging from 2 to 29 mol photon m^{-2} (Figure 5.A.2). Increased photodegradation with light absorption was linear for DOC and the DOM fractions a_{305}, humic-like C1, and tryptophan-like C4. The S_R also increased linearly with light absorption (Figure 5.2c). Tyrosine-like C5 exhibited both increases and decreases with light absorption (Figure 5.2f).

Photodegradation of DOM impacted its biodegradability, and the impacts differed among fractions of the DOM pool (Figure 5.3). Photodegradation of humic-like C1 and tryptophan-like C4, those DOM fractions most strongly photodegraded, resulted in a 2.0-fold and 3.3-fold lower biodegradability on average compared to dark controls, respectively (p < 0.001; Table 5.3). Photodegradation resulted in a 10.1% ± 3.8% greater decrease of S_R during biodegradation, on average, compared to dark controls (p < 0.05; Table 5.3). While photodegradation increased, decreased, or did not change subsequent biodegradation of a_{305} and tyrosine-like C5 (Figure 5.3), on average, there were no detectable changes in biodegradation of these fractions of DOM compared to dark controls (Table 5.3). On average, photodegradation increased the percent of

total BDOC by 2.5% ± 1.3% ($p < 0.001$; Table 5.3), ranging from a 9.1% ± 0.7% decrease to a 7.6% ± 3.0% increase (Figure 5.3a). Photodegradation also increased the percentage of labile DOC by 3.5% ± 1.6% on average (triangles; Figure 5.3a).

The extent of DOM photodegradation impacted subsequent differences in biodegradation of DOM in the light-exposed and dark control waters. The impacts differed among DOM fractions and were dependent upon the direction and magnitude of changes in the individual fractions during photodegradation (Figure 5.4). For example, as humic-like C1 and tryptophan-like C4 were increasingly photodegraded, the biodegradability of these fractions generally decreased (Figure 5.4). For humic-like C1, biodegradation decreased linearly with increasing photodegradation (Figure 5.4d). As the extent of photodegradation increased, there was a greater decrease of S_R during biodegradation compared to dark controls. That is, the light minus dark difference in decreased S_R during biodegradation was proportional to the change in S_R during photodegradation (Figure 5.4c). When photodegradation produced ≥ 10% of tyrosine-like C5 (plotting below the origin on the x-axis), biodegradation of this component was enhanced. Conversely, when photodegradation removed ≥ 10% of tyrosine-like C5 (plotting above the origin on the x-axis), there was a lower biodegradability of this component on average (Figure 5.4f). For a_{305}, there was either no impact of increasing photodegradation on subsequent biodegradation or an increase in biodegradation, until the highest extent of photodegradation, at which point biodegradation was diminished (Figure 5.4b). After low levels of photodegradation (i.e., < 10% of DOC photomineralized), biodegradation of DOC generally increased, although in one of the stream waters this was not the case. As the extent of photodegradation increased (i.e., > 10% of DOC photomineralized), no detectable changes in subsequent biodegradation were observed (Figure 5.4a). Differences in the effect of photodegradation on the biodegradability of

the total BDOC pool followed differences in the amount of light absorbed by CDOM, where the one stream water which showed less biodegradation of total BDOC (Figure 5.4a) experienced a higher amount of light absorbed by CDOM compared to most of the stream waters which showed enhanced biodegradation of total BDOC (Figure 5.5).

The magnitude of DOM photodegradation rates compared to rates of biodegradation in WCC was strongly dependent upon the lability pool within BDOC. For labile DOC, rates of photomineralization, photochemical production, and photochemical removal in the water column were on average 22, 53, and 62 times slower, respectively, than rates of its biodegradation in the streambed of WCC (Table 5.4). In contrast, rates of photomineralization, photochemical production, and photochemical removal of semi-labile DOC were each about two times slower than the rates of its biodegradation in the streambed (Table 5.4). Thus, the sum of the rates of DOC photomineralization and photochemical alteration of semi-labile DOC overlapped with the average rate of biodegradation of semi-labile DOC in WCC (Table 5.4).

5.5 Discussion

It is well established that photodegradation of terrestrially-derived DOM can involve both photomineralization[8-9] and photo-alteration.[10-12] Photomineralization removes carbon from the DOM pool, some of which may include BDOM. In contrast, photo-alteration can increase or decrease the BDOM pool by producing or removing biodegradable compounds, respectively, without reducing the size of the DOM pool.[14,16-17] Understanding what controls the balance between BDOM produced or removed by photomineralization and photo-alteration remains elusive, yet critical to assessing the impact of photodegradation on the biogeochemistry of DOM in stream ecosystems. Our research has provided new information concerning the overlap between fractions of DOM susceptible to both photo- and biodegradation as well as the role of

photon dose in altering the balance between BDOM production and removal. Additionally, we have used that information to estimate the lowest amount of light needed to impact DOM biodegradability and generate the first quantitative comparison of rates of DOM photo- and biodegradation in a temperate headwater stream. These advances help reconcile disparate observations of both positive and negative effects of sunlight on DOM biodegradability and to improve our understanding the role of photodegradation in the DOM biogeochemistry of stream ecosystems.

5.5.1 Overlap between fractions of DOM photo- and biodegraded

The large, significant changes in the biodegradability of DOC, CDOM, and FDOM following sunlight exposure (Figure 5.3) provide strong evidence for the overlap between fractions of DOM degraded by sunlight and microbes. These findings extend prior work showing that the biodegradability of DOC, CDOM, and FDOM changes after photodegradation.[13,15,20] Significant changes in the biodegradability of DOM following photodegradation are expected if sunlight competes with microbes by degrading the same fractions of DOM as microbes (Table 5.3). Changes in the biodegradability of DOC, CDOM, and FDOM after photodegradation could result from the loss of these fractions by photomineralization to CO_2. Following the photochemical loss of DOC, CDOM, and FDOM, lower concentrations of these fractions should be biodegraded because there was less of each fraction after sunlight exposure compared to dark controls (Table 5.3).

However, three lines of evidence suggest that photo-alteration, and not photomineralization, was primarily responsible for shifts in the biodegradability of DOM following photodegradation. First, there was only a small percentage of DOC photomineralized to CO_2 (on average 4.7% ± 1.1%; Table 5.3). Second, this loss of DOC by photomineralization

did not result in a decrease in BDOC concentration of equal mass after photodegradation. For example, a greater mass of DOC was biodegraded in some of the light-exposed waters compared to dark controls (Figure 5.5), despite less DOC available for microbes to degrade in light-exposed versus dark control waters. This finding strongly suggests that the remaining, photo-altered DOM in these waters was more biodegradable than the dark control DOM. Similarly, for the stream waters that exhibited decreased biodegradability of DOM after photodegradation, a smaller mass of DOC was biodegraded in the light-exposed versus dark control waters than the amount lost by photomineralization (Table 5.A.2). This finding suggests that, in these waters, the remaining, photo-altered DOM was less biodegradable than the dark control DOM. Third, photo-altered CDOM and FDOM differed in biodegradability compared to dark control CDOM and FDOM (Figure 5.3). These results demonstrate that photo-alteration of DOM included both photo-production and photo-removal of different moieties within the BDOM pool.

For example, BDOM was likely photochemically produced during the breakdown of HMW, aromatic compounds to form LMW aromatics, as indicated from an increase in S_R (Figure 5.2c). These LMW, aromatic photo-products were more biodegradable than the HMW, aromatic DOM in the dark control (Figure 5.4c). Many studies have shown that the molecular weight of terrestrially-derived DOM decreases with increasing photodegradation,[12,36,46] consistent with the fact that this DOM is comprised mostly of HMW, aromatic compounds.[10,33,47-48] BDOM may also be photochemically produced during the liberation of free amino acids from proteins within DOM.[15,49-50] Photochemical liberation of tyrosine may account for increased fluorescence of tyrosine-like FDOM after photodegradation in some instances (Figure 5.2f). Increased biodegradability of tyrosine-like FDOM in proportion to its

photochemical production (Figure 5.4f) is consistent with higher biodegradability of free amino acids compared to those associated with proteins.[51]

In contrast, lower biodegradability of the CDOM and FDOM remaining after photodegradation compared to dark controls (Figure 5.3) indicated photochemical removal of BDOM. Decreased biodegradability of humic-like FDOM remaining after photodegradation compared to dark controls (Figure 5.3d) is consistent with photo-oxidation of aromatic DOM to less biodegradable compounds compared to the parent compound.[14,16] Photo-alteration of tryptophan-like FDOM to oxidized amino acids,[52-53] expected to be less biodegradable,[15,20] is consistent with decreased biodegradability of this fraction of DOM compared to dark controls (Figure 5.3e).

Although we cannot relate changes to the biodegradability of CDOM and FDOM (Figure 5.4) to net changes in DOM biodegradability on a mass basis (Figure 5.5), photo-alteration of HMW, aromatic DOM likely had a larger impact on the net change in BDOM than photo-alteration of amino acid-like DOM given that HWM, aromatic DOM accounts for more of the DOM pool on a mass basis compared to amino acid-like DOM. For example, HMW, aromatic compounds comprise at least 20% of terrestrially-derived DOM,[10,54] whereas nitrogen comprises less than 1% of terrestrially-derived DOM by mass.[10] Thus, photo-alteration of amino acid-like DOM constitutes an insufficient mass of carbon to account for net changes in BDOM. Given that photochemical production of acetate and other identifiable LMW acids or aldehydes account for at most ~ 20% of the increased BDOC concentration following photodegradation of terrestrially-derived DOM,[17-18,21] closing the mass balance on the net change in BDOM following photodegradation requires quantifying the fractions of LMW, aromatic DOM that contribute to the increased BDOC concentration.[14,16]

5.5.2 BDOM changes with the amount of light absorbed by CDOM

The impact of photodegradation on DOM biodegradability depended on the amount of light absorbed by CDOM because photochemical production and removal of BDOM varied with light absorption by CDOM (Figure 5.5; as related to photon dose in Figure 5.A.2). The net change in BDOM on a mass basis following photodegradation must result from the sum of photochemical production and removal of BDOM. For example, at the lowest amounts of light absorbed by CDOM ($\leq$ 0.07 mol photon m^{-2}) when there was no significant difference in BDOC concentration between light-exposed and dark control waters (Figure 5.5), photochemical production of BDOM was offset by removal of BDOM. As light absorption by CDOM increased in the range of 0.08 to 0.21 mol photon m^{-2}, the significant increases in BDOC concentration relative to dark controls (Figure 5.5) suggest that photo-production of BDOM exceeded the removal of BDOM.

After CDOM absorbed higher amounts of light ($\geq$ 0.22 mol photon m^{-2}), there was either an increase or a decrease in BDOC concentration relative to dark controls (Figure 5.5). These large differences in the effect of photodegradation on BDOC concentrations after the same amount of light absorbed by CDOM (0.22 or 0.29 mol photon m^{-2}) may be in part due to differences in the extent of photomineralization of BDOM. For example, the stream waters that had decreased BDOC concentration after 0.22 or 0.29 mol photon m^{-2} of light was absorbed by CDOM lost a greater mass of DOC by photomineralization than the stream waters that had increased BDOC concentration after the same amount of light was absorbed (Table 5.A.2; Figure 5.5). These results suggest that with increasing loss of DOC by photomineralization, it is more likely that the loss includes BDOM, which can offset photo-production of BDOM.

Variability in the magnitude of increased BDOC concentration with light absorption by CDOM (i.e., photon dose) is consistent with prior work. Several studies have demonstrated smaller gains in microbial production or respiration after DOM received higher photon doses compared to lower photon doses.[17,29] This observation has been attributed in part to decreases in the yield of biodegradable photo-products with increasing photon dose.[27,29,45,55] For example, as HWM, aromatic DOM is increasingly altered by sunlight (Figure 5.2),[8-9,13] there is less of this DOM to be converted to biodegradable LMW compounds.[55] In addition, others have suggested that the smaller gains in microbial production or respiration after DOM received higher photon doses must also be due to photo-alteration of BDOM to compounds no longer biodegradable.[55] Thus, the simultaneous photochemical production and removal of BDOM observed in our study help explain changes in the magnitude or direction of the effect of sunlight on DOM biodegradability.

5.5.3 Photo- versus biodegradation of DOM in the stream reach

Photodegradation impacted DOM biodegradability in WCC water following sunlight exposure times that were comparable to hydraulic residence times in the stream reach. For example, we estimated that at least 30 minutes of sunlight exposure in unshaded reaches of WCC was needed to result in a change in BDOC concentration (Table 5.1; Figure 5.5). Given that the stream water in this headwater reach of WCC is replaced by groundwater approximately every 9 to 13 hours (in May and August, respectively; J. D. Newbold unpubl.) and, when the canopy is full (e.g., growing season), 16% and 14% of the reaches flow through semi-open canopy and meadows, respectively,[30] water column rates of light absorption by CDOM in WCC are fast enough for BDOM to be photochemically produced or removed. However, to impact organic

matter processing in the stream reach, rates of DOM photodegradation would need to be comparable to rates of DOM biodegradation.

Similar rates of photo- and biodegradation of the semi-labile pool in WCC suggest substantial cooperation and competition between sunlight and microbes to degrade semi-labile DOM (Table 5.4). For example, rates of photodegradation of recalcitrant DOM to produce more semi-labile DOM or photochemical removal of semi-labile DOM are fast enough to increase or decrease the semi-labile pool, respectively, before being biodegraded several kilometers downstream. In contrast, the nearly 60 times slower rates of photo-production or photo-removal of labile DOC in the water column compared to rates of its biodegradation in the streambed suggest little interaction between sunlight and microbes to degrade labile DOM. That is, even if all fractions of DOM that are photo-altered or photomineralized comprise the labile pool, the rate of photodegradation of DOM in the water column would still be too slow to impact its biodegradation in the streambed.

An essential aspect of our research involved converting measures of photodegradation in quartz tubes into areal rates of DOM photodegradation representative of those in the stream. We accomplished this by selecting a range of sunlight exposure times that mimicked natural sunlight exposure times in the stream and quantifying all terms needed to relate experimental results to rates of photodegradation in the stream. Additionally, the stream waters used for sunlight exposure experiments were collected at sunrise so that the DOM would have had little to no prior exposure to sunlight. Our estimated rates of DOM photodegradation are representative of those in streams like WCC because there were no mixing limitations on DOM photodegradation rates in low turbidity waters where CDOM is the main light-absorbing constituent in the water column and the rates of vertical mixing exceed rates of photodegradation in the water column.[56]

However, there remain large uncertainties bracketing our estimates of the areal rates of DOM photodegradation that call for caution in evaluating the comparisons between rates of photo- and biodegradation of DOM in streams and underscore the need for future studies to constrain these estimates. For example, areal rates of DOM photodegradation depend strongly on the wavelength dependence of the photochemical production and removal of BDOM, which are not known (see Methods Section 5.3.8).[7] In addition, the areal rates of DOM photodegradation were obtained from experiments using stream water collected on only five dates and exposed to sunlight on mostly cloudy days. Thus, the rates of DOM light absorption in this study may represent a relatively narrow range of DOM photodegradation taking place in unshaded reaches of WCC. Rates of DOM photodegradation in streams like WCC also depend on the extent to which the reach is shaded from UV and visible sunlight. For example, rates of light absorption by CDOM, and thus DOM photodegradation, would be much lower in shaded compared to unshaded streams. Nonetheless, these first comparisons between rates of DOM photodegradation and biodegradation in a headwater stream tentatively suggest that photomineralization and photochemical alteration of the semi-labile pool may substantially impact the biogeochemistry of DOM in stream ecosystems.

5.6 Conclusions and implications

This study demonstrated that just minutes of sunlight exposure in the stream can impact the biodegradability of DOM. The net effect of sunlight on DOM biodegradability changed with photon dose due to shifts in the balance of photochemical production and removal of biodegradable DOM. Overlap in the DOM fractions degraded by sunlight and microbes indicate that photo-alteration of DOM is relatively more important than photomineralization in the production and removal of BDOM. Given that water column rates of photochemical production

and removal of semi-labile DOM were similar to rates of its biodegradation in the streambed, DOM photodegradation disproportionally impacts biodegradation of semi-labile DOM over labile DOM in streams.

In stream ecosystems, as the spatial scale expands from the headwaters to the catchment level, photodegradation of the semi-labile pool should play an increasingly important role in organic matter processing. Semi-labile and recalcitrant DOM largely escape biodegradation at the reach scale, with the semi-labile pool transported several kilometers downstream before it is biodegraded.[32] Most streams increase in size with downstream distance, and based on hydrodynamics alone, biological uptake lengths should increase downstream as the product of increasing depth and velocity.[57-58] Thus, in downstream reaches there is greater likelihood that rates of photodegradation may equal or exceed rates of biodegradation of semi-labile DOM compared to upstream reaches. Furthermore, as semi-labile DOM is transported downstream, opportunities for photodegradation may increase in WCC, and streams in general, as shading from the riparian zone recedes to the edges of the widening channel and all of the available sunlight is absorbed by CDOM within the greater depth of water. Increasing export of terrestrially-derived DOM to streams in response to changes in climate or land-use[5] could also increase rates of light absorption, and thus rates of photodegradation of DOM in streams.

5.7 Acknowledgments

We thank M. Gentile, S. Roberts, and L. Treibergs for assistance with field and laboratory work. Support for this work came from NSF grants EAR-1451372 (R.M.C.), EAR-1452039 (L.A.K.), and the Scott Turner Research Award in Earth Sciences at the University of Michigan (J.C.B.).

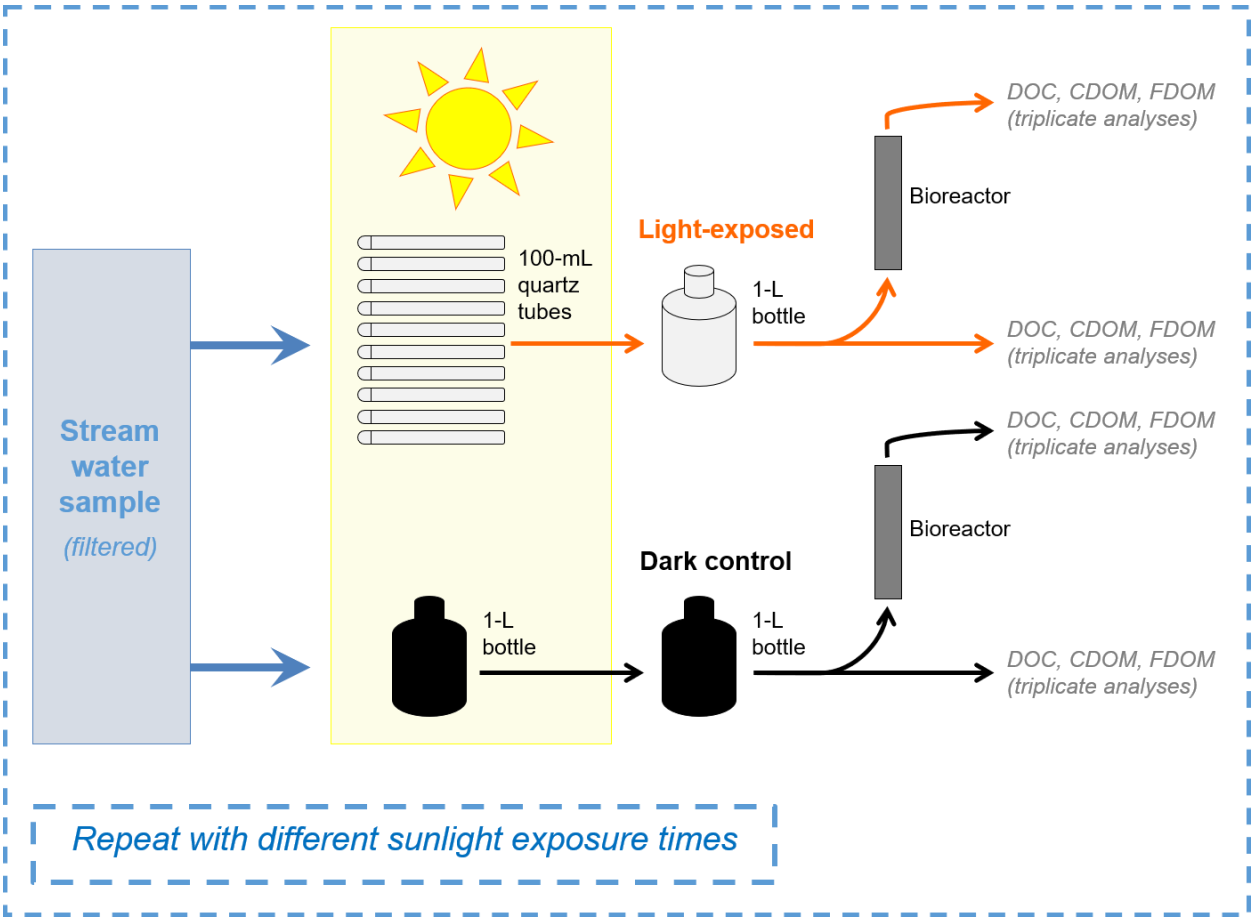

Figure 5.1. Experimental design for photodegradation and biodegradation of DOM used for each of the five stream water samples collected from White Clay Creek.

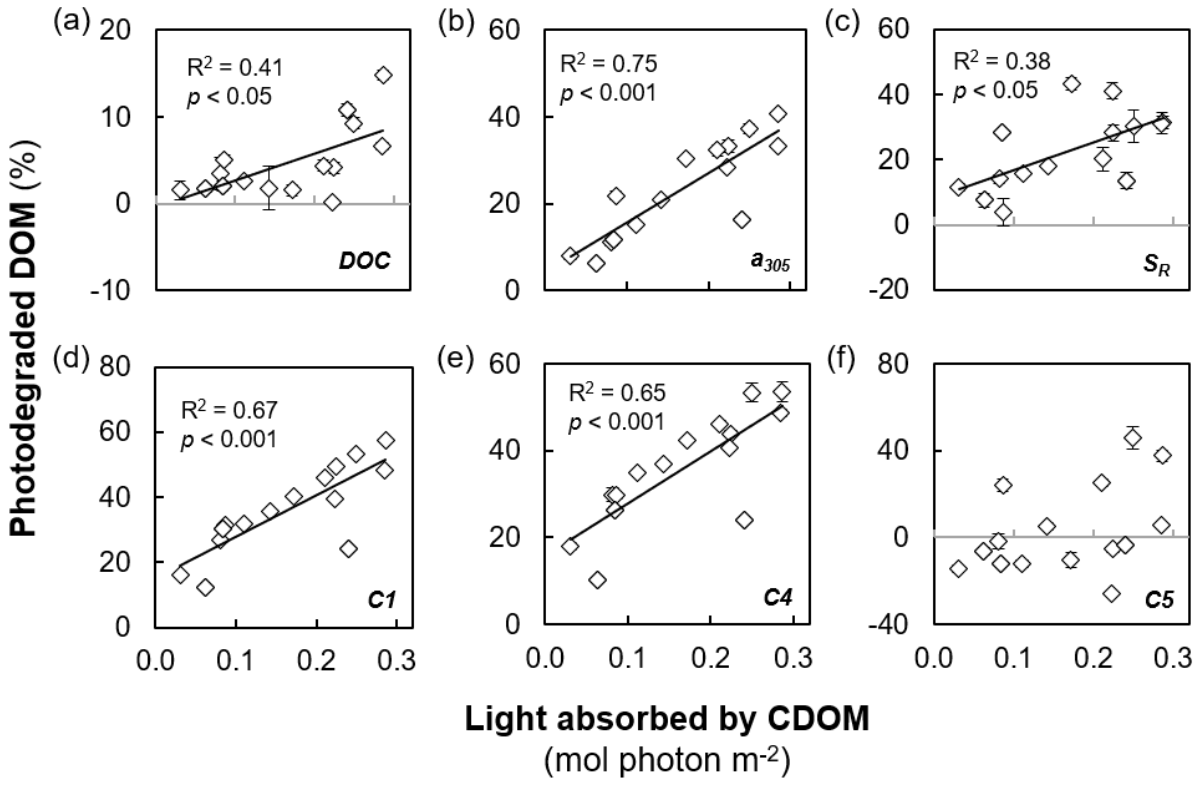

Figure 5.2. Percentage of DOM photodegraded as a function of the amount of light absorbed by CDOM. All values are average ± 1 standard error of triplicate measurements.

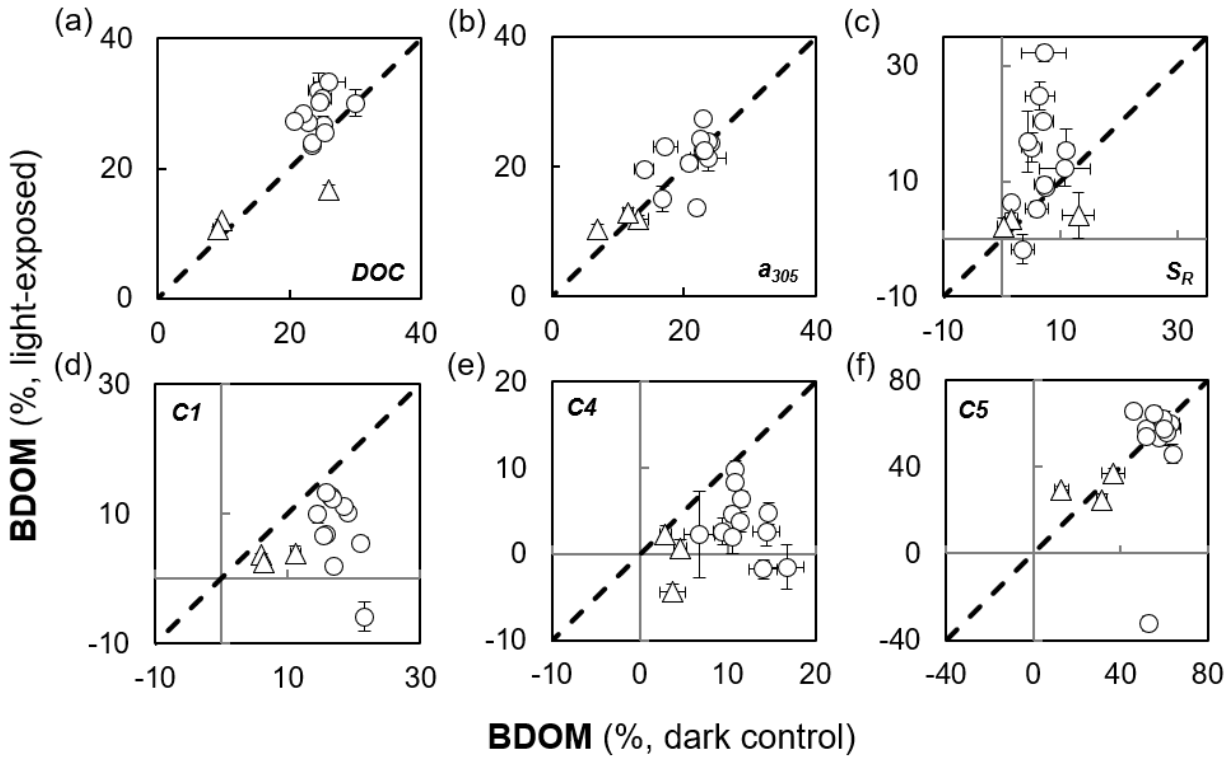

Figure 5.3. Percentage of biodegradable DOM (BDOM) in the light-exposed versus dark control waters plotted with the 1:1 line. Triangles (Δ) indicate the labile pool within BDOM and circles (O) indicate total BDOM. All data plotted as average ± 1 standard error of triplicate measurements.

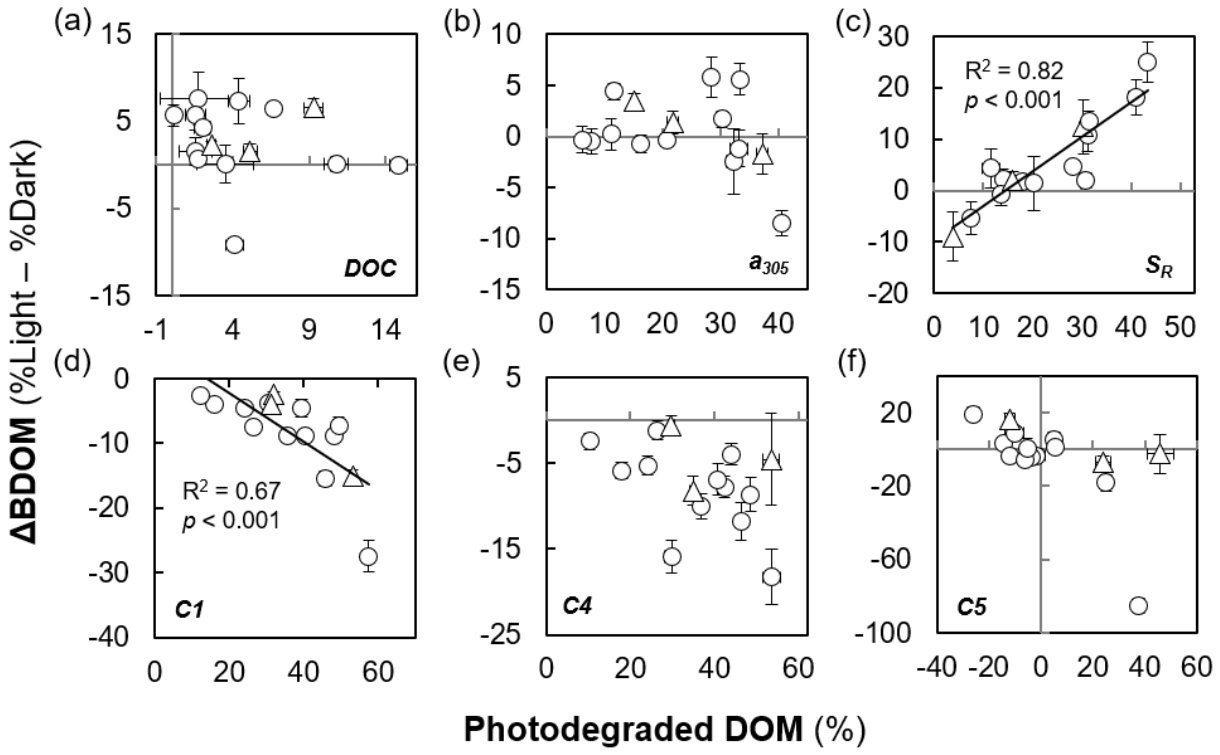

Figure 5.4. Effect of photodegradation on biodegradable DOM (BDOM) versus the percentage of DOM photodegraded. Triangles (Δ) indicate the labile pool within BDOM and circles (O) indicate total BDOM. All data plotted as average ± 1 standard error of triplicate measurements.

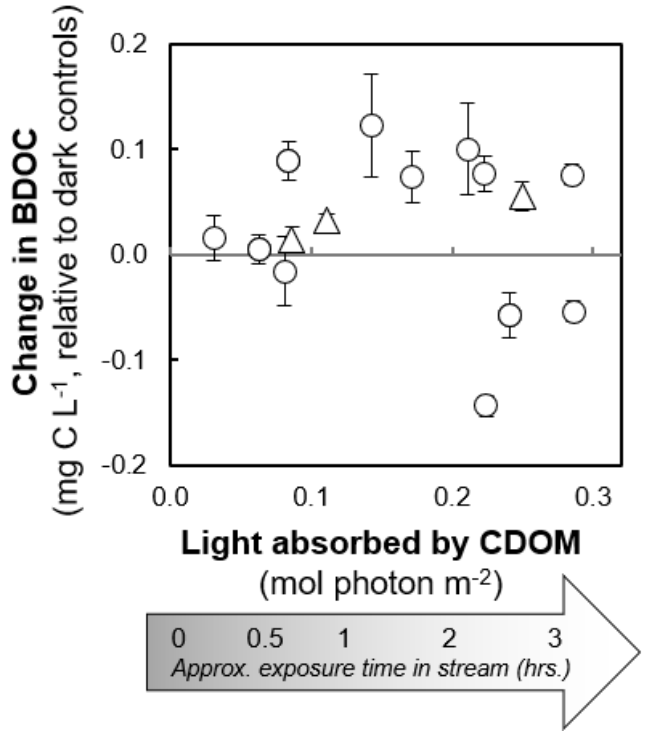

Figure 5.5. Effect of photodegradation on biodegradable DOC (BDOC) concentration as a function of the amount of light absorbed by CDOM. Triangles (Δ) indicate the labile pool within BDOC and circles (O) indicate total BDOC. All data plotted as average ± 1 standard error of triplicate measurements.

Date of collection	Sunlight exposure in quartz tubes (hr)	Photon dose (mol photon m^{-2})	Light absorbed by CDOM (mol photon m^{-2})	Equivalent sunlight exposure in WCC (hr)	Bioreactor EBCT (min)
14 August 2016	10	24	0.22	2.0	37
	12	26	0.25	2.2	1.5
	12	28	0.29	2.5	37
20 May 2017	5	5	0.08	0.9	37
	9	7	0.11	1.2	1.5
	10	9	0.14	1.6	37
	12	17	0.21	2.3	37
21 May 2017	5	2	0.03	0.4	37
	6	8	0.09	1.2	1.5
	11	18	0.17	2.5	37
	12	22	0.22	3.2	37
27 May 2017†	3	2	0.06	0.4	37
	4	3	0.08	0.5	37
	8	9	0.24	1.5	37
28 May 2017	17*	29	0.29	3.8	37

†Stream water collected 24 hours after a storm (41 mm of precipitation)
*Stream water was exposed to natural sunlight over a period of two days

Table 5.1. Summary of the sunlight exposure and biodegradation experiments conducted with White Clay Creek water. Biodegradation experiments were conducted using two bioreactors with different empty bed contact times (EBCT).

DOM constituent	Date of collection				
	14 August 2016	20 May 2017	21 May 2017	27 May 2017	28 May 2017
DOC concentration (mg C L^{-1})	1.46 ± 0.01^{a}	1.74 ± 0.01^{c}	1.43 ± 0.01^{a}	2.39 ± 0.01^{d}	1.69 ± 0.01^{b}
a_{305} (m^{-1})	5.77 ± 0.08^{b}	5.59 ± 0.01^{b}	4.71 ± 0.03^{a}	9.35 ± 0.01^{d}	6.05 ± 0.01^{c}
$SUVA_{254}$ (L mg^{-1} C m^{-1})	2.95 ± 0.02^{c}	2.56 ± 0.02^{a}	2.43 ± 0.03^{a}	2.99 ± 0.01^{c}	2.75 ± 0.01^{b}
S_R	0.68 ± 0.02^{ab}	0.74 ± 0.01^{c}	0.69 ± 0.01^{a}	0.71 ± 0.01^{b}	0.70 ± 0.01^{ab}
Humic-like C1 (RU)	0.41 ± 0.01^{b}	0.41 ± 0.01^{b}	0.36 ± 0.01^{a}	0.68 ± 0.01^{d}	0.49 ± 0.01^{c}
Tryptophan-like C4 (RU)	0.13 ± 0.01^{b}	0.13 ± 0.01^{b}	0.11 ± 0.01^{a}	0.21 ± 0.01^{d}	0.16 ± 0.01^{c}
Tyrosine-like C5 (RU)	0.05 ± 0.01^{a}	0.06 ± 0.01^{b}	0.05 ± 0.01^{a}	0.08 ± 0.01^{c}	0.06 ± 0.01^{b}

Table 5.2. Average concentrations of DOM fractions in White Clay Creek water. Letters indicate significant differences (ANOVA, $p < 0.05$) among stream waters. All values listed as average ± 1 standard error of triplicate measurements.

DOM constituent	Initial DOM (n = 5)	Photodegraded DOM (n = 15)	Total biodegradable DOM (n = 12)	
			Dark control	*Light-exposed*
DOC concentration (mg C L^{-1})	1.74 ± 0.17	0.08 ± 0.02 (4.7 ± 1.1)†	0.43 ± 0.02 (24.9 ± 0.6)	0.46 ± 0.03 (27.4 ± 1.3)*
a_{305} (m^{-1})	6.29 ± 0.80	1.36 ± 0.16 (23.1 ± 2.9)	1.34 ± 0.14 (20.8 ± 1.1)	1.09 ± 0.16 (21.1 ± 1.2)
$SUVA_{254}$ (L mg C^{-1} m^{-1})	2.74 ± 0.11	0.22 ± 0.04 (8.0 ± 1.4)	– 0.20 ± 0.04 (– 7.4 ± 1.5)	– 0.09 ± 0.02 (– 4.0 ± 1.1)
S_R	0.70 ± 0.01	– 0.16 ± 0.02 (– 22.8 ± 3.1)†	0.05 ± 0.01 (6.4 ± 0.8)	0.12 ± 0.03 (12.7 ± 2.8)*
Humic-like C1 (RU)	0.47 ± 0.06	0.16 ± 0.01 (36.2 ± 3.4)†	0.08 ± 0.01 (16.9 ± 0.8)	0.03 ± 0.01 (8.3 ± 1.6)*
Tryptophan-like C4 (RU)	0.15 ± 0.02	0.05 ± 0.01 (36.0 ± 3.3)†	0.02 ± 0.01 (11.7 ± 0.9)	0.01 ± 0.01 (3.5 ± 1.0)*
Tyrosine-like C5 (RU)	0.06 ± 0.01	0.01 ± 0.01 (3.5 ± 5.3)†	0.03 ± 0.01 (55.1 ± 2.2)	0.03 ± 0.01 (48.4 ± 7.7)

†Indicates significant differences between photodegraded DOM and total biodegradable DOM in the dark control (paired t-test, $p < 0.05$)
*Indicates significant differences between total biodegradable DOM in the dark control and light-exposed waters (paired t-test, $p < 0.05$)

Table 5.3. Average concentration of initial, photodegraded, and the total biodegradable DOM in White Clay Creek water. The percentage of DOM photodegraded or biodegraded is in parentheses. All values listed as average ± 1 standard error.

Lability class	Areal rate of DOC biodegradation (mg C m^{-2} d^{-1})	Areal rate of photomineralization (mg C m^{-2} d^{-1})	Areal rate of photo-production of BDOC (mg C m^{-2} d^{-1})		Areal rate of photo-removal of BDOC (mg C m^{-2} d^{-1})
			Calculated using a bioreactor with a 1.5-min EBCT	*Calculated using a bioreactor with a 37-min EBCT*	*Calculated using a bioreactor with a 37-min EBCT*
Labile	304 ± 20		9 ± 1	8 ± 3	6 ± 2
Semi-labile	25 ± 1			13 ± 5	9 ± 3
N/A		16 ± 4			

Table 5.4. Areal rates of DOC biodegradation, photomineralization, photochemical production of biodegradable DOC (BDOC), and photochemical removal of BDOC in White Clay Creek. All values listed as average ± 1 standard error.

5.8 Appendix

5.8.1 Percentages of labile and semi-labile DOM biodegraded in the 37-min EBCT bioreactor

Although prior studies have typically quantified total BDOM using a bioreactor with an EBCT of 150 minutes,[32] sample volume constraints required use of the 37-min EBCT bioreactor. The bioreactor with a 150-min EBCT would have required four times the sample volume needed to operate the bioreactor with a 37-min EBCT, which was too large a volume based on the number and volume of the quartz tubes available to expose stream water to sunlight. BDOM quantified using the bioreactor with a 37-min EBCT underestimates total BDOM because the ratio of BDOC concentration measured in the 37-min EBCT and the 150-min EBCT bioreactors, expressed as a percent, is 78.7% ± 0.9% (average ± 1 SE) based on feeding both bioreactors WCC water on 258 separate dates over several years (L. A. Kaplan unpubl.). Concentrations of the labile and semi-labile pools within total BDOC were estimated based on this larger dataset (*n* = 258 WCC water samples) showing that 38.5% ± 0.9% of the BDOC concentration degraded within a 37-min EBCT was in the labile pool (i.e., biodegraded within an EBCT of 1.5 minutes; L. A. Kaplan unpubl.), with the remaining 61% of BDOC in the semi-labile pool. For simplicity of presentation, we refer to the data from the 37-min EBCT bioreactor as total BDOM (Table 5.A.1), that was, on average, comprised of 39% and 61% labile and semi-labile DOM, respectively.

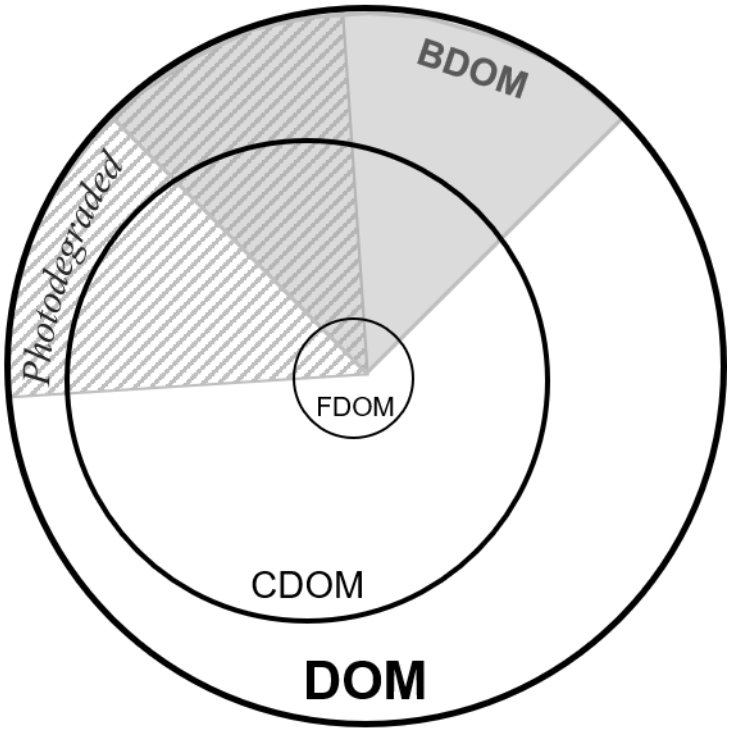

Figure 5.A.1. Conceptual diagram of the expected overlap between operational fractions of DOM and the impact of photodegradation on these fractions.

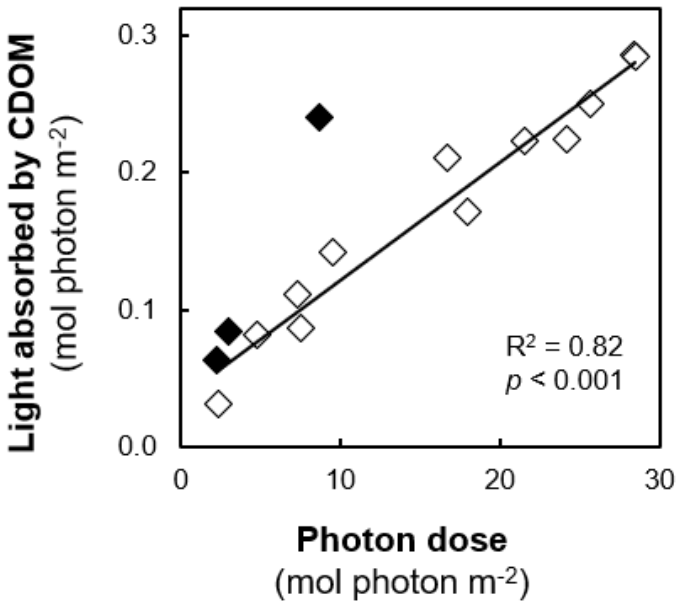

Figure 5.A.2. Light absorbed by CDOM in White Clay Creek water versus the total photon dose during the light exposure period. Open data points indicate stream water with CDOM at 305 nm (a_{305}) less than 6 m^{-1} and closed data points indicate stream water with a_{305} greater than 9 m^{-1} (collected on 27 May 2018).

Term	Operational definition	Units
DOM	All organic matter in water that passes through a GFF filter	N/A
DOC	Carbon concentrations of DOM	mg C L^{-1}
CDOM	Chromophoric or light-absorbing fraction of DOM	m^{-1}
FDOM	Fluorescent fraction of DOM	RU
Photodegraded DOM	Photodegradation is a term used to refer to all photochemical processes that breakdown any fraction of DOM	N/A
Photomineralization	Photochemical conversion to DOC to CO_2	mg C L^{-1}
Photo-alteration	Any photochemical change in DOM composition; in this study, photo-alteration was quantified as light-exposed vs. dark control differences in CDOM and FDOM	m^{-1}, RU or %
BDOM	DOM that is biodegradable	N/A
Total BDOM	The total biodegradable fraction of DOM, analyzed as the difference in DOM concentration and composition between the influent and effluent waters from a bioreactor with a 37-min empty bed contact time (EBCT)	N/A
Total BDOC	Carbon concentrations of total BDOM	mg C L^{-1}
Labile DOM	The pool of total BDOM degraded most rapidly by microbes, quantified as the difference in DOM concentration and composition between the influent and effluent waters from a bioreactor with a 1.5-min EBCT	N/A
Labile DOC	Carbon concentrations of labile DOM	mg C L^{-1}
Semi-labile DOM	The pool of total BDOM degraded more slowly by microbes, quantified as the difference in DOM concentration and composition between the effluent waters of bioreactors with 1.5-min and 37-min EBCTs	N/A
Semi-labile DOC	Carbon concentrations of semi-labile DOM	mg C L^{-1}

Table 5.A.1. Glossary table of terms.

Date of collection	Light absorbed by CDOM (mol photon m^{-2})	Photomineralized DOC (mg C L^{-1})	Biodegradable DOC (mg C L^{-1})	
			Dark control	*Light-exposed*
14 August 2016	0.22	0.06 ± 0.01 (4.1 ± 0.6)	0.38 ± 0.01 (25.9 ± 0.1)	0.23 ± 0.01 (16.8 ± 0.7)
	0.25	0.13 ± 0.01 (9.3 ± 0.6)	**0.29 ± 0.01** **(20.7 ± 0.8)**	**0.34 ± 0.01** **(27.2 ± 0.7)**
	0.29	0.21 ± 0.01 (14.8 ± 0.6)	0.36 ± 0.01 (25.5 ± 0.6)	0.31 ± 0.01 (25.4 ± 0.5)
20 May 2017	0.08	0.06 ± 0.03 (3.5 ± 1.8)	0.48 ± 0.01 (30.0 ± 0.8)	0.47 ± 0.03 (30.1 ± 2.1)
	0.11	0.04 ± 0.01 (2.6 ± 0.3)	**0.16 ± 0.01** **(9.6 ± 0.3)**	**0.19 ± 0.01** **(11.9 ± 0.4)**
	0.14	0.03 ± 0.04 (1.8 ± 2.5)	0.42 ± 0.03 (24.4 ± 1.5)	0.55 ± 0.04 (32.0 ± 2.6)
	0.21	0.08 ± 0.01 (4.4 ± 0.7)	0.45 ± 0.04 (26.0 ± 2.4)	0.55 ± 0.01 (33.3 ± 0.7)
21 May 2017	0.03	0.02 ± 0.02 (1.6 ± 1.1)	0.36 ± 0.01 (25.1 ± 0.7)	0.38 ± 0.02 (26.7 ± 1.4)
	0.09	0.07 ± 0.01 (5.1 ± 0.5)	**0.13 ± 0.01** **(9.1 ± 0.8)**	**0.15 ± 0.01** **(10.6 ± 0.5)**
	0.17	0.02 ± 0.01 (1.6 ± 0.6)	0.35 ± 0.02 (25.1 ± 1.2)	0.43 ± 0.02 (30.8 ± 1.2)
	0.22	0.01 ± 0.01 (0.1 ± 0.1)	0.34 ± 0.01 (24.6 ± 0.4)	0.41 ± 0.02 (30.2 ± 1.2)
27 May 2017†	0.06	0.04 ± 0.01 (1.8 ± 0.5)	0.56 ± 0.01 (23.4 ± 0.2)	0.56 ± 0.01 (24.0 ± 0.6)
	0.08	0.05 ± 0.01 (2.0 ± 0.5)	0.54 ± 0.01 (22.8 ± 0.5)	0.63 ± 0.01 (27.1 ± 0.6)
	0.24	0.26 ± 0.02 (10.8 ± 0.8)	0.56 ± 0.02 (23.4 ± 0.8)	0.50 ± 0.01 (23.5 ± 0.4)
28 May 2017	0.29	0.11 ± 0.01 (6.7 ± 0.4)	0.37 ± 0.01 (22.1 ± 0.5)	0.45 ± 0.01 (28.5 ± 0.3)

†Stream water collected 24 hours after a storm event (41 mm of precipitation)

Table 5.A.2. Concentrations of photomineralized and biodegradable DOC in White Clay Creek water. The percentage of DOC photomineralized or biodegraded is in parentheses. The three sets of light-exposed and dark control waters that were fed through a bioreactor with 1.5 minute empty bed contact time to quantify the labile DOC pool are indicated in bold font. All values listed as average ± 1 standard error of triplicate measurements.

5.9 References

1. Battin, T. J., L. A. Kaplan, S. Findlay, C. S. Hopkinson, E. Marti, A. I. Packman, et al. (2008). Biophysical controls on organic carbon fluxes in fluvial networks. *Nat. Geosci*. 1: 95-100.

2. Monteith, D. T., J. L. Stoddard, C. D. Evans, D. A. de Wit, M. Forsius, T. Høgåsen, et al. (2007). Dissolved organic carbon trends resulting from changes in atmospheric deposition chemistry. *Nature* 450: 537-540.

3. Laudon, H., J. Hedtjärn, J. Schelker, K. Bishop, R. Sørensen, and A. Ågren (2009). Responses of dissolved organic carbon following forest harvesting in a boreal forest. *Ambio* 38: 381-386.

4. Singh, N. K., W. M. Reyes, E. S. Bernhardt, R. Bhattacharya, J. L. Meyer, J. D. Knoepp, and R. E. Emanuel (2016). Hydro-climatological influences on long-term dissolved organic carbon in a mountain stream of the southeastern United States. *J. Environ. Qual*. 45: 1286-1295.

5. Oni, S. K., T. Tiwari, J. L. J. Ledesma, A. M. Ågren, C. Teutschbein, J. Schelker, et al. (2015). Local- and landscape-scale impacts of clear-cuts and climate change on surface water dissolved organic carbon in boreal forests. *J. Geophys. Res. Biogeosci.* 120: 2402-2426.

6. Biddanda, B. A. (2017). Global significance of the changing freshwater carbon cycle. *Eos* 98: 15-17.

7. Cory, R. M., and G. W. Kling (2018). Interactions between sunlight and microorganisms influence dissolved organic matter degradation along the aquatic continuum. *Limnol. Oceanogr.: Lett.* 3: 102-116.

8. Granéli, W., M. Lindell, and L. Tranvik (1996). Photo-oxidative production of dissolved inorganic carbon in lakes of different humic content. *Limnol. Oceanogr.* 41: 698-706.

9. Lindell, M. J., H. W. Granéli, and S. Bertilsson (2000). Seasonal photoreactivity of dissolved organic matter from lakes with contrasting humic content. *Can. J. Fish. Aquat. Sci.* 57: 875-885.

10. Cory, R. M., D. M. McKnight, Y.-P. Chin, P. Miller, and C. L. Jaros (2007). Chemical characteristics of fulvic acids from Arctic surface waters: Microbial contributions and photochemical transformations. *J. Geophys. Res.* 112, G04S51.

11. Gonsoir, M., B. M. Peake, W. T. Cooper, D. Podgorski, J. D'Andrilli, and W. J. Cooper (2009). Photochemically induced changes in dissolved organic matter identified by ultrahigh resolution Fourier transform ion cyclotron resonance mass spectrometry. *Environ. Sci. Technol*. 43: 698-703.

12. Ward, C. P., and R. M. Cory (2016). Complete and partial photo-oxidation of dissolved organic matter draining permafrost soils. *Environ. Sci. Technol.* 50: 3545-3553.

13. Moran, M. A., W. M. Sheldon, and R. G. Zepp (2000). Carbon loss and optical property changes during long-term photochemical and biological degradation of estuarine dissolved organic matter. *Limnol. Oceanogr.* 45: 1254-1264.

14. Cory, R. M., K. McNeill, J. P. Cotner, A. Amado, J. M. Purcell, and A. G. Marshall (2010). Singlet oxygen in the coupled photo- and biochemical oxidation of dissolved organic matter. *Environ. Sci. Technol*. 44: 3683-3689.

15. Amado, A. M., J. B. Cotner, R. M. Cory, B. L. Edhlund, and K. McNeill. (2015). Disentangling the interactions between photochemical and bacterial degradation of dissolved organic matter: Amino acids play a central role. *Microb. Ecol.* 69: 554-566.

16. Ward, C. P., S. G. Nalven, B. C. Crump, G. W. Kling, and R. M. Cory (2017). Photochemical alteration of organic carbon draining permafrost soils shifts microbial metabolic pathways and stimulates respiration. *Nat. Commun*. 8, 722.

17. Wetzel, R. G., P. G. Hatcher, and T. S. Bianchi (1995). Natural photolysis by ultraviolet irradiance of recalcitrant dissolved organic matter to simple substrates for rapid bacterial metabolism. *Limnol. Oceanogr*. 40: 1369-1380.

18. Bertilsson, S., and L. J. Tranvik (1998). Photochemically produced carboxylic acids as substrates for freshwater bacterioplankton. *Limnol. Oceanogr*. 43: 885-895.

19. Tranvik, L. J., and S. Bertilsson (2001). Contrasting effects of solar UV radiation on dissolved organic sources for bacterial growth. *Ecol. Lett.* 4: 458-463.

20. Amado, A. M., J. B. Cotner, A. L. Suhett, F.D. Assis Esteves, R. L. Bozelli, and V. F. Farjalla (2007). Contrasting interactions mediate dissolved organic matter decomposition in tropical aquatic ecosystems. *Aquat. Microb. Ecol*. 49: 25-34.

21. Pullin, M. J., S. Bertilsson, J. V. Goldstone, and B. M. Voelker (2004). Effects of sunlight and hydroxyl radical on dissolved organic matter: Bacterial growth efficiency and production of carboxylic acids and other substrates. *Limnol. Oceanogr.* 49: 2011-2022.

22. Obernosterer, I., and R. Benner (2004). Competition between biological and photochemical processes in the mineralization of dissolved organic carbon. *Limnol. Oceanogr.* 49: 117-124.

23. Fasching, C., and T. J. Battin (2012). Exposure of dissolved organic matter to UV-radiation increases bacterial growth efficiency in a clear-water Alpine stream and its adjacent groundwater. *Aquat. Sci.* 74: 143-153.

24. Coble, P. G (1996). Characterization of marine and terrestrial DOM in seawater using excitation emission matrix spectroscopy. *Mar. Chem.* 51: 325-346.

25. Guillemette, F., and P. A. del Giorgio (2011). Reconstructing the various facets of dissolved organic carbon bioavailability in freshwater ecosystems. *Limnol. Oceanogr*. 56: 734-748.

26. Cory, R. M., and L. A. Kaplan (2012). Biological lability of streamwater fluorescent dissolved organic matter. *Limnol. Oceanogr*. 57: 1347-1360.

27. Cory, R. M., C. P. Ward, B. C. Crump, and G. W. Kling (2014). Sunlight controls water column processing of carbon in arctic fresh waters. *Science* 345: 925-928.

28. Cory, R. M., K. H. Harrold, B. T. Neilson, and G. W. Kling (2015). Controls on dissolved organic matter (DOM) degradation in a headwater stream: the influence of photochemical and hydrological conditions in determining light-limitation or substrate limitation of photo-degradation. *Biogeosci.* 12: 6669-6685.

29. Reader, H. E., and W. L. Miller (2014). The efficiency and spectral photon dose dependence of photochemically induced changes to the bioavailability of dissolved organic carbon. *Limnol. Oceanogr*. 59: 182-194.

30. Newbold, J. D., T. L. Bott, L. A. Kaplan, B. W. Sweeney, and R. L. Vannote (1997). Organic matter dynamics in White Clay Creek, Pennsylvania, USA. *J. N. Am. Benthol. Soc.* 16: 46-50.

31. Kaplan, L. A., and J. D. Newbold (1995). Measurements of streamwater biodegradable dissolved organic carbon with a plug-flow bioreactor. *Water Res.* 29: 2696-2706.

32. Kaplan, L. A., T. N. Wiegner, J. D. Newbold, P. H. Ostrom, and H. Gandhi (2008). Untangling the complex issue of dissolved organic carbon uptake: A stable isotope approach. *Freshw. Biol*. 53: 855-864.

33. Sleighter, R. L., R. M. Cory, L. A. Kaplan, H. A. N. Abdulla, and P. G. Hatcher (2014). A coupled geochemical and biogeochemical approach to characterize the bioreactivity of dissolved organic matter from a headwater stream. *J. Geophys. Res. Biogeosci.* 199: 1520-1537.

34. Tyndall, J. (1877). On heat as a germicide when discontinuously applied. *Proc. R. Soc. Lond.* 25: 569-570.

35. Weishaar, J. L., G. R. Aiken, B. A. Bergamaschi, M. S. Fram, R. Fujii, and K. Mopper (2003). Evaluation of specific ultraviolet absorbance as an indicator of the chemical composition and reactivity of dissolved organic carbon. *Environ. Sci. Technol.* 37: 4702-4708.

36. Helms, J. R., A. Stubbins, J. D. Ritchie, E. C. Minor, D. J. Kieber, and K. Mopper (2008). Absorption spectral slopes and slope ratios as indicators of molecular weight, source, and photobleaching of chromophoric dissolved organic matter. *Limnol. Oceanogr.* 53: 955-969.

37. Cory, R. M., M. P. Miller, D. M. McKnight, J. J. Guerard, and P. L. Miller (2010). Effect of instrument-specific response on the analysis of fulvic acid fluorescence spectra. *Limnol. Oceanogr.: Methods* 8: 67-78.

38. Stedmon, C. A., and R. Bro (2008). Characterizing dissolved organic matter fluorescence with parallel factor analysis: A tutorial. *Limnol. Oceanogr.: Methods* 6: 572-579.

39. del Vecchio, R., and N. V. Blough (2004). On the origin of the optical properties of humic substances. *Environ. Sci. Technol*. 38: 3885-3891.

40. Hernes, P. J., B. A. Bergamaschi, R. S. Eckard, and R. G. M. Spencer (2009). Fluorescence-based proxies for lignin in freshwater dissolved organic matter. *J. Geophys. Res.* 114, G00F03.

41. Cory, R. M., and D. M. McKnight (2005). Fluorescence spectroscopy reveals ubiquitous presence of oxidized and reduced quinones in dissolved organic matter. *Environ. Sci. Technol.* 39: 8142-8149.

42. Murphy, K. R., C. A. Stedmon, T. D. Waite, and G. M. Ruiz (2008). Distinguishing between terrestrial autochthonous organic matter sources in marine environments using fluorescence spectroscopy. *Mar. Chem.* 108: 40-58.

43. Stedmon, C. A., and S. Markager (2005). Tracing the production and degradation of autochthonous fractions of dissolved organic matter by fluoresence analysis. *Limnol. Oceanogr.* 50: 1415-1426.

44. Vähätalo, A. V., M. Salkinoja-Salonen, P. Taalas, and K. Salonen (2000). Spectrum of the quantum yield for photochemical mineralization of dissolved organic carbon in a humic lake. *Limnol. Oceanogr.* 45: 664-676.

45. Cory, R. M., B. C. Crump, J. A. Dobkowski, and G. W. Kling (2013). Surface exposure to sunlight stimulates CO2 release from permafrost soil carbon in the Arctic. *Proc. Natl. Acad. Sci. USA* 110: 3429-3434.

46. Gonsoir, M., P. Schmitt-Kopplin, and D. Bastviken (2013). Depth-dependent molecular composition and photo-reactivity of dissolved organic matter in a boreal lake under winter and summer conditions. *Biogeosci.* 10: 6945-6956.

47. Kim, S., L. A. Kaplan, and P. G. Hatcher (2006). Biodegradable dissolved organic matter in a temperate and a tropical stream determined from ultra-high resolution mass spectrometry. *Limnol. Oceanogr*. 51: 1054-1063.

48. Ward, C. P., and R. M. Cory (2015). Chemical composition of dissolved organic matter draining permafrost soils. *Geochim. Cosmochim. Acta* 167: 63-79.

49. Jørgensen, N. O. G., L. Tranvik, H. Edling, W. Granéli, and M. Lindell (1998). Effects of sunlight on occurrence and bacterial turnover of specific carbon and nitrogen compounds in lake waters. *FEMS Microbol. Ecol.* 25: 217-227.

50. Buffam, I., and K. J. McGlathery (2003). Effect of ultraviolet light on dissolved nitrogen transformations in coastal lagoon water. *Limnol. Oceanogr.* 48: 723-734.

51. Volk, C. J., C. B. Volk, and L. A. Kaplan (1997). Chemical composition of biodegradable dissolved organic matter in streamwater. *Limnol. Oceanogr*. 42: 39-44.

52. Pattison, D. I., A. S. Rahmanto, and M. J. Davies (2012). Photo-oxidation of proteins. *Photochem. Photobiol. Sci.* 11: 38-53.

53. Janssen, E. M.-L., P. R. Erickson, and K. McNeill (2014). Dual roles of dissolved organic matter as a sensitizer and quencher in the photooxidation of tryptophan. *Environ. Sci. Technol.* 48: 4916-4924.

54. Hockaday, W. C., J. M. Purcell, A. G. Marshall, J. A. Baldock, and P. G. Hatcher (2009). Electrospray and photoionization mass spectrometry for the characterization of organic matter in natural waters: A qualitative assessment. *Limnol. Oceanogr.: Methods* 7: 81-95.

55. Biddanda, B. A., and J. B. Cotner (2003). Enhancement of dissolved organic matter bioavailability by sunlight and its role in the carbon cycle of Lakes Superior and Michigan. *J. Great Lakes Res*. 29: 228-241.

56. Li, A., A. F. Aubeneau, T. King, R. M. Cory, B. T. Neilson, D. Bolster, and A. I. Packman (2019). Effects of vertical hydrodynamic mixing on photomineralization of dissolved organic carbon in arctic surface waters. *Environ. Sci.: Processes Impacts* 21: 748-760.

57. McLaughlin, C., and L. A. Kaplan (2013). Biological lability of dissolved organic carbon in stream water and contributing terrestrial sources. *Freshw. Sci.* 32: 1219-1230.

58. Hall, R. O., M. A. Baker, E. J. Rosi-Marshall, J. L. Tank, and J. D. Newbold (2013). Solute specific scaling of inorganic nitrogen and phosphorus uptake in streams. *Biogeosci.* 10: 7323-7331.

Chapter 6

Conclusions

6.1 Controls on and the importance of DOM photodegradation in freshwaters

This dissertation investigated controls on the photochemical production of ammonium (NH_4^+), carbon dioxide (CO_2), and photo-altered dissolved organic matter (DOM) compounds because these sunlight-driven pathways have the potential to impact the amount of CO_2 emitted from freshwaters. The classes of DOM compounds undergoing each DOM photodegradation pathway were identified, mechanisms of their degradation were tested, and impacts of photo-altered products on bacterial respiration were quantified. The role of each DOM photodegradation pathway in impacting freshwater carbon (C) and nitrogen (N) cycles was then investigated. Findings from this dissertation demonstrate that (1) protein-like compounds within DOM undergo photodegradation to produce NH_4^+, (2) carboxyl groups associated with lignin- and tannin-like compounds within DOM undergo an iron-catalyzed mechanism of photo-decarboxylation to produce CO_2, (3) unsaturated hydrocarbons within permafrost DOM undergo partial photo-oxidation to form more oxidized photo-products, and (4) aromatic and protein-like compounds undergo photochemical alteration to form organic photo-products that are more or less susceptible to respiration by bacteria in freshwaters. They also show how and why (1) the photodegradation of DOM to NH_4^+ provides an important source of the N fueling primary production in arctic lakes, (2) DOM photodegradation in arctic freshwaters will increase in the future as permafrost soils thaw, (3) the oxidation state of permafrost DOM will change as it is exposed to sunlight in arctic freshwaters and (4) the photodegradation of semi-labile DOM

impacts the amount of DOM respired by bacteria in temperate streams. Here, I discuss three ways that this work improves our understanding of the impact of DOM photodegradation on freshwater CO_2 emissions, and our ability to predict changes to this DOM photodegradation in the future.

6.1.1 Mechanistic controls on DOM photodegradation

My results improve our ability to predict rates of DOM photodegradation in freshwaters by identifying chemical controls on the photochemical production of NH_4^+ and CO_2. Prior studies have been unable to determine how DOM chemical composition or water chemistry control apparent quantum yields for their formation in natural waters.[1-3] However, my findings show that major controls on DOM photodegradation pathways can be identified if potential controls can be accounted for and multiple lines of evidence can be gathered from different analytical techniques and mass balance approaches.

For example, I combined high-resolution mass spectrometry and fluorescence spectroscopy with mass balance calculations to show that the photo-production of NH_4^+ is controlled by the abundance of protein-like compounds within DOM in arctic freshwaters (**Chapter 2**). The photochemical production of amino acid-like compounds observed alongside NH_4^+ (Figure 2.3) suggests that the cleavage of peptide bonds within protein structures can increase the number of primary amine groups available to undergo photodegradation to produce NH_4^+.[4-6] Not all amide groups within protein-like compounds were susceptible to this photodegradation and thus, only a fraction of protein-like N was likely converted to NH_4^+. For example, concentrations of protein-like N within DOM were estimated to be 6.5-fold greater than maximum concentrations of NH_4^+ photo-produced across arctic freshwaters, on average (Discussion Section 2.5.1). These findings suggest that NH_4^+ will be photo-produced from the

protein-like compounds present in freshwaters, but can be limited by the replenishment of new protein-like N that can undergo this photodegradation.[7]

I also combined ^{13}C nuclear magnetic resonance with dissolved gas and carbon isotope measurements to show that the photo-production of CO_2 from permafrost DOM is controlled by concentrations of dissolved iron present because iron catalyzed a mechanism of photo-decarboxylation, where carboxyl groups associated with lignin- and tannin-like compounds are oxidized to CO_2 (**Chapter 3**). Although both dissolved iron and carboxyl groups are needed for this reaction to proceed, my findings show that the photo-production of CO_2 from permafrost DOM depends more strongly on the amount of dissolved iron, likely because there are more carboxyl groups available to undergo this mechanism[8-10] than the dissolved iron needed to facilitate it.[11-14] Consistent with this idea, concentrations of carboxyl C within permafrost DOM (Table 3.A.6) were on average 7-fold greater than concentrations of CO_2 photo-produced (Table 3.A.3).[8] Thus, these findings indicate that the amount of CO_2 produced during the photo-decarboxylation of DOM increases in proportion to the amount of dissolved iron present in freshwaters, as long as there is enough carboxyl C to undergo degradation.

Although this work was conducted in the Arctic, knowledge of these mechanistic controls also improves our ability to quantify NH_4^+ and CO_2 photo-production in other freshwaters on Earth. Nitrogen can make up <1 to 5% of the DOM pool in freshwaters[15-18] and anywhere from 35 to 70% of this N can be protein-like.[19-21] In addition, carboxyl groups can contain 10 to 25% of the C within DOM in freshwaters.[8,16-17,22-23] Thus, the protein-like N and carboxyl C present in nearly all freshwaters should undergo photodegradation once DOM is exposed to sunlight. My results suggest that NH_4^+ photo-production in other freshwaters will depend strongly on the

amount of protein-like N present and the amount of CO_2 produced during the iron-catalyzed photo-decarboxylation of DOM will depend strongly on dissolved iron concentrations.

Most freshwaters have low concentrations of dissolved iron (< 1 µM),[24-27] suggesting that a small amount of CO_2 is produced during the iron-catalyzed mechanism of photo-decarboxylation. Freshwater DOM also has a higher abundance of aromatic compounds compared to permafrost DOM,[8,16,22] indicating that a larger portion of the CO_2 produced during DOM photodegradation likely comes from other mechanisms involving these light-absorbing compounds.[28-30] While this suggests that dissolved iron may be a minor control on the amount of CO_2 photo-produced from DOM in freshwaters other than those in the Arctic, concentrations of dissolved iron have been increasing in some freshwaters over the past ~30 years in temperate[31-32] and boreal regions.[33-34] Thus, dissolved iron could become a more important control on the photo-production of CO_2 in temperate and boreal freshwaters in the future, and its measurement could be useful in quantifying the increase in freshwater CO_2 emissions as a result of this change.

6.1.2 Estimating the effect of DOM photodegradation on bacterial respiration

My results improve our ability to estimate the effects of DOM photodegradation on the amount of DOM that is respired by bacteria to CO_2 in freshwaters by identifying controls on the formation of photo-altered products that may impact bacterial respiration. For example, I found that sunlight exposure of permafrost DOM can result in the photo-production of DOM compounds that are more oxidized or less oxidized, depending on the aromatic content of DOM and the wavelength of light (**Chapter 4**). Less oxidized DOM compounds were photo-produced following exposure to visible light compared to UV light (Figure 4.1) likely due to the greater iron-catalyzed photo-decarboxylation of permafrost DOM taking place at longer versus shorter

wavelengths (Discussion Section 4.5.3). The extent that photo-decarboxylation removed oxygen from DOM relative to oxygen incorporation during partial photo-oxidation at visible wavelengths depended on concentrations of dissolved iron present to photo-decarboxylate lignin-like compounds and the abundance of aromatic compounds that initiated partial photo-oxidation reactions. Given that the oxidation state of DOM can impact its susceptibility to bacterial respiration,[10,35-36] the photo-production of more oxidized versus less oxidized DOM compounds could impact the amount of permafrost DOM that gets respired by bacteria to CO_2 once it drains to sunlit freshwaters in the Arctic.

My results also help explain the conceptual model on when and why sunlight has a positive or negative effect on bacterial respiration of DOM to CO_2. It has long been thought that the effect of sunlight on bacterial respiration depends on the source of compounds making up the DOM pool, where sunlight exposure of DOM compounds from terrestrial sources (e.g., high molecular weight aromatics) increases their respiration by bacteria and exposure of DOM compounds from microbial sources (e.g., N-rich compounds) decreases their respiration.[37-38] However, this conceptual model does not explain why these patterns are observed, which is needed to estimate the extent that DOM photodegradation impacts bacterial respiration in freshwaters.

I found that sunlight exposure increases and decreases the susceptibility of aromatic and N-containing DOM compounds to bacterial respiration simultaneously and that the balance of labile and recalcitrant photo-products formed determines the effect of sunlight on bacterial respiration (**Chapter 5**). For instance, high molecular weight, aromatic compounds underwent photodegradation to produce lower molecular weight aromatics, which increased their susceptibility to bacterial respiration (Figure 5.4), consistent with expectations.[38] However, they

were also photochemically altered to less labile forms. Protein-like compounds were photochemically altered to less labile forms, consistent with expectations that N-rich DOM compounds become less labile to bacteria following sunlight exposure.[38] Yet, these compounds were also photodegraded to produce amino acid-like compounds that were more susceptible to bacterial respiration. Given that terrestrially-derived DOM contains more high molecular weight aromatics than protein-like compounds,[16,39-40] my findings suggest that the positive effect of sunlight on bacterial respiration of terrestrially-derived DOM generally observed across freshwaters[2,41-44] is due to the greater production of lower molecular weight aromatics compared to the photochemically altered, high molecular weight compounds. Thus, findings from this work challenge the conceptual model by showing that the effect of sunlight on bacterial respiration of DOM depends less on the source of compounds making up the DOM pool and more on the extent that they are photodegraded to labile versus recalcitrant forms.

6.1.3 Importance of DOM photodegradation in the freshwater carbon and nitrogen cycles

Findings from this dissertation challenge the long-held understanding that nearly all DOM degradation in freshwaters is attributed to heterotrophic bacteria alone[16,45-48] and build on previous findings that DOM photodegradation rates are fast enough to contribute up to 30% of the CO_2 emitted from arctic freshwaters.[2] For instance, my results demonstrate that DOM photodegradation is a critical component of the N cycle in arctic freshwaters (**Chapter 2**) and show how and why DOM photodegradation will continue to provide an important source of CO_2 emitted from arctic freshwaters in the future as permafrost soils thaw (**Chapter 3**). Additionally, my findings demonstrate that DOM photodegradation can impact the amount of CO_2 emitted from temperate streams over relatively short timescales by affecting the amount of DOM

respired by bacteria to CO_2 (**Chapter 5**). By directly measuring apparent quantum yield spectra, measuring the radiocarbon age of CO_2 produced from permafrost DOM, and comparing water column rates of photodegradation to bacterial degradation for specific classes of DOM compound, my results improve our understanding of the impact of DOM photodegradation on freshwater CO_2 emissions now and in the future.

For example, my results build on previous work in the Arctic[2] by showing that DOM photodegradation plays an equally important role in the freshwater N cycle as the C cycle (**Chapter 2**). My finding that NH_4^+ photo-production rates (Table 2.3) were comparable to fluxes of dissolved inorganic N export from arctic soils to streams[49] and streams to lakes[50] demonstrates that the degradation of DOM draining from soils can supply similar amounts of DIN to freshwaters as other fluxes of DIN, creating a strong linkage between soil and freshwater ecosystems.[51] Photodegradation of DOM to NH_4^+ could provide 5% of the N required by primary producers during the ice-free summer in an arctic lake (Figure 2.5), indicating that sunlight exposure of DOM in the sunlit water column can facilitate the use of protein-like N by primary producers by converting it to an inorganic form that can be taken up into their cells.[52] Thus, these findings add to current N budgets on the sources of dissolved inorganic N supporting N demands by primary producers in arctic lakes[50,53-54] by constraining sources of inorganic N from DOM degradation.

My finding that 4,000-year-old CO_2 is produced during the photodegradation of arctic permafrost DOM also demonstrates for the first time that permafrost DOM will be rapidly converted to CO_2, contributing to the arctic amplification of climate change, once it reaches sunlit freshwaters (**Chapter 3**). Given that rates of CO_2 photo-production from permafrost DOM were 2-fold higher than those for the modern DOM currently draining soils to arctic freshwaters

(Figure 3.7),[2] findings from this work show that DOM photodegradation could account for more of the CO_2 produced from arctic freshwaters in the future as permafrost soils thaw. The magnitude of this increased CO_2 photo-production will depend strongly on the amount of dissolved iron present in the freshwaters draining thawing permafrost soils in the Arctic.

Arctic freshwaters currently contain concentrations of dissolved iron that span the range tested in this dissertation (0-30 μM; Tables 3.A.5, 3.A.6)[7,30,55] and are expected to maintain these high iron concentrations in the future. For instance, numerous studies have reported higher concentrations of dissolved iron in permafrost-impacted freshwaters compared to non-impacted arctic freshwaters.[56-59] Higher dissolved iron concentrations have also been observed in arctic freshwaters in late fall when active soil layer is at its greatest depth,[60] suggesting that the deeper permafrost soil layer delivers more dissolved iron to neighboring freshwaters than the surface soil. Thus, it is likely that the photo-production of CO_2 from permafrost DOM can exceed that from modern DOM, increasing the amount of freshwater CO_2 coming from DOM photodegradation in the future.

Lastly, my finding that it takes only minutes to hours of sunlight exposure in a temperate stream for photodegradation to impact bacterial respiration of terrestrially-derived DOM (Figure 5.5) demonstrates that stream DOM may be exposed to enough sunlight to impact its respiration by bacteria in the benthic zone of the streambed downstream (**Chapter 5**). This result suggests that photodegradation could play an increasingly important role in determining the fate of DOM as streams become less shaded due to shifts in land-use from forested and rural to urban and agricultural.[61] Given that the effect of sunlight – positive or negative – on bacterial respiration depended strongly on the extent that DOM was exposed to sunlight (Figure 5.5), my findings

demonstrate a need to constrain the role of DOM photodegradation in increasing or decreasing the amount of CO_2 from bacterial respiration in freshwaters.

6.2 Future work: Impact of DOM photodegradation on bacterial use of carbon and nitrogen

The findings from this dissertation generated a number of new questions related to the impact of DOM photodegradation on bacterial use of C and N in freshwaters:

i. What are the labile and recalcitrant products formed during the photodegradation of terrestrially-derived, high molecular weight compounds within freshwater DOM?

ii. At which wavelengths of sunlight are these labile and recalcitrant photo-products formed?

iii. Could the photodegradation of protein-like compounds in arctic lakes impact their susceptibility to uptake by bacteria?

Knowledge of the high molecular weight, aromatic compounds undergoing photodegradation to form labile and recalcitrant products and the chemical properties of photo-products formed are needed to quantify the extent that photodegradation of terrestrially-derived DOM impacts bacterial respiration in freshwaters. Preliminary results following the work in **Chapter 5** suggest that the labile, lower molecular weight aromatic compounds formed during the photodegradation of temperate stream DOM are less oxidized compared to the initial bulk DOM (Figure 6.1). This finding is consistent with prior work showing that the photodegradation of terrestrially-derived DOM produces less oxidized compounds that are labile to bacterial respiration.[10,62] Photodegradation of terrestrially-derived DOM has also been shown to reduce the need for bacteria to make oxygenase enzymes, suggesting that more oxidized, labile photo-products are also formed, which shortcut key metabolic pathways for the bacterial degradation of

DOM.[62] Thus, the increased bacterial respiration of less oxidized, lower molecular weight aromatics following photodegradation of temperate stream DOM (Figure 6.1) suggests that there may be fewer oxidized, labile photo-products compared to the less oxidized, labile compounds also formed.

In contrast to the labile photo-products, much less is known about the chemical properties of the recalcitrant, high molecular weight, aliphatic and aromatic compounds formed during the photodegradation of terrestrially-derived DOM. Given that bacteria preferentially respired less oxidized DOM compounds following sunlight exposure of stream DOM (Figure 6.1), it is possible that the recalcitrant compounds remaining were more oxidized. Aliphatic and aromatic compounds within terrestrially-derived DOM can undergo partial photo-oxidation by reactive oxygen species to form saturated and carboxylic-rich alicyclic compounds.[63-66] Previous studies have showed that the partially oxidized products formed from singlet oxygen, the reactive oxygen species expected to account for most of the partial photo-oxidation of terrestrially-derived DOM,[66-68] are less susceptible to bacterial respiration.[63] Thus, the recalcitrant high, molecular weight, aliphatic and aromatic compounds formed during the photodegradation of terrestrially-derived DOM may be products of partial photo-oxidation by singlet oxygen. Determining controls on the production of these labile and recalcitrant compounds that have the largest impact on bacterial respiration on a mass basis will help to further refine the conceptual model on the effect of sunlight on bacterial respiration in freshwaters.

Identifying the labile and recalcitrant products formed during DOM photodegradation and the wavelengths at which they are formed will also improve water column rate estimates for DOM photodegradation in freshwaters. The main control on water column rates of photo-product formation is the apparent quantum yield spectrum, which is the yield of product formed

as a function of the wavelength of sunlight absorbed by the aromatic compounds within DOM.[68] While apparent quantum yield spectra have been characterized for the net effect of sunlight on bacterial respiration of DOM,[69] yield spectra have never been characterized for each of the labile and recalcitrant photo-products that substantially impact bacterial respiration of DOM because these individual DOM compounds cannot be quantified on a mass basis. Thus, to get a conservative estimate of the rates at which they are formed in a temperate stream, this dissertation assumed a spectral shape for the apparent quantum yield spectra for the photo-production of labile and recalcitrant compounds (see Methods Section 5.3.8). However, small changes to the shape of this yield spectrum can drastically impact rates of photodegradation in freshwaters (as shown in Figures 3.7 and 3.A.1). Given that previous work has reported spectral shapes for the net effect of sunlight on bacterial respiration of DOM that vary widely across freshwaters,[69] these findings indicate that there remains high uncertainty in the estimated rates of DOM photodegradation and their impact on bacterial respiration in freshwaters.

Two findings from this dissertation suggest that water column rates for the photochemical production and removal of labile DOM in streams could be underestimated (Table 5.4). First, the photo-production of less oxidized DOM compounds following the iron-catalyzed removal of carboxyl groups from lignin-like compounds likely took place at visible wavelengths of light (Discussion Section 4.5.3). Second, preliminary findings following **Chapter 2** show that amino acid-like compounds are photo-produced at visible wavelengths of light (Figure 6.2). The photo-production of less oxidized and amino acid-like, labile compounds at visible light disproportionately impacts the rate at which DOM is photodegraded because there is 10-fold more visible light reaching freshwaters than ultraviolet (Table 3.A.4). As a result, higher apparent quantum yields for the photo-production of labile, amino acid-like compounds at visible

wavelengths than in the spectral shape assumed in **Chapter 5** (see Methods Section 5.3.8) could result in photo-production rates in streams that are closer in magnitude to rates of their bacterial respiration in the streambed (Table 5.4). If water column rates for the photo-production of amino acid-like compounds were 10 times faster, then photodegradation rates could be fast enough to increase bacterial respiration of these labile compounds in the streambed. Thus, these findings demonstrate the need to characterize the wavelength dependence of labile and recalcitrant photo-products formed from DOM to better constrain the impact of this DOM photodegradation pathway on freshwater CO_2 emissions.

Lastly, the photo-production of labile, amino acid-like compounds and recalcitrant protein-like compounds from stream DOM (Figure 5.4) suggests that the photodegradation of protein-like N in arctic lakes could be impacting bacterial uptake of organic N in the water column. The photodegradation of tryptophan-like DOM, a proxy for protein-like compounds (Figure 2.2),[33] and photo-production of tyrosine-like DOM were observed in both the arctic lake and temperate stream waters studied in this dissertation (Figures 2.3, 5.2). However, the faster rates of photodegradation for protein-like N in arctic lakes (Figure 2.4) compared to the temperate stream (Table 5.4) suggest that these processes could be more important in impacting bacterial use of organic N in lakes than streams. The photodegradation of protein-like compounds to amino acids could facilitate the uptake of N by bacteria in arctic lakes, reducing their need to produce and release extracellular enzymes.[70-72] In contrast, the photochemical alteration of protein-like compounds could increase the need for bacteria to release extracellular enzymes to obtain N from larger compounds within the DOM pool, increasing rates of bacterial degradation and reducing the capacity for sunlight to compete with bacteria for the degradation of protein-like compounds in the water column (Figure 2.5). Previous studies have showed that

recalcitrant organic N accumulates in lakes where there are large inputs of protein-like compounds and long residence times for these compounds to be exposed to sunlight,[16-17] suggesting that DOM photodegradation could be removing labile, protein-like N from the water column in lakes. Thus, future work should evaluate the extent that DOM photodegradation produces recalcitrant protein-like compounds in arctic lakes, and the impact that this has on the arctic N cycle.

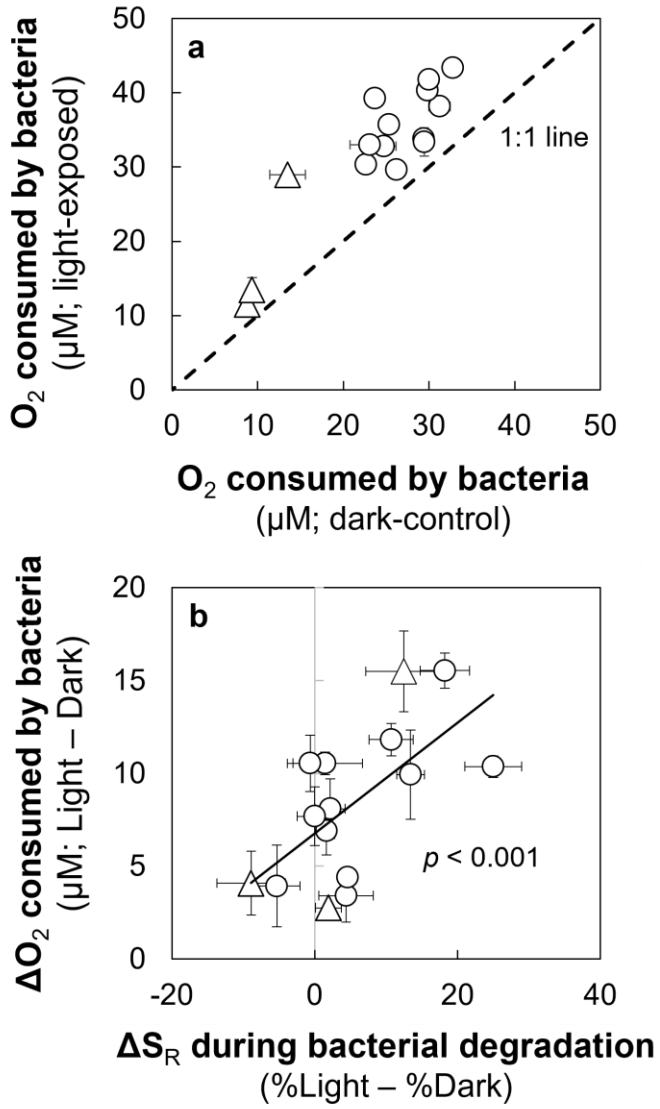

Figure 6.1. Effect of DOM photodegradation on the amount of dissolved oxygen (O_2) consumed by bacteria during the respiration of biodegradable DOM (BDOM) in White Clay Creek. (a) Concentration of O_2 consumed by bacteria in the light-exposed versus dark-control waters plotted with the 1:1 line (dashed). (b) Change in the average molecular weight of DOM (as indicated by the spectral slope ratio, S_R)[73] during bacterial degradation of DOM on the x-axis versus the impact of DOM photodegradation on O_2 consumption by bacteria on the y-axis. Triangles (Δ) indicate the labile pool within BDOM and circles (O) indicate total BDOM (see Appendix Section 5.8.1). Photodegradation decreased the molecular weight of DOM (Figure 5.2), resulting in greater bacterial degradation of lower molecular weight compounds (as indicated by positive values on the x-axis in (b)). O_2 consumption by bacteria increased in response to this bacterial degradation of lower molecular weight compounds within DOM. Dissolved O_2 was measured on a membrane inlet mass spectrometer (Bay Instruments).[74] When all data in (b) are fit using a least-squares regression, $p < 0.001$. All data plotted as average ± 1 standard error of triplicate measurements.

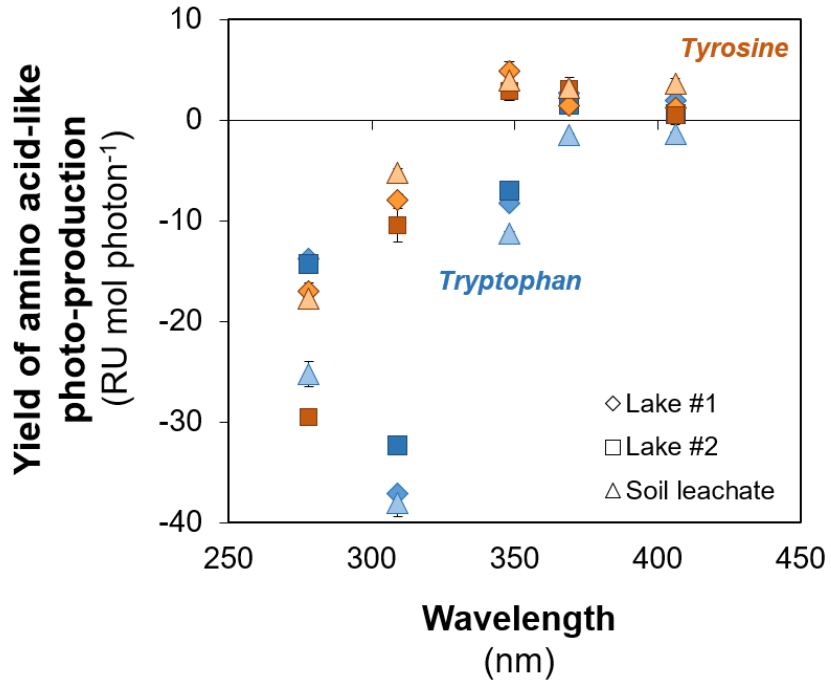

Figure 6.2. Wavelength-dependent apparent quantum yield spectra for the photo-production of tryptophan-like and tyrosine-like fluorescent DOM (FDOM) in arctic lake and soil waters. The photo-production yields ($\varphi_{,\lambda}$) for tryptophan-like (blue symbols) and tyrosine-like (orange symbols) FDOM are shown following exposures to light-emitting diodes (LEDs) at 278, 309, 348, 369, and 406 nm.[75] Tryptophan-like and tyrosine-like FDOM were measured alongside NH_4^+ as previously described (see Appendix Section 2.8.1). The abundance of tryptophan-like FDOM in each LED-exposed and dark-control water sample was calculated as the fluorescence intensity at an excitation wavelength of 292 nm and an emission wavelength of 385 nm in the excitation-emission matrix (Figure 2.A.1). The abundance of tyrosine-like FDOM was calculated as the fluorescence intensity at an excitation wavelength of 272 nm and emission wavelength of 318 nm (Figure 2.A.1). The yield at each wavelength was calculated as the amount of tryptophan-like or tyrosine-like FDOM photodegraded (light minus dark difference in Raman Unit, RU) divided by the total amount of light absorbed by chromophoric DOM in each beaker. All values are the average ± 1 standard error of replicate measurements (n = 3).

6.3 References

1. Stedmon, C. A., S. Markager, L. Tranvik, L. Kronberg, T. Slätis, and W. Martinsen (2007). Photochemical production of ammonium and transformation of dissolved organic matter in the Baltic Sea. *Mar. Chem*. 104: 227-240.

2. Cory, R. M., C. P. Ward, B. C. Crump, and G. W. Kling (2014). Sunlight controls water column processing of carbon in arctic freshwaters. *Science* 345: 925-928.

3. Powers, L. C., and W. L. Miller (2015). Photochemical production of CO and CO_2 in the Northern Gulf of Mexico: Estimates and challenges for quantifying the impact of photochemistry on carbon cycles. *Mar. Chem*. 171: 21-35.

4. Jørgensen, N. O. G., L. Tranvik, H. Edling, W. Granéli, and M. Lindell (1998). Effects of sunlight on occurrence and bacterial turnover of specific carbon and nitrogen compounds in lake waters. *FEMS Microbol. Ecol*. 25: 217-227.

5. Tarr, M. A., W. Wang, T. S. Bianchi, and E. A. Engelhaupt (2001). Mechanisms of ammonia and amino acid photoproduction from aquatic humic and colloidal matter. *Water Res*. 35(15): 3688-3696.

6. Zhang, Y., R. Zhang, S.-L. Li, K. M. G. Mostofa, X. Fu, H. Ji, et al. (2021). Photo-ammonification of low molecular weight dissolved organic nitrogen by direct and indirect photolysis. *Sci. Total Environ.* 764, 142930.

7. Cory, R. M., K. H. Harrold, B. T. Neilson, and G. W. Kling (2015). Controls on dissolved organic matter (DOM) degradation in a headwater stream: the influence of photochemical and hydrological conditions in determining light-limitation or substrate-limitation of photo-degradation. *Biogeosci.* 12: 6669-6685.

8. Ward, C. P., and R. M. Cory (2015). Chemical composition of dissolved organic matter draining permafrost soils. *Geochim. Cosmochim. Acta* 167: 63-79.

9. Feng, X., J. E. Vonk, C. Griffin, N. Zimov, D. B. Montluçon, L. Wacker, and T. I. Eglinton (2017). ^{14}C variation of dissolved lignin in arctic river systems. *ACS Earth Space Chem.* 1: 334-344.

10. Ward, C. P., S. G. Nalven, B. C. Crump, G. W. Kling, and R. M. Cory (2017). Photochemical alteration of organic carbon draining permafrost soils shifts microbial metabolic pathways and stimulates respiration. *Nat. Commun*. 8, 772.

11. Ping, C. L., J. G. Bockheim, J. M. Kimble, G. J. Michaelson, and D. A. Walker (1998). Characteristics of cryogenic soils along a latitudinal transect in Arctic Alaska. *J. Geophys. Res.* 103: 28917-28928.

12. Herndon, E. M., Z. Yang, J. Bargar, N. Janot, T. Z. Regier, D. E. Graham, et al. (2015). Geochemical drivers of organic matter decomposition in arctic tundra soils. *Biogeochem.* 126: 397-414.

13. Heslop, J. K., M. Winkel, K. M. Walter Anthony, R. G. M. Spencer, D. C. Podgorski, P. Zito, et al. (2019). Increasing organic carbon biolability with depth in yedoma permafrost: Ramifications for future climate change. *J. Geophys. Res. Biogeosci.* 124: 1-18.

14. Trusiak, A., L. A. Treibergs, G. W. Kling, and R. M. Cory (2019). The controls of iron and oxygen on hydroxyl radical (•OH) production in soils. *Soil Syst.* 3(1): 1-23.

15. Brown, A., D. M. McKnight, Y.-P. Chin, E. C. Roberts, and M. Uhle (2004). Chemical characterization of dissolved organic material in Pony Lake, a saline costal pond in Antarctica. *Mar. Chem.* 89: 327-337.

16. Cory, R. M., D. M. McKnight, Y.-P. Chin, P. Miller, and C. L. Jaros (2007). Chemical characteristics of fulvic acids from Arctic surface waters: Microbial contributions and photochemical transformations. *J. Geophys. Res.* 112, G04S51.

17. Goldberg, S. J., G. I. Ball, B. C. Allen, S. G. Schladow, A. J. Simpson, H. Masoom, et al. (2015). Refractory dissolved organic nitrogen accumulation in high-elevation lakes. *Nat. Commun.* 6, 6347.

18. Cao, X., G. A. Aiken, R. G. M. Spencer, K. Butler, J. Mao, and K. Schmidt-Rohr (2016). Novel insights from NMR spectroscopy into seasonal changes in the composition of dissolved organic matter exported to the Bering Sea by the Yukon River. *Geochem. Cosmochim. Acta* 181: 72-88.

19. Schmidt-Rohr, K., J.-D. Mao, and D. C. Olk (2004). Nitrogen-bonded aromatics in soil organic matter and their implications for a yield decline in intensive rice cropping. *Proc. Natl. Acad. Sci. USA* 101(17): 6351-6354.

20. Mao, J.-D., R. M. Cory, D. M. McKnight, and K. Schmidt-Rohr (2007). Characterization of a nitrogen-rich fulvic acid and its precursor algae from solid state NMR. *Org. Geochem.* 38: 1277-1292.

21. Mao, J.-D., L. Tremblay, J.-P. Gagné, S. Kohl, and K. Schmidt-Rohr (2007). Humic acids from particulate organic matter in the Saguenay Fjord and the St. Lawrence Estuary investigated by advanced solid-state NMR. *Geochim. Cosmochim. Acta* 71(22): 5483-5499.

22. Weishaar, J. L., G. R. Aiken, B. A. Bergamaschi, M. S. Fram, R. Fujii, and K. Mopper (2003). Evaluation of specific ultraviolet absorbance as an indicator of the chemical composition and reactivity of dissolved organic carbon. *Environ. Sci. Technol.* 37: 4702-4708.

23. Kaiser, E., A. J. Simpson, K. J. Dria, B. Sulzberger, and P. G. Hatcher (2003). Solid-state and multidimensional solution-state NMR of solid phase extracted and ultrafiltered riverine dissolved organic matter. *Environ. Sci. Technol.* 37: 2929-2935.

24. Allard, T., N. Menguy, J. Salomon, T. Calligaro, T. Weber, G. Calas, and M. F. Benedetti (2004). Revealing forms of iron in river-borne material from major tropical rivers of the Amazon Basin (Brazil). *Geochem. Cosmochim. Acta* 68(14): 3079-3094.

25. Hopwood, M. J., P. J. Statham, S. A. Skrabal, and J. D. Willey (2015). Dissolved iron(II) ligands in river and estuarine water. *Mar. Chem.* 173: 173-182.

26. Kaushal, S. S., A. J. Gold, S. Bernal, T. A. Newcomer Johnson, K. Addy, A. Bergin, et al. (2018). Watershed 'chemical cocktails': Forming novel elemental combinations in the Anthropocene fresh waters. *Biogeochem.* 141: 281-305.

27. Brezonik, P. L., J. C. Finlay, C. G. Griffin, W. A. Arnold, E. H. Boardman, N, Germolus, et al. (2019). Iron influences on dissolved color in lakes of the Upper Great Lakes States. *PLoS ONE* 14(2), e0211979.

28. Gao, H., and R. G. Zepp (1998). Factors influencing photoreactions of dissolved organic matter in a coastal river of the southeastern United States. *Environ. Sci. Technol.* 32: 2940-2946.

29. Mann, P. J., A. Davydova, N. Zimov, R. G. M. Spencer, S. Davydov, E. Bulygina, et al. (2012). Controls on the composition and lability of dissolved organic matter in Siberia's Kolyma River basin. *J. Geophys. Res.* 117, G01028.

30. Page, S. E., J. R. Logan, R. M. Cory, and K. McNeill (2014). Evidence for dissolved organic matter as the primary source and sink of photochemically produced hydroxyl radical in arctic surface waters. *Environ. Sci.: Processes Impacts* 16: 807-822.

31. Dillon, P. J., and L. A. Molot (1997). Effect of landscape form on export of dissolved organic carbon, iron, and phosphorus from forested stream catchments. *Water Resour. Res.* 33(11): 2591-2600.

32. Björnerås, C., G. A. Weyhenmeyer, C. D. Evans, M. O. Gessner, H.-P. Grossart, K. Kangur, et al. (2017). Widespread increases in iron concentration in European and North American freshwaters. *Global Biogeochem. Cycles* 31: 1488-1500.

33. Kritzberg, E. S., and S. M. Ekström (2012). Increasing iron concentrations in surface waters – a factor behind brownification? *Biogeosci.* 9: 1465-1478.

34. Weyhenmeyer, G. A., Y. T. Prairie, and L. J. Tranvik (2014). Browning of boreal freshwaters coupled to carbon-iron interactions along the aquatic continuum. *PLoS ONE* 9(2), e88104.

35. Vallino, J. J., C. S. Hopkinson, and J. E. Hobbie (1996). Modeling bacterial utilization of dissolved organic matter: Optimization replaces Monod growth kinetics. *Limnol. Oceanogr.* 41(6): 1591-1609.

36. Sun, L., E. M. Perdue, J. L. Meyer, and J. Weis (1997). Use of elemental composition to predict bioavailability of dissolved organic matter in a Georgia river. *Limnol. Oceanogr*. 42(4): 714-723.

37. Bertilsson, S., and L. J. Tranvik (1998). Photochemically produced carboxylic acids as substrates for freshwater bacterioplankton. *Limnol. Oceanogr*. 43: 885-895.

38. Tranvik, L. J., and S. Bertilsson (2001). Contrasting effects of solar UV radiation on dissolved organic sources for bacterial growth. *Ecol. Lett.* 4: 458-463.

39. Volk, C. J., C. B. Volk, and L. A. Kaplan (1997). Chemical composition of biodegradable dissolved organic matter in streamwater. *Limnol. Oceanogr*. 42: 39-44.

40. Hockaday, W. C., J. M. Purcell, A. G. Marshall, J. A. Baldock, and P. G. Hatcher (2009). Electrospray and photoionization mass spectrometry for the characterization of organic matter in natural waters: A qualitative assessment. *Limnol. Oceanogr.: Methods* 7: 81-95.

41. Amado, A. M., J. B. Cotner, A. L. Suhett, F. D. Assis Esteves, R. L. Bozelli, and V. F. Farjalla (2007). Contrasting interactions mediate dissolved organic matter decomposition in tropical aquatic ecosystems. *Aquat. Microb. Ecol.* 49: 25-34.

42. Moran, M. A., W. M. Sheldon, and R. G. Zepp (2000). Carbon loss and optical property changes during long-term photochemical and biological degradation of estuarine dissolved organic matter. *Limnol. Oceanogr.* 45: 1254-1264.

43. Vähätalo, A. V., K. Salonen, U. Münster, M. Järvinen, and R. G. Wetzel (2003). Photochemical transformation of allochthonous organic matter provides bioavailable nutrients in a humic lake. *Arch. Hydrobiol*. 156(3): 287-314.

44. Fasching, C., and T. J. Battin (2012). Exposure of dissolved organic matter to UV-radiation increases bacterial growth efficiency in a clear-water Alpine stream and its adjacent groundwater. *Aquat. Sci.* 74: 143-153.

45. Granéli, W., M. Lindell, and L. Tranvik (1996). Photo-oxidative production of dissolved inorganic carbon in lakes of different humic content. *Limnol. Oceanogr.* 41: 698-706.

46. Ziegler, S., and R. Benner (2000). Effects of solar radiation on dissolved organic matter cycling in a subtropical seagrass meadow. *Limnol. Oceanogr*. 45(2): 257-266.

47. Jonsson, A., M. Meili, A.-K. Bergström, and M. Jansson (2001). Whole-lake mineralization of allochthonous and autochthonous organic carbon in a large humic lake (örträsket, N. Sweden). *Limnol. Oceanogr*. 46(7): 1691-1700.

48. Remington, S., A. Krusche, and J. Richey (2011). Effects of DOM photochemistry on bacterial metabolism and CO_2 evasion during falling water in a humic and a whitewater river in the Brazilian Amazon. *Biogeochem.* 105: 185-200.

49. Hobbie, J. E., and G. W. Kling (Eds.). (2014). *Alaska's Changing Arctic: Ecological Consequences for Tundra, Streams, and Lakes.* Oxford, UK: Oxford University Press.

50. Whalen, S. C., and J. C. Cornwell (1985). Nitrogen, phosphorus, and organic carbon cycling in an arctic lake. *Can. J. Fish. Aquat. Sci.* 42: 797-808.

51. Kling, G. W. (1995). Land-Water Interactions: The Influence of Terrestrial Diversity on Aquatic Ecosystems. In F. S. Chapin and C. Körner (Eds.), *Arctic and Alpine Biodiversity: Patterns, Causes and Ecosystems* (pp. 297-310). Berlin, Germany: Springer.

52. Anita, N. J., P. J. Harrison, and L. Oliveira (1991). The role of dissolved organic nitrogen in phytoplankton nutrition, cell biology and ecology. *Phycologia* 30(1): 1-89.

53. Gettel, G. M. (2006). Rates, importance, and controls of nitrogen fixation in oligotrophic arctic lakes, Toolik, Alaska. Cornell University. Ithaca, New York.

54. Luecke, C., A. E. Giblin, N. D. Bettez, G. A. Burkart, B. C. Crump, M. A. Evans, et al. (2014). The Response of Lakes Near the Arctic LTER to Environmental Change. In J. E. Hobbie and G. W. Kling (Eds.), *Alaska's Changing Arctic: Ecological Consequences for Tundra, Streams, and Lakes* (pp. 238-286). Oxford, UK: Oxford University Press.

55. Pokrovsky, O. S., and J. Schott (2002). Iron colloids/organic matter associated transport of major and trace elements in small boreal rivers and their estuaries (NW Russia). *Chem. Geol.* 190: 141-179.

56. Pokrovsky, O. S., L. S. Shirokova, S. N. Kirpotin, S. Audry, J. Viers, and B. Dupré (2011). Effect of permafrost thawing on organic carbon and trace element colloidal speciation in the thermokarst lakes of western Siberia. *Biogeosci.* 8: 565-583.

57. Shirokova, L. S., O. S. Pokrovsky, S. N. Kirpotin, C. Desmukh, B. G. Pokrovsky, S. Audry, and J. Viers (2013). Biogeochemistry of organic carbon, CO_2, CH_4, and trace elements in thermokarst water bodies in discontinuous permafrost zones of Western Siberia. *Biogeochem.* 113: 573-593.

58. Pokrovsky, O. S., R. M. Manasypov, S. V. Loiko, and L. S. Shirokova (2016). Organic and organo-mineral colloids in discontinuous permafrost zone. *Geochim. Cosmochim. Acta* 188: 1-20.

59. Loiko, S. V., O. S. Pokrovsky, T. V. Raudina, A. Lim, L. G. Kolesnichenko, L. S. Shirokova, et al. (2017). Abrupt permafrost collapse enhances organic carbon, CO_2, nutrient and metal release into surface waters. *Chem. Geol.* 471: 153-165.

60. Barker, A. J., T. A. Douglas, A. D. Jacobson, J. W. McClelland, A. G. Ilgen, M. S. Khosh, et al. (2014). Late season mobilization of trace metals in two small Alaskan arctic watersheds as a proxy for landscape scale permafrost active layer dynamics. *Chem. Geol.* 381: 180-193.

61. Sulzberger, B., A. T. Austin, R. M. Cory, R. G. Zepp, and N. D. Paul (2019). Solar UV radiation in a changing world: Roles of cryosphere-land-water-atmosphere interfaces in global biogeochemical cycles. *Photochem. Photobiol. Sci*. 18: 747-774.

62. Nalven, S. G., C. P. Ward, J. P. Payet, R. M. Cory, G. W. Kling, T. J. Sharpton, et al. (2020). Experimental metatranscriptomics reveals the costs and benefits of dissolved organic matter photo-alteration for freshwater microbes. *Environ. Microbiol*. 22(8): 3505-3521.

63. Cory, R. M., K. McNeill, J. P. Cotner, A. Amado, J. M. Purcell, and A. G. Marshall (2010). Singlet oxygen in the coupled photochemical and biochemical oxidation of dissolved organic matter. *Environ. Sci. Technol*. 44: 3683-3689.

64. Waggoner, D. C., H. Chen, A. S. Willoughby, and P. G. Hatcher (2015). Formation of black carbon-like and alicyclic aliphatic compounds by hydroxyl radical initiated degradation of lignin. *Org. Geochem.* 82: 69-76.

65. Waggoner, D. C., A. S. Wozniak, R. M. Cory, and P. G. Hatcher (2017). The role of reactive oxygen species in the degradation of lignin derived dissolved organic matter. *Geochim. Cosmochim. Acta* 208: 171-184.

66. Ward, C. P., and R. M. Cory (2020). Assessing the prevalence, products, and pathways of dissolved organic matter partial photo-oxidation in arctic surface waters. *Environ. Sci.: Processes Impacts* 22: 1214-1223.

67. Latch, D. E., and K. McNeill (2006). Microheterogeneity of singlet oxygen distributions in irradiated humic acid solutions. *Science* 311(4981): 1743-1747.

68. Cory, R. M., and G. W. Kling (2018). Interactions between sunlight and microorganisms influence dissolved organic matter degradation along the aquatic continuum. *Limnol. Oceanogr.: Lett.* 3: 102-116.

69. Reader, H. E., and W. L. Miller (2014). The efficiency and spectral photon dose dependence of photochemically induced changes to the bioavailability of dissolved organic carbon. *Limnol. Oceanogr*. 59: 182-194.

70. Münster, U., P. Einiö, J. Nurminen, and J. Overbeck (1992). Extracellular enzymes in a polyhumic lake: important regulators in detritus processing. *Hydrobiol.* 229: 225-238.

71. Tranvik, L. J., and N. O. G. Jørgensen (1995). Colloidal and dissolved organic matter in lake water: Carbohydrate and amino acid composition, and ability to support bacterial growth. *Biogeochem*. 30: 77-97.

72. Siuda, W., and R. J. Chróst (2002). Decomposition and utilization of particulate organic matter by bacteria in lakes of different trophic status. *Polish J. Environ. Stud.* 11(1): 53-65.

73. Helms, J. R., A. Stubbins, J. D. Ritchie, E. C. Minor, D. J. Kieber, and K. Mopper (2008). Absorption spectral slopes and slope ratios as indicators of molecular weight, source, and photobleaching of chromophoric dissolved organic matter. *Limnol. Oceanogr.* 53: 955-969.

74. Kana, T. M., C. Darkangelo, M. D. Hunt, J. B. Oldham, G. E. Bennett, and J. C. Cornwell (1994). Membrane inlet mass spectrometer for rapid high-precision determination of N2, O2, and Ar in environmental water samples. *Anal. Chem*. 66(23): 4166-4170.

75. Ward, C. P., J. C. Bowen, D. H. Freeman, and C. M. Sharpless (2021). Rapid and reproducible characterization of the wavelength dependence of aquatic photochemical reactions using light emitting diodes (LEDs). *Environ. Sci. Technol. Lett.* 8(5): 437-442.